'Some mechanistic aspects of the environmental sensitive cracking of an 18Ni maraging steel'

by

I H Craig, B.Sc

A thesis submitted as part requirement
for the degree Doctor of Philosophy

Department of Metallurgy &
Engineering Materials
Haymarket Lane
Newcastle upon Tyne

July 1977

SYNOPSIS

The stress assisted cracking of high strength steels in aqueous environments is regarded by many to occur by a hydrogen embrittlement mechanism no matter to what potential the bulk surface of the material is electrochemically polarised.

Some data is presented in this work for a high strength 18Ni maraging steel in aqueous chloride environments and interpreted in terms of a dual mechanism of cracking according to the applied potential relative to the free corrosion potential. Several experimental techniques were employed; including the use of smooth and pre-cracked stress corrosion specimens, to assess the cracking mechanisms operative under given conditions with mixed success. The electrochemical hydrogen permeation technique whilst found to be useful for the determination of hydrogen diffusivities during cathodic charging was found to be unsuitable for a mechanistic experimental approach based on the observation of hydrogen permeating through the steel during anodic polarisation. However, the detection of acoustic emissions accompanying environmental cracking of pre-cracked specimens of the steel and the influence on the stress corrosion cracking susceptibility of chemical poisons or catalysts of the hydrogen evolution reaction suggested that a dual cracking mechanism was operative.

CONTENTS

1 Review of the Literature

1.1 The Physical Metallurgy of Maraging Steels

1.1.1 Uses of maraging steels

The Ni-Co-Mo maraging steels are a relatively new class of high strength steels deriving their strength from the precipitation hardening of a non-carbon martensite.

These steels have found increasing uses in applications requiring combinations of high strength and ductility which, combined with their excellent fabrication and machining properties, makes their use particularly attractive in situations where normally only low alloy high strength steels would be considered. It has been shown[1] that the reduced manufacturing costs associated with their excellent fabricability can more than compensate for the difference in price between maraging steel and low alloy steels of equivalent strength.

Uses include:-

i) In aerospace and marine applications:- rocket motor cases, load cells capable of measuring rocket motor thrusts, torsion bar suspension system for the Lunar Rover vehicle, flexible drive shafts for helicopters, aircraft landing gear, hinges for swing wing planes, foils for hydrofoil ships and deep submergence marine vessels etc.

ii) In structural and machine components:- pressure vessels, bolts and fasteners, barrels for rapid firing guns etc.

iii) In tooling applications:-

die casting dies or their components, moulds for the plastics industry, rams for extrusion of lead or lead-tin alloy sheaths and cold forming dies.

1.1.2 Compositions

The development of maraging steels proceeded from the initial alloys containing 20% and 25% Ni to the present day 18 Ni maraging steels. Other varieties have been developed including the 12 Ni-5Cr-3Mo series, a 17% Ni variety used for castings and the chromium containing stainless varieties.

This review will be confined to the 18Ni-Co-Mo variety often classified according to their tensile strengths in thousands of pounds per square inch i.e. 200, 250, 300 grades. Nominal compositions of the Ni-Co-Mo maraging steels are shown in Table 1.1. Fracture toughness properties of maraging steels are closely related to the impurity levels of P, C, S etc and as a consequence maraging steels are now produced by techniques involving at least one vacuum melting step, the best values of K_{IC} being achieved by vacuum induction melting alone or followed by vacuum arc remelting. Typical impurity levels produced by the latter techniques are:-

0.01P, 0.005C, 0.005S, 0.01N

1.1.3 Processing and heat treatment

Processing of maraging steels usually involves homogenisation and hot working at between 1200 and 1260°C followed by further hot working at temperatures below 1000°C.

TABLE 1.1

Maraging steel	Composition %						Nominal Yield Str. Ksi
	Ni	Cr	Co	Mo	Ti	Fe	
18Ni(200)	18	-	8.5	3	0.2	Bal	200
18Ni(250)	18	-	8	5	0.4	Bal	250
18Ni(300)	18	-	9	5	0.6	Bal	300
18Ni(350)	17.5	-	12.5	3.75	1.7	Bal	350
Cast Alloy	17	-	10	4.6	0.3	Bal	230
12-5-3	12	5	-	3	0.2	Bal	180

Prolonged exposure at temperatures between 760°C and 1095°C after hot working or during annealing are to be avoided since they induce chemical embrittlement, attributed to TiC(N) or Ti_2S films that form at prior austenite grain boundaries. The recommended post-working heat treatment consists of annealing for 1 hour at 820°C followed by air cooling. Because of the high nickel content and the absence of carbon hardenability is not a problem and therefore the cooling rate after annealing is unimportant.

The austenite to martensite phase transformation occurs in the temperature range 143°C to 199°C depending upon the specific alloy content. The transformation produces a structure consisting of packets of parallel lath-like platelets of martensite which is relatively soft. (Rc 30), untwinned and has a high dislocation density. The martensitic structure so formed creates favourable conditions for uniform nucleation and distribution of precipitates during subsequent ageing.

In the as annealed condition the maraging steels can be readily machined or fabricated.

The martensitic structure is aged at 480° - 520°C for 3 hours to develop the desired strength level. The precipitates that have been identified in Ni-Co-Mo maraging steels after ageing include Ni_3Mo and a titanium bearing precipitate which may be Eta Ni_3Ti or sigma titanium.[2,3] Ageing at higher temperatures or for longer times causes the Ni_3Mo precipitates to be replaced by the more stable Fe_2Mo precipitate. In addition, the martensite matrix partially reverts to austenite; the latter usually forming at martensite lath boundaries and at the prior austenite grain boundaries. Since large amounts of austenite significantly lowers the strength of maraging steels, over-ageing is avoided for commercial applications of the steel.

1.1.4 The role of alloying elements

i) Nickel

It has been shown that alloying ferrite with nickel not only ensures a martensitic structure which can increase the strength of the matrix but also reduces the solubility of other elements, e.g. Ti, Mo, Al in α iron. Furthermore, nickel lowers the resistance of the crystal lattice to the movement of dislocations and reduces the energy of interaction of dislocations with interstitial atoms.[4] Stress relaxation is, thereby, assisted thus reducing the susceptibility of the steels to brittle failure.

The remaining alloying elements found in the 18Ni maraging steels can be classified according to their hardening capabilities as 'strong' Be, Ti, moderate Al, Nb, Mn, Si, Ta, V, W or weak Co, Cu, Zr hardeners.

ii) Titanium

Titanium plays a double role in its use in the maraging steels; as a hardener and refining agent to tie up residual carbon. According to Castagné and Legendre[5] during the solidification of maraging steels, titanium tends to segregate or precipitate in the austenite grain boundaries in the form of titanium carbide or carbon-nitrides causing anisotropy of plasticity and reducing ductility. Cheng[6] et al have also identified the precipitation of titanium compounds with carbon, nitrogen or oxygen on ageing maraging steels between 370 and 480^{o}C.

iii) Molybdenum

Molybdenum lowers the diffusion coefficients of a number of elements in the grain boundaries and so restricts preferential precipitation of second phase particles at these localities during ageing. However, like titanium, molybdenum also tends to segregate during solidification from the melt which contributes to anisotropy of plasticity and ductility.

iv) Aluminium

Aluminium appears to have only a minor effect; in that it limits hardening of the martensite and at concentrations in excess of 0.2 to 0.3% lowers ductility both before and after ageing.

v) Manganese

Manganese additions assist in the formation of a martensitic structure at low nickel contents but they have a detrimental effect on the ductility properties after ageing.

vi) Cobalt

Cobalt appears to have several affects, e.g. By lowering the solubility of Mo and W in α iron cobalt indirectly increases the degree of hardening that occurs upon ageing. The decrease in solubility of hardener elements leads to an increase in the volume per cent of precipitates formed and reduces the work of formation of nucleii of the precipitation phase. Consequently the number of nucleii capable of growth at a given temperature is increased and therefore the average distance between particles is reduced. All of these factors influence the phenomenon of age hardening.

The Cobalt-molybdenum interaction provides one of the most significant contributions to the strengthening of maraging steels. It has been found[7,8,9] that the hardening effect obtained when cobalt and molybdenum are present together was much greater than the sum of the strength increments produced when these elements are added individually.

1.2 Stress Corrosion Cracking Mechanisms

By definition, stress corrosion cracking is the phenomenon in which a material will fail prematurely when subjected to both stress and a corrosive environment but not when subjected to either alone. This definition is of course entirely general, describing as it does the basic requirements of stress corrosion crack propagation and to be more precise it is convenient to consider a spectrum of stress corrosion cracking processes ranging from those systems in which stress or strain is the predominating influence to those in which dissolution processes appear to be dominant. Fig. 1.1[10] shows some of the metal environment systems in which stress corrosion cracking is observed arranged in such a series.

CORROSION DOMINANT — STRESS DOMINANT

WELD DECAY	MILD STEELS IN NO_3^-	Al-Zn -Mg IN Cl^-	Cu-Zn IN NH_3	18/8 IN Cl^-	Mg-Al IN CrO_4^- Cl	Ti ALLOYS IN CH_4OH	HIGH STR. STEELS IN H_2O	BRITTLE FRACTURE
	PRE-EXISTING ACTIVE PATHS		STRAIN GENERATED ACTIVE PATHS		SPECIFIC ADSORPTION AT SUB-CRITICALLY STRESSED SITES			

FIG. 1.1 Stress Corrosion Spectrum

It is convenient, for discussion purposes, to divide the spectrum into 3 zones describing the three principle cracking mechanisms that can operate in the phenomenon of stress corrosion cracking namely:-

i) Pre-existing active paths

ii) Strain generated active paths

iii) Specific adsorption at sub-critically stressed sites.

Whilst this subdivision is made for the convenience of discussion, it should be recognised that the spectrum is, in reality, continuous; in that there is a continuous change in emphasis in moving from one end of the spectrum to the other.

Mechanisms i) and ii) differ from iii) in that when the former mechanisms are operative crack propagation is usually considered to take place by a dissolution process whereas in the case of iii) crack propagation is regarded to be predominantly mechanical in nature.

1.2.1 Dissolution mechanisms via pre-existing or strain generated active paths

Bearing in mind the fact that in order for the crack morphology to be maintained, the anodic current density at the crack tip must be maintained at a much higher value than on the crack faces; then the crack velocity, V can be expressed as a function of the anodic current density at the crack tip as:-

$$V = \frac{ia\ M}{Z \rho F} \qquad 1.1$$

where ia = anodic current density at the crack tip

M = atomic weight of metal of valency, Z and density, ρ undergoing dissolution

and F = Faraday constant.

The anodic current density at the crack tip and hence V will depend upon the nature of the phase being dissolved and also upon the nature and location of any cathodic processes that occur elsewhere. The question now arises 'how does a tensile stress (or strain) influence the situation to produce stress corrosion cracking?' It has been demonstrated[11] that the dissolution rate of iron in acid solutions undergoes a marked increase when straining passes from the elastic to the plastic regimes in dynamic straining experiments and this effect was due to the exposure of high index planes and edges of slip steps as well as increases in surface roughness as plastic deformation occurs. Stresses greater than the yield stress may therefore produce enhanced local activity at surfaces intersected by slip planes and so ia (and hence V) are increased as a result of plastic straining.

However, the above phenomenon still does not explain why the corrosion process proceeds along a narrow front to maintain the geometry of a crack implying that most of the exposed surface area (including the crack sides) must remain relatively inactive. It seems most likely that this inactivity results from the formation of a passive layer (usually oxide) layer at such sites. This implies that, with reference to equation 1.1 stress corrosion cracking conditions are met when ia represents the film free anodic current density. In this context, the function of stress is to maintain the crack tip film free in film forming mechanisms.

Two crack propagation mechanisms may now be envisaged depending upon the presence or otherwise of structural features (either segregate or precipitate) usually at grain boundaries which cause a local galvanic cell to be set up i.e. a pre-existing path is involved. In the latter context the precipitate or segregate may act as the anode in a local cell or by acting as an efficient cathode may cause attack to be localised in the immediately adjacent matrix material (see Fig. 1.2). The function of stress in such a situation is presumably to prevent the dissolution reaction from becoming stifled by film formation.

When such pre-existing paths are non-existant or are inoperative because of environmental effects, the stress may act to disrupt a protective film formed on the metal surface to expose bare metal and so maintain the relatively high localised anodic current density (see Fig. 1.3). The active path in this case is, therefore, cyclically generated as disruptive strain and film build up compete with one another. Such 'strain generated active paths' would be expected to result in transgranular stress corrosion cracking.

1.2.2 Specific adsorption at sub-critically stressed sites (hydrogen embrittlement mechanism)

The fracture stress, σ_{FR} to pull apart two planes of atoms in a metal lattice is given by the formula:-

$$\sigma_{FR} = \left(\frac{E\gamma}{b}\right)^{\frac{1}{2}} \qquad 1.2$$

where E = Youngs modulus of elasticity, γ = surface energy of lattice

b = interatomic spacing.

If, therefore, the surface energy term is lowered so also will the fracture stress of the solid and this led Orowan to explain the fracture of glass by the adsorption of some atmospheric species on surface Griffith cracks; thereby lowering the surface energy and so reducing the stress required to propagate the surface cracks. The same argument has been used by many authors to explain some or all stress corrosion failures in metals or alloys.

The adsorbed species may act to embrittle the material in one of two ways

a) Directly by adsorbing at the crack tip and lowering γ or

b) Indirectly by subsequent diffusion of the

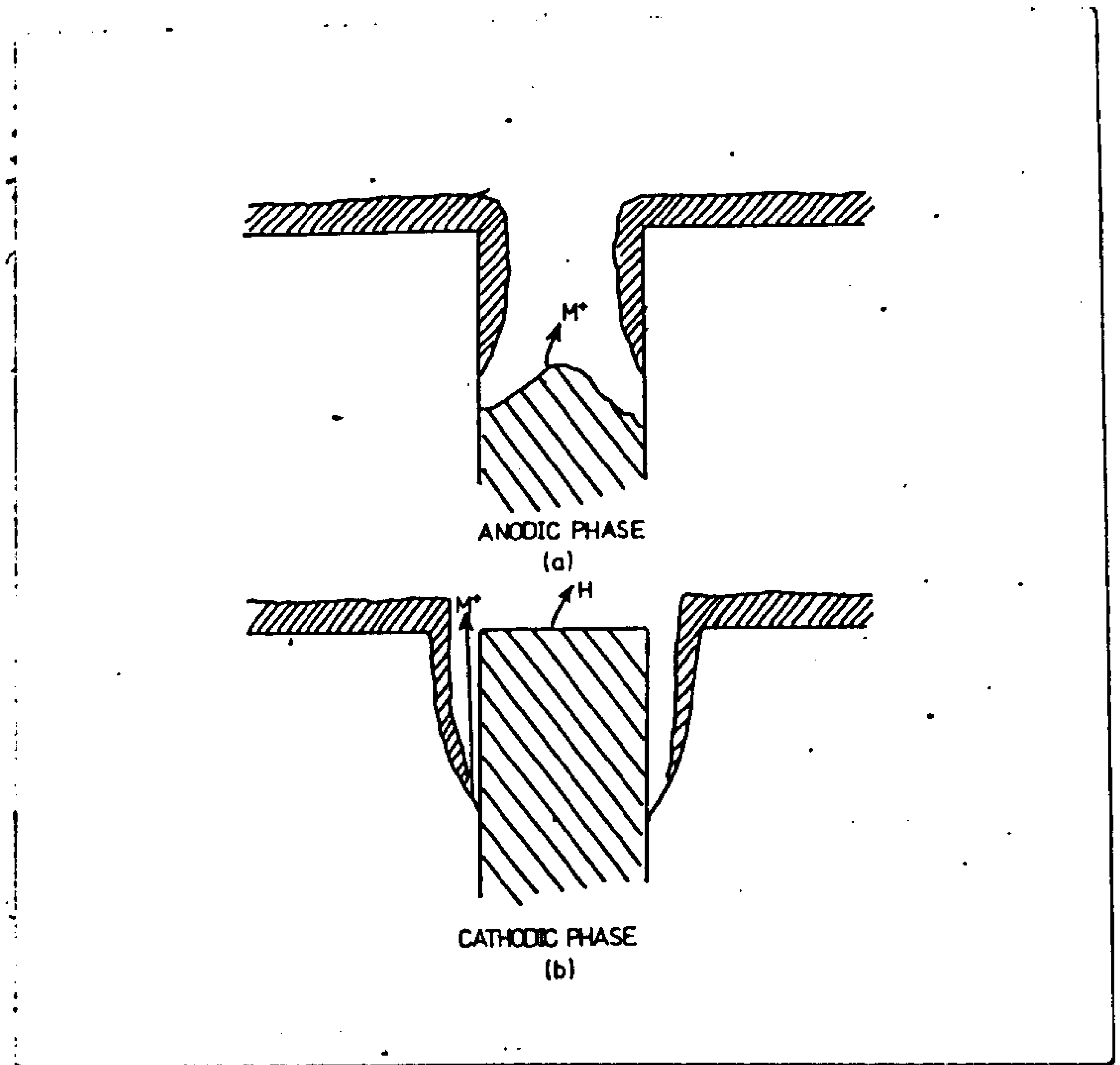

Fig. 1.2 Stress Corrosion via Pre-existing Active Paths

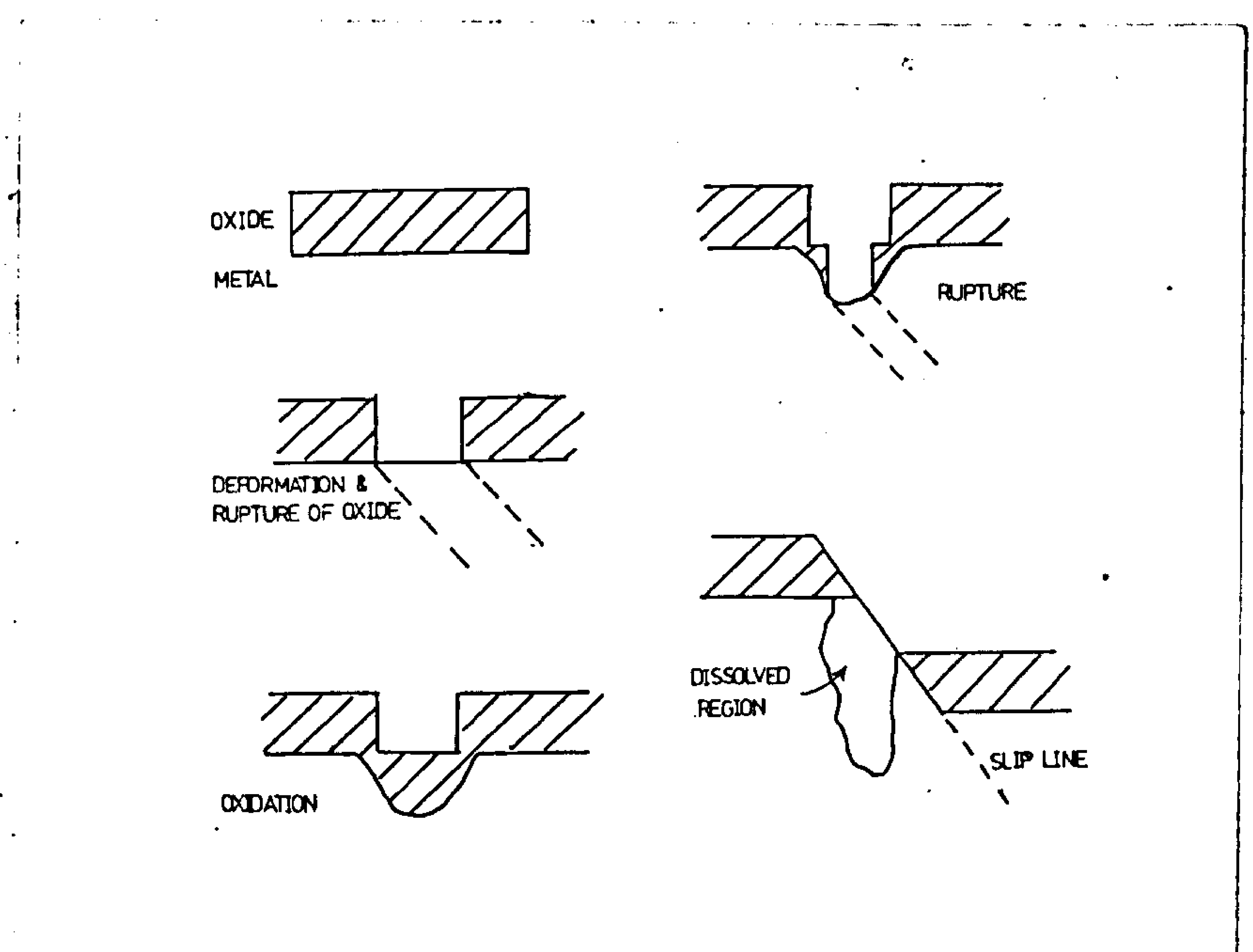

Fig. 1.3 Stress Corrosion via Strain-Generated Active Paths.

adsorbed species to some region in advance of the crack tip where the stress or strain conditions are particularly favourable for the nucleation of cracks e.g. at regions of maximum stress triaxiality usually considered to be located at the elastic-plastic interface of the plastic zone formed at the crack tip.

In the case of mechanism b) hydrogen is regarded to be the only species that can diffuse sufficiently rapidly to explain observed crack propagation rates and in this respect hydrogen embrittlement, with the hydrogen being cathodically produced at the metal surface as a result of corrosion reactions is considered to be a special instance of stress corrosion cracking.

The strongest evidence put forward in support of the adsorption theory is the observed grain size dependancy of the stress corrosion fracture stress, $\sigma_{FR.SCC}$ as given by the Hall-Petch relationship:-

$$\sigma_{FR.SCC} = \sigma_o + kd^{-\frac{1}{2}} \qquad 1.3$$

where σ_o and k are constants, d = grain size and $k = \left(\frac{6\pi G}{1-\nu}\right)^{\frac{1}{2}}$

with G = modulus of rigidity, ν = Poisson's ratio.

Using equation 1.3, γ may be calculated and has been observed to be less than that determined under different circumstances where surface energy lowering could not operate and thus lending support to the adsorption theory. However, the above arguments have been applied to metals and alloys in which cracking is associated with negligible plastic deformation.

Where plastic deformation is involved, equation 1.3 may simply be reflecting the variation of the work hardened flow stress and yield stress with grain size. In such cases equation 1.1 must be modified to include a plastic work term γp.

$$\text{Thus } \sigma_{FR} = \left[\frac{E(\gamma_s + \gamma_p)}{b}\right]^{\frac{1}{2}} \qquad 1.4$$

where σ_{FR}, E, b are as defined previously and γ_s is the specific surface energy

γ_p is the work required for plastic deformation.

In general, γ_p is greater by several orders of magnitude than γ_s so that any reduction of γ_s by adsorption will have a negligible effect on the fracture stress and so fracture is insignificantly easier with adsorption than without.

Furthermore, plastic deformation associated with S.C.C is important since it allows the crack tip to yawn which results in crack blunting. In such circumstances the adsorption model would not predict an increased crack propagation rate; yet this is precisely what is observed with some metals and alloys.

It is reasonable to suggest therefore that specific adsorption is only likely to be of any significance in the cracking of the less ductile materials where plastic deformation is negligible and γ_p is not $\gg \gamma_s$.

In view of this it is hardly surprising therefore, that hydrogen embrittlement is widely regarded to be the principle cause of stress corrosion cracking in the high strength steels.

1.3 A Review of the Stress Corrosion Cracking of High Strength Steels (With Particular Reference to 18Ni Maraging Steels)

Since stress corrosion cracking resistance is a material property often restricting the use of high strength steels in certain applications it is, perhaps, understandable that a large amount of research work has been carried out for particular alloys when exposed to selected environments.

As a consequence the mechanisms operating in the environmental cracking of the high strength steels are less well understood.

1.3.1 The influence of composition on the S.C.C. susceptibility of high strength steels

Although no systematic investigation appears to have been carried out concerning the influence of composition on the stress corrosion cracking susceptibility of high strength steels; the results of several comprehensive investigations[12,13,14] carried out on several compositionally different steels tends to suggest that the stress corrosion cracking susceptibility of high strength steels is more dependant on the yield strength of the material than any other single factor. As such, the influence of compositional changes may be associated with their influence on material strength properties by their influence on, for example, solid solution hardening or precipitation reactions during tempering or ageing.

Of all the different types of maraging steel it has been established that the 18Ni varieties offer the best all round stress corrosion resistance. However there is only a limited amount of published work concerning the effects of composition on-the stress corrosion cracking resistance of maraging steels. The influence of various residual elements on stress corrosion cracking behaviour have been extensively investigated,[15,16] however, and with somewhat conflicting results.

Stavros and Paxton[15] investigated the effects of various residual elements on the $K_{I\ SCC}$ values of an 18Ni (300) grade maraging steel tested in 3.5 wt % sodium chloride solution. The residual elements were varied in the following composition ranges S.003-.031%, P.002-.03, C.005-.062%, Cr.01-.24%, Si + Mn .036 - .29%.

Their results indicated that all of the alloys studied had similar stress corrosion resistances with $K_{I\ SCC}$ varying between 8 and 13 KSI $\sqrt{IN}$. They concluded that C and P may be beneficial at the higher levels, Cr was slightly detrimental, whilst S, Si and Mn had no effect on the stress corrosion cracking resistance. Looking at their results, however,(Table 1.2)[15] it would appear that they can be more readily explained by experimental scatter than any compositional differences associated with the residual element content.

Table 1.3 taken from Dautovitch and Floreens paper, lists the compositions, yield strengths and $K_{I\ SCC}$ data for an 18Ni maraging steel basis material tested in 3.5%NaCl solution. The investigation was carried out in order to determine the influence of the residual elements C, S, P, N and O on the stress corrosion cracking resistance of maraging steels. They concluded that $K_{I\ SCC}$ had no correlation with the P and N content but was strongly correlated with the S and to a lesser extent with the C content. A regression equation was derived relating $K_{I\ SCC}$ to yield strength, σy and the C, S

TABLE 1.2

The influence of various residual elements on the $K_{I\ SCC}$ data of an 18Ni maraging steel tested in 3.5 wt % NaCl[15]

Steel Composition	A HIGH PURITY	B COMMERCIAL PURITY	C SULPHUR ADDED	D PHOSPH ADDED	E CARBON ADDED	F CHROMIUM ADDED	G Si + Mn ADDED
Ni	18.1	18.0	18.0	18.1	18.2	18.2	18.1
Co	8.87	9.00	8.90	8.97	9.00	8.87	8.53
Mo	5.00	4.97	4.85	4.98	4.90	4.97	4.97
Ti	0.69	0.76	0.79	0.76	0.76	0.76	0.75
Al	0.11	0.12	0.11	0.12	0.12	0.11	0.11
B	0.001	0.001	0.001	0.001	0.001	0.001	0.001
Zr	0.01	0.01	0.01	0.01	0.01	0.01	0.01
N_2	0.007	0.007	0.002	0.006	0.001	0.005	0.001
S	0.003	0.005	0.031	0.014	0.004	0.004	0.004
P	0.007	0.008	0.002	0.030	0.006	0.008	0.002
C	0.005	0.019	0.005	0.027	0.062	0.016	0.015
Cr	0.011	0.012	0.010	0.014	0.010	0.24	0.015
Si	0.014	0.015	0.014	0.018	0.011	0.017	0.15
Mn	0.024	0.025	0.025	0.025	0.025	0.025	0.14
Yield Strength 0.2% offset (KSI)	244	246	240	243	240	248	241
K_{IC} (KSI$\sqrt{IN}$)	66	59	67	56	58	55	45
$K_{I\ SCC}$ (KSI$\sqrt{IN}$)	10	10	10	13	13	8	11

TABLE 1.3

The influence of minor compositional changes on the $K_{I\ SCC}$ data for an 18 Ni maraging steel tested in 3.5 wt % NaCl [16]

Heat	Ni	Co	Mo	Ti	Al	P	N	C	S	Mo+ Co+ Ti	Yield Strength (KSI)	$K_{I\ SCC}$ ($KSI\sqrt{IN}$)
1	18.3	8.55	3.10	0.25	0.07	0.005	0.0036	0.026	0.0030	11.9	206	120
2	18.0	8.70	3.75	0.32	0.04	0.007	0.0025	0.001	0.0010	12.77	227	120
3	17.8	7.95	4.68	0.43	0.18	0.011	0.0020	0.001	0.0040	13.06	245	30
4	17.6	7.90	4.60	0.51	0.19	0.011	0.0076	0.034	0.0040	13.01	247	35
5	17.7	8.00	4.53	0.45	0.13	0.003	-	0.004	0.0040	12.98	252	42
6	17.9	7.95	4.95	0.52	0.13	0.003	0.005	0.002	0.0022	13.42	257	21
7	18.0	8.20	4.90	0.48	0.02	0.009	0.0028	0.012	0.0015	13.58	260	36
8	18.5	7.40	4.95	0.72	0.05	0.010	0.0020	0.003	0.0030	13.07	262	20
9	18.4	7.48	4.88	0.37	0.05	-	0.0020	0.001	0.0017	12.73	269	45
10	18.2	7.63	4.72	0.47	0.10	0.008	0.0215	0.035	0.0010	12.82	270	50
11	17.9	8.90	5.1	0.48	0.08	-	-	0.011	0.0050	14.48	273	14
12	18.6	8.90	5.05	0.63	0.07	0.003	0.0005	0.004	0.0017	14.58	280	23
13	18.6	8.90	5.00	0.65	0.07	0.003	0.0005	0.004	0.0014	14.55	284	27
14	18.2	9.10	5.2	0.65	0.08	-	-	0.010	0.0017	14.95	243	11

residual element contents.

$$\text{Thus } K_{I\ SCC} = 363 - \frac{2.48\times10^5}{\sigma y} + \frac{4.01\times10^7}{\sigma y^2} + \frac{80.9}{C} + \frac{542}{S}$$

where $K_{I\ SCC}$ is in units of KSI $\sqrt{IN}$, σy is in Ksi and C, S contents in p.p.m.

The final column in the above table was added by the author and, as indicated, represents the total concentration of the principal strengthening element elements Co, Mo and Ti. It can be seen that although the correlation is not perfect, the $K_{I\ SCC}$ data can be just as easily explained by the effects of the total concentration of these elements in the steels as by any effect of differences in the concentrations of the residual alloying elements.

1.3.2 The influence of structure on the stress corrosion cracking susceptibility of the high strength steels

i) High Strength Steels

Phelps and Loginow[17] investigated a wide range of commercial high strength steels in marine and 'semi-industrial atmospheres, using cantilever beam specimens. Their results indicated that martensitic and alloy steels when heat treated to yield strengths in excess of 200,000 psi were susceptible to stress corrosion cracking in both of these environments. Semi-austenitic precipitation hardenable steels, however, though susceptible in marine atmospheres were not so in semi-industrial ones. Tempering of the latter steels above 590^{o}C conferred a resistance to cracking which was, however, probably a consequence of an associated reduction in the yield strength of the material.

Davis (et al)[18] found a similar yield strength dependancy of stress corrosion cracking resistance in AlSl 4330M, 4340 and hot work die steels tested in aqueous chloride environments. At yield strengths below 200,000 psi these steels were resistant to cracking, but above this stress level stress corrosion cracking was observed. Fürthermore, the failure times in these tests correlated reasonably well with notch sensitivites measured on circumferentially notched tensile specimens.

Figure 1.4[19] shows the results of cantilever beam tests performed on AlSl 4340 steel in flowing sea water. The results indicate that the difference between K_{IC} and $K_{I\ SCC}$ is more marked at the higher yield strength levels above about 150 Ksi, thus confirming the trends observed by Phelps[17] and Davis.[18]

Similarly, Figure 1.5[20] reflects the dependance of stress corrosion cracking resistance on yield strength for five high strength steels exposed to a natural marine environment.

Very little work appears to have been done on the effects of cold working on the resistance to stress corrosion cracking of high strength steels other than maraging steels however Davis[18] found that cold worked and stress relieved austenitic stainless steels were found to have excellent resistance to stress corrosion cracking despite high yield strength levels developed of 215 - 264 Ksi.

Procter and Paxton[21] and Webster[22] have investigated the influence of prior austenite grain size on

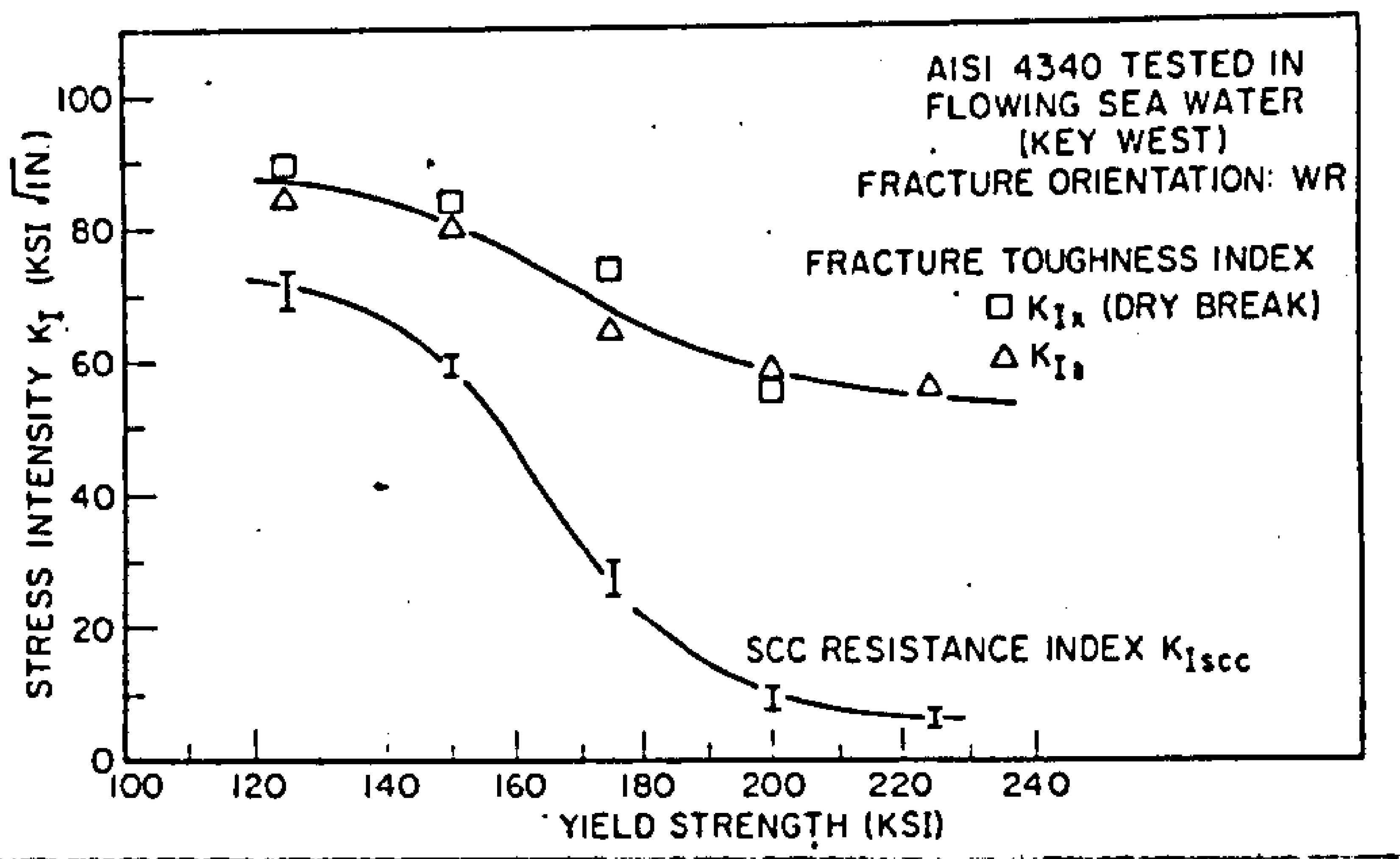

Fig. 1.4 The relationship between the fracture toughness and stress corrosion cracking index and yield strength for A.I.S.I. 4340 steel.[19]

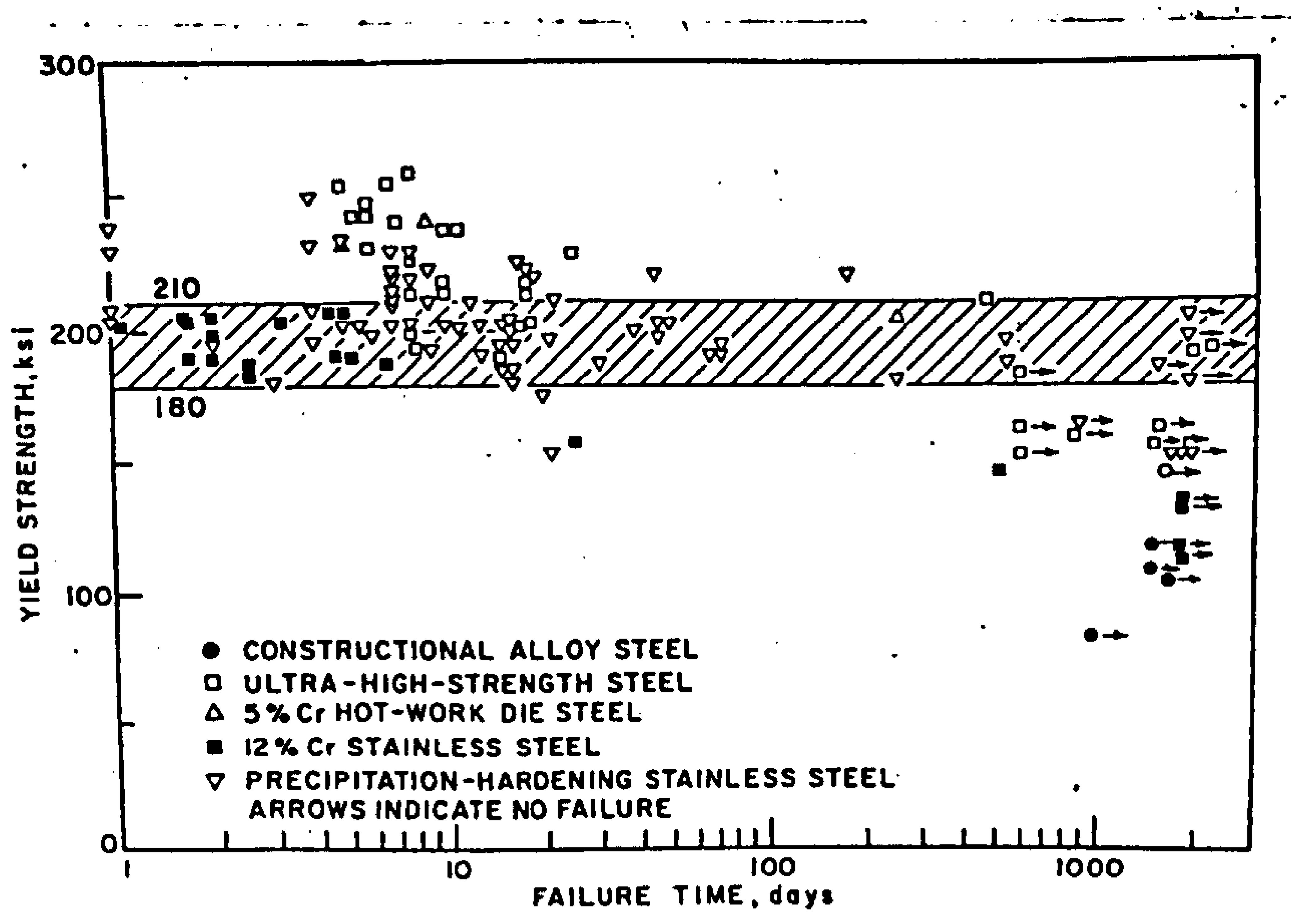

Fig. 1.5 The dependance of stress corrosion failure times of cantilever bend precracked specimens on the yield strength for several high strength steels exposed to marine atmospheres at 75% of their yield strengths.[20]

the stress corrosion cracking susceptibilities of A.I.S.I. 4340 and 14Cr - 13Co - 5Mo precipitation hardening steels respectively on aqueous chloride environments. In both cases, a decrease in the prior austenite grain size was found to increase both fracture toughness values (K_{1C}) and threshold stress intensities for stress corrosion cracking ($K_{I\ SCC}$).

ii) Maraging Steels in Particular

The influence of heat treatment on the resistance to stress corrosion cracking of maraging steels has been the subject of several investigations.

Parkins and Haney[23] investigated the influence of austenitising temperature in the range 760-1000°C on the stress corrosion cracking susceptibility of 18Ni(250) grade maraging steel. They found that in the range 800-1000°C, the influence of austenitising temperature was negligible but that material austenitised at 760°C was significantly more resistant to stress corrosion cracking. There was an insignificant change in strength level with austenitising temperature and the controlling factor appeared to be the variation in austenite grain size which increased considerably with austenitising temperature as Table 1.4, taken from their results shows.

Castagne[24] compared the influence of annealing temperatures of 850°C and 1088°C (which produced grain sizes of ASTM Nos. 10 and 1 respectively. i.e. 512 and 1 grains/in^2 respectively) On the stress corrosion cracking resistance of an 18Ni(250) maraging steel tested as smooth cantilever bend specimens in 5% NaCl solution. He found that the lower annealing temperature with its smaller grain size produced the greater resistance to cracking.

TABLE 1.4

The influence of austenitising temperature on the grain size of an 18Ni maraging steel.

AUSTENITISING TEMP.	No. of Grains/IN ^{2} at MAG×100
As received	1100
760°C	840
799°C	370
899°C	450
999°C	128

Dautovitch[16] in his review paper reports of unpublished work of a similar nature carried out on 18Ni(270) grade and 18Ni(200) grade maraging steels. He investigated the influence of austenitising temperature, in the range 760°-1210°C, on the stress corrosion cracking resistance of these steels presumably (though he does not say so) in aqueous chloride solutions. In the case of the 270 grade maraging steel austenitising temperatures of 760, 816° and 1210°C had no effect on the $K_{I\ SCC}$ values (45-50 KSI $\sqrt{IN}$) nor did hot rolling at 927°C. The crack path was found to be intergranular after the 1210°C heat treatment and transgranular after the other heat treatments. The 200 grade maraging steel, however, suffered a reduction in $K_{I\ SCC}$ from 120 KSI $\sqrt{IN}$ to 90 KSI $\sqrt{IN}$ when the austenitising temperature was increased from 816°C to 1210°C.

In summary, therefore it would appear that high annealing temperatures may cause some loss of cracking resistance in maraging steels; however, the results are by no means consistent particularly with respect to the grain size dependency of cracking resistance.

Investigations of the influence of ageing temperature on the cracking resistance of maraging steels have usually been confined to testing the material heat treated to optimum strength conditions i.e. ageing temperatures in the range 420-580°C. Consequently, only slightly over and under aged conditions have been investigated.

There is general agreement that the standard ageing temperature of 31 hours at 480°C produces better stress corrosion cracking resistance than slightly underaged heat treatments (i.e. between 425° and 450°C); however, overageing can prove beneficial but with the loss of considerable strength. Thus underageing was found to increase the crack propagation rate[24,25,26,27] and in some cases reduce $K_{I\ SCC}$[16,25] whilst overageing decreased the crack propagation rate[25,26] and slightly increased $K_{I\ SCC}$[16] at the loss of considerable strength.

Haigh[28] investigated a broader range of ageing temperatures (300-600°C) and found that the threshold stresses determined on smooth tensile specimens for ageing heat treatments of 3 hours at 400, 450 and 480°C were approximately half those for ageing treatments of 350, 530 and 600°C. Furthermore, he found a close correlation between times of failure at a given stress level for different ageing temperatures and corresponding ultimate tensile strengths. Maximum susceptibility to stress corrosion cracking corresponded almost exactly with maximum tensile strengths attained at ageing temperatures of between 400 and 500°C.

Cold work before or after ageing has been found[28,29,30] to have a beneficial effect on the stress corrosion cracking resistance of maraging steels. Copsen and Van Rooyen[29] investigated the effect of cold working before aging on the resistance to stress corrosion cracking of U-bend specimens of an 18Ni(250) grade alloy in 3.5% NaCl. A 30% reduction caused only slight improvement whilst reductions of 40 and 50% produced increasingly greater resistances to cracking. Similarly Setturlund[30] found that cold working before ageing improved the cracking resistance of smooth tensile specimens of 18Ni and 20Ni maraging steels stressed to 75% of their yield strengths in distilled water. The beneficial influence of cold working is probably a consequence of the elongation of the prior austenite grain boundaries produced by working and/or to an increase on the dislocation density of the material which, by providing more numerous sites for the nucleation of precipitate particles during subsequent ageing, produces a more uniform microstructure. Prestressing above the subsequent service load has been successfully applied to increase the air fracture stress in a number of structural materials. The resistance to fracture conferred by prestressing may be due to blunting of pre-existing crack like defects in the structure by local yielding or to residual compressive stresses at defects after prestressing.

The effect of prestressing on the stress corrosion cracking resistance has been the subject of a number of studies.[31,32,33,34] Navak[31] found that prestraining 1-5% before machining precracked specimens from the material was detrimental to HY130 steel but had no effect on a 12Ni-5Cr-3Mo maraging steel.

The effect of prestressing already precracked bars has been investigated by Carter[32,33] and Dautovitch[34]. Carter investigated the effect of prestressing precracked bars of a 200 KSI yeild strength 4340 steel and an 18Ni(300) maraging steel. He found that prestressing of the 4340 steel at stress intensities of up to 90% of K_{IC} was effective in improving the stress corrosion cracking resistance raising $K_{I\ SCC}$ from 9 to about 25 KSI $\sqrt{IN}$. Prestressing of the 18Ni 300 alloy was not as effective, however, raising $K_{I\ SCC}$ from 7.5 to about 10 KSI $\sqrt{IN}$.

Dautovitch[34] studied the effect of both room temperature and 260°C prestressing of precracked bars and 260°C prestressing of notched tensile specimens (KT = 10) on the resistance to cracking of an 18Ni(270) grade maraging steel tested in artificial sea water. Fig. 1.6 shows the results obtained by Dautovitch plotted in terms of critical stress intensity for stress corrosion cracking ($K_{I\ SCC}$) as a function of prestressing stress intensity (K_{IP}). It is apparent from Fig. 1.6 that room temperature prestressing was only effective after the prestressing stress intensity exceeded $K_{I\ SCC}$. The 260°C prestress was much more effective than the room temperature prestress, though in both cases a substantial improvement in $K_{I\ SCC}$ was effected. The improvement in $K_{I\ SCC}$ observed in the case of the 260°C prestress could not be attributed to the formation of a protective oxide film formed at these temperatures since $K_{I\ SCC}$ was determined in these tests after a slight extension of the initial crack.

The reason why prestressing improves the stress corrosion cracking resistance of specimens containing a discontinuity appears to be associated with the nature of the plastic zone formed at the tip of the discontinuity upon prestressing. Thus, the plane stress plastic zone size, b increases with applied stress intensity factor K_I according to[3]

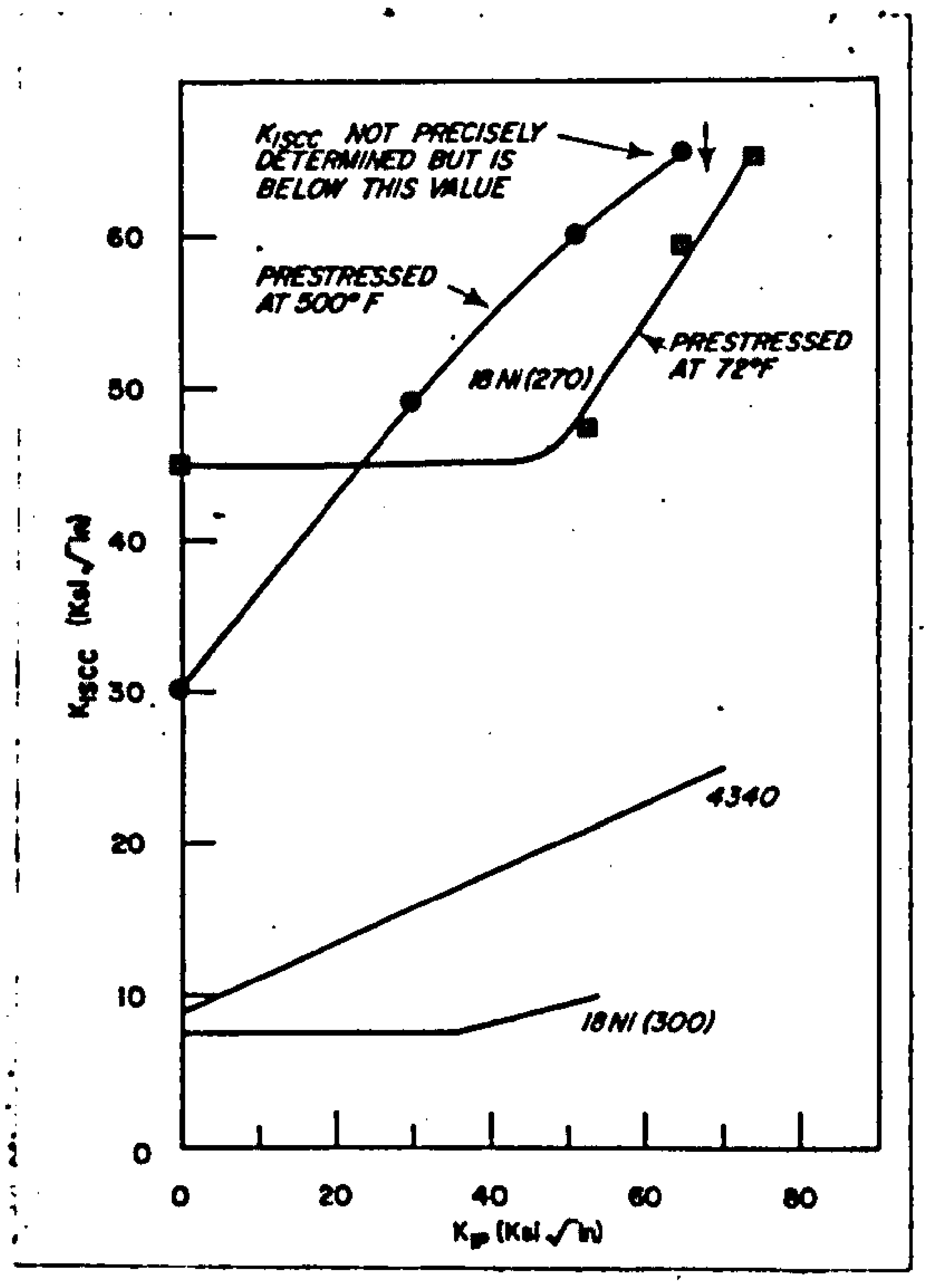

Fig. 1.6 The influence of pre-stressing on the stress corrosion cracking index of an 18 Ni (270) grade maraging steel tested in 3.5 wt % NaCl.[34]

$$b = \frac{K^2}{E\sigma y}$$

where σy = yield stress of the material,

E = Youngs modulus of elasticity.

Now for reasons which are not fully understood stress corrosion cracks are disinclined to propagate through plane stress plastic zones so that the higher the prestressing stress intensity factor the more important becomes the effects of plane stress plasticity and the cracks are unlikely to propagate. Alternatively, residual compressive stresses (the magnitude of which are proportional to K_{IP}) may be formed within the plastic zones on unloading the specimen from K_{IP} so that on reloading in the corrosive environment crack propagation can only occur when the stress level is sufficient to overcome these residual compressive stresses hence $K_{I\ SCC}$ is effectively raised.

In summary then; the results of a large number of investigations on several high strength steels strengthened by heat treatment have shown that steels with yield strengths above about 200,000 psi are susceptible to stress corrosion cracking in natural environments. Furthermore, this behaviour appears to be more dependant on yield strength than any other single factor such as alloy type structure or heat treatment, etc.

The maraging steels however have been shown[30,36,37] to exhibit longer failure times than martensitic alloy and stainless steels tested at the same strength level. Furthermore, a comparison of fatigue precracked specimen data has shown that maraging steels in general show higher $K_{I\ SCC}$ values and slower crack growth rates that many other high strength steels of similar strength. Thus, Fig. 1.7[16] shows that 18Ni maraging steels compare favourably with other high strength steels offering as good or better $K_{I\ SCC}$ values over a wide strength range. Fig. 1.8[26] shows a comparison of region II crack growth rates of 18Ni maraging steels with those for 4340, 300M, H-11, 9Ni-4Co-.45C, 9Ni-4Co-.25C and D6AC steels as a function of yield strength. Clearly, the crack growth rates of 18Ni maraging steel at the 250 ksi yield strength level were comparable with those for 9Ni-4Co-.25C and H-11 steels of yield strength 200 ksi but two orders of magnitude slower than the crack growth rates of 4340 and 300M steels also of yield strength 200 ksi.

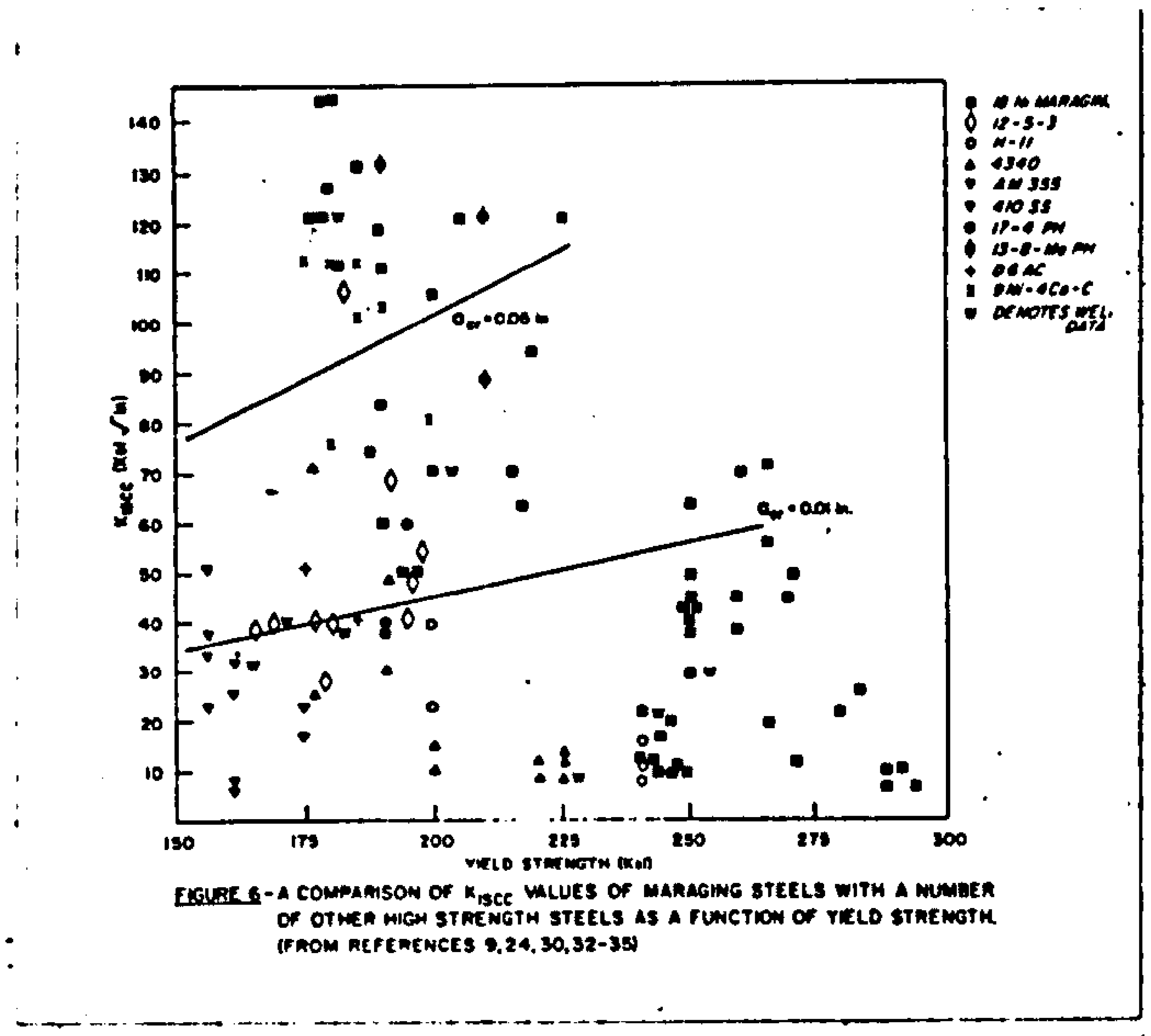

Fig. 1.7 A comparison of $K_{I\ SCC}$ values for maraging steel with a number of other high strength steels as a function of yield strength.[16]

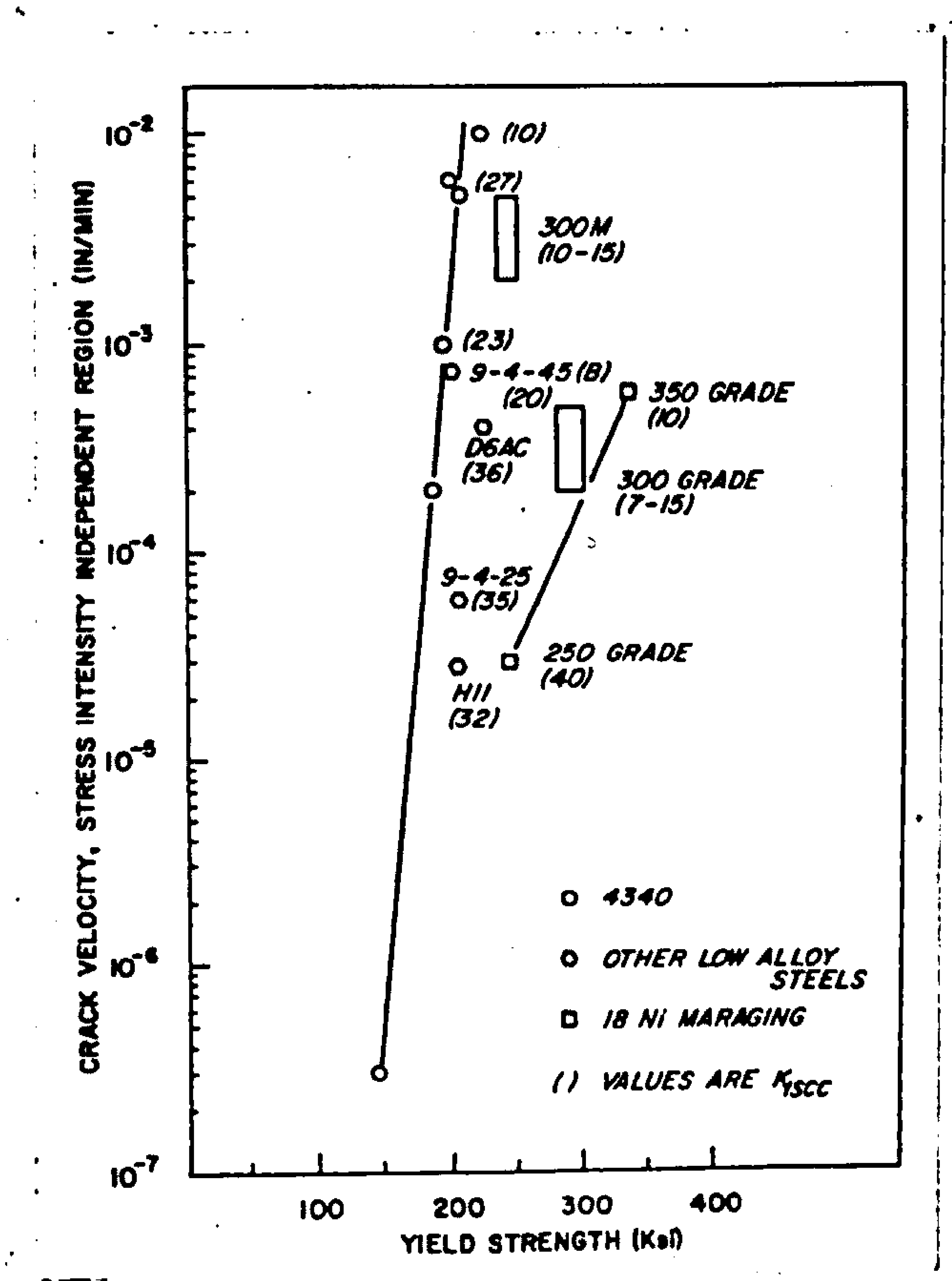

Fig. 1.8 A comparison of the stress corrosion crack velocities in the stress intensity independant region of maraging steels with those of some low alloy steels.[26]

1.3.3 The influence of environment on the stress corrosion cracking behaviour of high strength steels

a) AQUEOUS ENVIRONMENTS

(i) High Strength Steels

One of the characteristic features of the stress corrosion cracking of high strength steels is the wide variety of environments, some of which at first sight appear to be totally innocuous, in which cracking has been observed to occur.

Phelps and Mears[38] investigated the effects different anions had on the resistance to cracking of a 12Mo-V stainless steel heat treated to a high strength level. Their results are summarised in Table 1.5, which indicate that a large number of anions other than chloride cause cracking and that the anion present has a pronounced effect on cracking times.

Several other investigations[17,30,39] have been carried out in natural environments with the principle aim of selecting the most suitable alloys for a given job in a given environment and in general the results indicate that marine and simulated marine atmospheres are more aggresive than industrial atmospheres and that natural marine environments are more severe than artificial ones. Possibly the worst possible environment as far as the stress corrosion cracking of high strength steels is concerned is one containing hydrogen sulphide. Naturally, this particular aspect of stress corrosion cracking is of particular interest to the oil and gas industries since a large proportion of the crude oil and gas found in various parts of the world contains hydrogen sulphide and consequently the steels used for drilling and recovery of these

TABLE 1.5

Stress Corrosion Behaviour of VSS 12MoV Stainless in various Salt Solutions

Material tempered at 425°C to give a yield strength of 207 Ksi

Environment	Initial pH	Average Failure Time
NaF (1.0M)	7.7	22 min
NaCl (1.0M)	6.2	28 min
NaBr (1.0M)	6.7	11 min
NaI (1.0M)	8.9	6 min
NaH_2PO_4(1.0M)	3.6	6 min
Na_2HPO_4 (1.0M)	8.9	NF 620 hr
Na_3PO_4 (Sat)	12.3	60 min
Na_2SO_4(1.0M)	7.0	5 min
$NaNO_3$(1.0M)	5.7	18 hr
Na_2SO_4(1.0M)	9.4	49 hr
$NaClO_3$ (1.0M)	7.8	205 hr
$NaC_2H_3O_2$(1.0M)	8.2	520 hr
NaOH (1.0M)	12.0	NF 840 hr
$NaNO_3$(1.0M)	8.1	NF 840 hr
$NaHCO_3$ (Sat)	8.9	NF 840 hr
Na_2CO_3 (1.0M)	11.5	NF 840 hr
NaCN (1.0M)	11.8	NF 840 hr

products must have inherent resistance to cracking or else be appropriately protected. As a result, a great deal of literature[40-43] is available on the performance of different steels in sulphide containing environments.

The stress corrosion cracking of high strength steels in sulphide containing environments is regarded to be a special case of hydrogen embrittlement cracking. Several workers[44,45] have shown, for example, that hydrogen sulphide promotes hydrogen entry into the steel by poisoning the hydrogen adatom recombination reaction and thereby decreasing the S.C.C. resistance in these environments. The embrittling tendency is most pronounced in acid solutions[45] where hydrogen sulphide is thermodynamically stable and particularly so when acetic acid is also present in the solution.[46]

Bhatt and Phelps[47] investigated the effect of solution pH in the range 1-13 on the stress corrosion cracking susceptibility of a 12Mo-V stainless steel in 3% by wt sodium chloride solutions. They found that the times to failure increased and the corrosion rate decreased as the pH was increased from 3 to 11. At pH values greater than 11.0 stress corrosion cracking did not occur and the rate of corrosion was negligible. Green and Haney,[48] however, found minima in the times to failure versus pH curves of tensile foil specimens of 4340, H-11 and maraging steels at a pH of between 11.0 and 12.0. The minimum was observed to be more pronounced for the maraging steel.

An interesting feature of the stress corrosion cracking of high strength steels is the fact that many environments which under most circumstances would be considered to be fairly innocuous have been found to induce cracking or slow crack propagation in the high strength steels when the latter are heat treated to very high yield strength levels.

Thus, Steigerwald[49] investigated the stress corrosion cracking susceptibility of fatigue precracked tensile specimens of 300M steel, heat treated to a yield strength of 245 ksi, in various liquid environments, The specimens were stressed to 75 ksi or 84% of the strength obtained in the absence of a liquid environment. His results are shown in Table 1.6 and indicate that even apparently innocuous environments such as lubricating oil and acetone can induce slow crack propagation in this steel although the failure times in these environments were always longer than in aqueous environments. Similarly, fatigue precracked tensile specimens of a 12% Cr stainless steel tested in the martensitic condition have recently been observed[50] to show slow crack propagation in organically based crack detecting fluids.

Steels heat treated to high yield strengths have also been observed to exhibit slow crack growth in gaseous environments containing various amounts of water vapour as well as in distilled water. Hanna,[51] et al found that air with a dew point of 35^{o}F and moist argon with a dew point of 45^{o}F were as effective in promoting crack propagation of precracked tensile specimens of 4340 steel of yield strength 214 ksi as was exposure to distilled water. The critical dew point to initiate failure in moist argon was estimated to be -5^{o}F corresponding to moisture content of only 1 grain per cubic foot of gas. The authors attributed cracking to embrittlement by hydrogen absorbed as a result of corrosion processes occurring on the specimen surface.

In work of a similar nature, Johnson and Willner[52]

TABLE 1.6

Influence of Various Environments
on Failure Time of 300M Steel

Material tempered at 315 °C to give a yield strength of 245 KSI

Environment	Failure Time (MIN)
Recording Ink	0.5
Distilled Water	6.5
Amyl Alcohol	35.8
Butyl Alcohol	28.0
Butyl Acetate	18.0
Acetone	120
Lubricating Oil	150
Benzene	2247
CCl_4	N.F. 1280
Air	N.F. 6000

found that the stress intensity for crack initiation in precracked specimens of H-11 steel (Y.S. 230 KSI) decreased from the air fracture value (40 KSI$\sqrt{IN}$) at 0.1% R.H 80^{o}F to half that value at 100% R.H 80^{o}F. For relative humidities in excess of 60%, crack initiation and growth characteristics were identical to those in distilled water. The authors suggested that at such high humidities water vapour condenses at the crack tip. At lower relative humidities cracking was attributed to a lowering of surface energy by adsorption.

(ii) Maraging Steels in Particular

In general those environments found to cause cracking in the other high strength steels, and the respective differences in severity observed between them, are also found to produce stress corrosion cracking of maraging steels and wth similar differences in their severity. Thus, as was found to be the case for other high strength steels, Kenyon,[53] et al and Leckie and Loginow[54] both found that natural sea water tended to be more severe than 3.5% sodium chloride solution with the proviso that, as has already been seen, crack velocities of maraging steel were generally lower and $K_{I\ SCC}$ values higher than other high strength steels heat treated to the same yield strength.

The effects of pH and chloride ion concentration on the cracking resistance of maraging steels have been investigated using both smooth[28,55] and precracked specimens.[27,56-59] In smooth specimen tests pH and chloride ion concentration have both been found to influence cracking times. Green and Haney[55] working with .002" thick foil tensile specimens of an 18Ni maraging steel found that a reduction in chloride ion concentration increased the resistance to stress corrosion cracking. pH changes in the range 9 to 13 produced a prounced minimum in the time to failure, the position of which varied as the chloride ion concentration was changed (in general to higher pH's as Cl^- concentration was increased). Leckie[59] observed a similar minimum in the time to failure of precracked specimens of a 12Ni-5Cr-3Mo maraging steel at a pH of 12.

Stavros and Paxton,[27] however, found no systematic effect of pH changes in the range 0.5 to 11 on the $K_{I\ SCC}$ values or cracking times of precracked specimens of an 18Ni (300) grade maraging steel tested in a 3% (by weight) sodium chloride solution. Furthermore they found no differences in $K_{I\ SCC}$ values or crack growth rates between tests carried out in 3% NaCl or distilled water. Freedman[56] observed no effect on $K_{I\ SCC}$ data of tests carried out in 20% NaCl solutions as compared to marine atmospheres, whilst Carter[58] and Mostovy et al[57] found no consistent effect of chloride ion concentration on crack growth rates in 9Ni-4Co-0.45C, 9Ni-4Co-.25C, H-11 and 300M steels.

It would appear therefore that pH and Cl^- ion concentration have a definite effect on the cracking resistance of smooth tensile specimens where pre-existing cracks are absent and this probably reflects the influence of these variables on the crack initiation through their effects on pitting chracteristics.

Finally, as was found to be the case in other high strength steels, the stress corrosion cracking susceptibility of maraging steels tested at high stress levels in saline solutions saturated with hydrogen sulphide (pH5·0) is described as large.

b <u>GASEOUS HYDROGEN ENVIRONMENTS</u>

(i) <u>High Strength Steels in General</u>

Although previous studies had indicated that high strength steels were susceptible to cracking in high pressures of hydrogen gas it was only in 1966 that Johnson and Hancock[61] demonstrated that atmospheric pressures of hydrogen could induce embrittlement of high strength steel (actually H-11 steel heat treated to a yield strength of 230 ksi). Their results on precracked tensile specimens of H-11 steel indicated that crack velocities in one atmosphere of hydrogen were greater than in water or moist argon environments. The addition of 0.7 volume % of oxygen terminated crack growth in dry hydrogen gas or humid argon environments.

Similar behaviour to the latter has been observed by other workers. Thus Sawicki[62] reports 0.4 volume % O_2 prevented cracking in gaseous hydrogen environments at temperatures between -28 and 100°C. McIntyre (et al)[63] found 1% O_2 was sufficient to stop crack growth in dry hydrogen gas whilst Kerno[64] suggests that the oxygen level is more significant than the oxygen/hydrogen ratio. This inhibiting effect of oxygen is probably related to its preferential adsorption at the crack tip thus providing a barrier to the adsorption of the embrittling hydrogen species.

The pressure dependance of crack growth in hydrogen gas has been reported[62-64] as ranging from $pH_2^{\frac{1}{2}}$ to pH_2^{2} depending upon temperature[62] and applied stress intensity.[64] Sawicki reports that at 27 and 47°C H-11 steel shows a pH_2^{1} dependance of crack velocity but at 80°C a $pH_2^{3/2}$ dependence was observed whereas McIntyre observed a $pH_2^{\frac{1}{2}}$ dependence of crack velocity for high strength 835M30 steel in sub-atmosphere pressures of hydrogen gas at ambient temperatures.

(ii) Maraging Steels in Particular

The cracking behavior of maraging steels in gaseous hydrogen has been the subject of several recent investigations. Thus, Walter (et al)[65] noted a severe loss in ductility in 18Ni(250) grade smooth tensile specimens in 10 ksi of hydrogen gas. Hudak and Wei[66] have shown that the activation energies for crack growth and crack growth rates in the temperature range $-60^{o}C$ to $+23^{o}C$ for an 18Ni(250) grade steel agreed quite well with those found in similar tests on a 4130 steel by Williams and Nelson.[67] This agreement suggests that composition and structural differences between maraging and high strength low alloy steels play a minor role in influencing cracking behaviour of high strength steels in gaseous hydrogen which, in turn, implies that it is reactions at the specimen surface rather than within the alloy that control the cracking behaviour of high strength steels in these environments.

Oriani and Josephic[68] have investigated the hydrogen gas pressures required to start and stop slow crack growth in fatigue precracked 18Ni (250) grade maraging steel specimens. Hydrogen gas pressures as low as 10-20 cm of mercury were found to be sufficient to induce slow crack growth; the pressure required decreasing slowing with increasing stress intensity. Arrested cracks generally required about a 30% increase in hydrogen pressure to restart them, which was attributed to preferential adsorption of impurities, probably oxygen, at the crack tip providing a barrier to the adsorption of hydrogen.

More significantly, however, it was observed that an increase or decrease of hydrogen pressure of about 4 TORR produced a noticeable change in crack velocity within a fraction of a second which implies that the distance over which the hydrogen atoms must diffuse to affect embrittlement is small and of the order of a few atomic diameters from the surface of the crack tip.

The influence of hydrogen precharging on the cracking susceptibility of maraging and other high strength steels has been the subject of a number of studies.[69-73] These studies, in general have shown that whilst maraging steels are subject to embrittlement, the degree of embrittlement is much less than that observed in other high strength steels. For example, Gray and Troiano[70] found that under conditions of either equal charging times or equal hydrogen contents the degree of embrittlement (as indicated by % RIA) in tensile tests was much less for an 18Ni(200) grade maraging steel than for a 4340 steel quenched and tempered to a similar strength level.

More recently Dautovitch and Floreen[72] measured the critical stress intensities required to produce slow crack growth in hydrogen precharged fracture toughness samples of 18Ni(250), (270) and (290) grades of maraging steel and quenched and tempered 300M steel. Their results shown in Fig. 1.9 demonstrate that the 3 grades of maraging steel display a significantly greater resistance to hydrogen embrittlement than the quenched and tempered 300M steel.

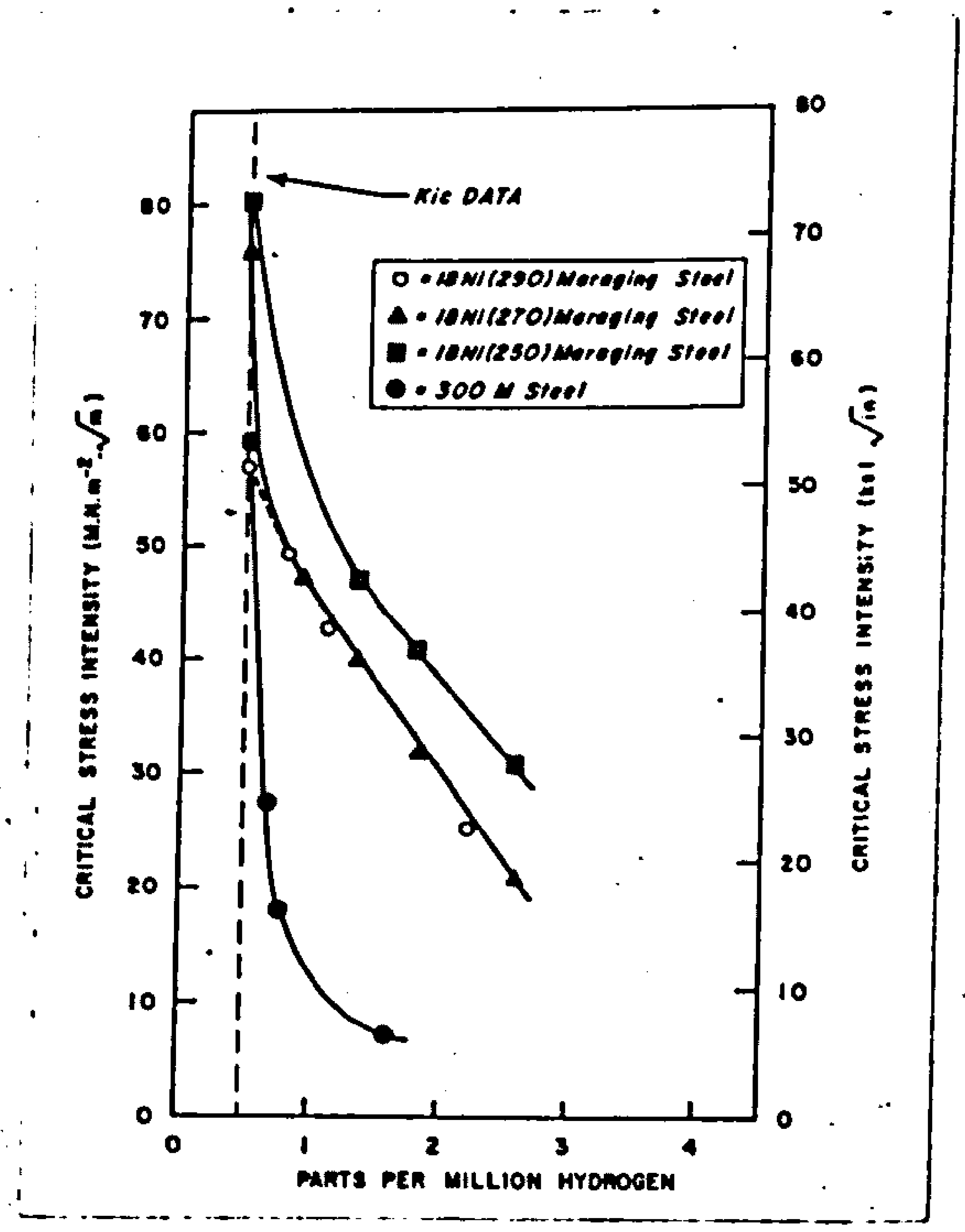

Fig. 1.9 The relationship between the critical stress intensity for cracking and the average hydrogen concentration for hydrogen precharged maraging steels and quenched and tempered 300M steel.[72]

The greater resistance to hydrogen embrittlement of the maraging steels compared with high strength low alloy steels may be associated with the fine scale dislocation and precipitate microstructure of the former e.g. in view of the significant hydrogen-dislocation interaction energies observed in the iron base alloys it is likely that dislocations and precipitate interfaces would act as effective traps for absorbed hydrogen in maraging steels. If such sites are innocuous with respect to the cracking processes then the concentration of hydrogen available to produce cracking would be reduced. The results of Dautovitch and Floreen,[72] for example, would appear to confirm this hypothesis. At a stress intensity of 30 KSI$\sqrt{IN}$ (Fig. 1.9) the 300M steel would start to crack when the average hydrogen concentration has reached approximately 0.7 ppm whereas at this stress intensity 2.7 ppm of hydrogen would be required to cause crack growth in the 18Ni(250) grade maraging steel. Furthermore, measurements of the diffusion coefficient of hydrogen in maraging steel have shown[74,75] that the values of between 10^{-8} and 10^{-9} cm^2 s^{-1} observed are 3 to 4 orders of magnitude lower than those of hydrogen in iron or mild steel.[76] The much higher density of trapping sites in the microstructure of the maraging steels is considered to be the reason for the abnormally low diffusion coefficients observed in these steels.

In summary, therefore, a combination of the lower rate of hydrogen diffusion and the higher concentration of hydrogen needed to induce cracking (both as a result of the higher density of trapping sites for hydrogen compared with other steels) is probably responsible for the lower crack growth rates and higher critical stress intensities for stress corrosion cracking observed for maraging steels compared with other high strength steels subjected to the same hydrogen embrittling environments.

1.3.4 <u>Microstructural aspects of SCC in the high strength steels - the crack path</u>

(i) <u>High Strength Steels in General</u>

The crack path in high strength steels has been observed to be either intergranular or transgranular with respect to the prior austenite grain boundaries depending upon microstructure, environment and the level of applied stress.

Most investigations[38,41,46,77] have found that the crack path in hydrogen sulphide saturated environments is transgranular with respect to the prior austenite grain boundaries.

However, intergranular cracking in hydrogen containing environments has also been observed. Thus, Prange[78] observed intergranular cracking in a 9% Ni tube steel which had failed in a sour condensate well. In gaseous hydrogen environments and environments not containing hydrogen sulphide, however, intergranular stress corrosion cracking is the rule rather than the exception. Phelps and Loginow,[17] Davis,[18,79] and Dean and Copson[36] all report predominantly intergranular cracking in their investigations on several high strength steels.

Lillys and Nehrenberg[80] studied the microstructural factors influencing the SCC of several martensitic stainless steels exposed at the free corrosion potential in 5% NaCl solution and also as cathodes in a cell containing .1N H_2SO_4 plus 3mg of arsenic/litre as electrolyte. The former was chosen to be representative of a true stress corrosion system whereas the latter was considered to be representative of hydrogen embrittlement. It was observed that SCC was minimised when 5-10% delta ferrite was present in the structure; the cracks being deflected around the ferrite phase and so interfering with crack propagation. Exclusively intergranular cracking was only observed after tempering at 510°C for specimens subjected to 'stress corrosion conditions' and after tempering at 538°C for specimens exposed to 'hydrogen embrittle -ment conditions' despite the fact that precipitates could be detected in grain boundaries after tempering at 454°C.

Trozzo and McCartney[81] using electron microscopy and diffraction techniques investigated three heats of AISI410 stainless steel exhibiting degrees of susceptibility to stress corrosion cracking in a high temperature water environments. It was found that in two heats which were susceptible to intergranular cracking, a continuous constituent was observed in the prior austenite grain boundaries after quenching. This constituent was later found to consist of enriched austenite and martensite. Tempering at 345^{o}C resulted in the retained austenite transforming to martensite, so creating a brittle grain boundary network of untempered martensite which thereby provided an easy path for intergranular crack propagation.

The influence of microstructure on the nature of the microscopic crack paths observed in the stress corrosion cracking of the high strength steels can be most easily rationalised on the basis of the presence or otherwise of grain boundary precipitates located at the prior austenite grain boundaries. Thus, if an active path dissolution cracking mechanism is considered to be operative then the grain boundary precipitate may have sufficiently different electrochemical characteristics from the surrounding alloy matrix to either be preferentially anodically dissolved or by acting as a particularly efficient cathode the matrix material immediately adjacent to the ppte may be preferentially dissolved. In either case, the net result is the same (i.e. cracking). Alternatively, if the cracking mechanism operative is considered to be hydrogen embrittlement then the precipitate interface may be a preferential site for the location of absorbed hydrogen atoms which lower the cohesive forces[82] between atoms of precipitate and matrix.

The macroscopic details of crack propagation are also of interest. Thus cracks can propagate either as a single crack in the plane of the precrack or as branched cracks inclined to the plane of the precrack. The different crack morphologies have been referred to as Types 1 and 2 respectively.[83] Attempts have been made to quantify the conditions under which crack branching will occur.

In general crack branching is observed in Region II (Fig. 1.10) for slow crack growth in aqueous environments i.e. where crack velocity is independent of stress intensity. In Fig. 1.10 in region I, which maybe absent in some materials, crack velocity is strongly dependant upon stress intensity. In region II, crack velocity is independent of stress intensity; the constant crack velocity in this region is thought[58] to be a consequence of a limiting mass transport or diffusion controlled mechanism operating. In region III, where crack velocity is again strongly dependent upon stress intensity, mechanical failure is regarded[58,84,85] to be playing an increasingly important role in crack propagation. Speidel,[86] for example, has observed crack branching in an AFC 77 quenched and tempered high strength steel tested in distilled water as the results in Fig. 1.11 show. Crack microbranching with branch separations of the order of one grain diameter was observed at stress intensities 1.4 times the $K_{I\,SCC}$ value (or greater). Macro-branching was only observed at stress intensities 1.4 times the minimum K value observed in region II (i.e. K_I^* in Fig. 1.10). Carter,[87] however, observed crack macrobranching in high strength steels to occur at a value of stress intensity $K_{BT} = n\, K_{I\,SCC}$ where n varies from 2 to 4. Another important requirement that must be satisfied before macrobranching is observed is that the velocity of the branched cracks must not be significantly less than the velocity of the main crack from which they grow otherwise the main crack may continue to grow to the point where the branched cracks are unloaded.

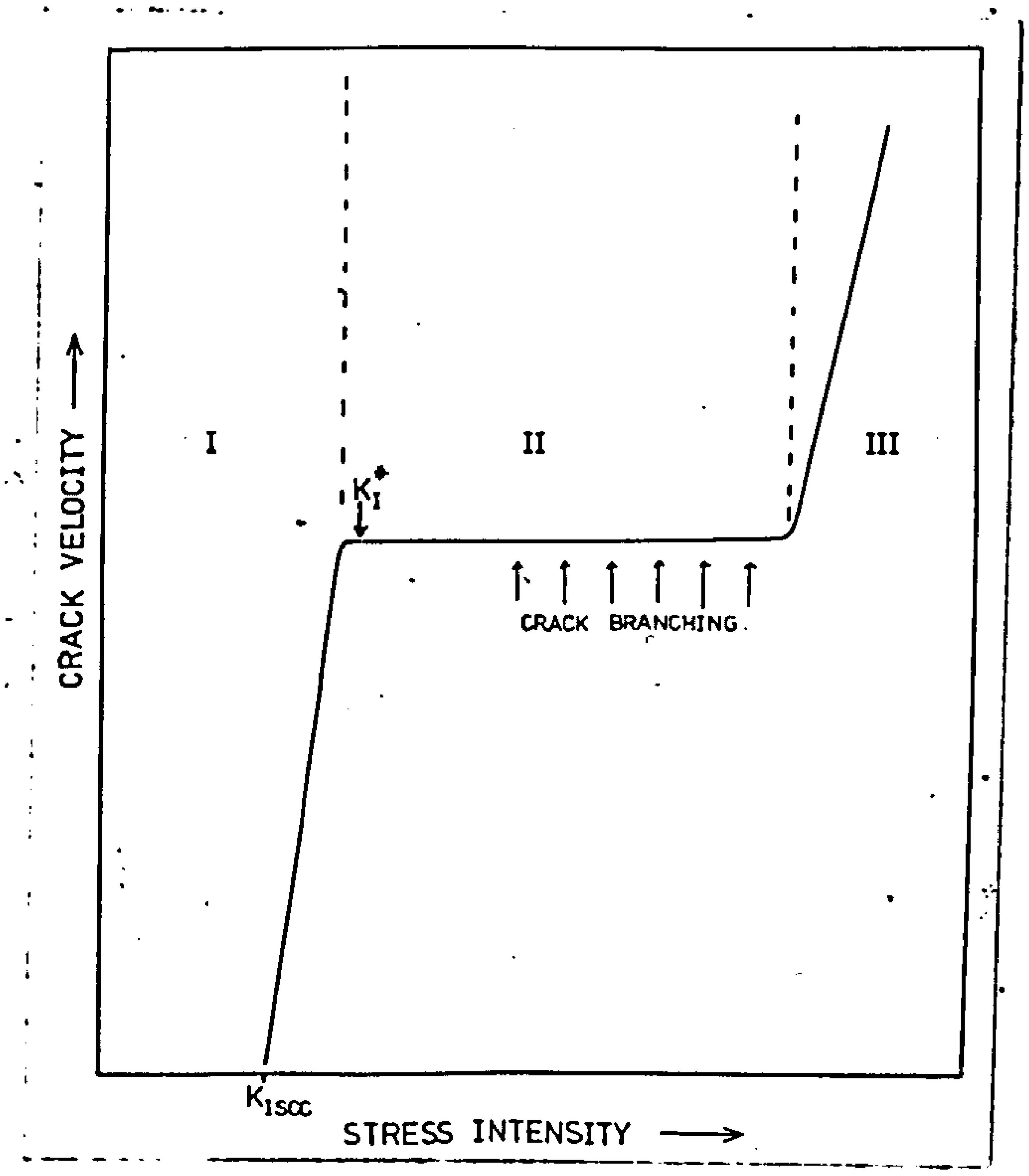

Fig. 1.10 The schematic relationship between crack growth rate and stress intensity factor during stress corrosion cracking of a typical steel.

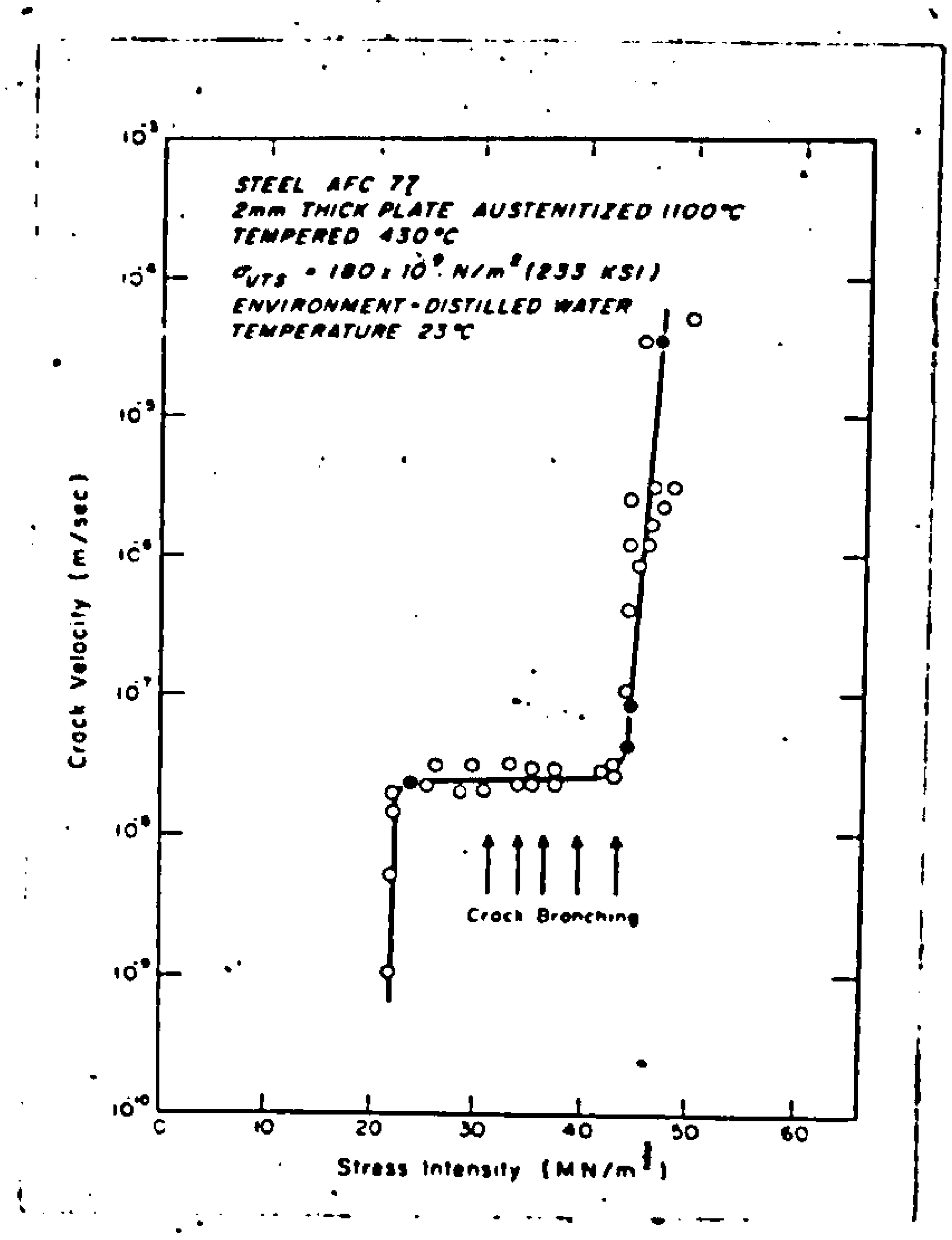

Fig. 1.11 The dependance of crack growth rate on stress intensity factor for AFC quenched and tempered high strength steel tested in distilled water.[86]

(ii) Maraging Steels in Particular

Stress corrosion crack paths in maraging steels are generally intergranular[23,25,27,36] along prior austenite grain boundaries though transgranular cracking has been reported.[16] Ti_2S or TiC(N) precipitates which have been observed[16,23] at prior austenite grain boundaries may provide a favourable path for cracking in a manner as outlined above. Where transgranular cracking has been observed the martensite platelet boundaries have been suggested as being preferential sites for attack.[16,88]

Fracture paths observed in hydrogen precharged maraging steels are usually intergranular or transgranular quasi-cleavage type fractures or mixtures of both. Tritium autoradiography[89,90,91] or the formation of neodynium surface films[92] that form hydrides have been used to demonstrate that the hydrogen tends to accumulate at the prior austenite grain boundaries and along martensite platelet boundaries. The quasi-cleavage fracture mode observed on some fracture surfaces of hydrogen charged maraging steel specimens may thus be indicative of fracture along the martensite platelet boundaries.

As was observed to be the case in the other high strength steels, cracks in maraging steels have been observed to propagate either as a single crack in the plane of the precrack or as branched cracks inclined to the plane of the precrack and the requirements for macrobranching appear to be identical to those for other high strength steels.[87]

An explanation of the crack branching phenomenon in high strength steels has been given by Clark and Irwin[93] and Syrett and Trudeau.[94]

They point out that the stress distribution around the tip of a propagating crack is such that extensional stresses along planes inclined at 60^{o} to the precrack is greater than along the plane of the precrack. These planes are referred to as 'zero isoclinics' by Syrett and Trudeau since they are characterised by zero shear and separation may occur along these planes purely in the direction of loading.

1.3.5 The influence of stress on the S.C.C. behaviour of high strength steels

In general the effect of increasing the stress level in stress corrosion tests on smooth specimens of any metal in any environment is to shorten the cracking times. Furthermore, for many metal-environment systems a distinct threshold stress is observed below which cracking does not occur in the maximum time allowed for the test e.g. Phelps and Loginow[17] showed that for a number of high strength steels exposed to a marine environment the failure times generally decreased as the stress level was increased and a threshold stress of between 50 and 75% of the yield strength was observed for some of the steels.

The above refers to tests carried out on smooth tensile specimens and it is as well to point out at this stage that stress corrosion data from different sources may be obtained using widely different specimen types and employing significantly different loading modes. As such, caution should be observed at all times in comparing data from different laboratories. An example of the effect that various modes of loading can have on failure times of a given material in a given environment; is given in a recent paper by Hayden and

Floreen.[95] They investigated the effect of various modes of loading on the failure times of an 18Ni maraging steel in 3.5 wt % NaCl solution. In order of increasing severity the loading modes investigated were shear loading by torsion no failures, plane stress bending (approximated by U-bend or thin bent beam specimens), tensile loading of smooth specimens, and fatigue precracked plane strain bending. It was observed that the threshold stress increased from ~40 to 275 ksi as the loading was changed from the most severe to the least severe case (Fig. 1.12).

Notwithstanding, the necessity for caution in comparing data from different sources, the results of many investigations suggests that in general, the maraging steels show superior threshold stresses, higher threshold stress intensities and longer times to failure than other high strength steels heat treated to the same or similar strength levels.

1.3.6 The influence of Electrochemical Polarization

The influence of applied electrochemical polarization and in particular the influence of applied current, on the stress corrosion cracking susceptibility of high strength steels has been used to provide information enabling a distinction to be made between anodic dissolution and hydrogen embrittlement as the cracking mechanism operating at the free corrosion potential in a given environment. As such, the influence of electrochemical polarization will be discussed fully in the following section.

1.4 The Mechanism of Stress Corrosion Cracking

The mechanism of stress corrosion cracking of high strength steels in aqueous environments has been the subject of much controversial debate in recent years and it is fair to say that most systems of metal and environment that exhibit stress corrosion cracking have at one time or another been explained in terms of a hydrogen embrittlement mechanism. The evidence adduced in favour of a hydrogen embrittlement mechanism is often based on such factors as the observation of hydrogen bubbles emanating from cracks, fractrographic evidence suggesting a quasi-cleavage crack propagation process, the demonstration of the presence of hydrogen in the metal or to measurements indicating that conditions are favourable for hydrogen discharge.

Evidence of an indirect nature which has been cited as evidence of a hydrogen embrittlement cracking mechanism concerns the change in cracking response to various modes of loading. Hayden and Floreen[95] suggest that the variation in failure times with the state of stress they observed in an 18Ni maraging steel could not be explained on the basis of an active path corrosion mechanism and was more consistent with an explanation of cracking via hydrogen embrittlement. Fig. 1.12 taken from their paper, indicates that the severity of stress corrosion cracking of unnotched samples decreased in the sequence plane strain bending - tension - plane stress bending. The significant difference in the apparent threshold stresses between fatigue precracked plane strain bending and essentially smooth plane strain bending samples can be readily explained in terms of electro-

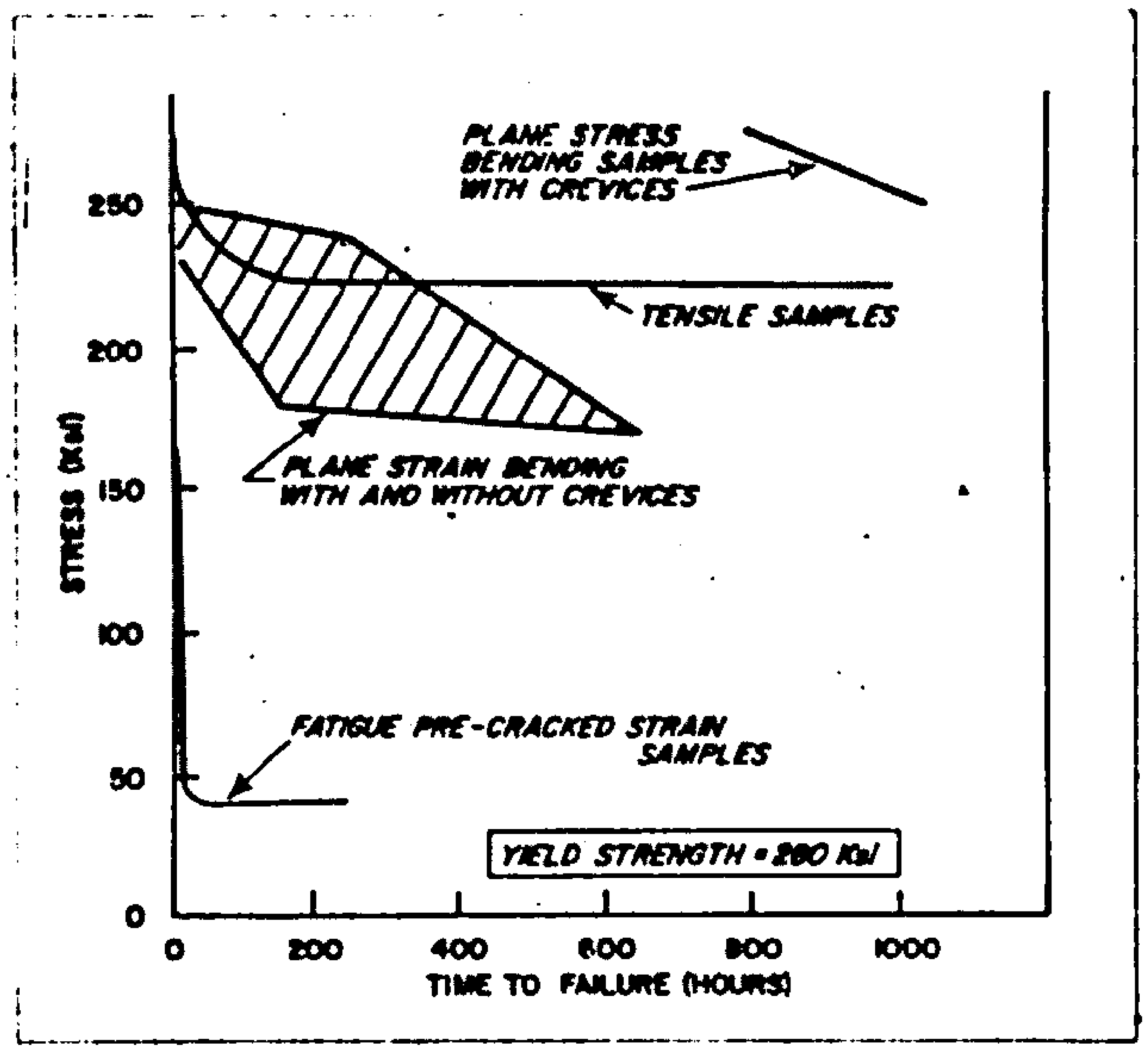

Fig. 1.12 The influence of specimen type on the resistance to stress corrosion cracking of an 18Ni (280) grade maraging steel corroded in 3.5 wt % NaCl.[95]

chemical changes taking place more readily in the former case within the confines of the precrack than in the latter case. Although electrochemical changes result in potential and pH changes such that conditions become conducive to hydrogen discharge within the cracks it should be recognised that a reduction in pH can also result in enhanced metal dissolution so that enhanced cracking in such circumstances is just as likely to be a consequence of enhanced metal dissolution as it is to hydrogen absorption. Alternatively the explanation may lie in the greater amount of plastic deformation that is produced at the tip of a sharp fatigue precrack as compared with that produced at the tip of a relatively blunt machined starter notch.

The differences between the results of plane strain and plane stress bending are a little more difficult to explain. One possible explanation has already been mentioned, i.e. the fact that stress corrosion cracks, for reasons that are not fully understood, are disinclined to propagate through regions of plane stress. Another explanation, not totally unconnected, may be associated with the differences in specimen size necessitated by plane strain bending and plane stress bending. Thus, by definition, plane stress specimens (for a given material) are considerably thinner than plane strain specimens and if one assumes that the probability of cracking is reduced as the exposed area is reduced[96] then one might anticipate that at a given stress level the plane stress specimen would exhibit a correspondingly greater time to failure than the plane strain specimen.

One of the earliest techniques[97] used to distinguish between an active path corrosion and hydrogen embrittlement mechanism operating under freely corroding conditions is based upon the influence of applied anodic and cathodic currents (or potentials) upon the times to failure of specimens tested in the environments under consideration. Bhatt and Phelps[98] have described in detail the different types of curves which could be obtained using this electrochemical polarisation technique. These curves are reproduced in Fig. 1.13.

In Fig. 1.13(A) it is suggested that since the time to failure are decreased by the application of small cathodic currents and increased by the application of anodic currents, the cracking mechanism at the free corrosion potential is one involving hydrogen embrittlement. In Fig.

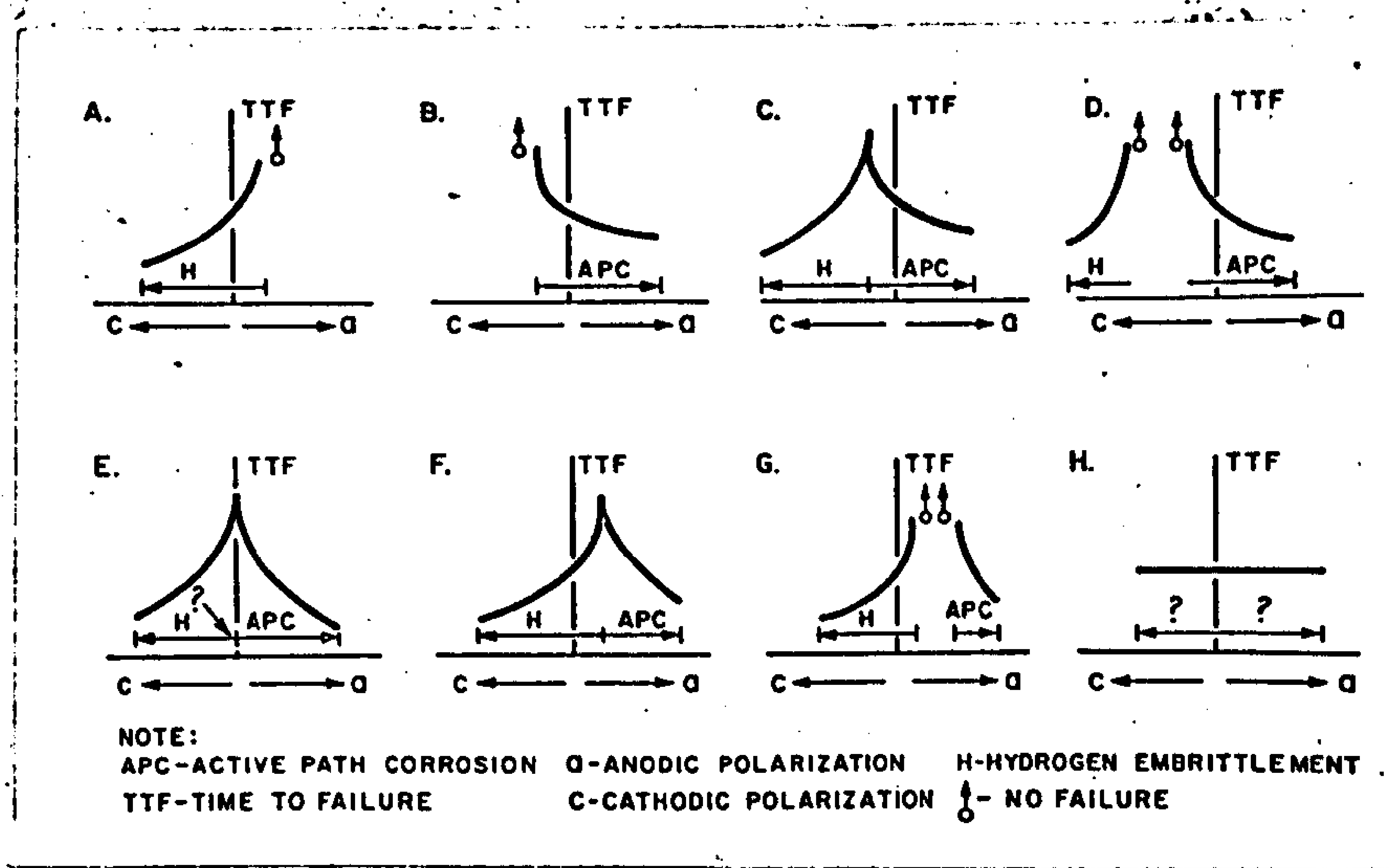

Fig. 1.13 The several possible effects of anodic and cathodic polarisation on the failure times of high strength steels.[98]

1.13(B), since the times to failure are increased by the application of small cathodic currents - a situation presumed to result in an increase in the rate of proton discharge - the cracking mechanism at the free corrosion potential is assumed to involve anodic dissolution. Figs. 1.13(C), (D), (F) and (G) represent different combinations of the above described cases in which the cracking mechanisms at the free corrosion potential are said to be active path corrosion and hydrogen embrittlement respectively. Where both anodic and cathodic polarization shortens the cracking times, as in curve (E) it is not possible to determine the cracking mechanism operating at the free corrosion potential by this method. In the case of a curve such as (H) neither anodic or cathodic polarization influence the cracking time and it has been suggested that a possible explanation is that a hydrogen embrittlement mechanism is operating but that the mechanism by which hydrogen enters the steel is not electrochemical.

Several investigations[17,19,47,98,99,100-103] have been carried out in which the polarization technique was employed to try to determine the cracking mechanism at the free corrosion potential of several different steels in different environments. Brown[101] working with heat treated AISI 410 stainless steel found that in aqueous chloride environments times to failure were shortened by the application of anodic currents and greatly lengthened by the application of small cathodic currents; behaviour characteristic of an active path corrosion mechanism operating at the free corrosion potential i.e. Type (C). In aqueous solutions containing 0.5% acetic acid + 0.1% NH_4S however, small cathodic currents decreased fracture times whereas anodic currents greatly increased failure times. Brown was led to the conclusion that in this environment A1S1 410 stainless steel cracked via a hydrogen embrittlement process at the free corrosion potential i.e. Type (A).

Bhatt and Phelps[47] found that in polarization tests on a high strength 12% Cr stainless steel containing Mo and V (12 MoV stainless) in aqueous chloride environments, the mechanism of cracking at the free corrosion potential was dependant upon the initial pH of the solution. In neutral solutions the failure times were shortened by anodic currents.

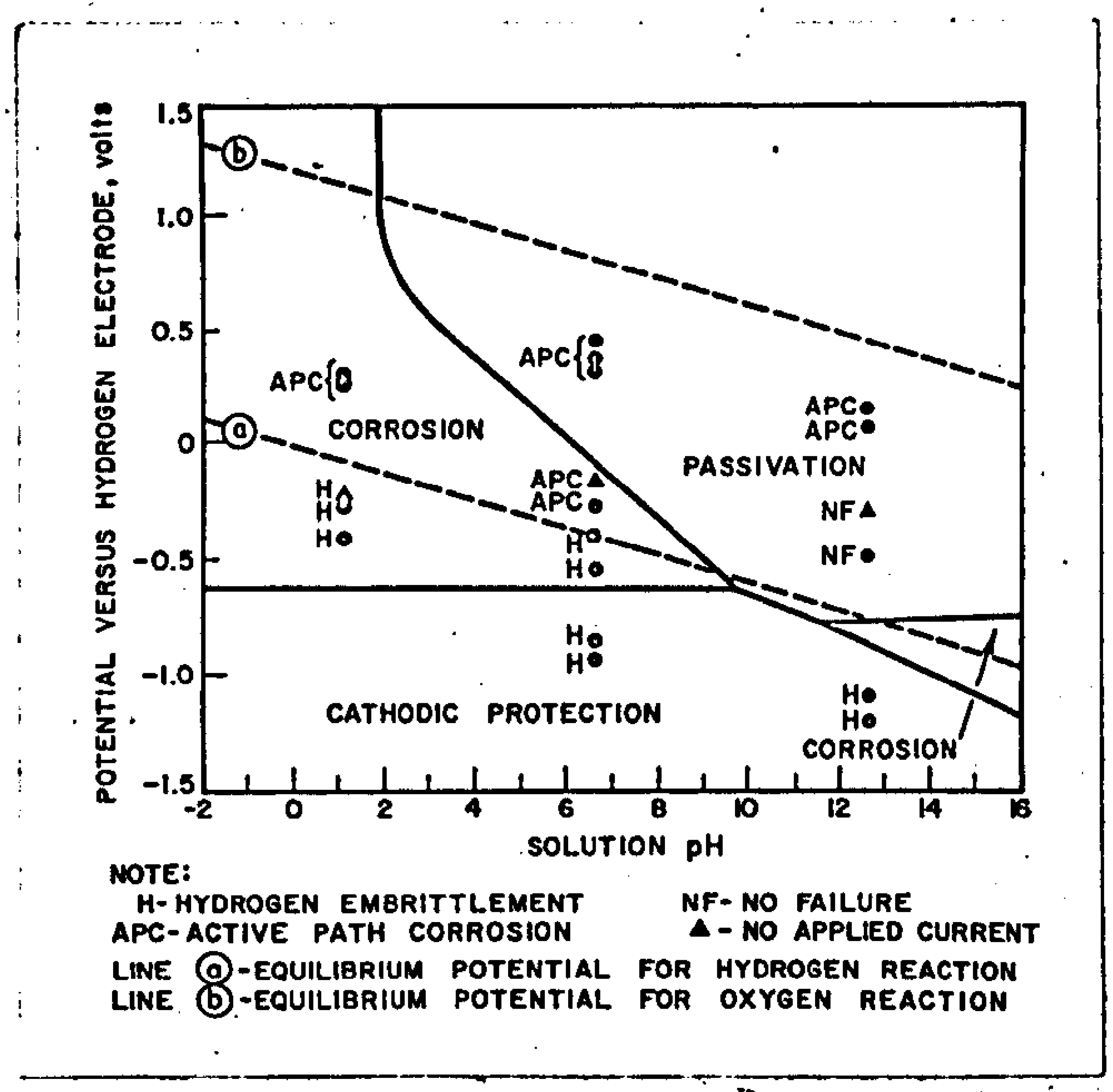

Fig. 1.14 The equilibrium pH - potential diagram for iron showing the stress corrosion results obtained in a 12% Cr stainless steel in 3% NaCl solution.[47]

and lengthened by small cathodic currents indicative of an active path dissolution mechanism operating at the free corrosion potential. In a solution acidified to pH 1 both anodic and cathodic polarization shortened the failure time with respect to the failure time observed at the free corrosion potential. Consequently, the mechanism of cracking at the free corrosion potential could not be deduced from the polarization data but other evidence suggested it to be hydrogen embrittlement. In a solution of pH 12.5 no cracking was observed under freely corroding conditions which was attributed to the onset of passivity. Their results could be interpreted in terms of the potential - pH diagram for iron. Fig. 1.14; it being noteworthy that the cracking mechanism was diagnosed to be hydrogen embrittlement for experiments in which the potential was equal to or more active than the reversible hydrogen potential and active path corrosion for all experiments in which the potential was noble to the reversible hydrogen potential. The above observations were supported by hydrogen permeation experiments in which it was observed that hydrogen permeated the steel only in conditions diagnosed to be hydrogen embrittlement in electrochemical polarization tests.

Parkins and Haney [23] found a relationship of the type illustrated in Fig. 1.13(c) in smooth tensile tests performed on an 18Ni maraging steel in acidified 3.5 wt % sodium chloride solution which, in view of the above, implies that the cracking mechanism operating on freely corroded maraging steel in this environment is active path corrosion.

The arguments concerning the use of the polarisation technique to distinguish between active path corrosion and hydrogen embrittlement cracking mechanisms at the free corrosion potential, of necessity assume that the electrochemical conditions within a growing crack, once initiated, are identical to the bulk surface conditions at all times. However it has long been postulated by a number of corrosion scientists[104-106] that electrochemical conditions within a stress corrosion crack, initiating pit, crevice or precrack may be significantly different from those in bulk solution, particularly with respect to solution pH. In the last decade Brown[107] et al claim to have ended the speculation by measuring the pH and potential in the crack tip region of a propagating stress corrosion crack in a heat treated low alloy high strength steel (AlSl 4340). Their measurements indicated that at the crack tip; irrespective of conditions in the bulk solution, conditions were always conducive to hydrogen absorption. This was true even when the bulk surface of the specimen was anodically polarized (see Fig. 1.15). The above evidence is confirmed to some extent by the observations of Brown[107] and Leckie and Loginow,[54] who both reported hydrogen gas escaping from precracking cantilever specimens corroding in sodium chloride solution.

Clearly such evidence lends strong support to a hydrogen embrittlement cracking mechanism but two points are worthy of mention in this context. In the first place to show that hydrogen is liberated within a crack is one thing but to show that the hydrogen actually causes crack

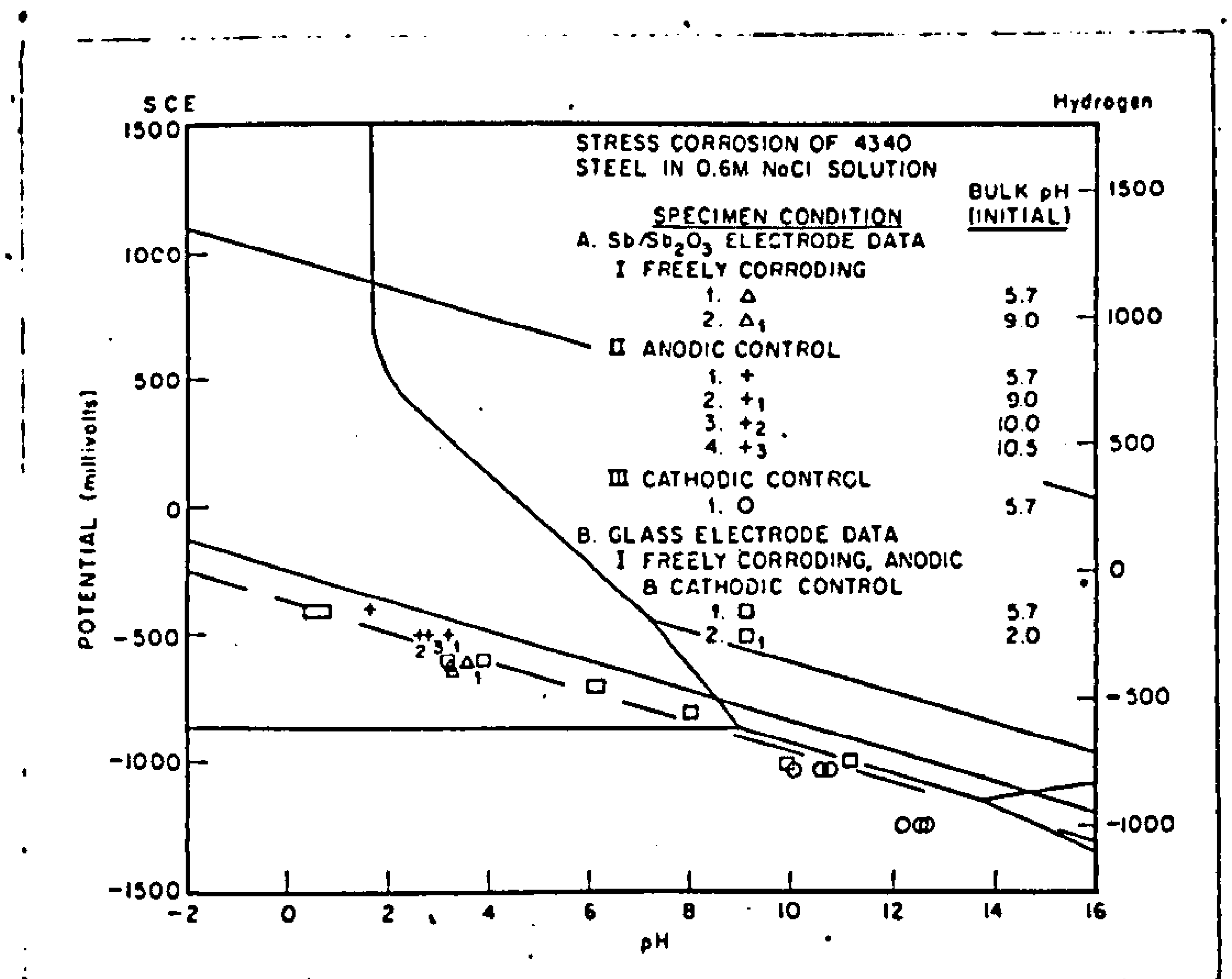

Fig. 1.15 The potential pH relationships measured on precracked specimens of a 4340 steel stress corroded in 3.5 wt % NaCl solution.[107]

propagation is another. Indeed, it could be argued that since hydrogen is appearing in molecular form as bubbles emanating from the crack it is less likely to be entering the metal lattice in atomic form and producing embrittlement. Secondly, it is as well to remember that the electrochemical conditions necessary for hydrogen discharge are not exclusive to this process. Thus, the demonstration of a lowering of pH within the confines of a stress corrosion crack is not solely conducive to hydrogen evolution since acidification can also result in enhanced metal dissolution.

In a recent paper by Ateya and Pickering[108] it was demonstrated that under conditions of bulk surface cathodic polarization of Fe and Ni in $1MHClO_4$ and 0.5M in sodium acetate/acetic acid buffer (pH 5.0) potential drops measured down slots of width 0.5-1.5 mm were often large ($\approx$ 0.5V) with the result that potentials at the base of the slots were sufficiently noble to allow metal dissolution to take place. The latter fact was confirmed by color-metric orthophenanthroline tests carried out on solutions extracted from the base of the slots.

Thus we are in the situation where, just as observations of hydrogen bubbles emanating from cracks or pits during strong anodic bulk polarization has been cited as evidence of an all embracing hydrogen embrittlement mechanism, if this recent evidence i.e. of metal dissolution occurring within slots of Fe and Ni undergoing strong cathodic polarization, is believed then an all embracing dissolution model for stress corrosion cracking could be postulated.

In recent years hydrogen permeation techniques, initially developed to determine hydrogen diffusivities in various metals and alloys, have been increasingly employed to demonstrate that stress corrosion cracking of various high strength steels can be explained by an all embracing hydrogen embrittlement mechanism. Thus, Barth (et al)[109] and Wilde[110] have studied hydrogen permeation through 9-4-45, 4340 and 12% Cr martensitic stainless steel membranes respectively subjected to various conditions of applied polarization in simulated marine environments.

The results of Wilde on a 4340 steel are typical and consequently only the latter will be discussed in detail here. The influence of applied current on the failure times of this steel are shown in Fig. 1.16 which is the type of curve typified by Fig. 1.13(c) i.e. where it may be implied that cracking is via an active path dissolution mode at the free corrosion potential. However, when the absorption and permeation of hydrogen through thin membranes of the steel, exposed on one side to 3.5 wt % NaCl, was measured under various conditions of applied current density, the results implied that hydrogen was absorbed into the steel under conditions of anodic polarization almost as readily as when cathodic polarization was applied (see Fig. 1.17).

The implication of these results was that at the free corrosion potential and with applied anodic polarization pitting occurred and with increasing facility as the current density was increased. Acidification of the solution within the confines of the pits thereby facilitated hydrogen absorption and so failure times decreased with increasing anodic current density. The pronounced increase in the time to failure in aerated solutions as a result of the application of a cathodic current density of about 20μA/

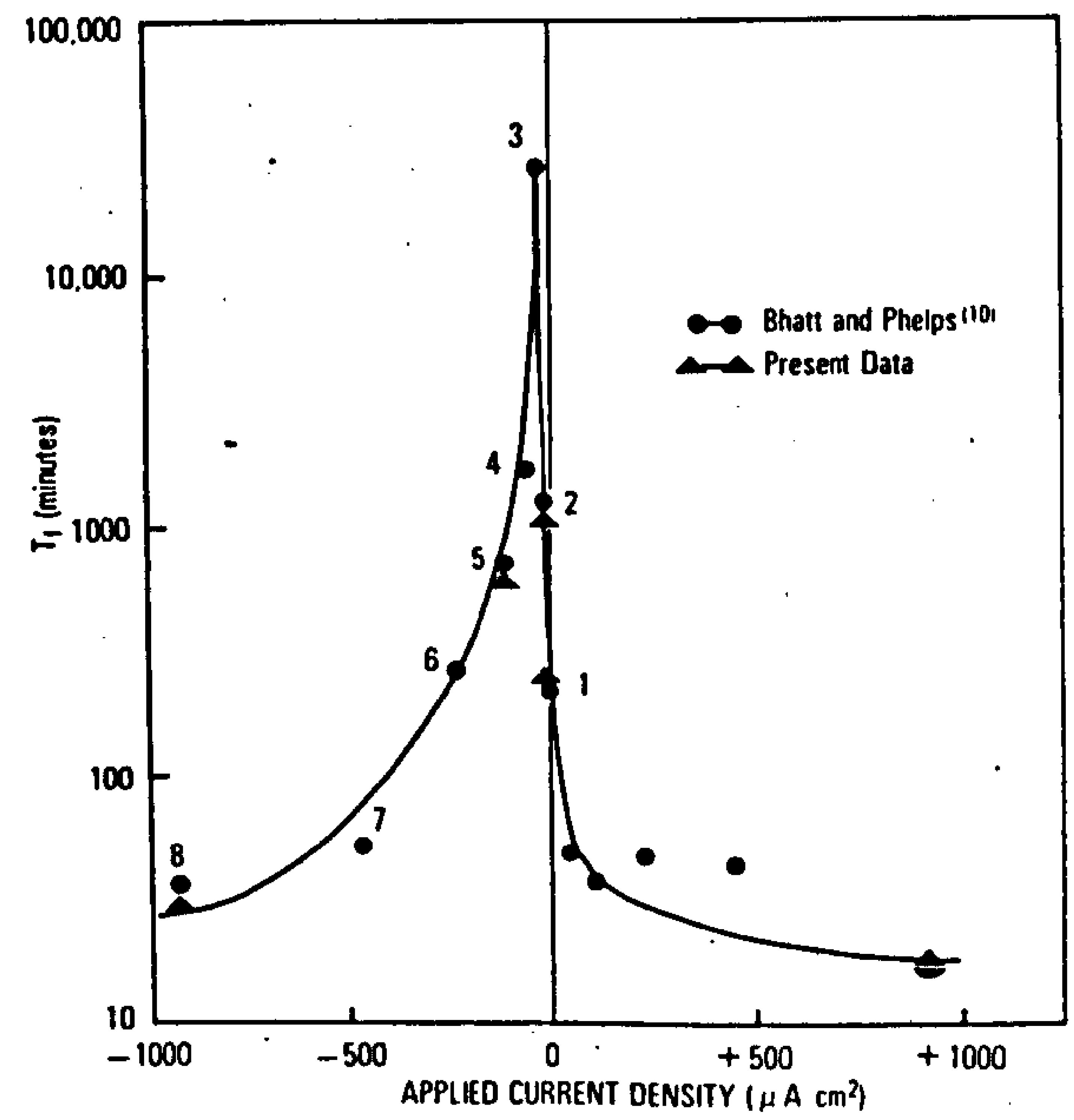

Fig. 1.16 The influence of applied current on the failure times of smooth tensile specimens of a 4340 steel tested in 3.5 wt % NaCl solution.[110]

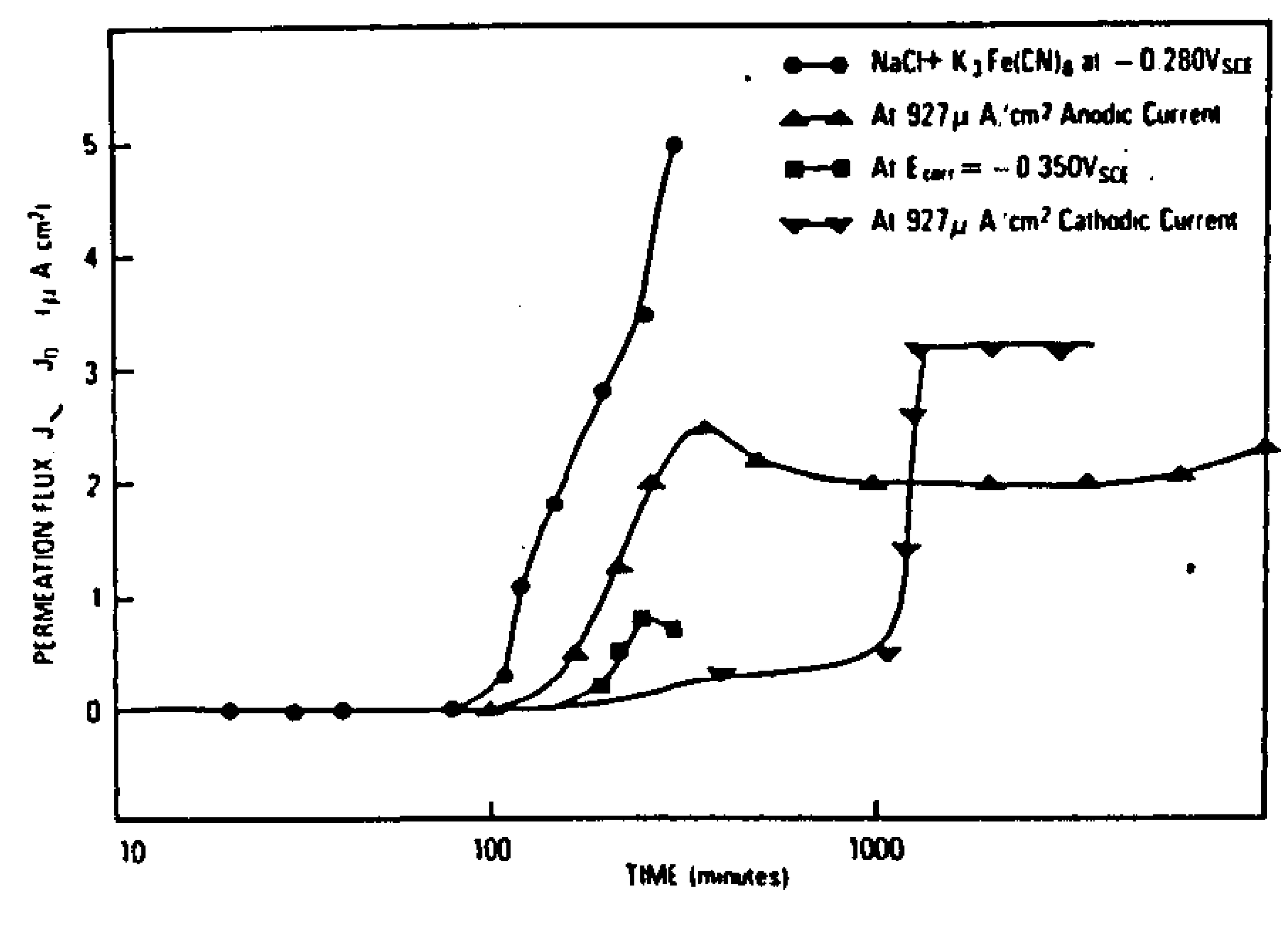

Fig. 1.17 The hydrogen permeation transients for thin membranes of 4340 steel exposed on one side to 3.5 wt % NaCl solution.[110]

cm^2 was explained as follows. The potential at this current density was observed to be active to the pitting potential (Fig. 1.18) so that no pitting corrosion could occur and the only source of hydrogen would be from the direct reduction of water, which if it occurred would tend to increase the pH and thereby make hydrogen adsorption even slower and time to failure longer. Fig. 1.18 indicates that at cathodic current densities above about $25\mu A/cm^2$ hydrogen evolution is the major cathodic reaction and the decreased failure times at higher cathodic current densities were simply reflecting the easier adsorption and absorption of hydrogen under these conditions. If the above arguments are correct then the time to failure of a test performed with an applied cathodic current density of $-20\mu A\ cm^{-2}$ in a de-aerated solution ought to be no less than that observed in an aerated solution at the same current density. Experiments performed in helium saturated solutions showed this to be the case.

Although the evidence provided by the hydrogen permeation technique appears at first sight to be fairly conclusive it is hoped to demonstrate in a subsequent section that evidence provided by the technique may not be as significant as a cursory examination suggests.

The latest technique claimed to provide evidence enabling the cracking mechanism to be identified in a given metal-environment system is the monitoring of acoustic (stress wave) emissions. In the latter technique a piezo-electric transducer attached to the surface of the specimen close to the anticipated direction of crack growth is used to detect the emission of stress waves induced by discontinuous crack propagation and converts the microscopic

Fig. 1.18(a) The potentiostatic anodic and
(b) galvanostatic cathodic polarisation curves for 4340 steel in helium and air saturated 3.5 wt % NaCl solutions. 110

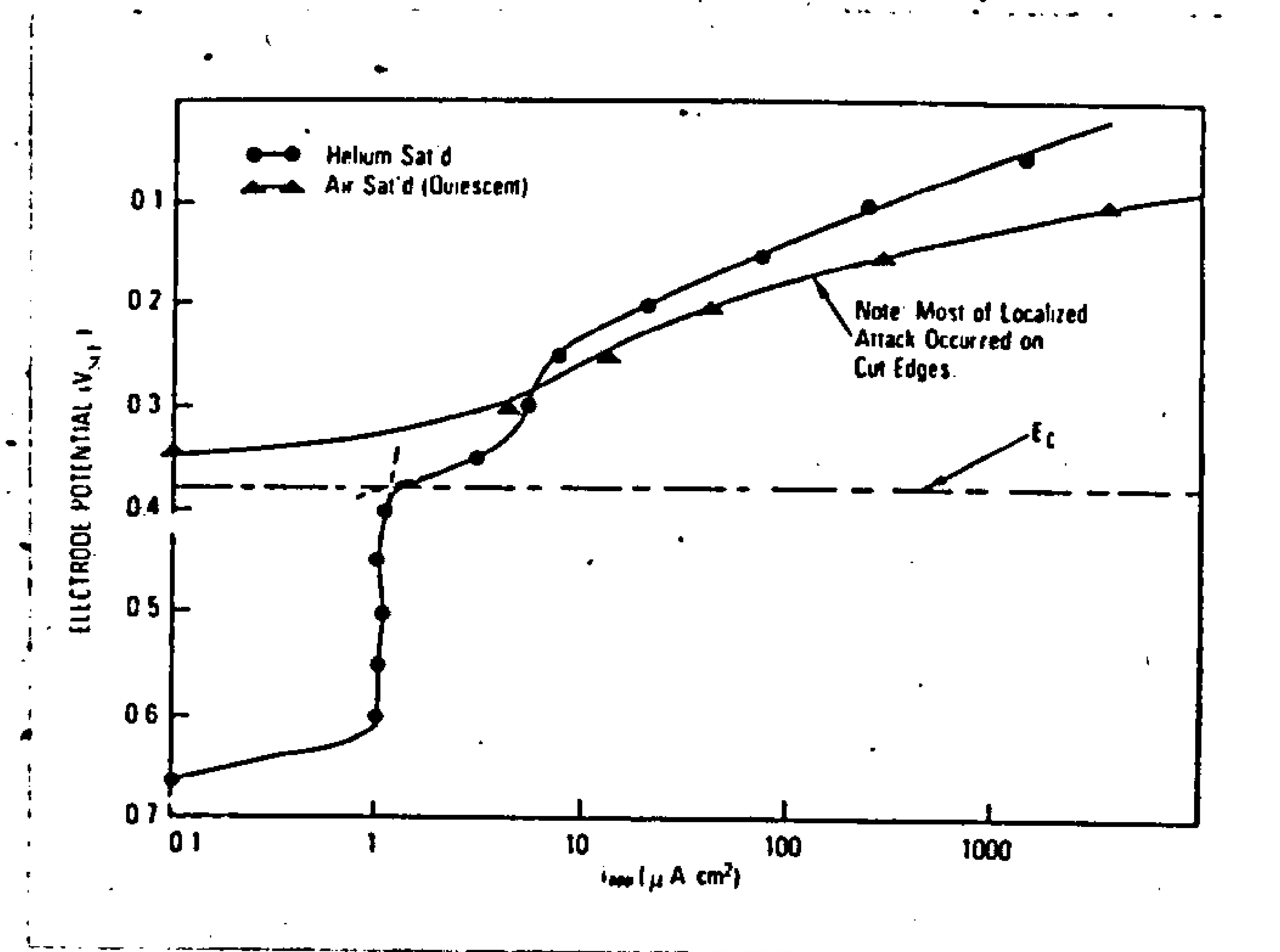

Fig. 1.18a

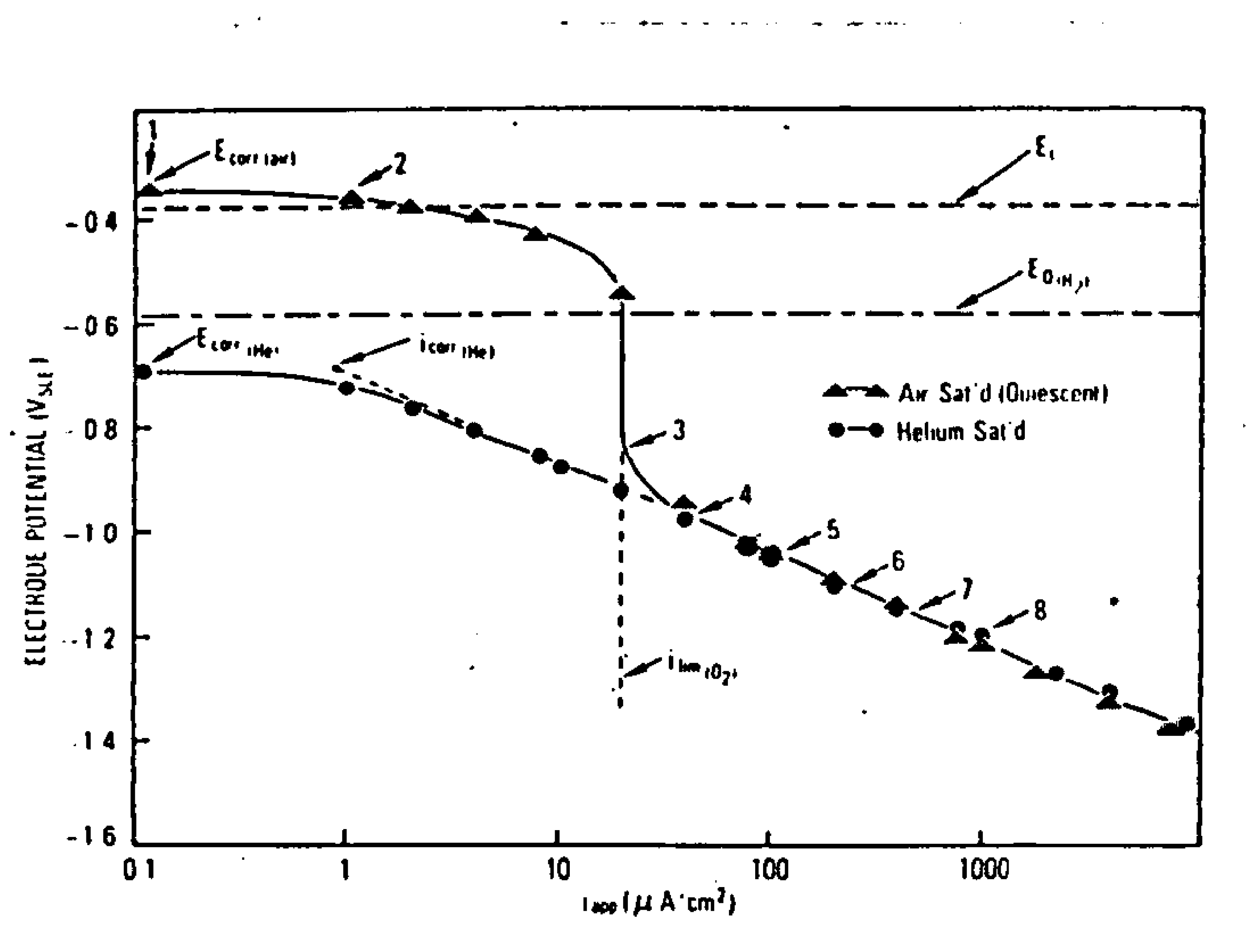

Fig. 1.18b

surface movements to an electrical signal which is suitably amplified, counted and analysed. The justification of its use in the present context depends upon the assumption that crack propagation via a dissolution mechanism is continuous and therefore 'quiet' whereas propagation as a consequence of hydrogen embrittlement involves a brittle crack propagation step which is associated with bursts of energy (stress wave emissions) which can, therefore, be detected as outlined above.

Thus Swann and Embury[111] report that stress corrosion cracking by dissolution in a copper based alloy produced no significant increase in acoustic emissions when compared to non-environmental crack propagation tests. On the other hand Elsea[112] observed that crack propagation in hydrogen embrittled steels was a discontinuous process producing readily detectable stress wave emissions.

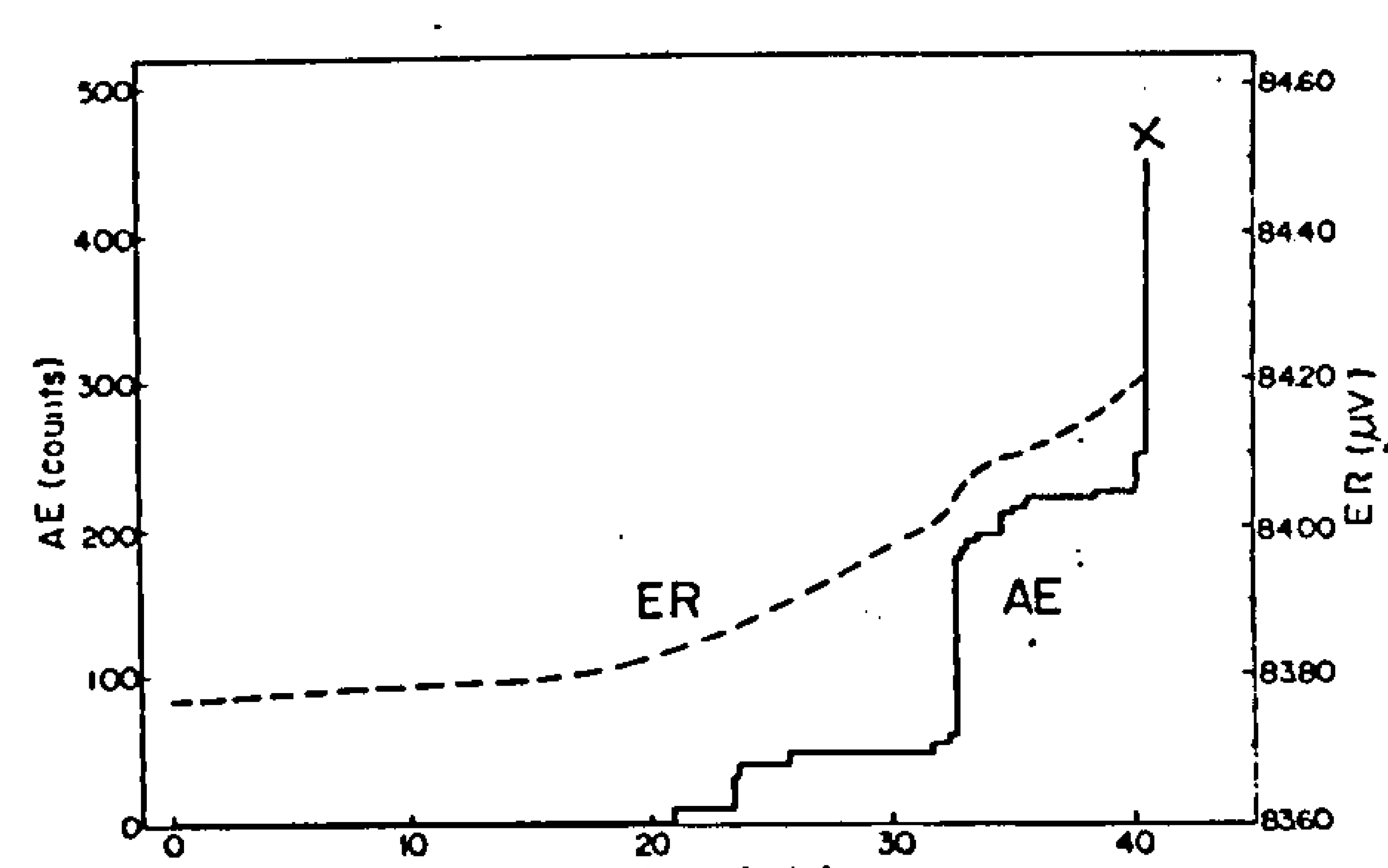

Fig. 1.19 Acoustic emission cumulative counts and electrical resistance change as a function of time for martensitic stainless steel stressed to $\approx 0.7\ \sigma_y$ in 3 wt % NaCl solution at 25°C.[113]

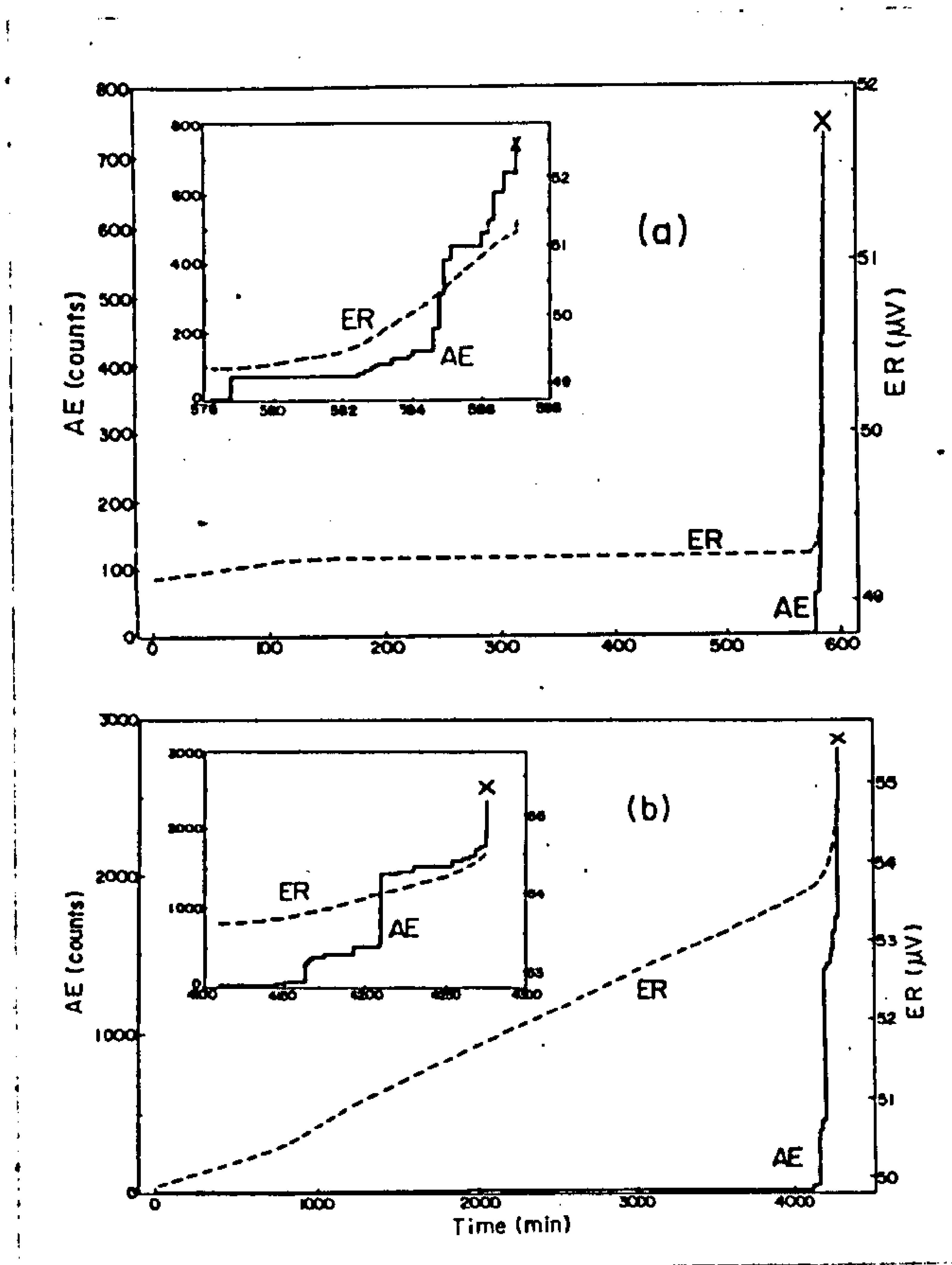

Fig. 1.20 Acoustic emission cumulative counts and electrical resistance change as a function of time for a low alloy steel stressed to 0.75σy in 3 wt % NaCl solution at 25°C (a) under cathodic polarisation (current density 2mA cm^{-2}), and (b) under anodic polarisation (current density 2mA cm^{-2}).[113]

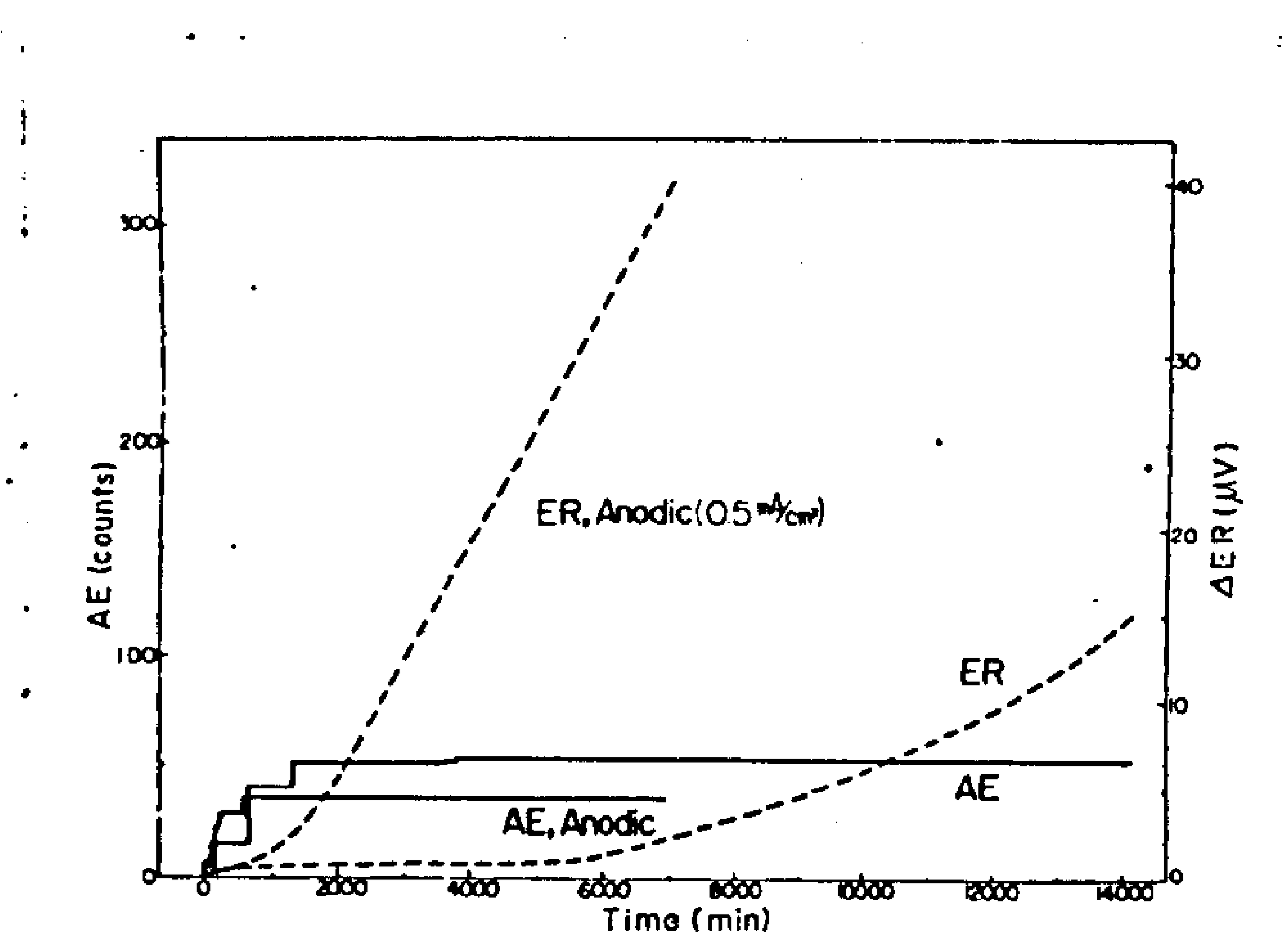

Fig. 1.21 Acoustic emission counts and electrical resistance change as a function of time for TYPE 304 stainless steel stressed to 0.85 σ y in 5N H_2SO_4 + 5MNaCl solution at 25°C.[113]

More recently, Hideya Okada[113] (et al) describe work performed on precracked cantilever bend specimens of 4 different steel types (low alloy, martensitic stainless steel, AlSl 304 and a ferritic stainless steel) in environments ranging from 3% NaCl in the former case to boiling (154°C) $MgCl_2$ in the latter case. Crack growth was measured by monitoring either the change in electrical resistance or displacement of the cantilever beam and stress wave emissions were detected by an acoustic emission transducer mounted on the upper surface of the specimen outside the corrosion cell. The signals from the transducer were amplified 70 dB and filtered to remove extraneous noise e.g. due to boiling before further amplification and counting. Figs. 1.19, 1.20, 1.21 taken from the Okada paper shows some typical results obtained on 3 of the steels and under different conditions of applied polarization.

The results of Figs. 1.19 and 1.20 were interpreted by Okada as being indicative of a hydrogen embrittlement cracking mechanism. The results of Fig. 1.21 were interpreted as being indicative of an active path dissolution mechanism being operative in Type 304 stainless steel tested in 5N H_2SO_4 + 5N NaCl at the free corrosion potential and with applied anodic polarization. The steady increase in electrical resistance in Fig. 1.20(b) was claimed to be a consequence of a reduction in specimen cross sectional area due to uniform anodic dissolution and <u>not</u> as one might expect a consequence of crack propagation as a result of active path dissolution.

Though the results of Figs. 1.19, 1.20(a), 1.21 appear to be straight forward to explain, those of Fig.

1.20(b) are less so. Thus, in the latter case the steady increase in electrical resistance could be interpreted as crack propagation via an active path, as explained above and the final rapid rise in electrical resistance towards the end of the test being a consequence of an increase in the crack propagation rate on approaching final fracture (i.e. a transition from stage II to stage III crack growth c.f. Fig. 1.9). The associated increase in the emission count rate in this late stage of crack propagation may well be symptomatic of an increasing contribution from mechanical processes in crack propagation. In this respect a more sensible experimental approach would have been to unload the specimen well before K_{IC} was attained, i.e. around the 2000 min mark and break open the specimen to see whether in fact any crack propagation had occurred up to this point in time.

2 Experimental Procedure

2.1 Material

The material used in these investigations was nominally an 18Ni (300) grade maraging steel and was received in the form of ¾" and 1" diameter hot rolled bar.

The chemical analysis of the two batches of material used are shown in Table 2.1.

TABLE 2.1

	BATCH A	BATCH B
Carbon	.01	.01
Sulphur	.01	.01
Phosphorous	.01	.01
Nickel	18.6	18.5
Molybdenum	5.2	5.4
Cobalt	9.3	8.1
Aluminium	.12	.07
Titanium	.72	.59

2.2 Specimen Preparation

2.2.1 Constant strain and constant strain rate specimens

The as received bar was hot rolled at a temperature of between 900^{o} and 950^{o}C to a diameter of 0.5". This ½" diameter bar was then finished to remove the heavy oxide layer and swaged to a diameter of .365" (47% total reduction), through two dies before annealing for 1 hour at 800^{o}C under an argon atmosphere. Two further swaging passes reduced the diameter to .250" (total reduction 53%). The material was then annealed once more for 1 hour at 800^{o}C and cold drawn to the final size of .1875" through dies of diameter .230", .197" and .1875" (total reduction 44%).

Tensile specimens to the dimensions indicated in Fig. 2.1(a) were machined from the.1875" cold drawn wire, solution treated for one hour at the desired temperature, air cooled and aged for three hours in an Heraeus forced air furnace. Solution treatment was carried out under vacuum to restrict oxidation. The heat treated specimens were polished to 2/0 emery and coated with Bakelite lacquer to the shoulders of the gauge length and to within 1-1½" of each end of the specimen.

A few specimens were prepared in which the original rolling direction of the as-received rod was arranged to be perpendicular to the tensile axis of the finished specimens. The latter specimens were prepared by forging the as received 1" diameter bar to produce a roughly rectangular cross section and hot rolling parallel to the

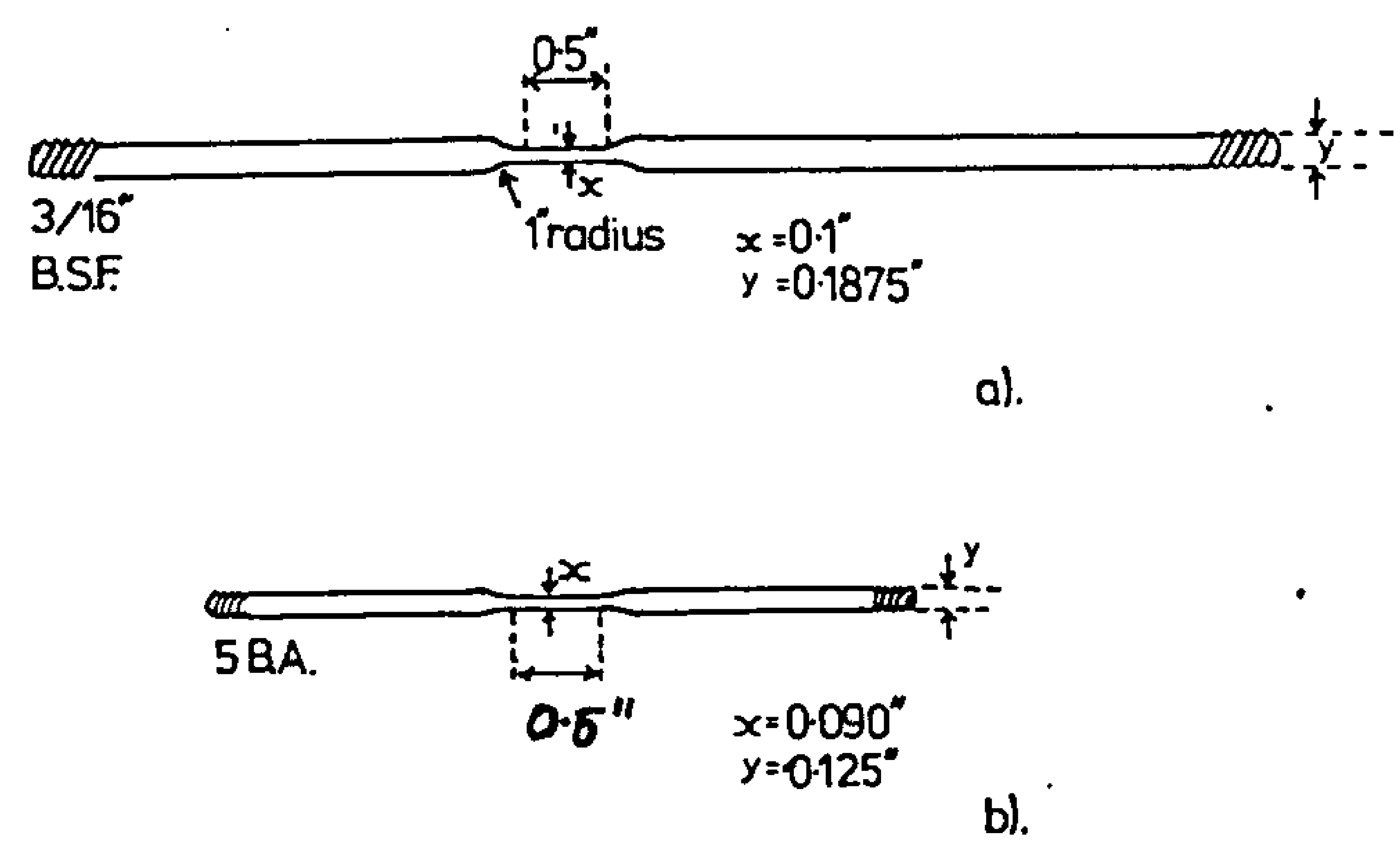

Fig. 2.1 Smooth stress corrosion tensile specimens.

original diameter of the bar. The resulting flat plate was cut into strips (such that the original rolling direction of the so received bar was perpendicular to the long axis of the strips) and machined to the dimensions indicated in Fig. 2.1(b). The reduced specimen dimensions were necessary because the maximum thickness and length of plate that could be hot rolled from the 1" diameter bar were insufficient to enable full sized specimens to be made.

2.2.2 Constant strain rate specimens for hydrogen precharged & gaseous hydrogen testing and for the determination of mechanical properties

Hounsfield No. 11 specimens (Fig. 2.2) were machined from .230" diameter cold drawn wire fabricated as described in section 2.2.1. The specimens were solution treated, air cooled aged and polished to 2/0 emery and the shoulders coated with Bakelite lacquer.

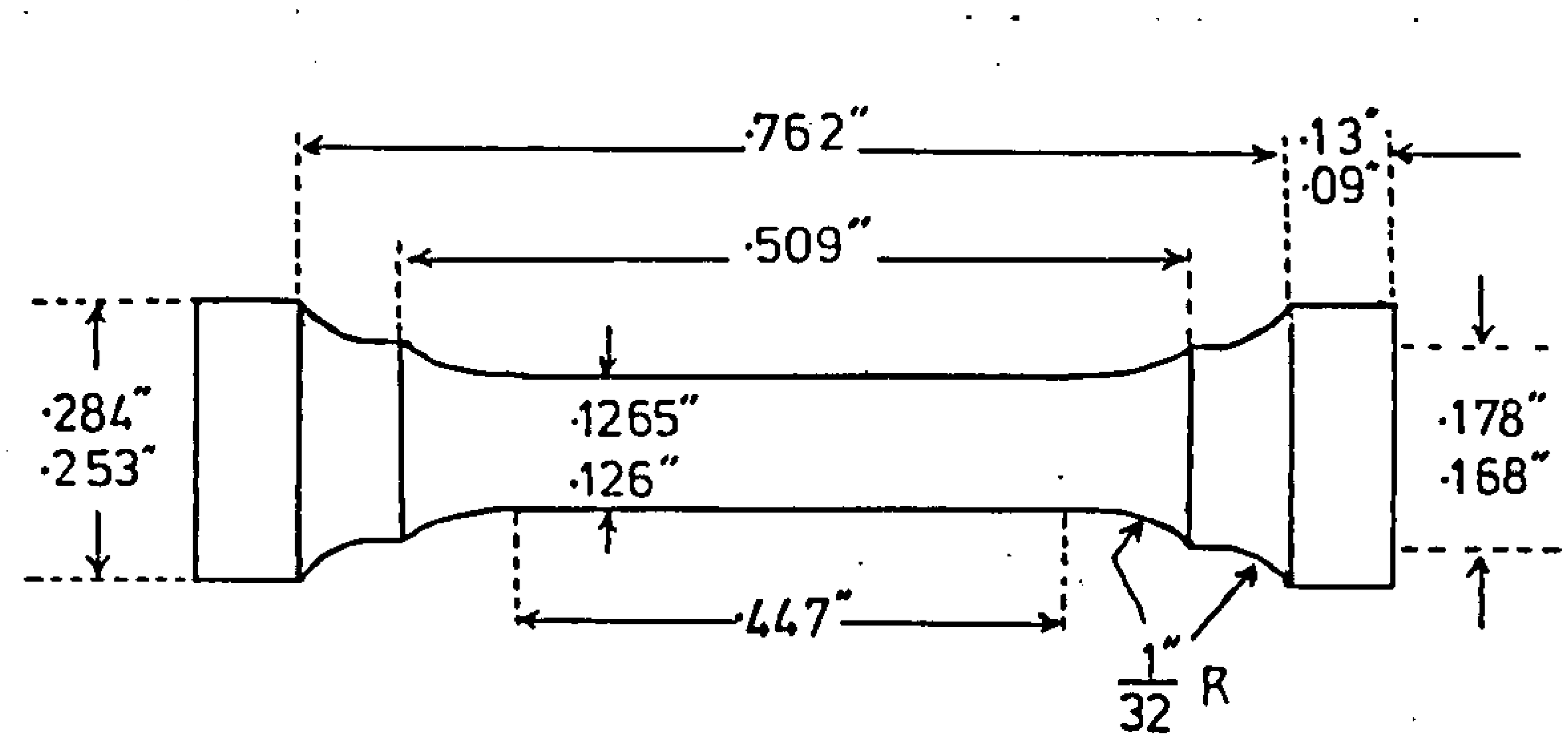

Fig. 2.2 Hounsfield No.11 tensile specimens.

2.2.3 Fatigue precracked specimens

Two loading modes were employed for fatigue precracked specimen work.Fig. 2.3 shows the dimensions of specimens tested as cantilever beams. Fig. 2.4 shows the dimensions of specimens tested in the pin loaded tensile mode. The specimens were fabricated as follows. The as-received bar was hot forged to produce a roughly rectangular cross section before hot rolling at temperatures of between 900° and $950^{\circ}C$ to a cross section approximating that of the finished specimens. The resulting flat bar was solution treated at the desired temperature and machined to the final dimensions. The specimens were then aged and cooled.

Two iron wires 6" long and .030" in diameter were spot welded to the specimen on either side of the chamfered notch and about 2mm from the notch to enable mesurements to be made of the potential drop across the crack using the D.C.electrical resistance technique. Current leads for the resistometric technique were provided in the form of 3"and 4" long .1875" diameter rods which were soldered into the drilled and tapped holes on either side of the pre-notch of the specimens (Fig. 2.5). Fatigue precracks were then introduced into the specimen to a depth of about 1mm below the base of the machined pre-notch. The required length of precrack was arranged to be produced in approximately 45-50 min.

2.2.4 Hydrogen permeation specimens

Hydrogen permeation discs were prepared in three different ways, for reasons that will be made clear in the appropriate section.

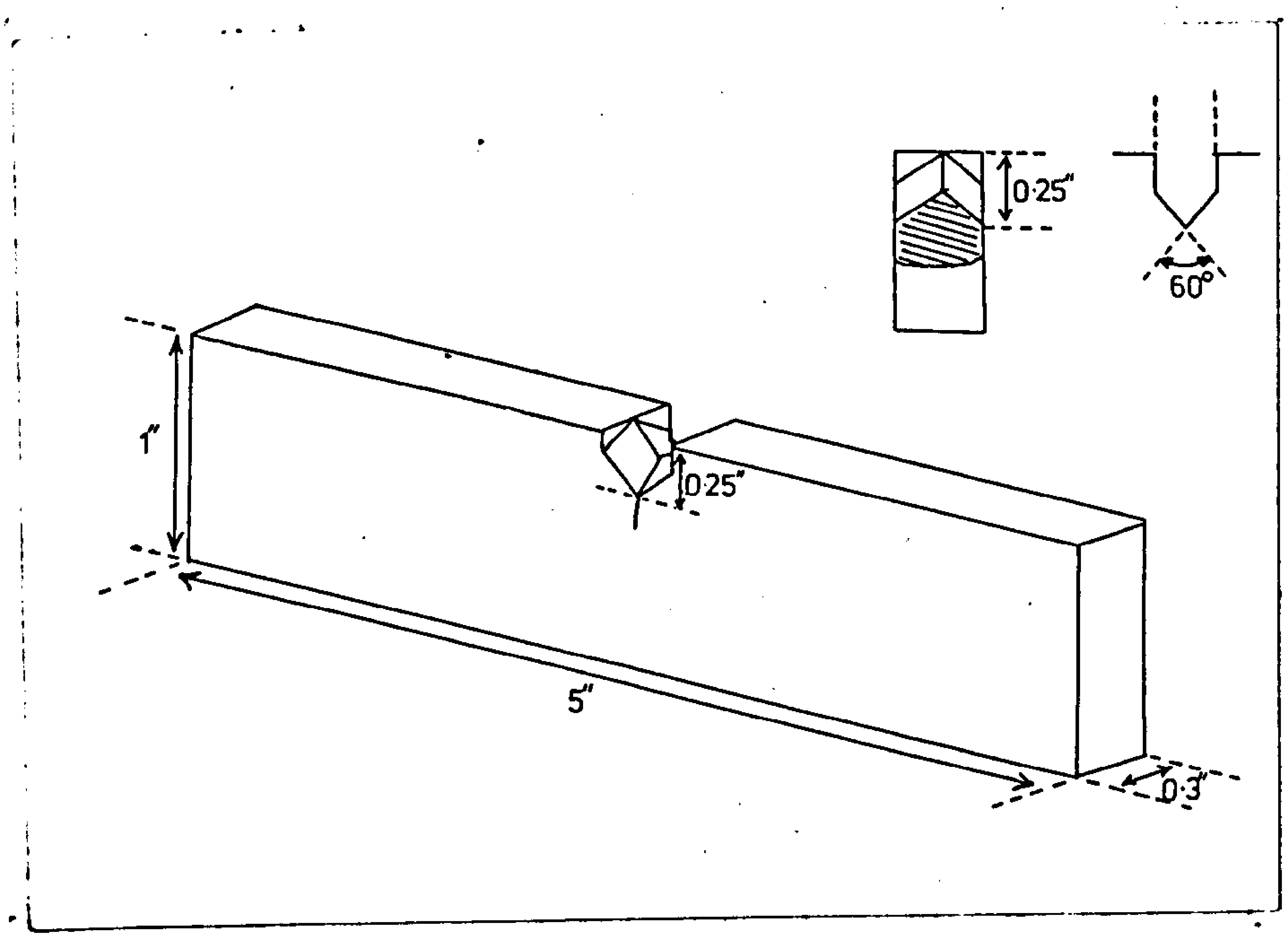

Fig. 2.3 Brown type cantilever beam fatigue precracked specimens.

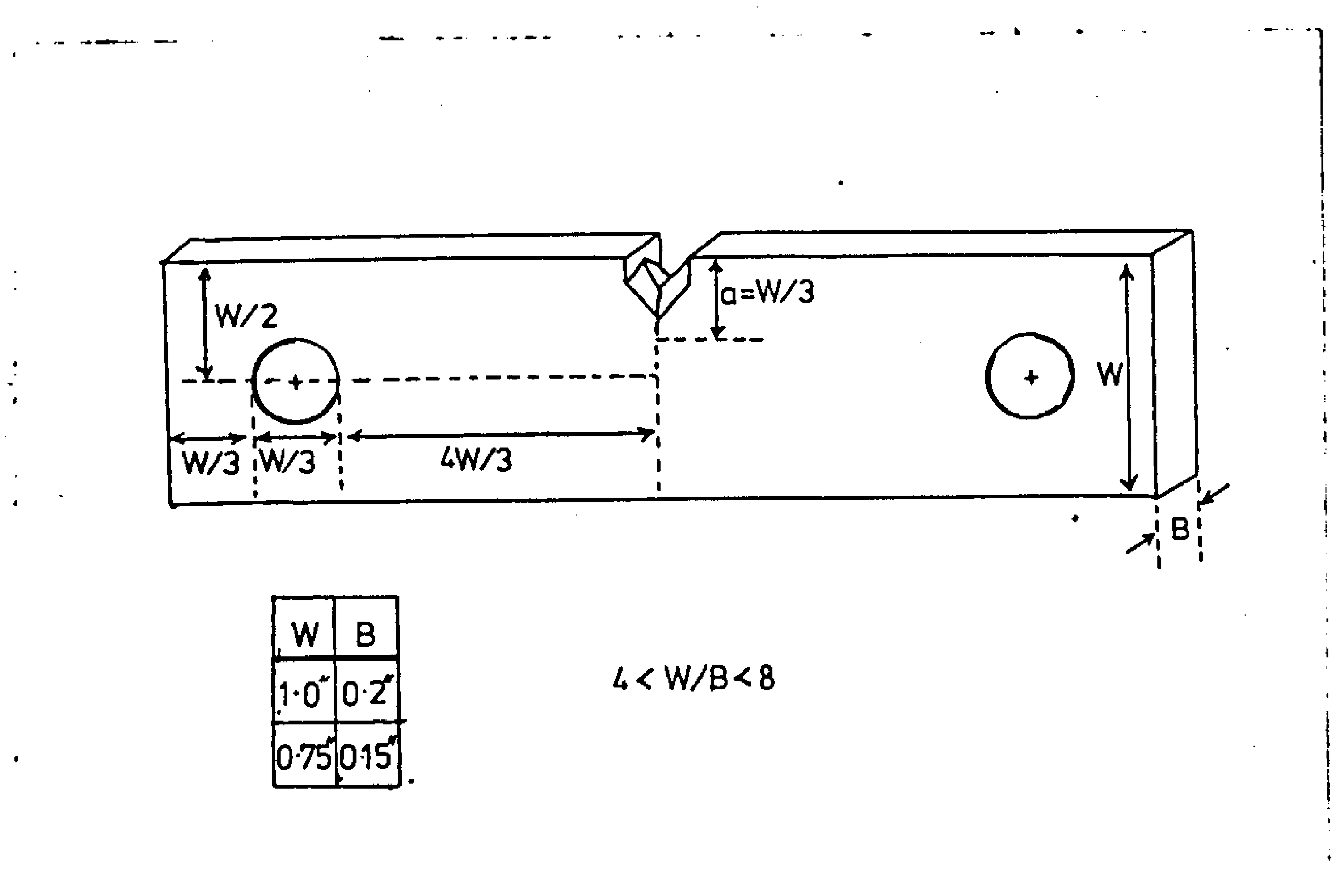

Fig. 2.4 Pin loaded single edge notch fatigue precracked specimens.

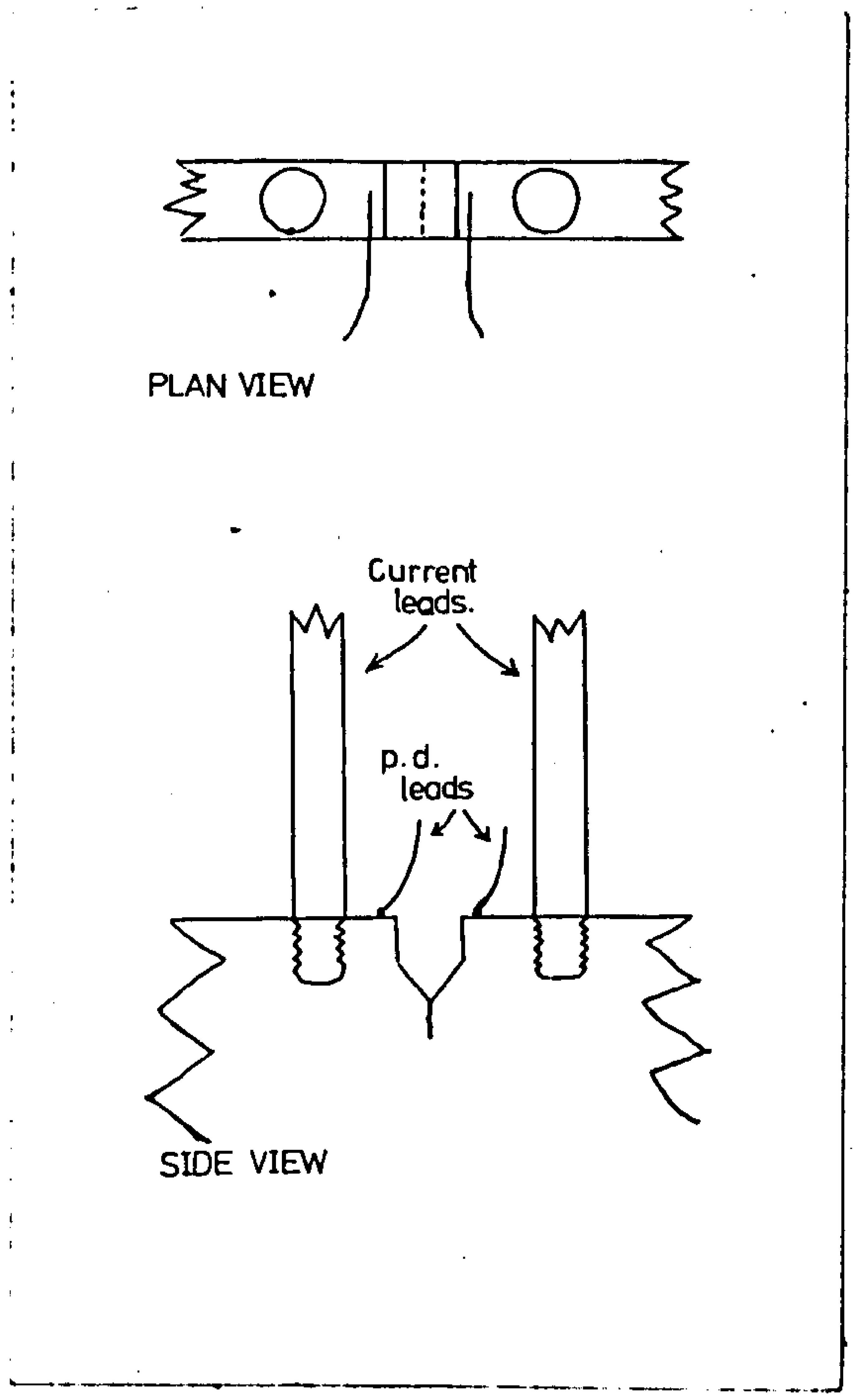

Fig. 2.5 Arrangement of current and p.d leads for the resistometric crack monitoring technique - on fatigue precracked specimens.

(1) The majority of specimens were prepared as follows. 1" diameter, approximately .030" thick discs were cut from the as-received bar stock after solution treatment at the desired temperature. The discs were mounted on flat steel bases using double sided adhesive tape and carefully ground to the desired thickness.

(2) As-received bar was hot rolled to approximately .050" thick strip. The strip was ground to the desired thickness after solution treatment and 1" diameter discs stamped out of the strip.

(3) A few specimens were prepared by machining a 1" wide strip of the desired thickness directly from the as-received bar stock after solution treatment and 1" diameter discs stamped out of the resulting strip.

The machined discs were then aged and cooled in vacuo and a 1" length of multistrand copper wire soldered to the edge of each to provide electrical contact with the specimen.

2.2.5 Polarization curve and potential-time specimens

Specimens for the determination of polarization and potential-time curves were prepared by polishing 3" lengths of .1875" diameter wire to 2/0 grade emery and stopping off an exposed area of 2cm^2 near one end with bakelite lacquer.

2.3 Solutions

The environment mostly used in the present work was a 3.5 wt % (0.6N) NaCl solution prepared from Analar grade sodium chloride and de-ionised water. pH adjustments were made with dilute, 0.6N hydrochloric acid or sodium hydroxide solutions depending upon the initial solution pH required.

In addition, some tests were performed in which the following additions were made to the basic 3.5 wt % NaCl solution.

i) 25cc/litre chloroplatinic acid solution. (5% w/v $H_2\ PtCl_6\ 6H_2O$)

ii) 5g /l thiourea

iii) 5g /l sodium arsenate

iv) 2%v/v hydrogen peroxide solution

All chemicals were analar grade.

2.4 Equipment and Procedure

2.4.1 Constant strain and constant crosshead speed tensile testing

Constant strain and constant crosshead speed tests were carried out on a hardbeam tensometer which is illustrated in Fig. 2.6. The apparatus has been described in detail elsewhere.[114]

Constant strain tests were performed on the machine by disconnecting the chain drive from the worm gear and loading the specimen to the desired initial stress by rotating the handle on the worm gear. The crosshead was then locked in position and the load allowed to relax as crack propagation proceeded.

Constant crosshead speed tests were carried out using crosshead speeds in the range 10^{-7} to 10^{-5} IN.S^{-1} by suitable selection of gearing and chain drive.

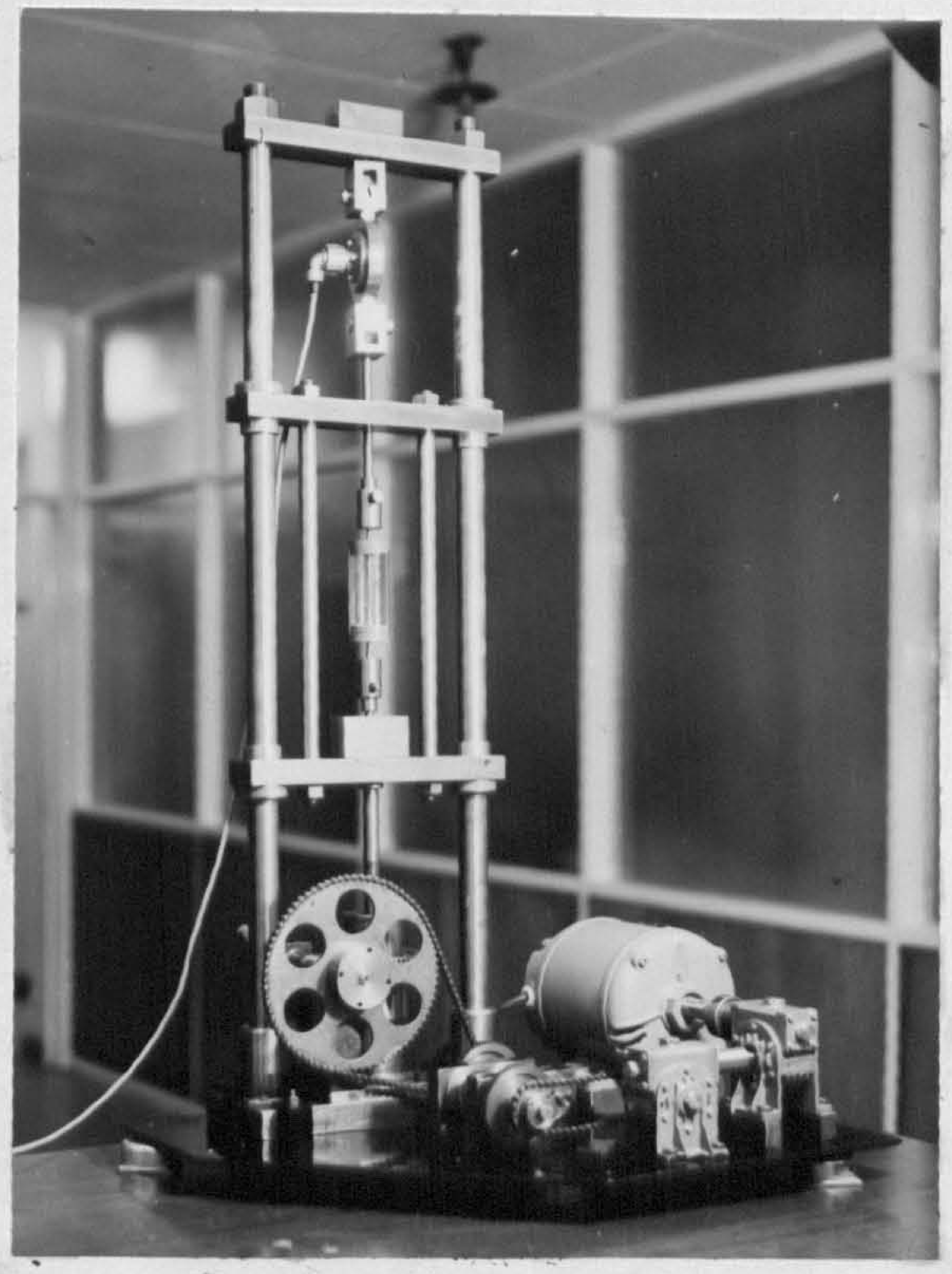

Fig. 2.6 Constant crosshead speed hardbeam tensometer.

The load was monitored continuously throughout a test by means of a load cell employing a Wheatstone bridge arrangement of strain gauges cemented within a hardened steel stressing ring. The power to the Wheatstone bridge circuit was supplied from a FARNELL instrument stabilised power supply. (Model No. M3A 30/.5) and the output was monitored on a Servoscribe potentiometric chart recorder. The schematic circuit diagram of the load cell arrangement is shown in Fig. 2.7. The load cells were calibrated on a Hounsfield tensometer using a 2 ton beam prior to use.

The corrosion cell employed in these investigations is illustrated in Fig. 2.8 and consists of 1½" diameter Pyrex glass tubing 4" in length. The specimen was held in place within the corrosion cell by tightly fitting rubber bungs. A platinum counter electrode, a filling tube and a string bridge connecting the corrosion cell to the reference electrode (see following page) were also incorporated into the uppermost rubber bung. The cell so constructed had a solution capacity of approximately 70 cc of solution.

Tests other than at the free corrosion potential were performed using potentiostatic or galvanostatic polarization.

Potentiostatic tests were performed by polarizing the specimen to the desired potential (with respect to a saturated calomel electrode of potential +241 mV versus the normal hydrogen electrode) using a Wenking operational power amplifier (Model Nos. OPA69 or OPA72M).

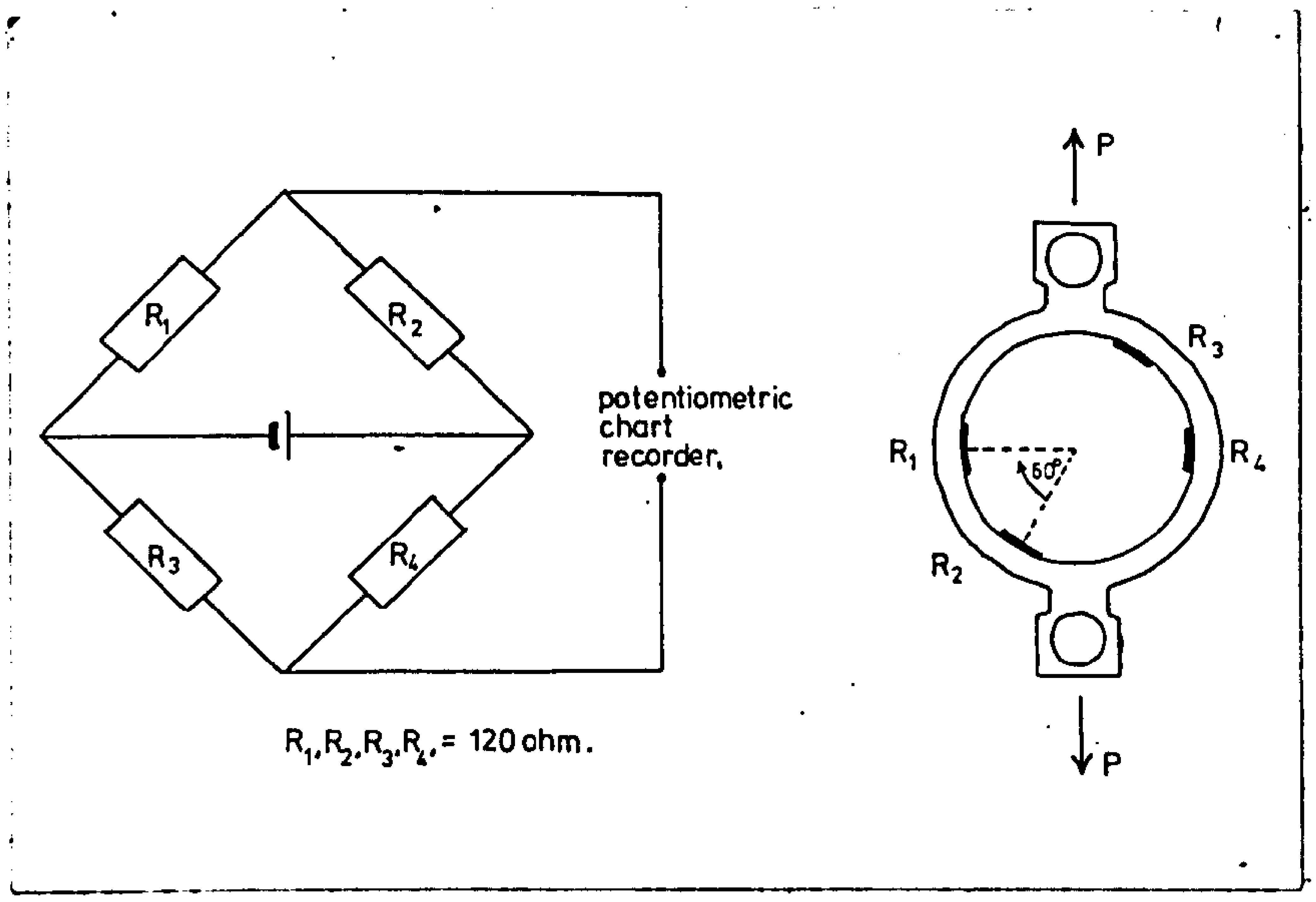

Fig. 2.7 Schematic circuit diagram and arrangements of strain gauges in load cells.

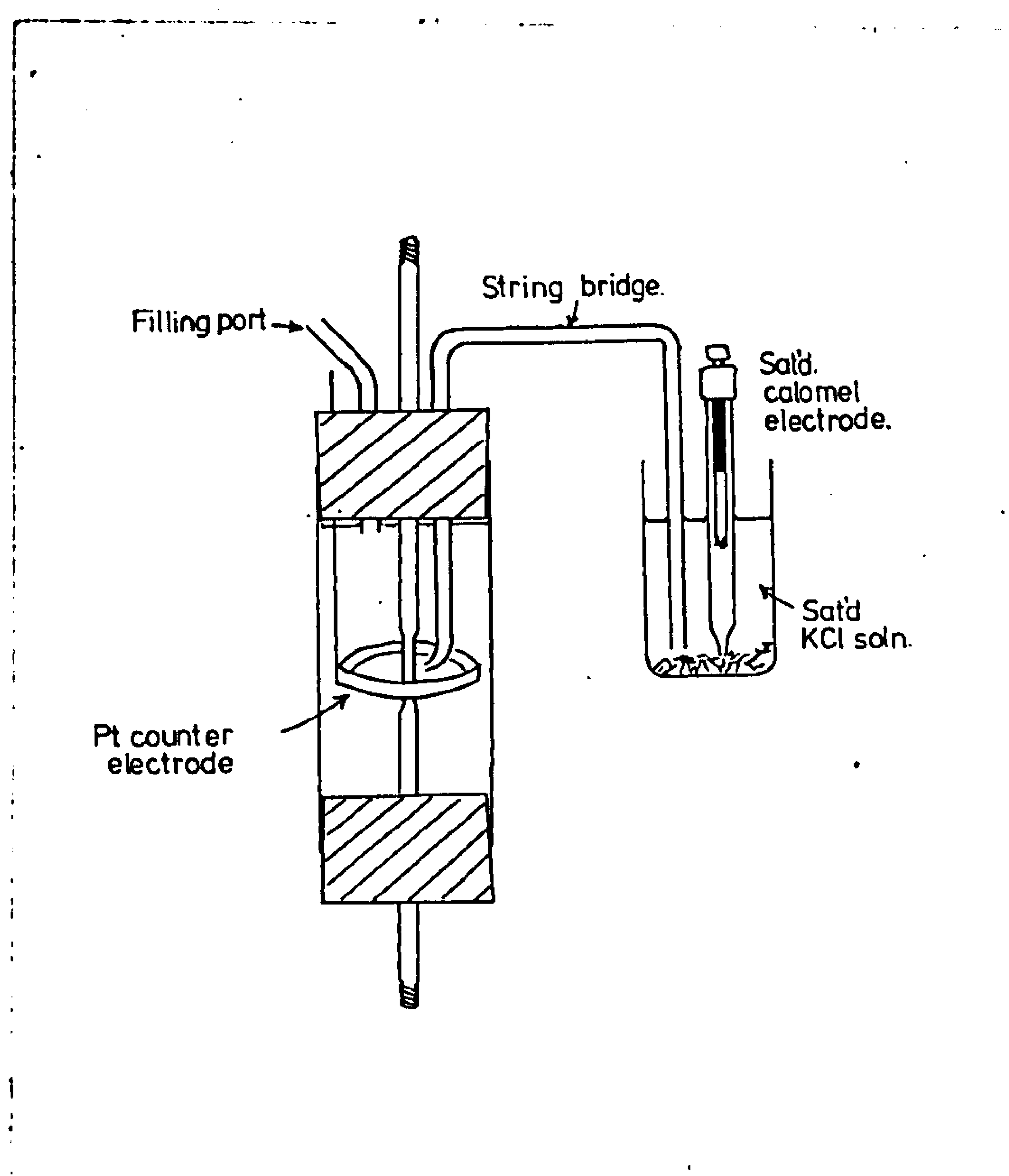

Fig. 2.8 Stress corrosion test cell employed in constant strain and constant crosshead speed tensile tests showing the positioning of reference and auxiliary electrodes.

Galvanostatic tests were performed by polarizing the specimen to the desired anodic or cathodic current density using the simple galvanostatic circuit illustrated in Fig. 2.9.

Constant crosshead speed tests in gaseous hydrogen were performed on a Hounsfield tensometer rig surrounded by a vacuum chamber into which purified hydrogen was introduced to the desired pressure after evacuation. Load was monitored during a test using a load cell of Wheatstone bridge circuit design and strain was monitored using a linear displacement transducer. The signals from load cell and transducer were passed to a Bryans X-Y plotter, thus enabling load extension curves to be automatically plotted out during testing.

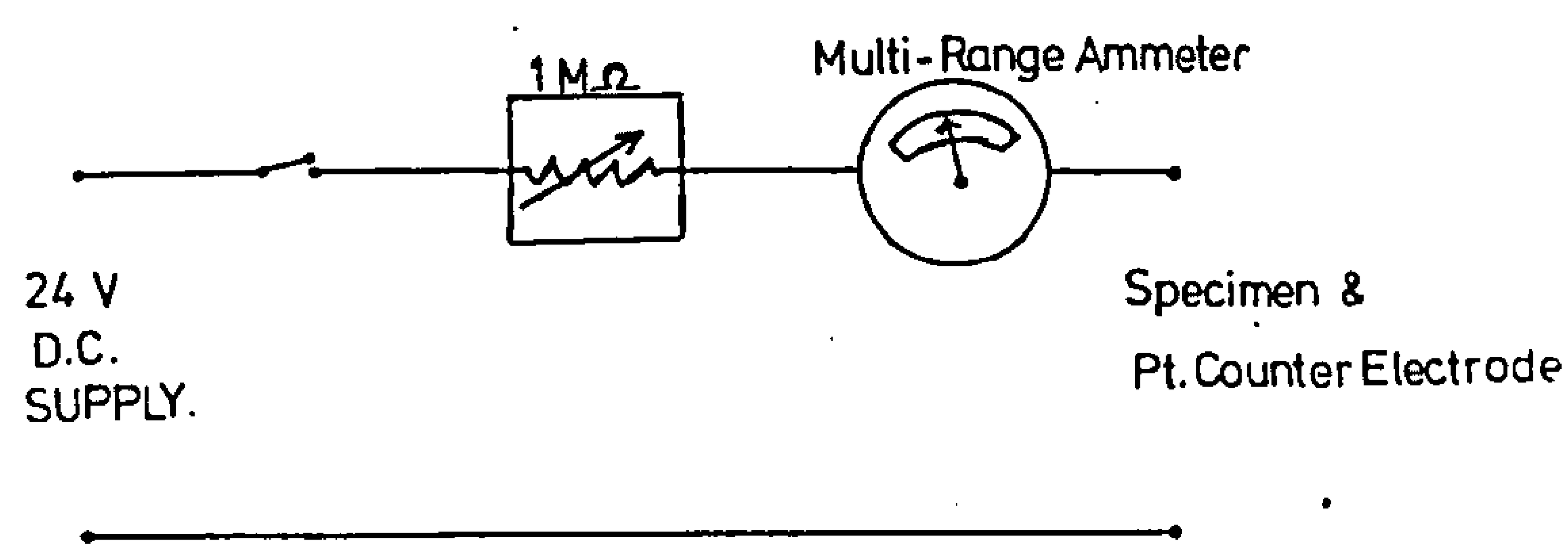

Fig. 2.9 Galvanostat circuit diagram.

2.4.2 Fatigue precracked specimen tests

a) Loading arrangements

Two loading arrangements were employed for stress corrosion testing of precracked specimens.

i) Cantilever bending

These were carried out by clamping one end of the specimen rigidly in position and attaching a lever arm (36" in length) to the other end. From the arm, weights could be hung to produce stress intensities K_I at the tip (assuming plane strain conditions) given by[115]

$$K_I = \frac{4.12M\left(\frac{1}{\alpha^3} - \alpha^3\right)^{\frac{1}{2}}}{B\ D^{3/2}} \qquad 2.1$$

where $\alpha = 1 - a/D$

and a = total crack length

D = height of specimen

B = specimen thickness

M = bending moment = (distance between crack plane and point of load application x load) + (distance between crack plane and c. of gravity of lever arm x wt of lever arm).

The notch of the specimen was surrounded by a corrosion cell fabricated from a polyethylene bottle cut to fit the specimen and fitted with a platinum ribbon to act as a counter electrode. The cell was bonded to the specimen with silicone rubber solution to provide a leak proof seal. The loading arrangement with specimen and fitted corrosion cell is shown in Fig. 2.10.

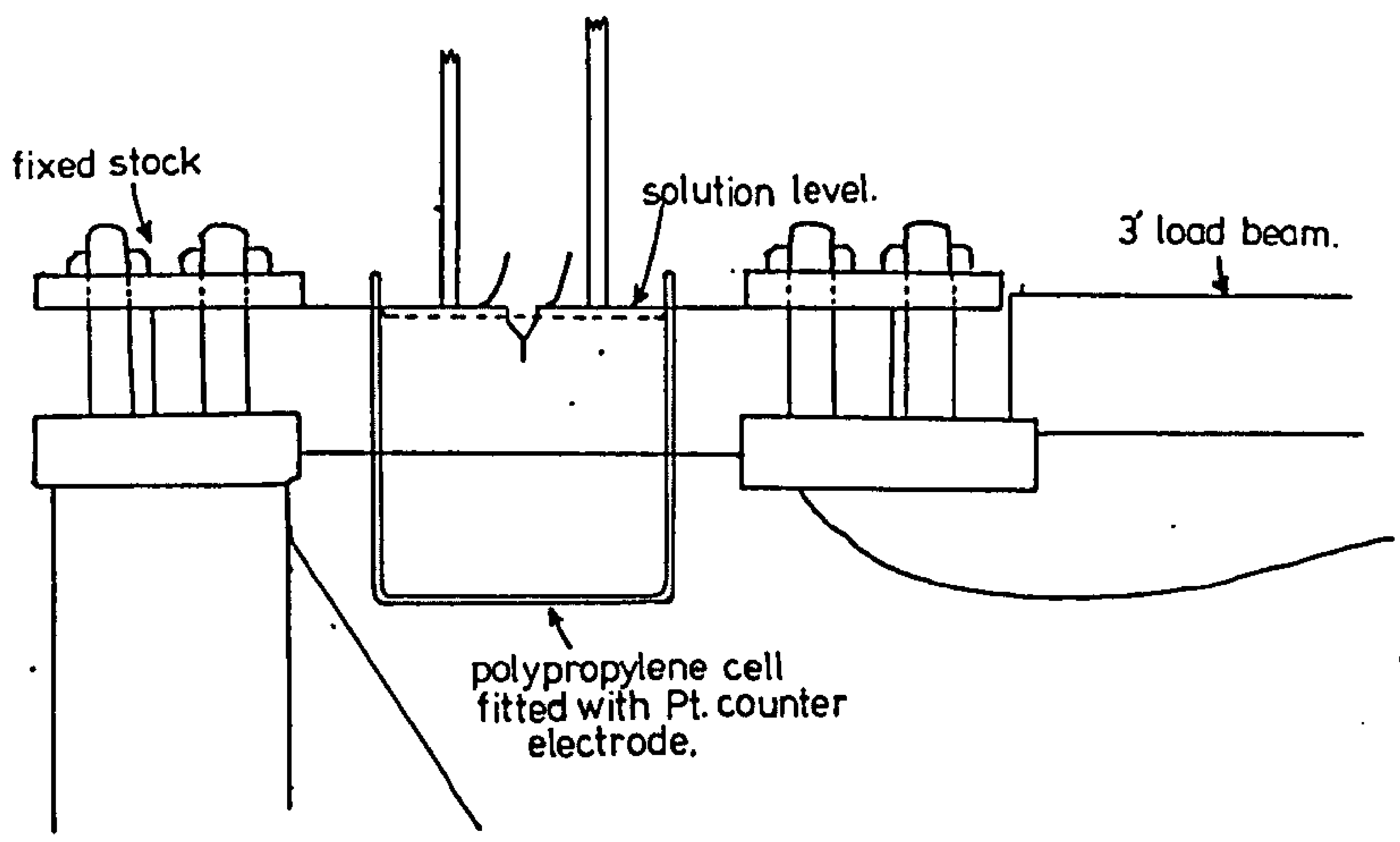

Fig. 2.10 Arrangement of specimen and corrosion cell in cantilever bend tests.

ii) Pin loaded single edge notch tensile loading

These tests were performed on the hardbeam tensometer described in the previous section. The specimens were loaded to the desired initial stress intensity, the crosshead locked in position and the load and crack growth monitored continuously throughout the duration of a test. The pins were greased with silicone grease prior to loading. Stress intensities were calculated using the relationship:[116]

$$K_I = \frac{P}{B}\left(\frac{a}{W}\right)^{\frac{1}{2}}\left[1.99-0.4124(a/W)+18.7(a/W)^2 - 38.48(a/W)^3+53.85(a/W)^4\right]$$

which is valid for $a/W < 0.6$

where P = load

B = specimen thickness

a = total crack length

W = height of specimen

The corrosion cell employed on this series of tests was in the form of a shallow polyethylene dish surrounding the prenotch and bonded to the specimen with silicone rubber solution to provide leak proof seals. The specimen, with attached corrosion cell is illustrated in Fig. 2.11.

b) <u>Crack growth monitoring</u>

The D.C. electrical resistance technique was the principle crack growth monitoring technique employed in these investigations. However, a small number of tests were performed in which crack growth was monitored by observing compliance changes from deflections of the loading arm as

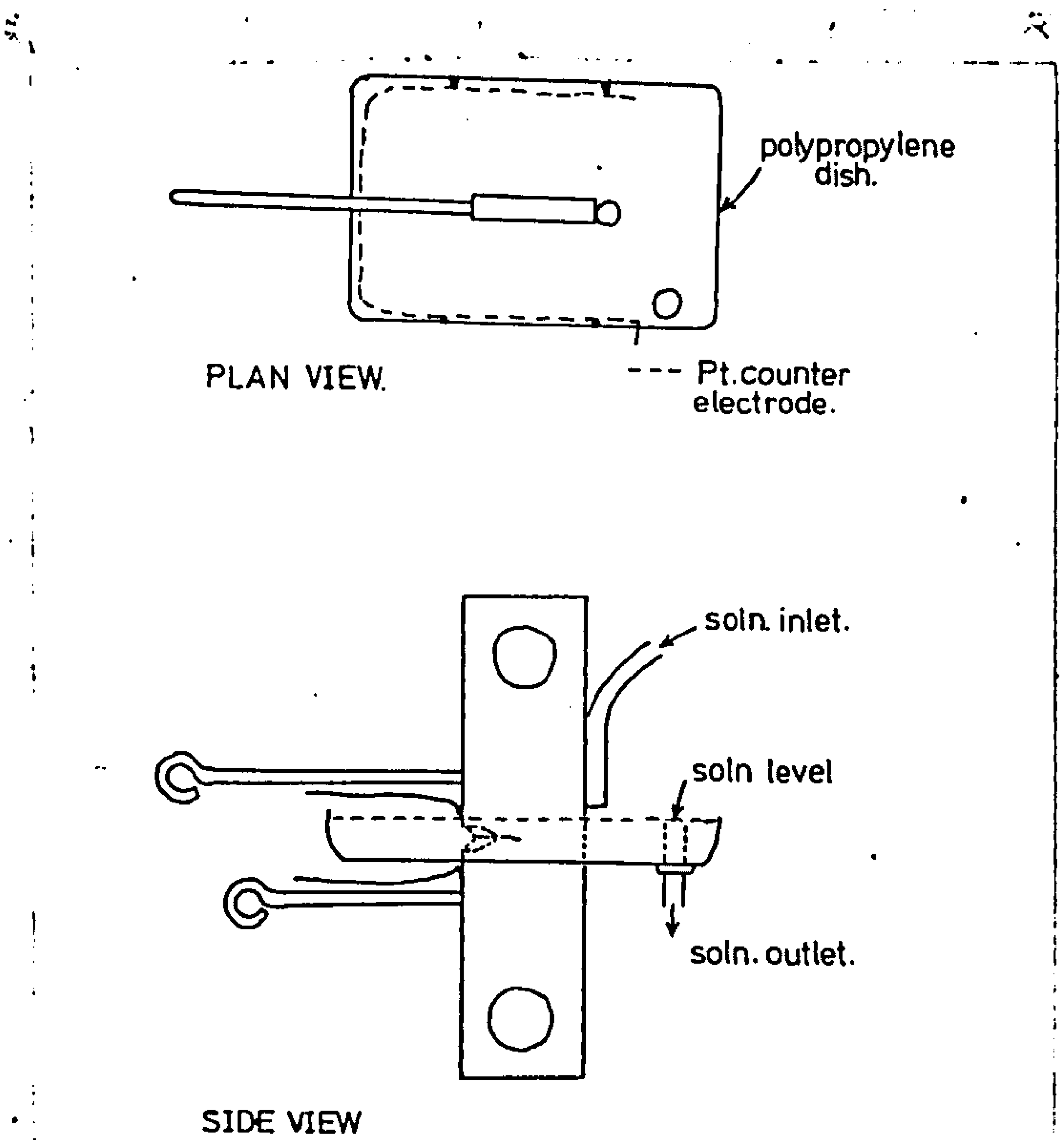

Fig. 2.11 Arrangement of specimen and corrosion cell in pin loaded single edge notch tensile tests.

measured by a linear displacement transducer. The chief disadvantage of the latter technique is that since crack lengths are indirectly deduced from measuring the deflection of a beam it is possible that contributions to the observed deflection other than from crack propagation may be detected e.g. plastic deformation at the crack tip or production of internal voids in the specimen due to hydrogen charging. Thus, for example, Procter and Paxton[117] using a cantilever bend jig demonstrated it to be impossible to distinguish between sub-critical flaw growth and plastic crack blunting in the initial stages of a stress corrosion test.

In the present work the measurement of beam deflection using the linear displacement transducer was used only to give a more precise indication of crack initiation, than otherwise would have been possible, in tests carried out in order to determine the influence on cracking susceptibility of passing a current of the order of 30 amperes through the specimen as is required by the D.C. electrical resistance technique for crack growth monitoring. Doubts have been expressed, chiefly by electrochemists as to the wisdom of measuring an absolute value of the rate of crack propagation by passing 30A through the specimen because it is felt that this may well affect the anodic dissolution rate at the crack tip.

Table 2.2 lists the $K_{I\ SCC}$ values and average crack velocities determined on fatigue precracked cantilever bend specimens freely corroded in de-ionised water with and without employment of the D.C. resistance technique for crack growth monitoring.

TABLE 2.2

	$K_{I\ SCC}$	Mean crack velocity INS^{-1}
Without	23-26 KSI $\sqrt{IN}$	5.54×10^{-6}
With	24-27 KSI $\sqrt{IN}$	6.3×10^{-6}

De-ionised water was chosen as the corrosive environment since it was felt that the true test of the effect of the passage of 30A through the specimen would be to carry out the tests under freely corroding conditions in the least aggresive environment likely to be encountered. From the above results, it was concluded that the effect of passing 30A through the specimens during crack growth monitoring using the D.C. resistance technique was negligible.

The D.C. electrical resistance technique of crack growth measurement was first developed by Barnett and Troiano[118] to allow analysis of crack growth kinetics in an investigation of hydrogen embrittlement in sharply notched round tensile specimens. The basis for this technique is when a current is passed through a body containing a discontinuity e.g. a crack, there will be a disturbance of the potential field in the region of the crack. As the crack grows, the p.d. developed between fixed points on either side of the crack will increase provided the current is maintained at a constant value.

In the present investigations a 30 ampere current was supplied to the specimen leads on either side of the specimen from a commercially available power pack (Farnell Instruments. Model F211) and the potential drop developed across the crack monitored with a Servoscribe potentiometric recorder. The schematic circuit arrangement is shown in Fig. 2.12.

To prevent parasitic currents, the specimen was electrically insulated from the test machine with thin mica strips.

In a report by McIntyre and Priest[119] the electrical resistance technique is described in great detail and calibration curves for several specimen types are included. Fig. 2.13 taken from their work shows typical calibration curves for C.K.S and ½ in. T-type W.O.L. specimens. It is apparent that most of the curves are characterised by an initial linear relationship between p.d. and crack length up to the so called limit of linearity, followed by a region of more rapidly increasing p.d. per unit increase in crack length. Consequently, for a given specimen type and in the absence of any complicating sources of error; it is reasonable to assume that if crack growth is not allowed to exceed the 'limit of linearity' then the p.d. can be taken to be a linear function of crack growth. McIntyre and Priest, by measuring crack growth using both resistance and ultrasonic techniques simultaneously have shown the D.C. resistance technique to be susceptible to two sources of error. The first is associated with crack front curvature; and the second from the rough fracture surfaces generally encountered in stress corrosion tests coupled with the small crack opening displacements at the relatively low stress intensities employed.

The former is a common source of error in any crack monitoring system and its effects can only be

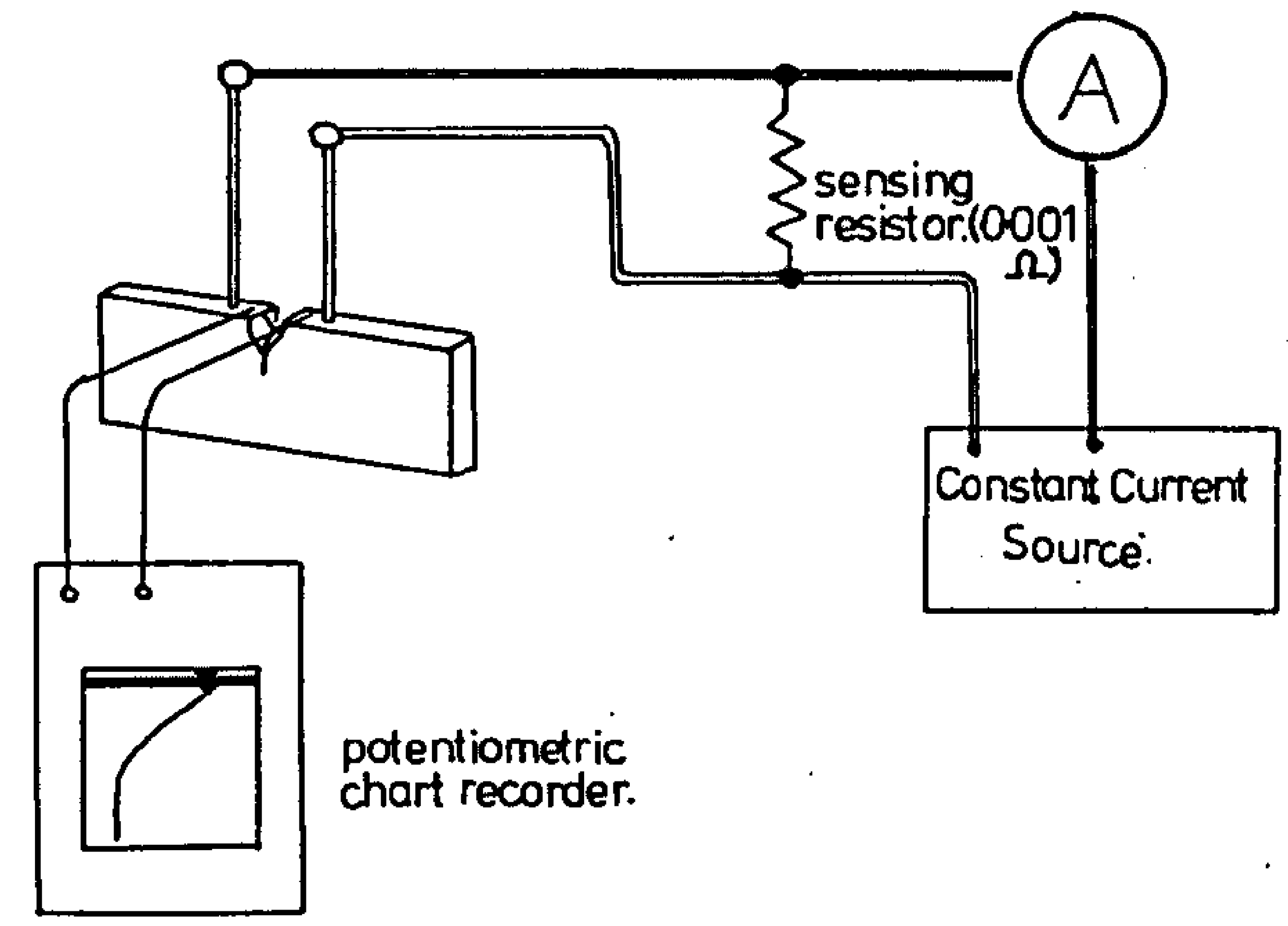

Fig. 2.12 Schematic circuit diagram for the D.C. electrical resistance technique for crack growth monitoring.

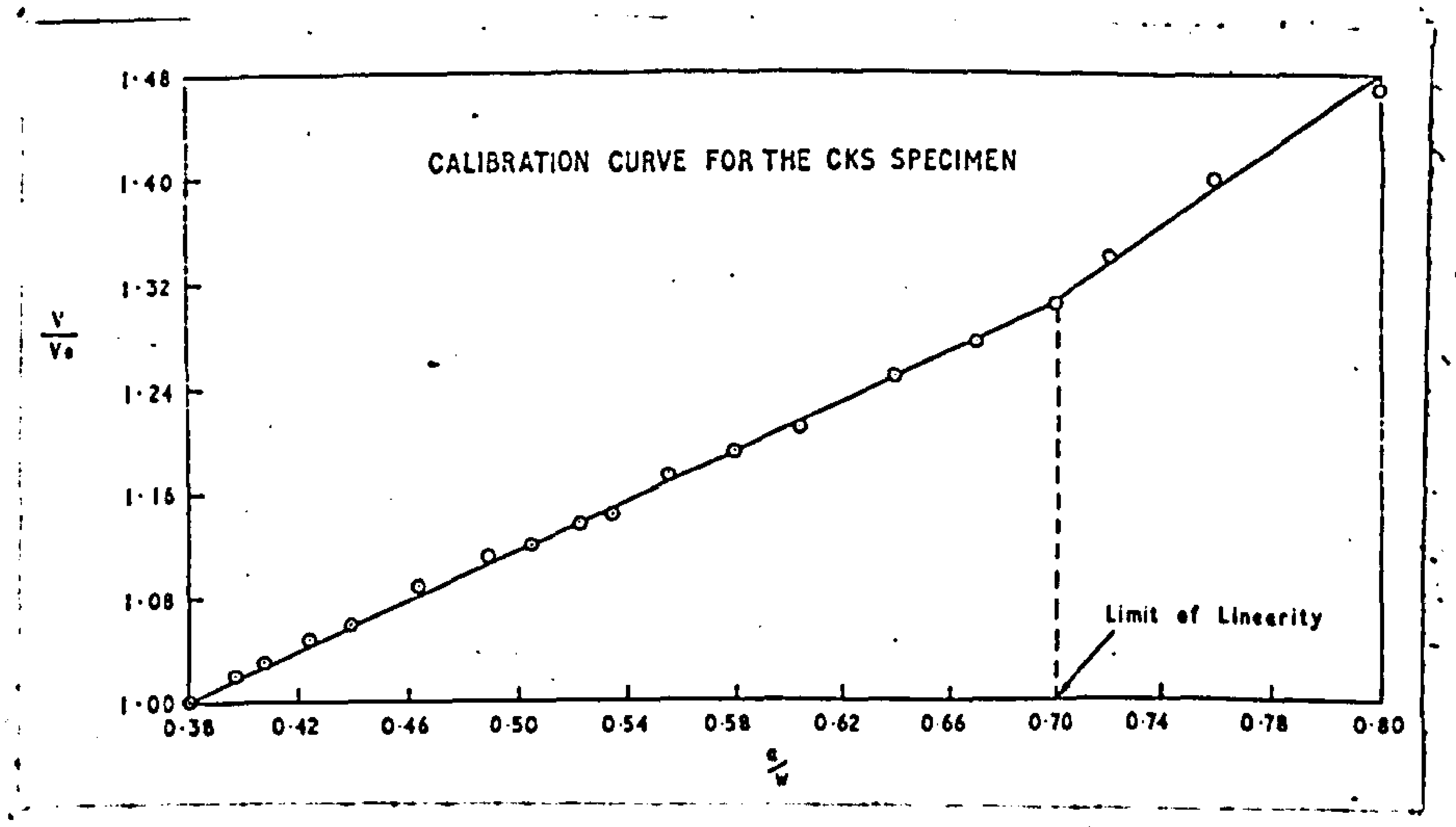

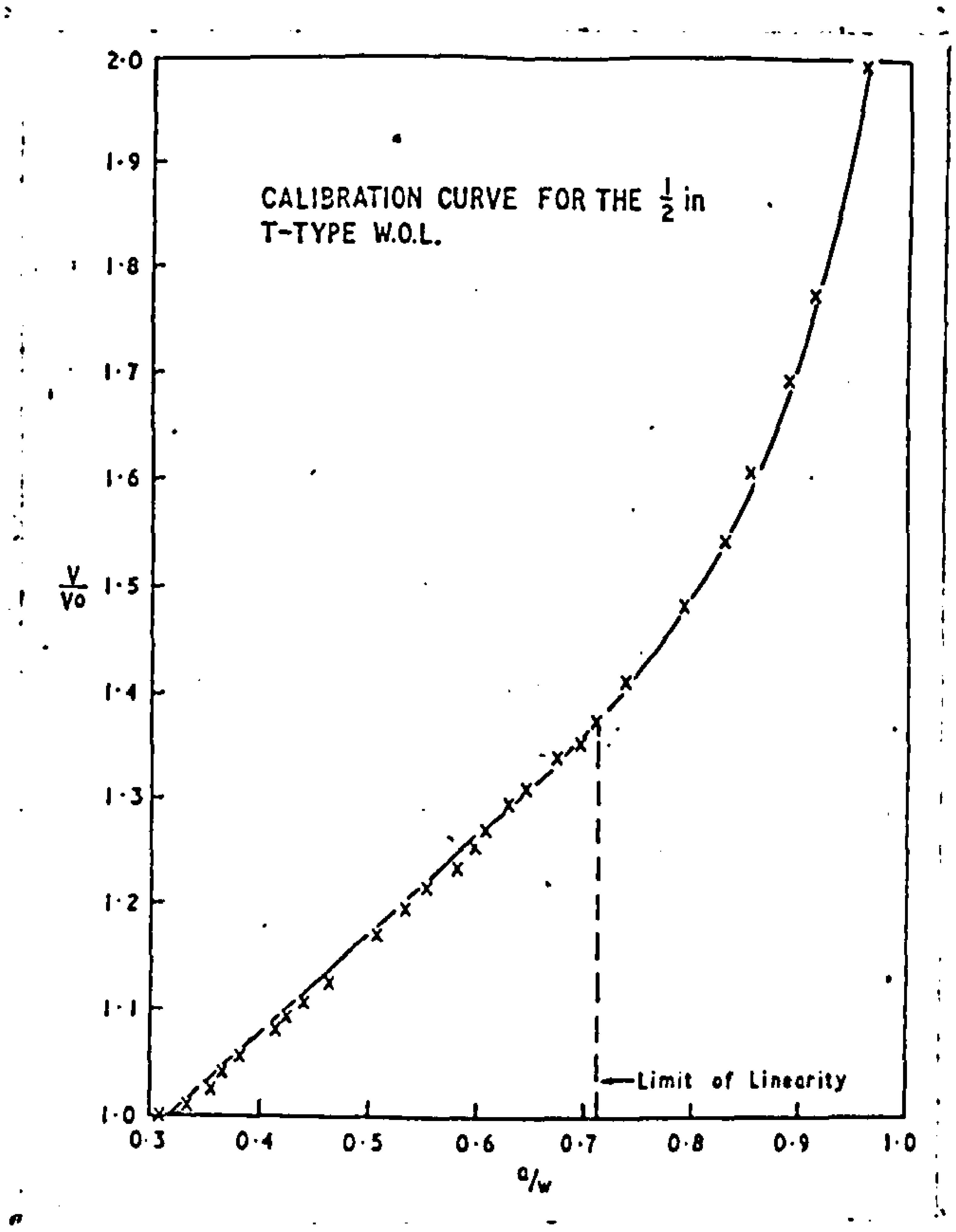

Fig. 2.13 D.C. electrical resistance technique. Calibration curves for C.KS and ½IN. T. TYPE W.O.L specimens.119

eliminated by checking the curvature of the crack front after testing and rejecting results of those tests on which crack front curvature was deemed to be excessive. The two factors contributing to the second source of error act together to produce what has been termed the 'interlocking zone' by McIntyre and Priest in which incomplete separation of the fracture surfaces behind the crack front results in short circuiting of the current and a corresponding reduction in the potential drop across the crack compared with that obtained across a saw-cut of the same length during the calibration procedure.

McIntyre and Priest describe a calibration procedure for ½ in C.K.S. specimens in which the effect of short circuiting was taken into account. The assumption was made that in specimens such as the C.K.S. specimens where the stiffness of the arms is such that complete separation of the crack faces does not occur prior to final failure by rapid fracture, the extent of short circuiting increases in proportion to crack growth. Measurement of the mean length of the S.C. crack from the fracture surface enabled the potential drop that would have occurred in the absence of any short circuiting to be derived from the calibration curve. The expected change in p difference was then compared with the actual change in p.d. recorded during the test and the change in p.d. at any time during a test was then multiplied by a correction factor equal to the ratio of the two.

In the present investigations, because of this uncertainty as to the effect of the 'interlocking zone', it was decided to determine the limit of linearity for each specimen type employed and thereafter ensure that in actual

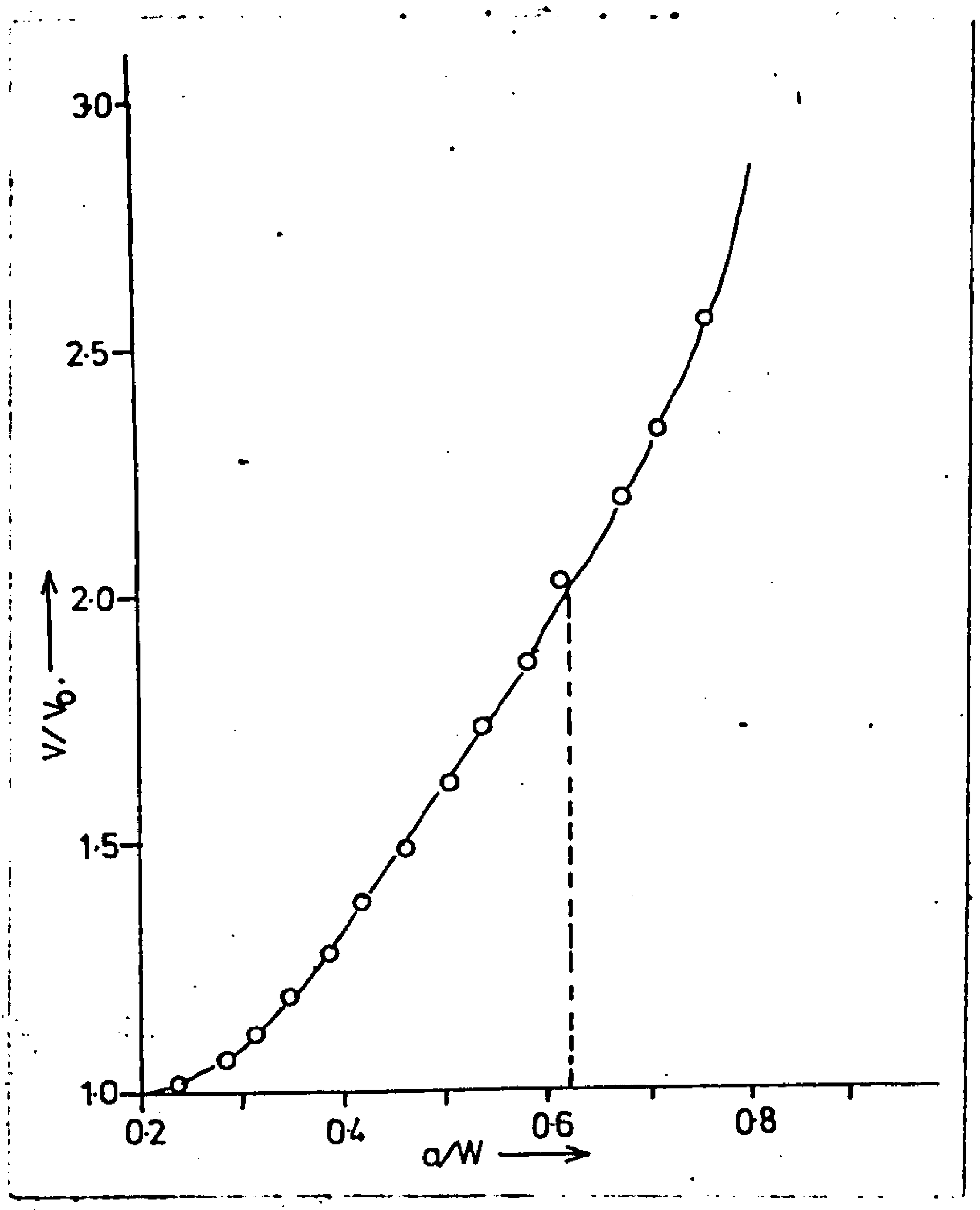

Fig. 2.14 Calibration curve for 0.3" x 5" x 1" cantilever bend specimens. (Nomenclature Vo = initial p.d. across crack, V = p.d. across crack at crack length, a and W = height of specimen).

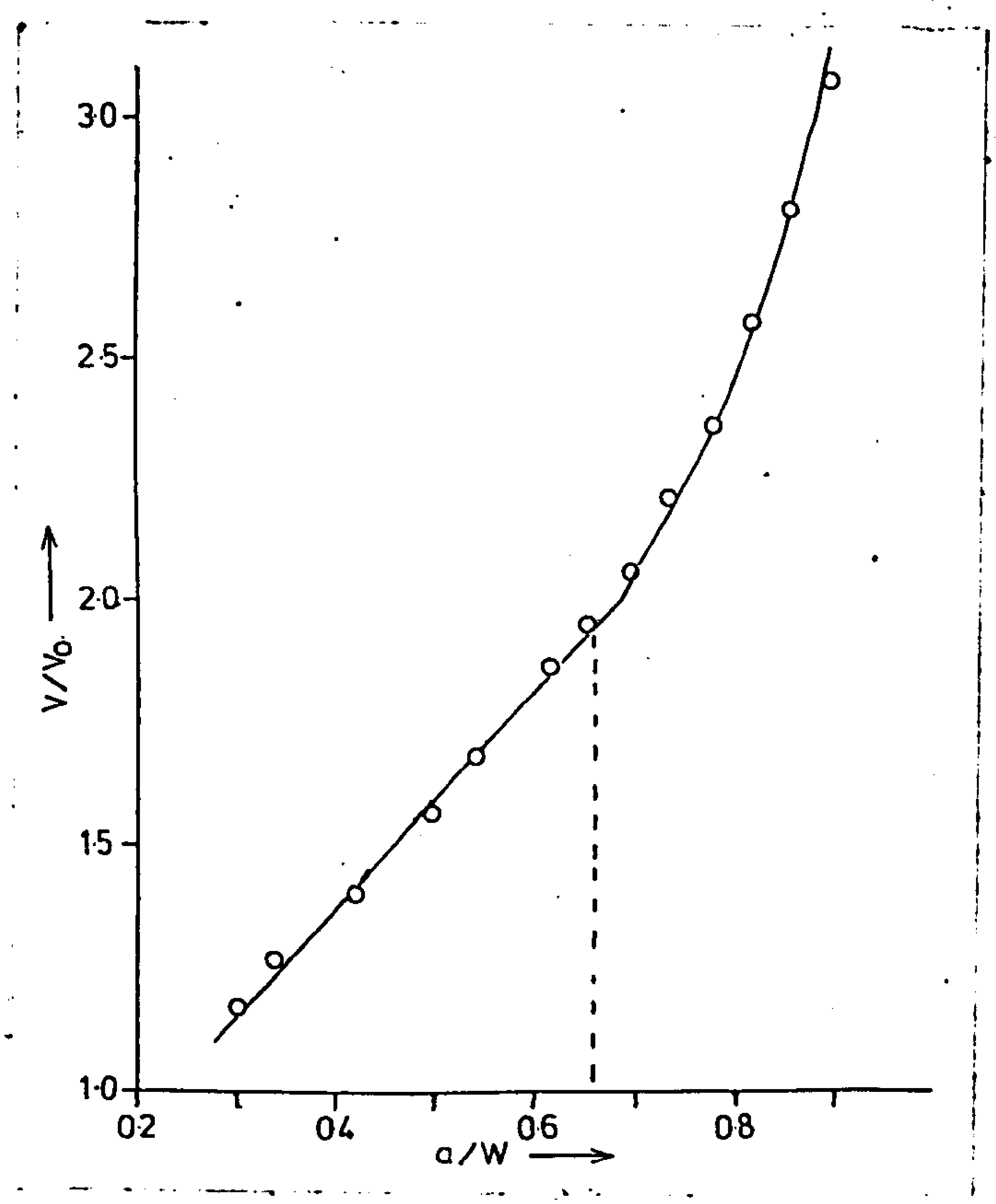

Fig. 2.15 Calibration curve for the 0.2" x 4" x 1" single edge notch tensile specimens (Nomenclature as in Fig. 2.14).

stress corrosion tests cracking did not exceed that crack length corresponding to the limit of linearity. The simplified assumption was then made that the p.d. difference remained linear with crack growth so that, in effect, each specimen was self calibrating. Fig. 2.14 shows the calibration curve for the 0.3" x 5" x 1" cantilever bend specimens determined by sawing an artificial crack with a jeweller's saw (blade thickness .008"). The initial portion of the curve, at values of $^a/W \leqslant 0.3$, is curved upwards because the saw cut was made from the tip of the chevron fatigue starter notch which was machined to a total depth of 0.3in in these specimens. From this curve the limit of linearity for the 0.3" thick cantilever bend specimens was deduced to occur at a value of $^a/W = 0.65$.

Fig. 2.15 shows the calibration curve for the 0.2" x 4" x 1" single edge notch tensile specimens which was determined by growing a fatigue precrack in the cantilever bending mode and measuring the crack growth and potential difference in situ. It was thought that this method of calibration would more closely resemble conditions in actual stress corrosion cracking tests and in particular it was felt that the degree of short circuiting in a fatigue precrack more closely approximates that of a stress corrosion crack than is possible with a saw cut in which short circuiting effects are absent. The limit of linearity was assumed to occur at a value of $^a/W = 0.65$.

c) Acoustic Emission Investigations on S.E.N. Tensile Specimens

Fig. 2.16 shows a schematic diagram of the acoustic emission equipment employed. The piezo-electric

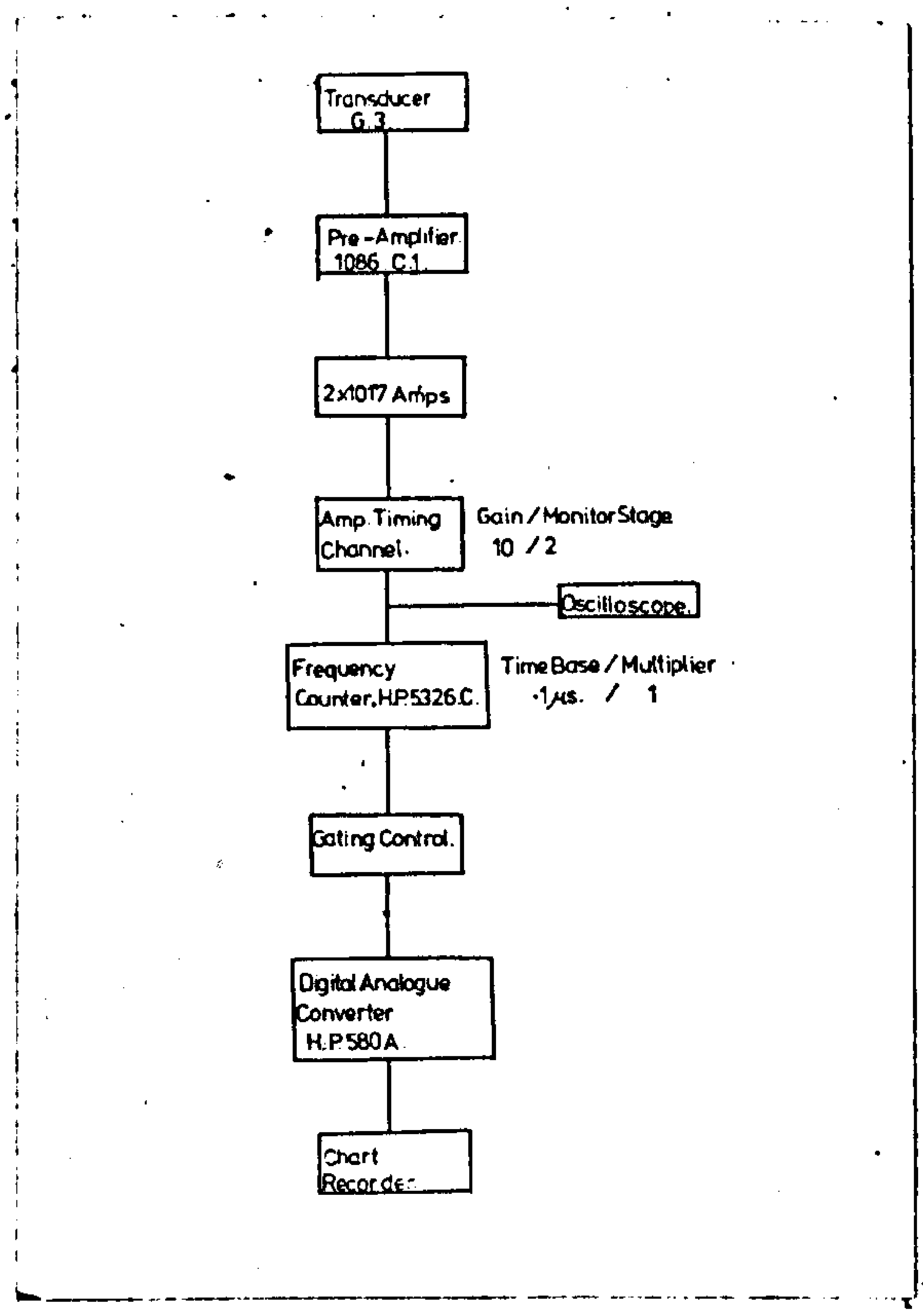

Fig. 2.16 Block diagram of the acoustic emission equipment.

transducer, developed at the Admiralty Materials Laboratory, Poole, Dorset was in the form of a 3mm cube of P.Z.T. 5A piezo-electric ceramic bonded to a brass shim inside a housing of very low transfer impedance and working at its resonance frequency of 372 KHZ. The signal from the transducer was fed into a high impedance, low noise pre-amplifier (24dB gain, $1mV/\sqrt{H_Z}$ noise level; $.1 \rightarrow 1MH_Z$ band width) before further amplification and data processing. The sensitivity of the transducer was arbitrarily set at between -87 and -88 dBM using a Dunegans S9201 (Serial No. AB01) transducer driven from a signal generator at the resonant frequency of 372 KH_Z. Standard 0.2" thick x 1" high single edge notch pin loaded tensile specimens were employed in these

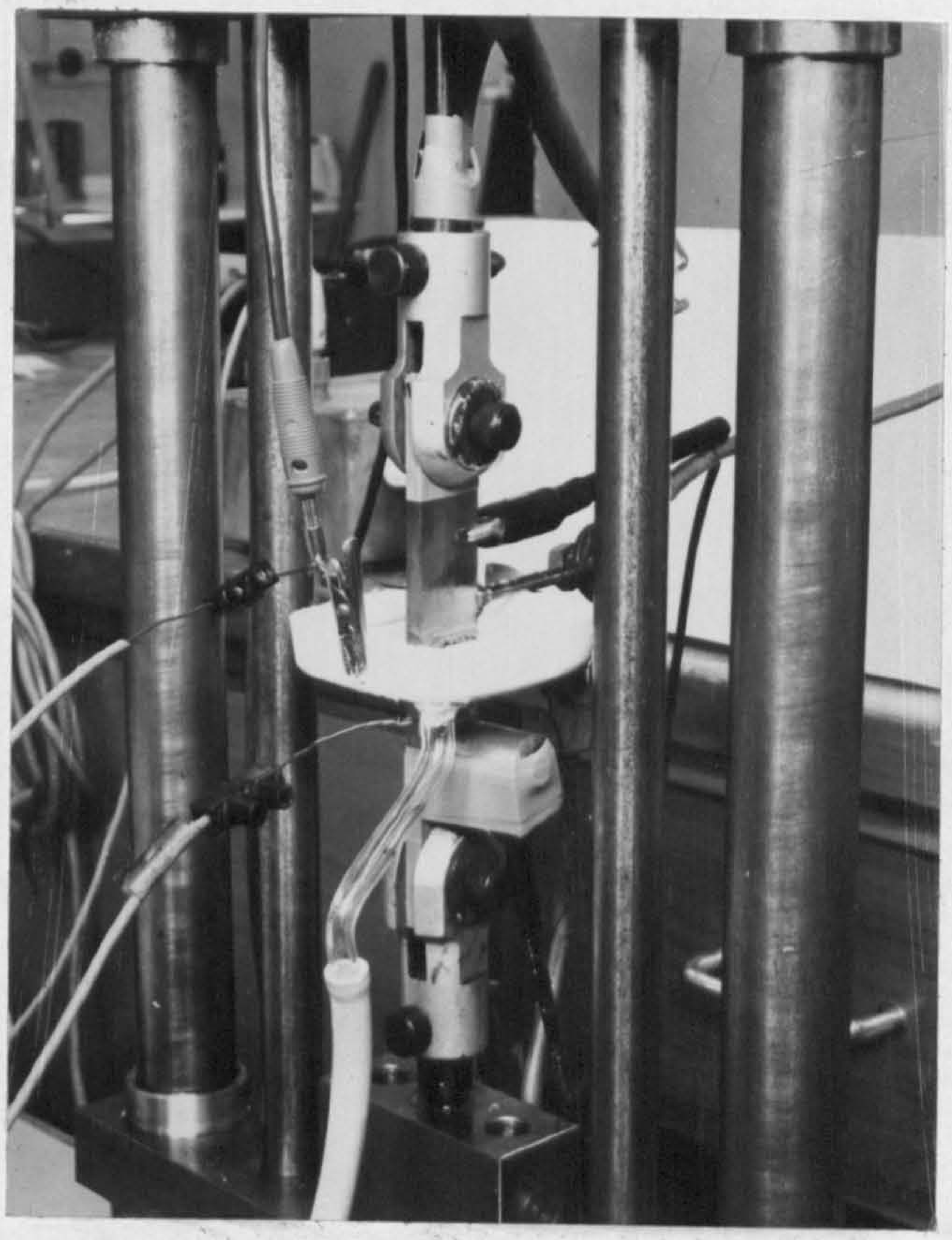

Fig. 2.17 Arrangement of specimen and acoustic emission transducer in acoustic emission experiments.

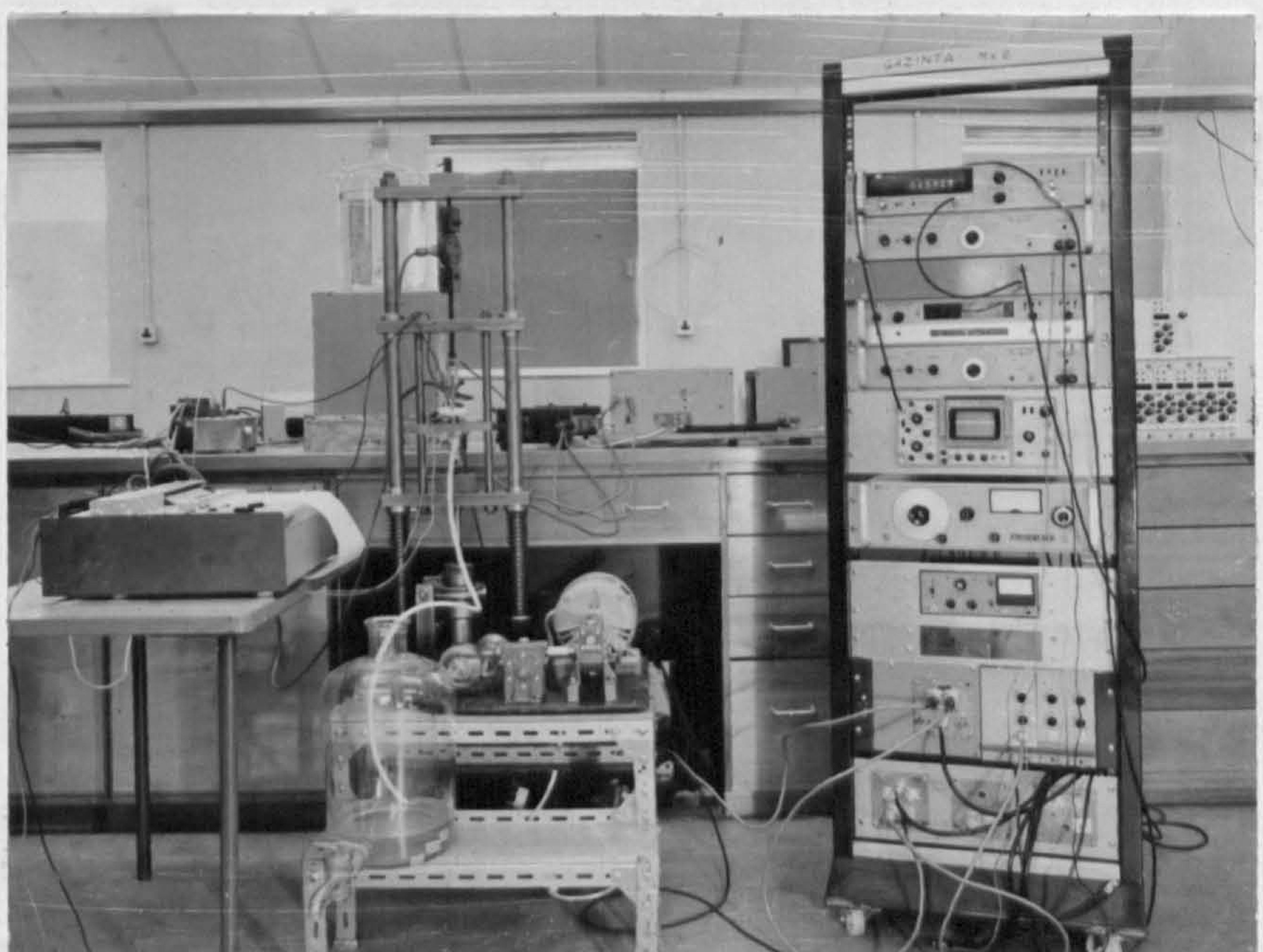

Fig. 2.18 Full experimental set-up for acoustic emission experiments.

investigations, but the total length of the specimens was increased to 6" to accommodate the piezo-electric transducer. The specimens were loaded to the desired stress intensity level on a hardbeam tensometer (described previously) and the crosshead locked in position.

All tests were performed in a 3.5 wt % sodium chloride solution of 'as made up' pH (6.0) and polarization applied to the specimen, as required, using a simple galvanostatic circuit (described previously). Crack initiation and propagation was monitored continuously throughout a test using the D.C. electrical resistance technique.

Fig. 2.17 shows the specimen in position on the hardbeam tensometer with corrosion cell, current and p.d leads for the D.C. electrical resistance crack monitoring technique and acoustic emission transducer attached. Fig. 2.18 shows the full experimental set-up. In certain tests it was found desirable to continuously replenish the test solution within the corrosion cell. This was accomplished by running the solution under gravity from a reservoir through the cell.

2.4.3 Hydrogen permeation measurements

Hydrogen permeation measurements were performed by an electrochemical technique using a permeation cell similar in design to that devised by Devanathan and Stachurski[120] for their studies of hydrogen permeation through palladium. The permeation cell used for the permeation studies is shown schematically in Fig. 2.19 and was constructed

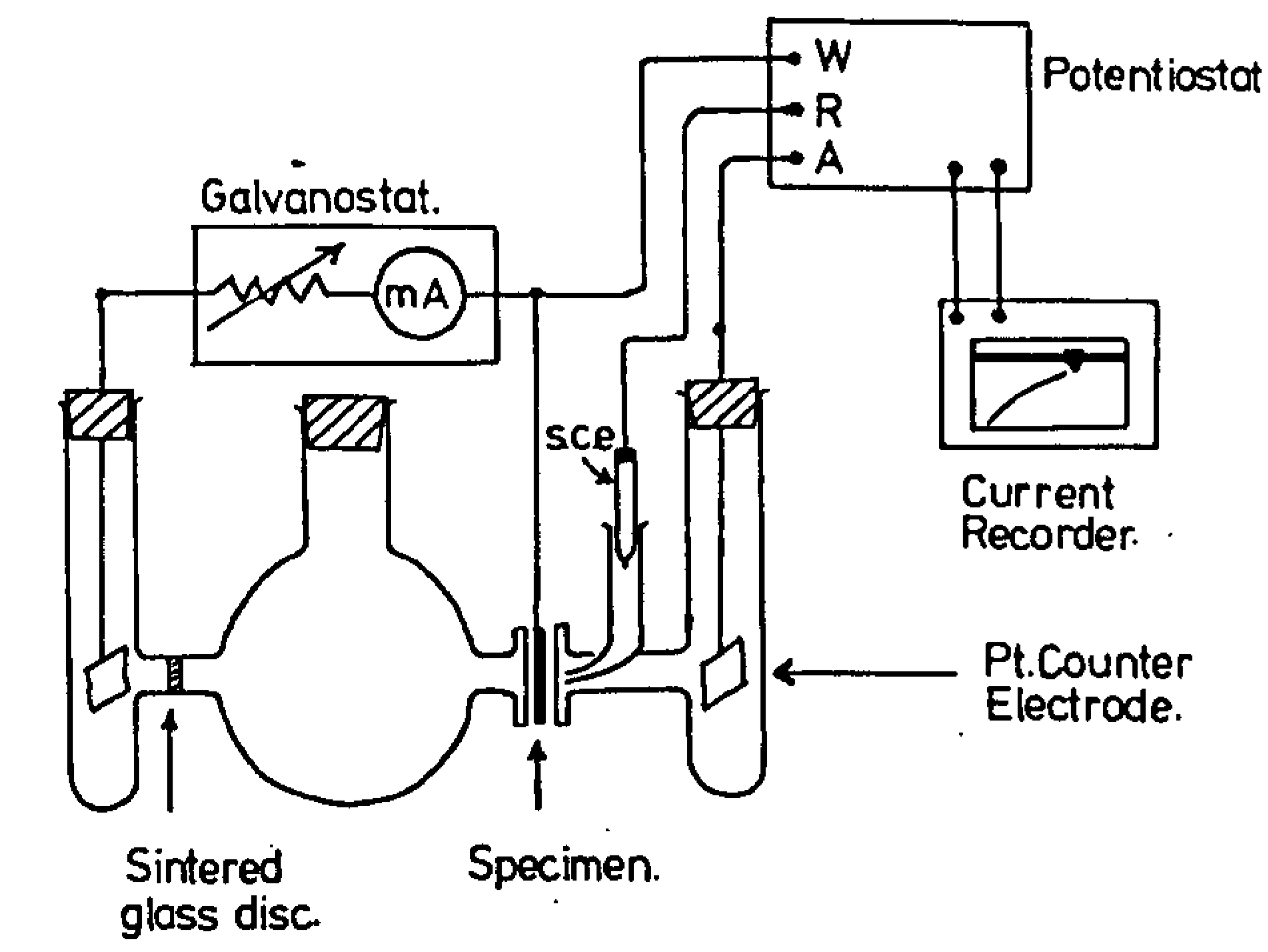

Fig. 2.19 Hydrogen permeation cell and schematic circuit diagram.

from borosilicate glassware. The cell consisted of a central compartment connected to a second compartment via a sintered glass disc in the configuration of a typical H cell. A platinum counter electrode was located in the second compartment. The working electrode was the steel membrane specimen mounted in a specimen holder of the design illustrated in Fig. 2.20. The specimen holder was clamped in position between the glass flanges; leak proof seals were provided by rubber 'O' rings located on the circumference of the specimen holder.

Hydrogen permeation fluxes were measured in N NaOH solution at +100 mV w.r.t. a saturated

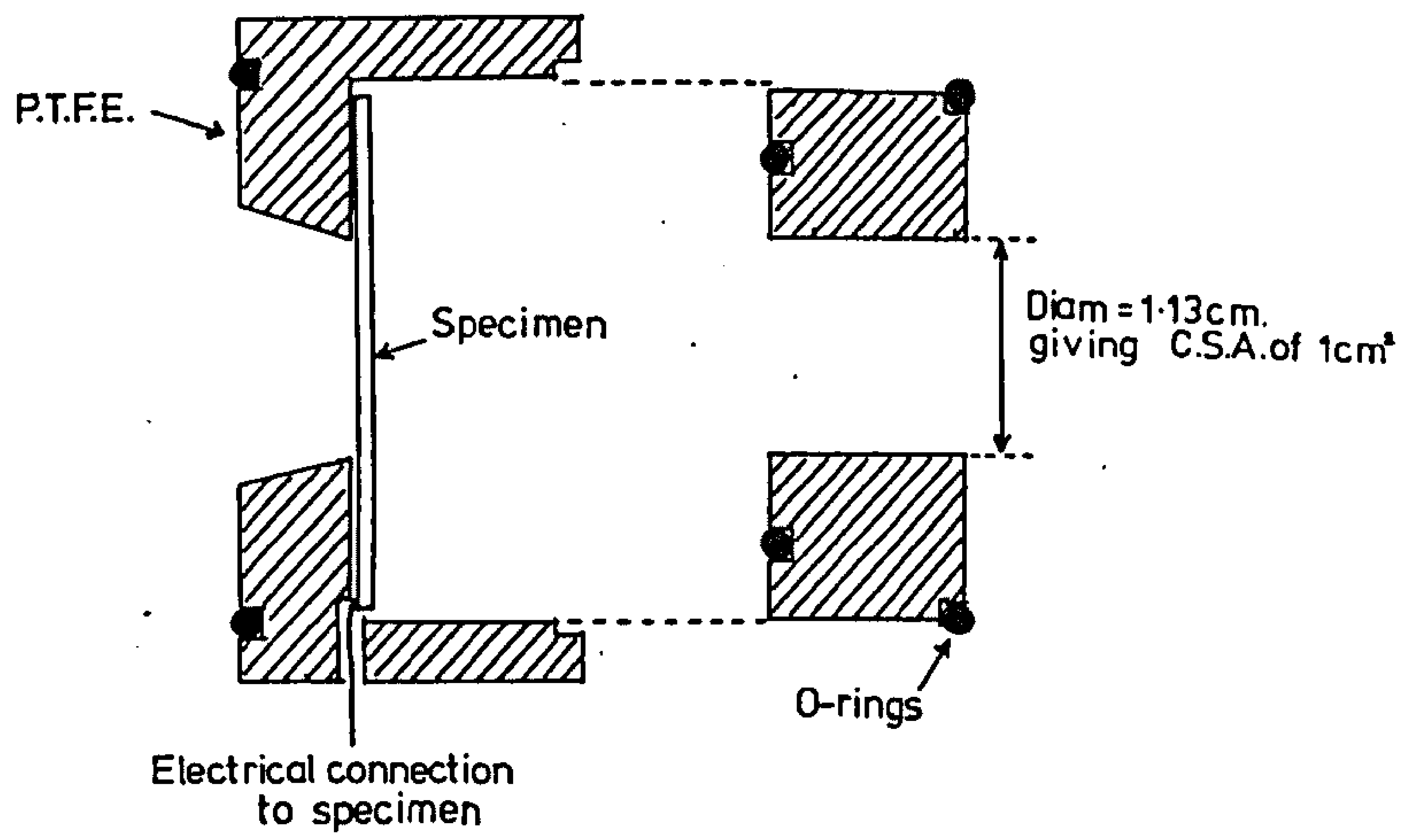

Fig. 2.20 Specimen holder for hydrogen permeation membranes.

calomel electrode at 25°C using the circuit shown in Fig. 2.19. Membranes were degreased in acetone washed in ethanol and dried before clamping between the glass flanges in the specimen holder. The 1N NaOH solution was then added to compartment D and the membrane polarized to +100 mV SCE with a Wenking Model OPA69 potentiostat and the residual current in the auxiliary current circuit monitored by measuring the p. d. across a standard resistance using a Servoscribe potentiometric chart recorder. When a steady state residual current was attained the corrodent was added to compartments A and B and the desired polarizing conditions applied to the opposite side of the membrane working electrode using the simple galvanostatic circuit described previously. The change in flux with time was recorded to a steady state.

2.4.4 Microscopy

(i) Optical microscopy

Specimens for examination under the optical microscope were prepared by mounting in bakelite, polishing on silicon carbide paper to 600 grit and finally polishing on diamond impregnated Selvyt to $\frac{1}{4}$ μm diamond. Two etchants were found to be satisfactory for etching specimens given the standard ageing heat treatments (i.e. 480-530^{o}C), These were i) aqueous ferric chloride and

ii) 1% nitric, 1% picric acid in alcohol. 30 seconds exposure time was found to be adequate for both etchants to enable the principle metallographic features to be delineated without staining. In certain cases however deliberate over etching was carried out for periods up to 4 minutes in order to emphasise certain metallographic features for examination on the scanning electron microscope.

(ii) Scanning electron microscopy

The scanning electron microscope was used in these investigations principally for examination of fracture surfaces. In such circumstances the specimens were usually mounted on .5" diameter aluminium stubs with contact adhesive, and electrical contact was provided to the specimen by a coat of silver paint applied to the junction between stub and specimen.

3 Results

3.1 The Influence of Structure on Stress Corrosion Cracking Resistance

As has been seen (cf. literature review) the influence of austenitising and ageing temperatures on the resistance to stress corrosion cracking of maraging steels has been reasonably well documented. However, most of this work has been concerned with investigating the effect of different heat treatments on the stress corrosion cracking susceptibility in aqueous environments only under freely corroding conditions. It was thought that further insight into the mechanisms of corrosion cracking of maraging steels might be obtained by determining the influence of heat treatment on the cracking susceptibility at the free corrosion potential and comparing with the corresponding influence of heat treatment on the cracking susceptibility of specimens subjected to anodic or cathodic polarisation. Consequently, constant crosshead speed tensile tests were performed at the free corrosion potential, and with the galvanostatic application of $\pm$ 10 mA to the exposed gauge lengths, in 3.5 wt % sodium chloride acidified to an initial pH of 2.0 with diluted hydrochloric acid solution, on specimens given the appropriate heat treatments.

3.1.1 The influence of austenitising temperature

Austenitising heat treatments investigated were as follows:-

1 hr at 760^{o}C, 800^{o}C, 850^{o}C, 900^{o}C, 950^{o}C, 1000^{o}C followed by air cooling and ageing for 3 hrs at 530^{o}C in all cases.

Previous work had indicated that, particularly in the case of the higher austenitising temperatures, differences in the cracking susceptibilities between specimens given different austenitising heat treatments could be slight. Consequently, preliminary experiments were carried out in which the cracking susceptibilities were determined as a function of crosshead speed for material given the 1hr 760°C and 1hr 950°C heat treatments. The results of these investigations were then used to select the most appropriate crosshead speed for subsequent investigations into the effect of the complete range of austenitising temperatures on cracking susceptibilities. Additionally, however the results would provide confirmatory evidence as to the influence of austenitising temperature on the environmental cracking resistance of maraging steels. The results are shown in Fig. 3.1.

Notwithstanding the fact that only two austenitising temperatures were investigated these results do give a favourable preliminary indication of the deleterious effect excessive austenitising temperatures have on cracking resistance irrespective of whether or not anodic or cathodic stimulation is employed. As a consequence of the form of these curves it was decided to employ a crosshead speed of 2.5×10^{-7} INS^{-1} to investigate the effect on cracking susceptibility of the full range of austenitising temperatures quoted above.

As above, failure times in solution for a given heat treatment were normalised on the corresponding air failure times; and the results plotted as normalised

Fig. 3.1 The influence of austenitising for 1hr at 760°C and 950°C on the stress corrosion cracking resistance of maraging steel specimens tested at various crosshead speeds in 3.5 wt % NaCl solution (initial pH 2.0), a) under freely corroding conditions b) with anodic polarisation (3.65 mA cm^{-2}) and c) with cathodic polarisation (3.65mA cm^{-2}) respectively.

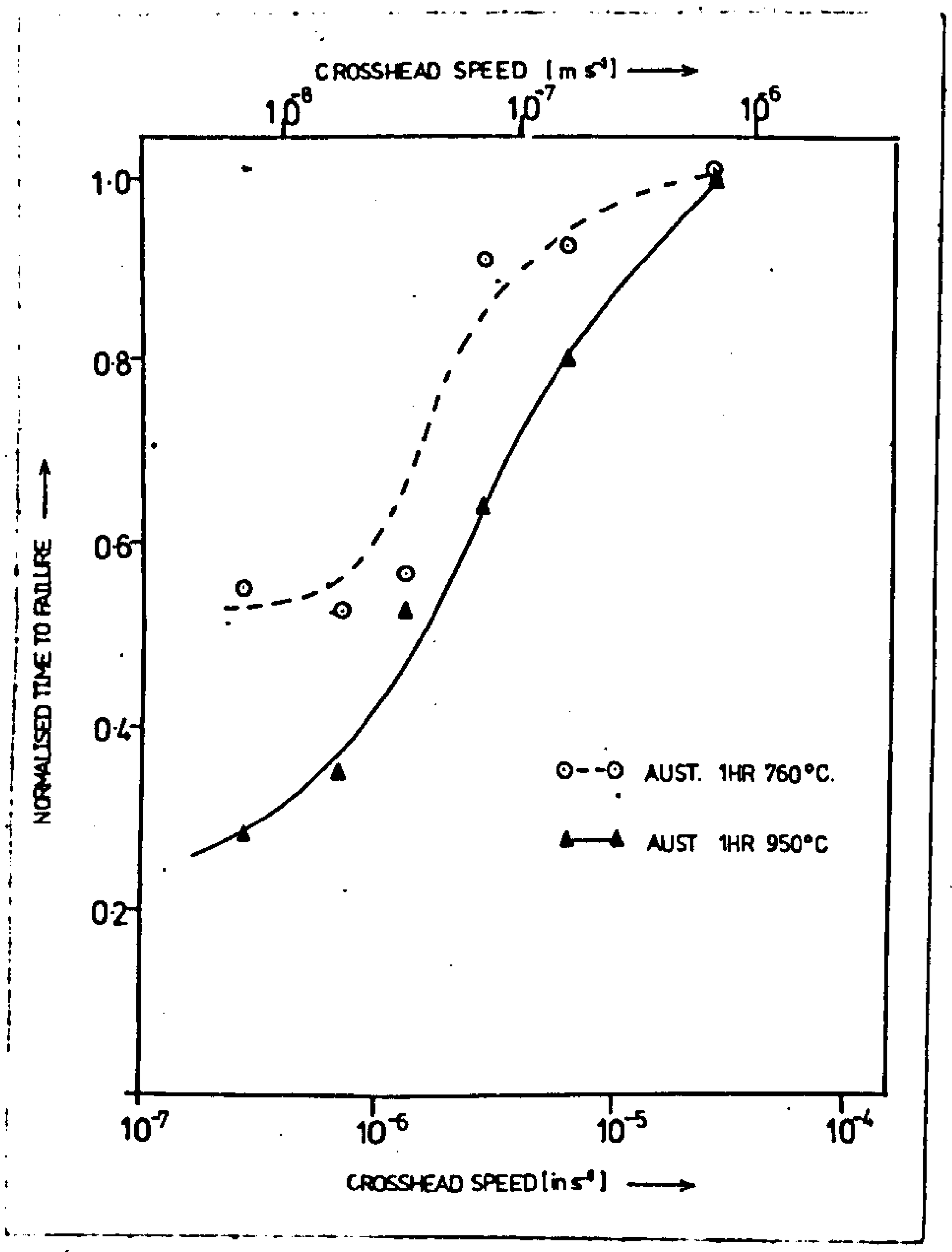

Fig. 3.1a

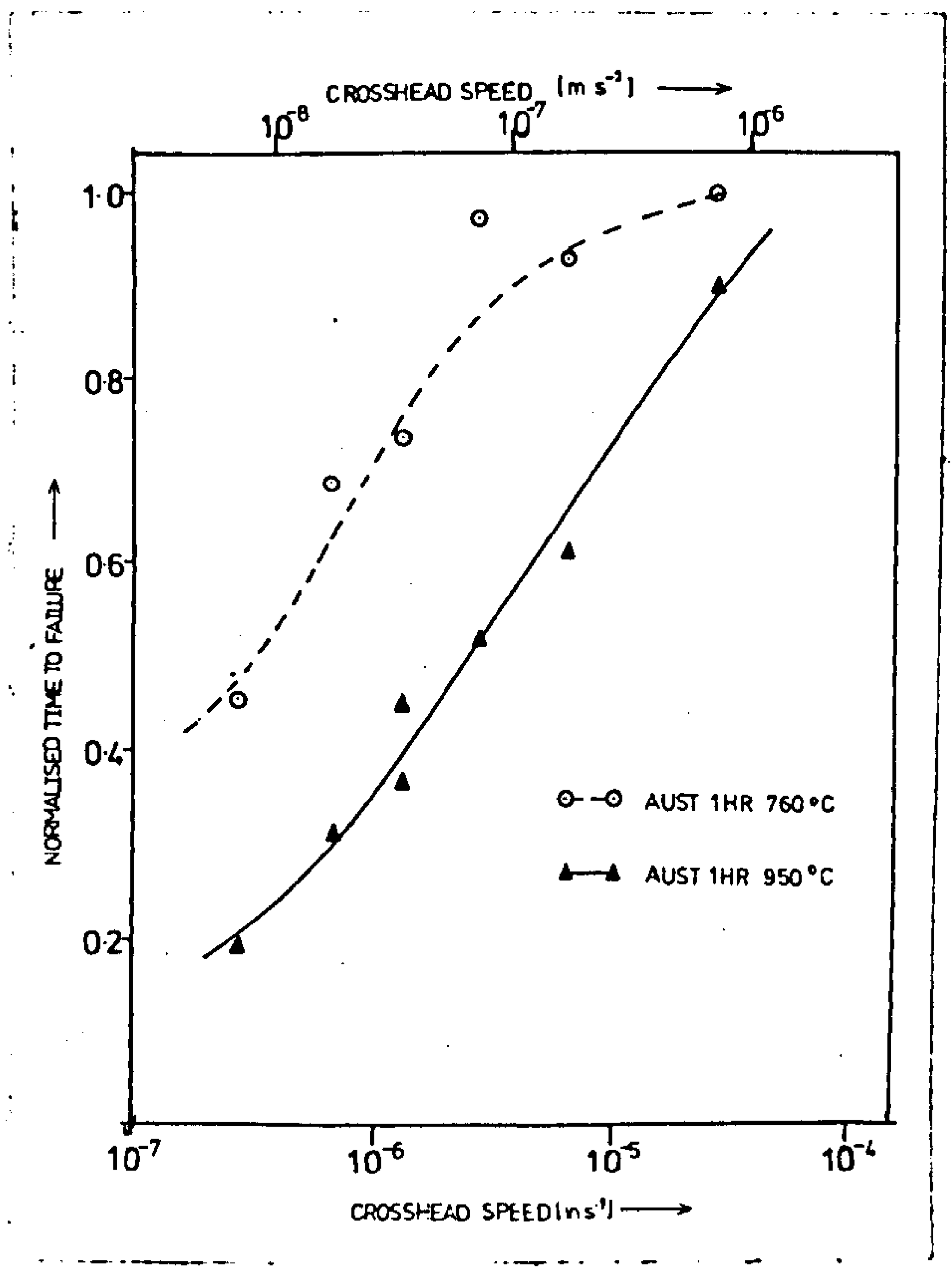

Fig. 3.1b

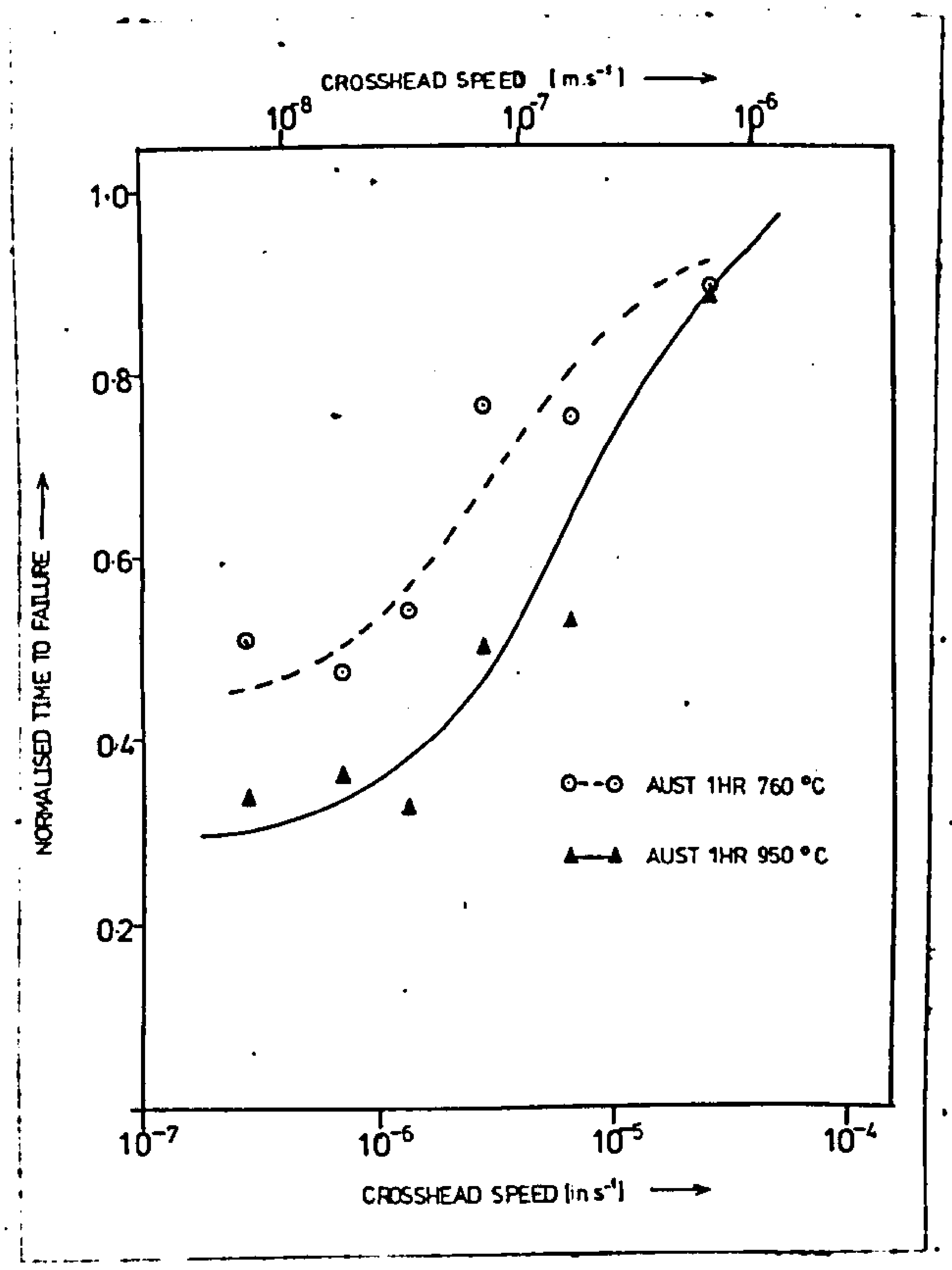

Fig. 3.1c

time to failure versus austenitising temperature. The results are shown in Fig. 3.2 and confirm the general trend suggested by the previous results i.e. that of increasing susceptibility to cracking with increasing austenitising temperature irrespective of the nature of applied polarisation.

Metallographic examination of failed specimens indicated that cracking in the more susceptible heat treatment conditions (i.e. $\gg$ 850°C) was intergranular presumably along prior austenite grain boundaries irrespective of whether or not anodic or cathodic stimulation was applied to the specimen surface. In the case of the less susceptible heat treatments (i.e. 760, 800°C) the crack path was not readily identified because of the fine grain sizes encountered however, it was thought the crack path was probably intergranular. Examination of fracture surfaces on the scanning electron microscope

Fig. 3.2 The influence of austenitising temperature on the stress corrosion cracking resistance of maraging steel specimens strained at a crosshead speed of 2.5x10^{-7} INS^{-1} in 3.5 wt % NaCl solution (initial pH 2.0), a) under freely corroding conditions b) with anodic polarisation (3.65mA cm^{-2}) and c) with cathodic polarisation (3.65mA cm^{-2}) respectively.

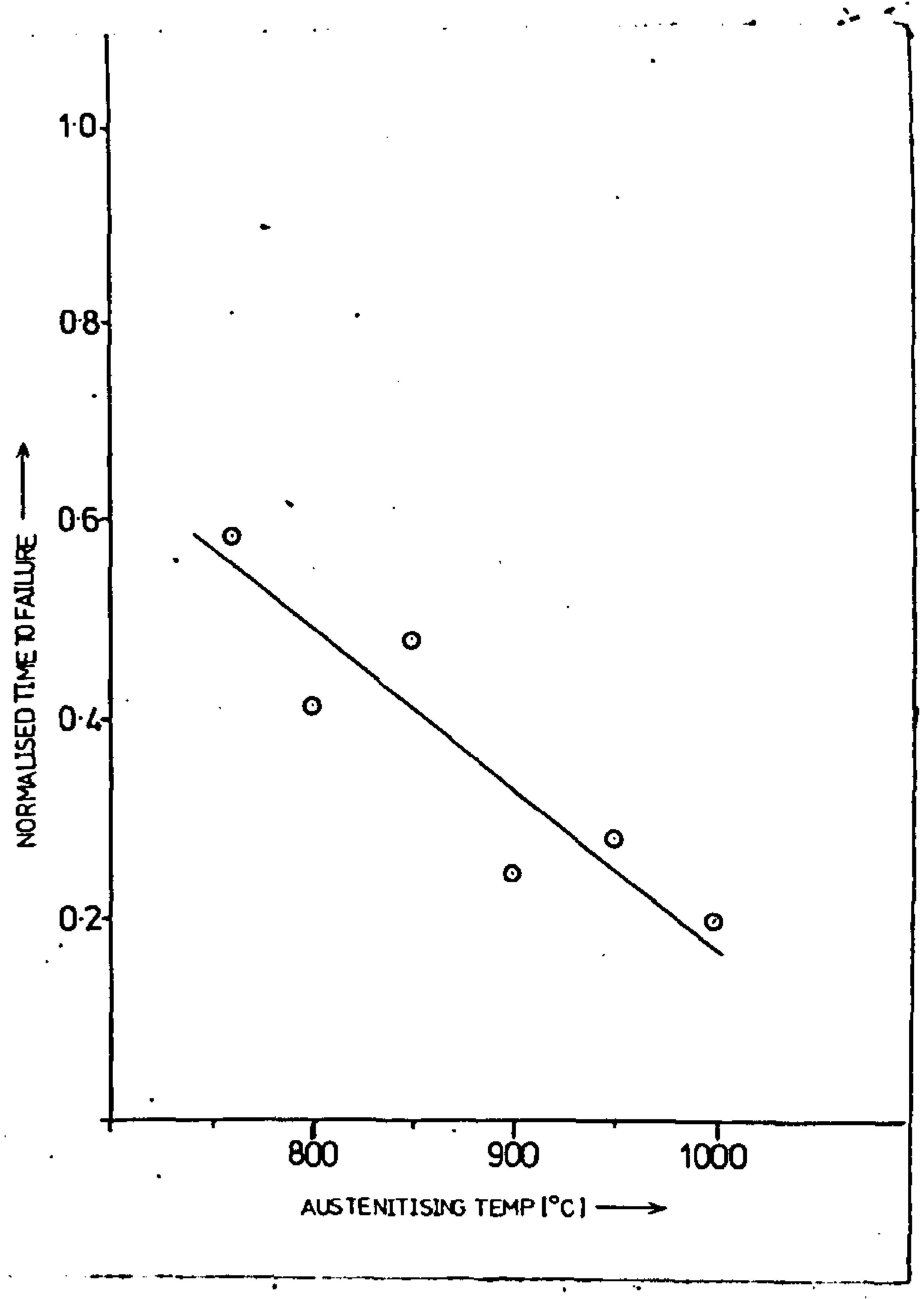

Fig. 3.2a

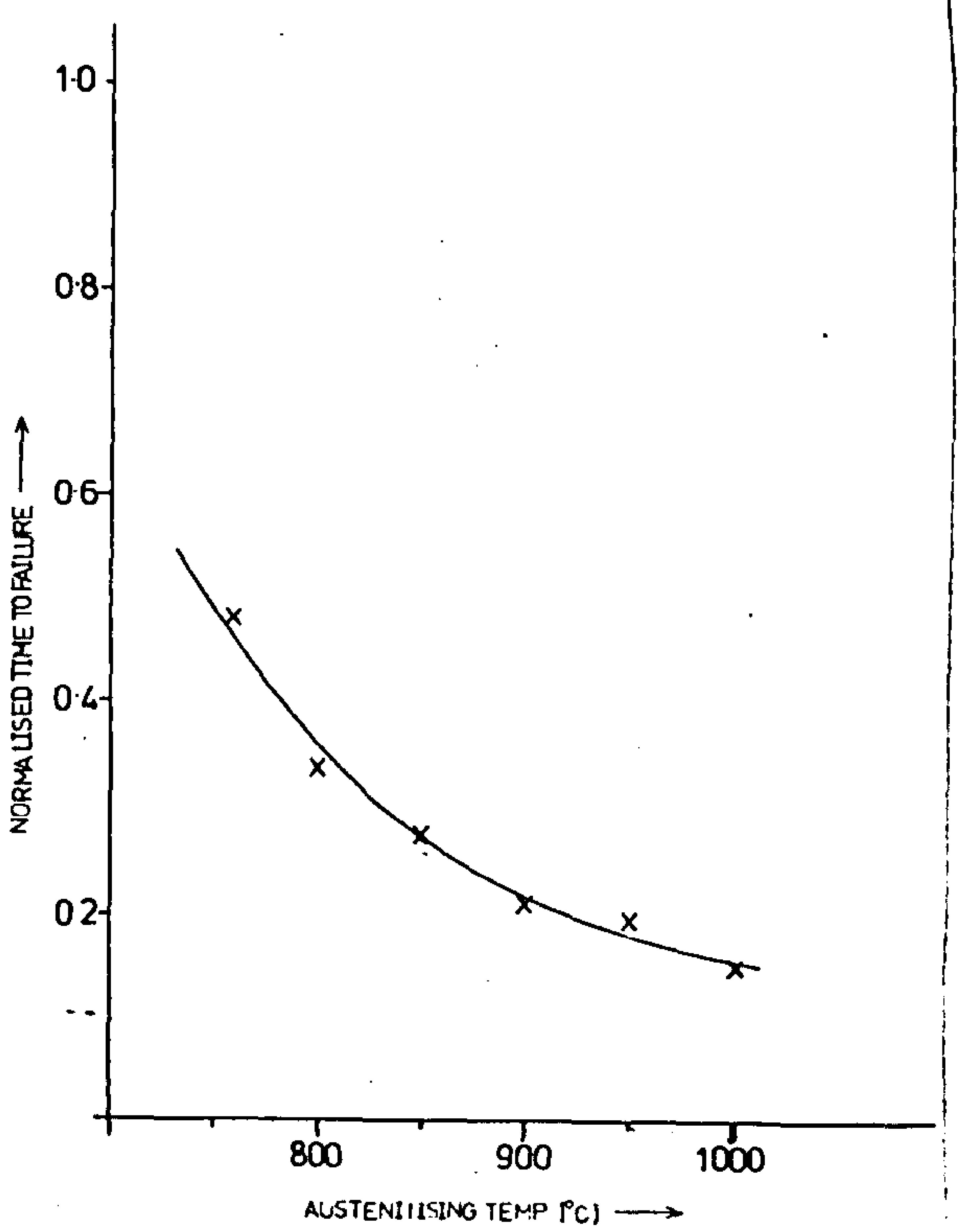

Fig. 3.2b

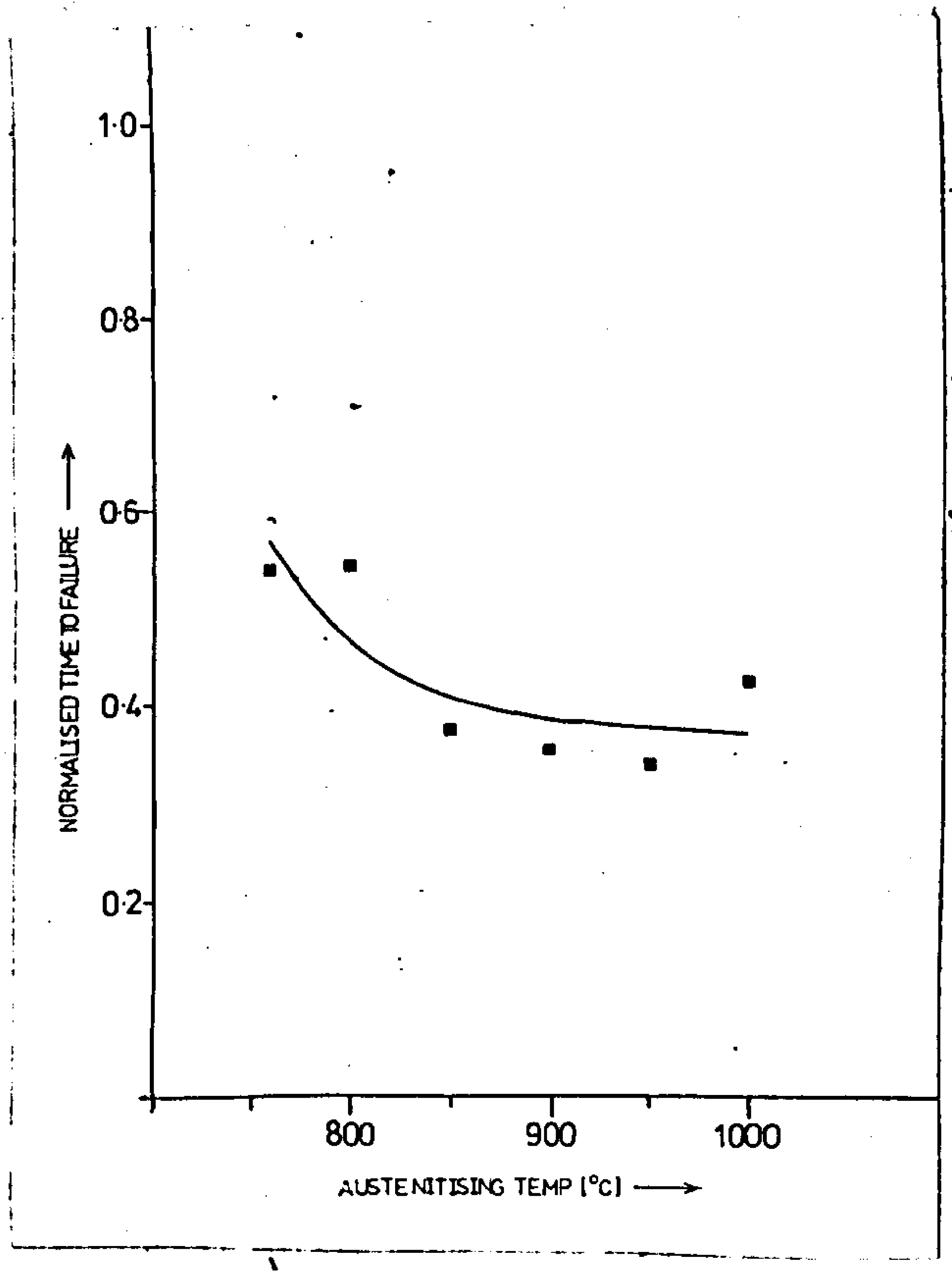

Fig. 3.2c

confirmed that the crack path in the latter cases was indeed intergranular along prior austenite grain boundaries.

Figs. 3.3, 3.4 are scanning electron micrographs of the fracture surfaces of specimens given the 800°C and 950°C austenitising heat treatment respectively. The photographs serve to demonstrate not only the intergranular nature of cracking but also the significantly different grain sizes between heat treatments producing significantly different cracking susceptibilities.

Table 3.1 lists grain diameters and ultimate tensile strengths as a function of austenitising temperature. Since grain boundaries were difficult to see on metallographic specimens, particularly at lower austenitising temperatures, grain diameters were estimated from the fracture surfaces of specimens examined on the scanning electron microscope.

Fig. 3.3 Scanning electron micrograph of the fracture surface of a maraging steel tensile specimen (Austenitised 1hr 800°C) tested at a crosshead speed of 2.5×10^{-7} INS^{-1} in 3.5 wt % NaCl (pH 2.0) under freely corroding conditions.

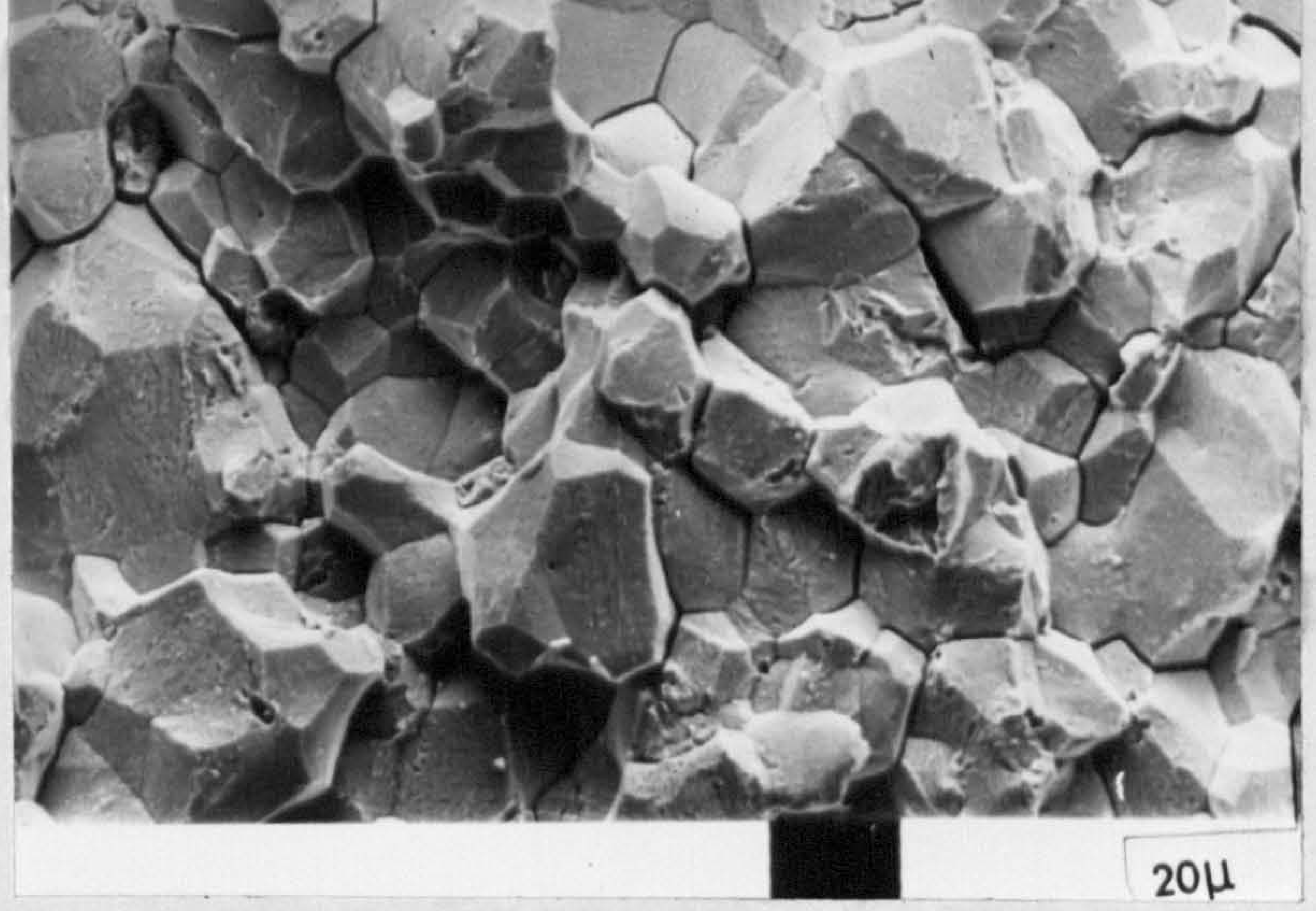

Fig. 3.4 Scanning electron micrograph of the fracture surface of a maraging steel tensile specimen (Austenitised 1hr 950°C) tested at a crosshead speed of 2.5×10^{-7} INS^{-1} in 3.5 wt % NaCl (pH 2.0) under freely corroding conditions.

TABLE 3.1

The influence of austenitising temperature on the grain diameters and ultimate tensile strength of 18 Ni maraging steel.

AUSTENITISING TEMP. (^{o}C)	GRAIN DIAMETER μm	ULTIMATE TENSILE STRENGTH p.s.i.	MNm^{-2}
760	1-3	280,000	1931
800	2-4	283,711	1956
850	5-10	289,051	1993
900	10-20	287,968	1986
950	20-40	271,203	1870
1000	40-50	277,923	1916

These results suggest there is a dependence of cracking susceptibility on grain size which is not merely related to any influence the latter may have on effecting differences in mechanical properties. The grain size dependency is probably related to a) the influence of grain size on the nature and distribution of residual elements which preferentially segregate to austenite grain boundaries during annealing

and/or (b) the influence of grain size on the size and distribution of precipitates formed during subsequent ageing.

In so far as the above results were derived from tests performed on smooth tensile specimens, and since it is known that a significant proportion of the total time to failure in smooth tensile tests can be attributed to crack initiation, then it seems reasonable to suggest that the above results simply reflect differences in crack initiation times between differently heat treated specimens rather than differences in absolute crack propagation rates.

Table 3.2 lists average macroscopic crack velocities determined on single edge notch fatigue pre-cracked, tensile specimens austenitised for 1hr at 760°C and 950°C respectively.

TABLE 3.2

The average crack velocities determined on S.E.N. tensile specimens austenitised for 1hr at 760°C and 950°C, as a function of applied current density.

APPLIED CURRENT	MEAN CRACK VELOCITY			
	1HR 760°C		1HR 950°C	
mA	INS^{-1}	ms^{-1}	INS^{-1}	ms^{-1}
-2.0	$1.3x10^{-5}$	$3.3x10^{-7}$	$1.7x10^{-5}$	$4.32x10^{-7}$
0	$1.8x10^{-6}$	$4.57x10^{-8}$	$1.0x10^{-6}$	$2.54x10^{-8}$
+2.0	$2.3x10^{-6}$	$5.84x10^{-8}$	$5.4x10^{-6}$	$1.37x10^{-7}$

Galvanostatic anodic and cathodic polarisation was performed at initial current densities approximating those used on smooth tensile specimens.

An initial stress intensity of 20 KSI $\sqrt{IN}$ was employed in all cases and crack initiation was detected using the electric resistance technique for crack growth monitoring.

Within the limits of experimental error, the above results indicate that macroscopic crack propagation rates are virtually independent of austenitising temperature.

This implies that the original supposition, (i.e. that the results obtained on smooth tensile tests reflects differences in crack initiation periods rather than differences in crack propagation rates) was correct.

3.1.2 The influence of ageing temperature

Five ageing temperatures in the range 250^{o}C to 650^{o}C were investigated in addition to material in the unaged condition. All specimens were austenitised for 1hr at 950^{o}C and air cooled prior to ageing for 3hr at 250^{o}C, 350^{o}, 450^{o}, 530^{o}, or 650^{o}C respectively.

A crosshead speed of 1.29×10^{-6} INS^{-1} was chosen for these investigations. The times to failure in solution were normalised on the corresponding air failure times and the results plotted as normalised time to failure versus ageing temperature. After failure, metallographic examination of test pieces was used to identify the crack path.

Fig. 3.5(a) shows the ultimate tensile strength plotted as a function of ageing temperature whilst Figs. 3.5(b), (c), (d), show normalised failure times as a function of ageing temperature for specimens tested at the free corrosion potential and with cathodic and anodic polarisation respectively. It can be seen from these results that there appears to be a direct correlation between tensile strength and susceptibility to environmental cracking such that maximum tensile strength corresponds almost exactly with the maximum susceptibility to cracking. Evidently these effects are related to the precipitation reactions occurring during ageing.

Fig. 3.5 The influence of ageing temperatures on a) the ultimate tensile strength and b), c), d) the stress corrosion cracking susceptibility under freely corroding conditions with cathodic polarisation (3.65mA cm^{-2}) and with anodic polarisation (3.65mA cm^{-2}) respectively of maraging steel tested at a crosshead speed of 1.29 x 10^{-6} INS^{-1} in air and 3.5 wt % NaCl solution.

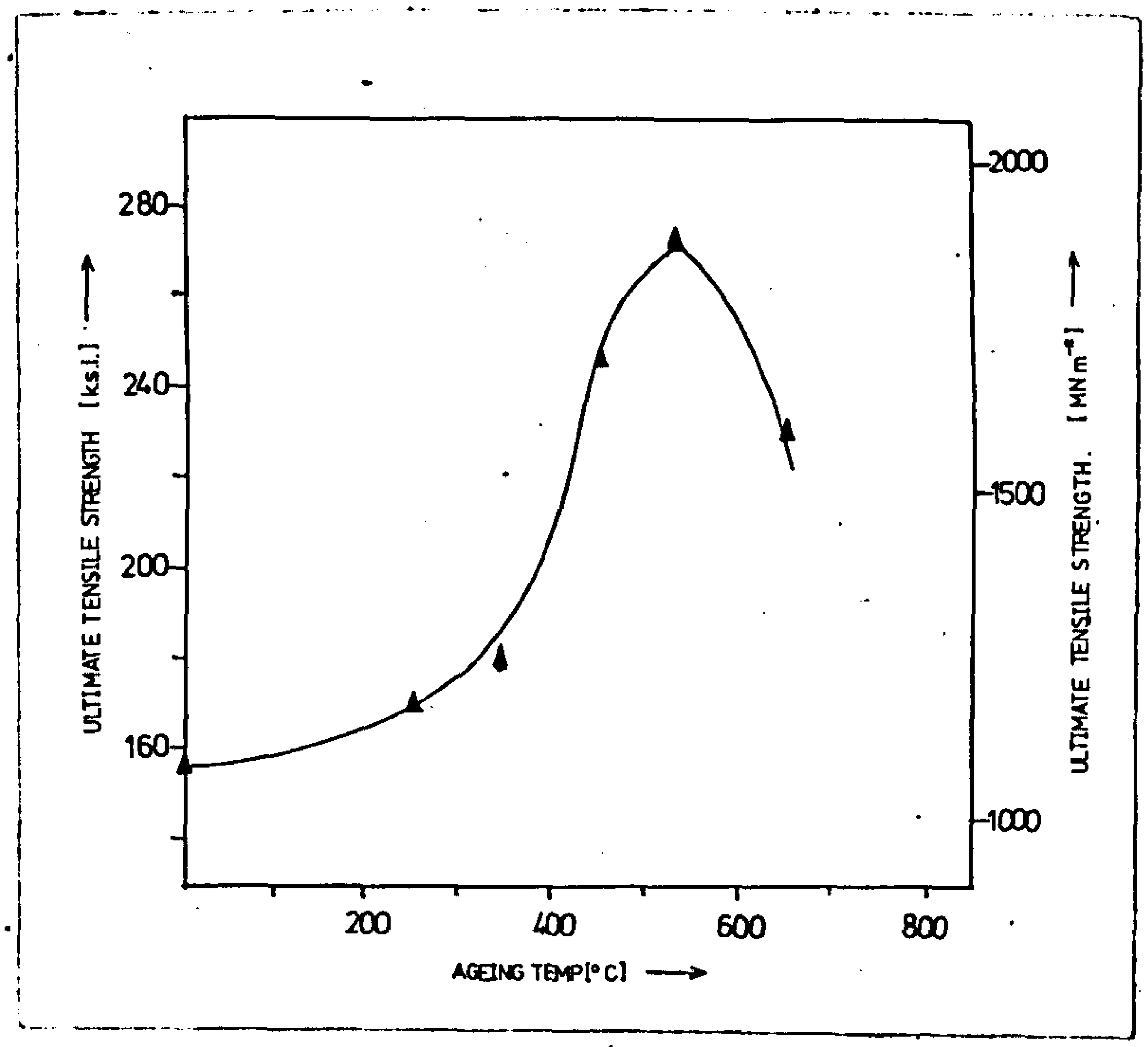

Fig. 3.5a

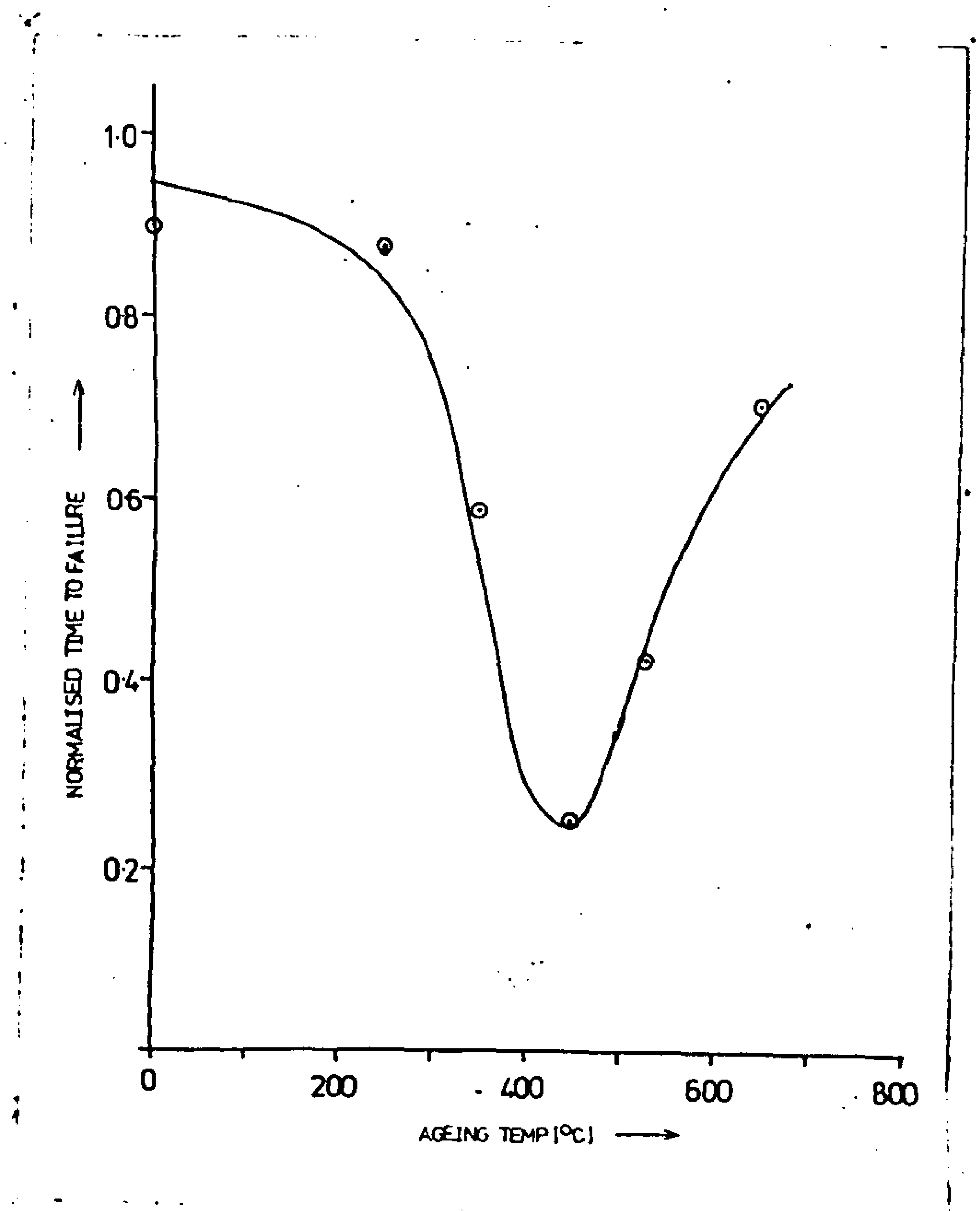

Fig. 3.5b

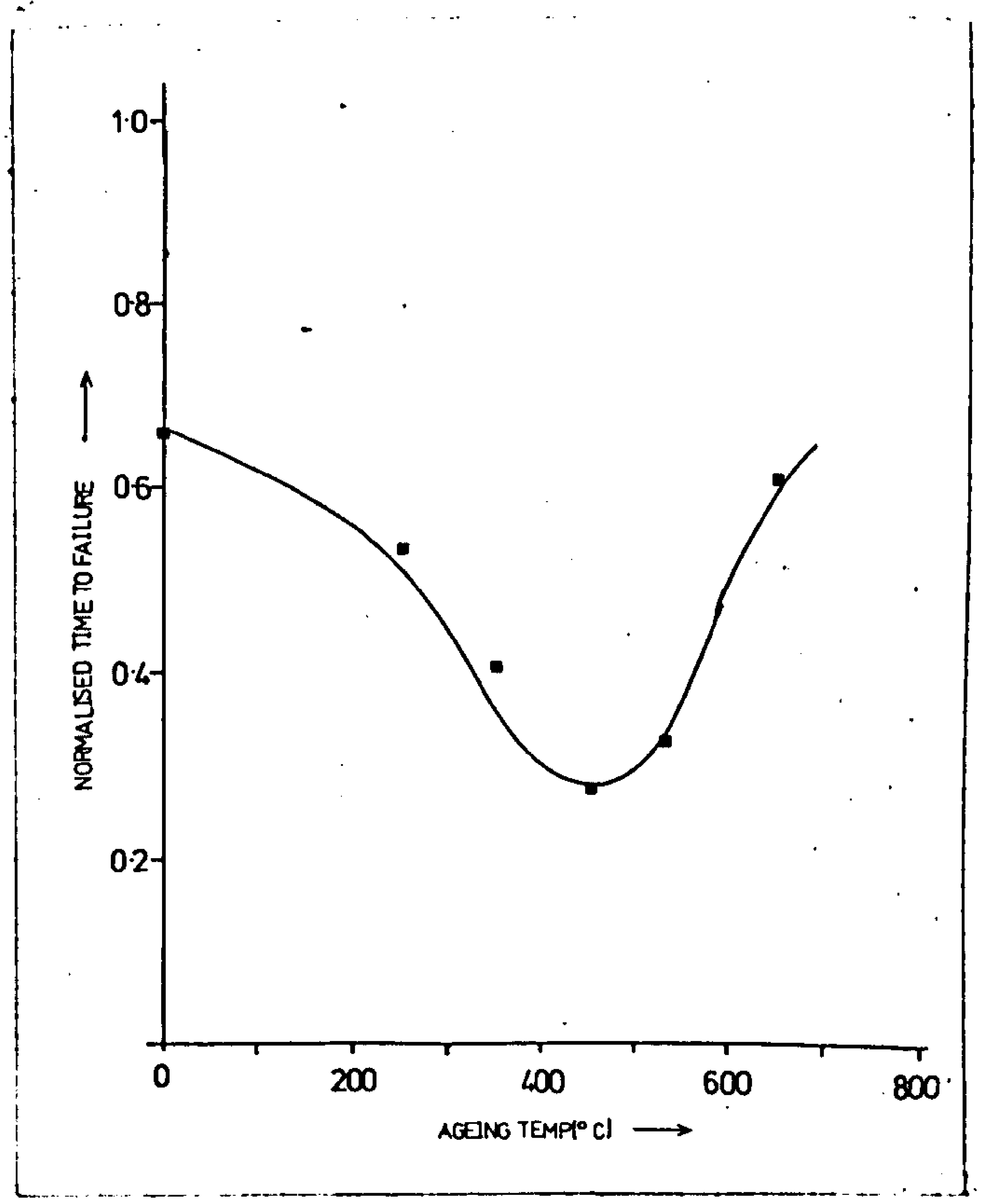

Fig. 3.5c

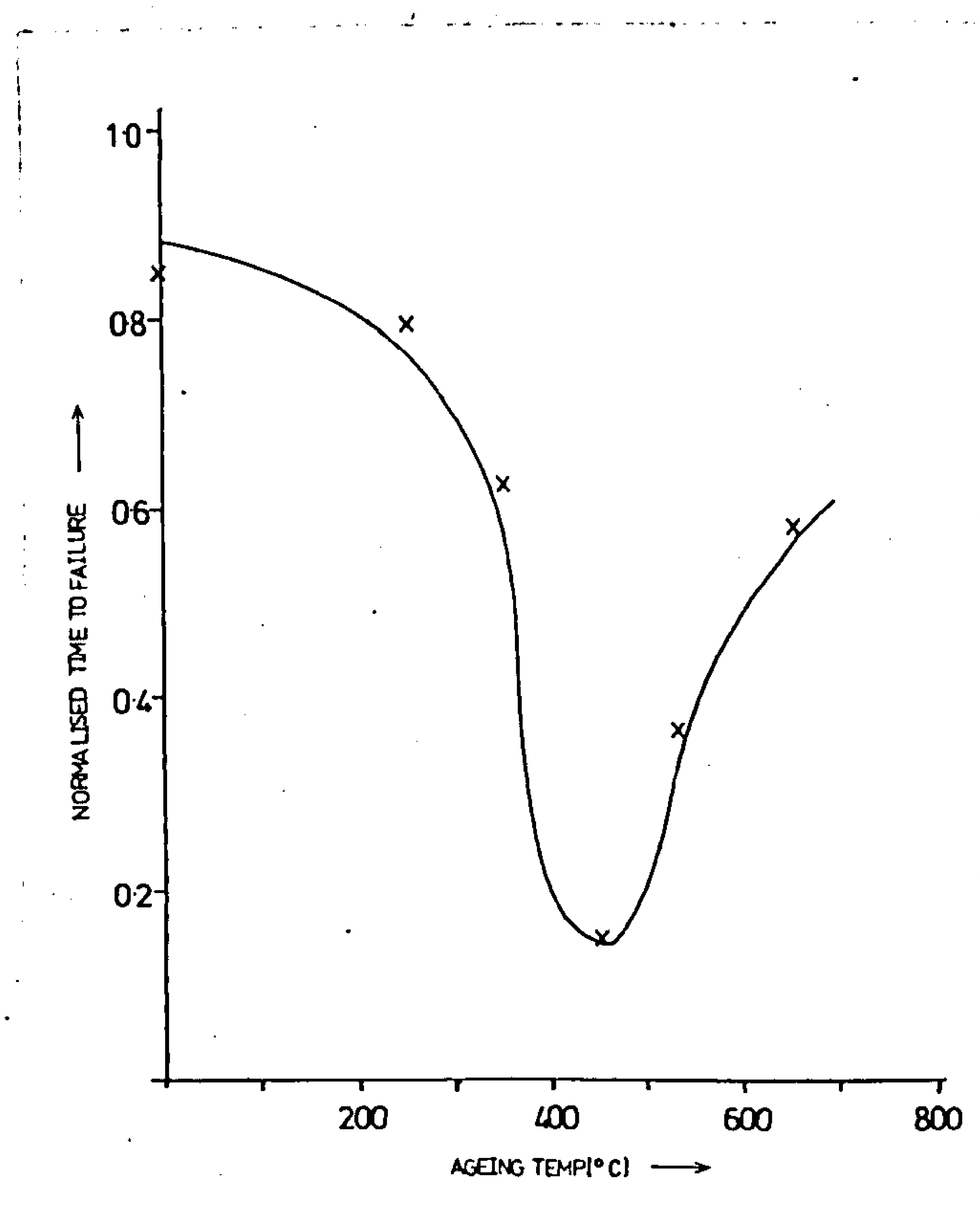

Fig. 3.5d

Furthermore the variation in cracking susceptibility with ageing temperature was associated with a corresponding change in the cracking mode from predominantly transgranular (or fissuring) below 400°C through a regime of predominantly intergranular cracking (between 400 and 600°C) and reverting to a mixed mode of cracking above 600°C. Table 3.3 summarises the cracking modes as a function of ageing temperature and applied polarisation.

The most important deduction that can be made from these results is that the precipitate formed during ageing appears to precipitate preferentially at prior austenite grain boundaries and so provides active paths for crack propagation. The similarity in cracking modes observed between anodically and cathodically polarised specimens could be cited as proof of an explanation of cracking by an all embracing hydrogen embrittlement mechanism. However, it should not be overlooked that the presence of a grain boundary precipitate can just as easily provide an active site for anodic dissolution as it can for hydrogen embrittlement especially if that precipitate is particularly active (or noble) to the matrix material. In this latter respect, for example, it has been suggested that titanium carbides (or carbonitrides) can preferentially precipitate at prior austenite grain boundaries during ageing. As will be seen in a later section, the free corrosion potential of titanium carbide is some 300-400 mV noble to the bulk free corrosion potential determined on maraging steel. Therefore, if titanium carbide precipitation occurs at grain boundaries during ageing it might be anticipated that this

TABLE 3.3

Metallographic examination of specimens aged at various temperatures

HEAT TREATMENT	APPLIED CURRENT DENSITY (mA/cm^2) -3.65	0	+3.65
Aust. 1hr 950°C; unaged.	Predominantly transgranular cracking	Transgranular fissuring especially in necked region	Transgranular fissuring
Aust. 1hr 950°C; aged 3hr 250°C.	Mixed intergranular and transgranular	Small transgranular fissures 3 grain diameters	Transgranular fissuring 5-10 grain diameters
Aust. 1hr 950°C; aged 3hr 350°C.	Predominantly intergranular cracking.	Small transgranular fissures. 3 grain diameters but principle cracks intergranular, the latter showing evidence of transgranular fissures branching out.	Transgranular fissuring 10 grain diameters deep. Evidence of intergranular cracking.
Aust. 1hr 950°C; aged 3hr 450°C.	Intergranular	Intergranular	Small V-shaped fissures intergranular cracks.
Aust. 1hr 950°C; aged 3hr 530°C.	Intergranular	Intergranular	Small V-shaped fissures intergranular cracking.
Aust. 1hr 950°C; aged 3hr 650°C.	Mainly intergranular with some evidence of transgranular.	Mainly intergranular.	Nature of cracking obscured by spongy mass of dissolution products.

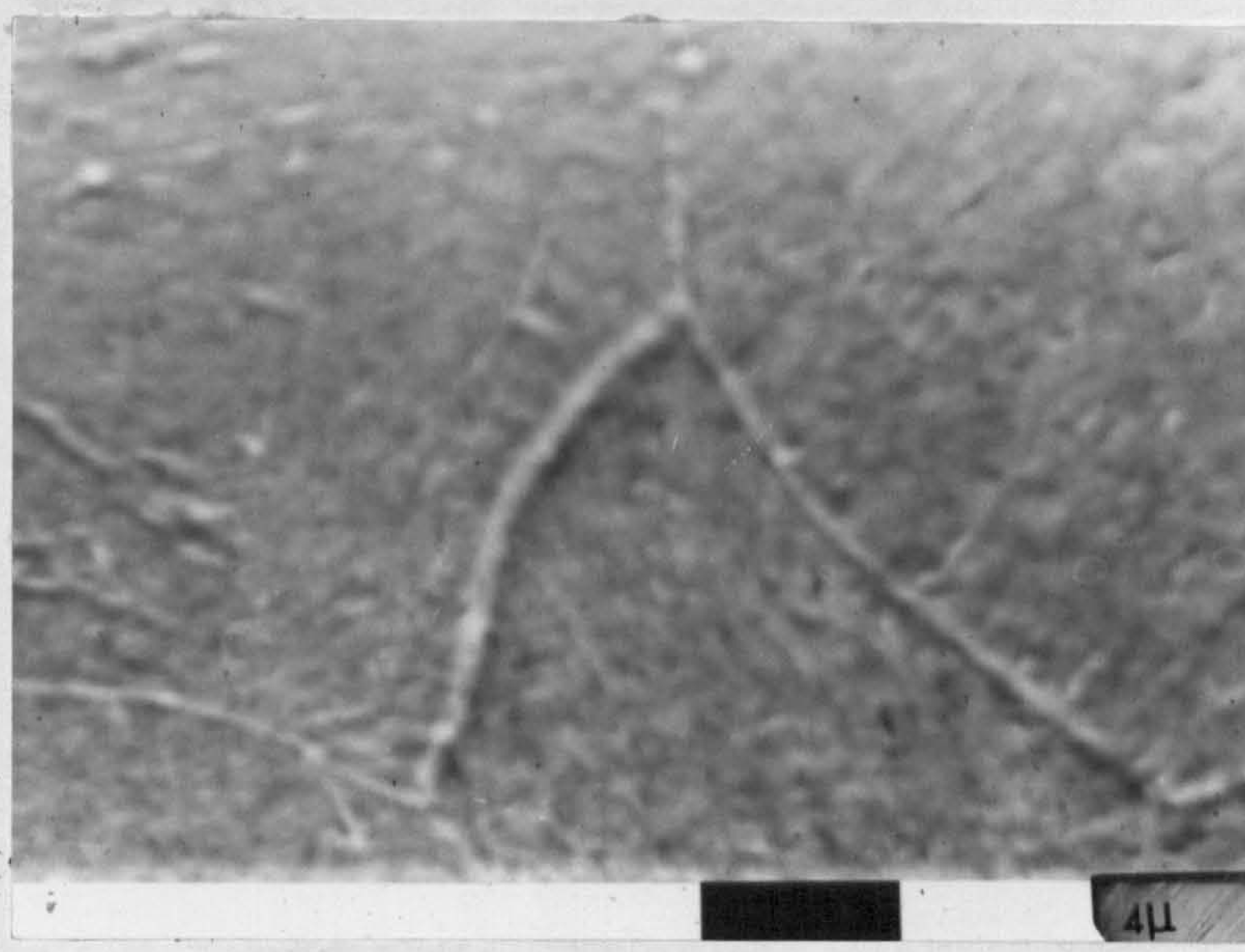

Fig. 3.6 Appearance of the grain boundary precipitate produced in a maraging steel specimen austenitised for 1hr at 950°C and aged for 3hr at 530°C revealed by etching for 10 minutes in 3.5 wt % NaCl test solution of initial pH 2.0. Backscattered scanning electron microscope image.

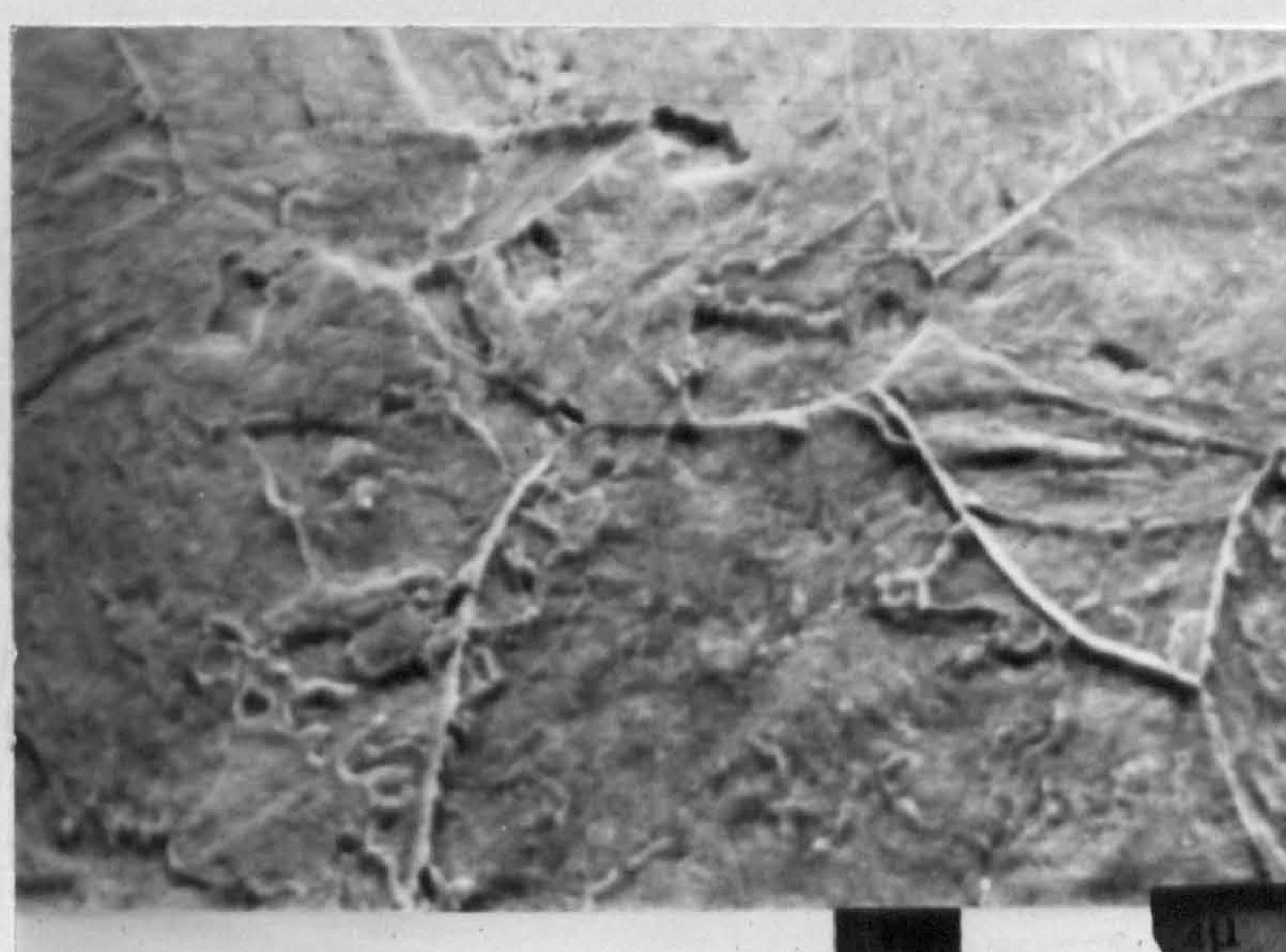

Fig. 3.7 Appearance of the grain boundary precipitate produced in a maraging steel specimen austenitised for 1 hr at 950°C and aged for 3hr at 530°C delineated by etching in acid ferric chloride solution for 30 seconds. Backscattered scanning electron microscope image.

precipitate would provide conditions suitable for a local galvanic cell to be set up between the carbide acting as cathode and the material, immediately adjacent to the grain boundaries acting as anode, such that the latter would be preferentially dissolved. Although no evidence can be supplied concerning the identity of the grain boundary precipitate; etch tests in 3.5 wt % NaCl and Ferric chloride solution indicated that the grain boundary precipitate remained unattacked, at least during the initial stages of corrosion in the above solutions; and is therefore probably cathodic (noble) to the matrix material. (See Figs. 3.6, 3.7).

3.2 The Influence of Environment and Applied Polarisation on S.C.C. Resistance

3.2.1 The influence of pH on the potential dependence of stress corrosion cracking

i) Smooth Tensile Specimens

Potentiodynamic fast and slow potential sweep rate polarisation curves (2000mV/MIN and 20 mV/MIN respectively) were determined on maraging steel specimens in 3.5 wt % NaCl solution adjusted to various initial pH values (2.0, as made up (6.0) and 11.0) and over the potential range - 1500 mV to +500 mV versus the S.C.E.

Potentiostatic constant crosshead speed tensile tests were also performed under similar test conditions and covering the same range of potentials. All specimens were austenitised for 1hr at 950^{o}C and aged for 3hr at 530^{o}C. A crosshead speed of 1.29x10^{-6} INS^{-1} was chosen for this series of tests.

Fig. 3.8(a) shows the polarisation curves and Fig. 3.8(b) the normalised time to failure versus applied potential curve for tests performed in a solution of initial pH = 2.0. Figs. 3.9, 3.10 show the corresponding curves obtained in solutions of initial pH's 6.0 and 11.0 respectively. The polarisation curves are characterised by 2 (in the case of the initial pH 2.0 solution) or 3 (in the case of pH 6.0 and 11.0 solutions) distinctly different ranges of potential each of which is closely related to stress corrosion cracking susceptibility and the presence or otherwise of visible corrosion films. At potentials noble to the free corrosion potential - the latter being virtually independent of solution pH - cracking in all 3 solutions was associated with metal dissolution and the formation of a black corrosion film over the entire surface of the exposed gauge length. At potentials active (-ve) to the free corrosion potential cracking, in a solution of initial pH 2.0, was observed to occur over the entire range of potentials investigated and in the absence of visible corrosion films. It was apparent from the bubbles of gas evolving from the specimen surface that cracking was a consequence of hydrogen embrittlement under these circumstances.

In 3.5 wt % NaCl solution of pH 6.0 and solutions made alkaline to an initial pH of 11.0, however, a range of cathodic protection extending from approximately -350 mV to approximately -850 mV versus S.C.E. was observed. At potentials active to -850 mV S.C.E. cracking was a consequence

Fig. 3.8 The potentiodynamic fast and slow sweep rate polarisation curves, a) and the normalised time to failure versus applied potential relationship b) for maraging steel specimens tested in a 3.5 wt % NaCl solution of initial pH 2.0.

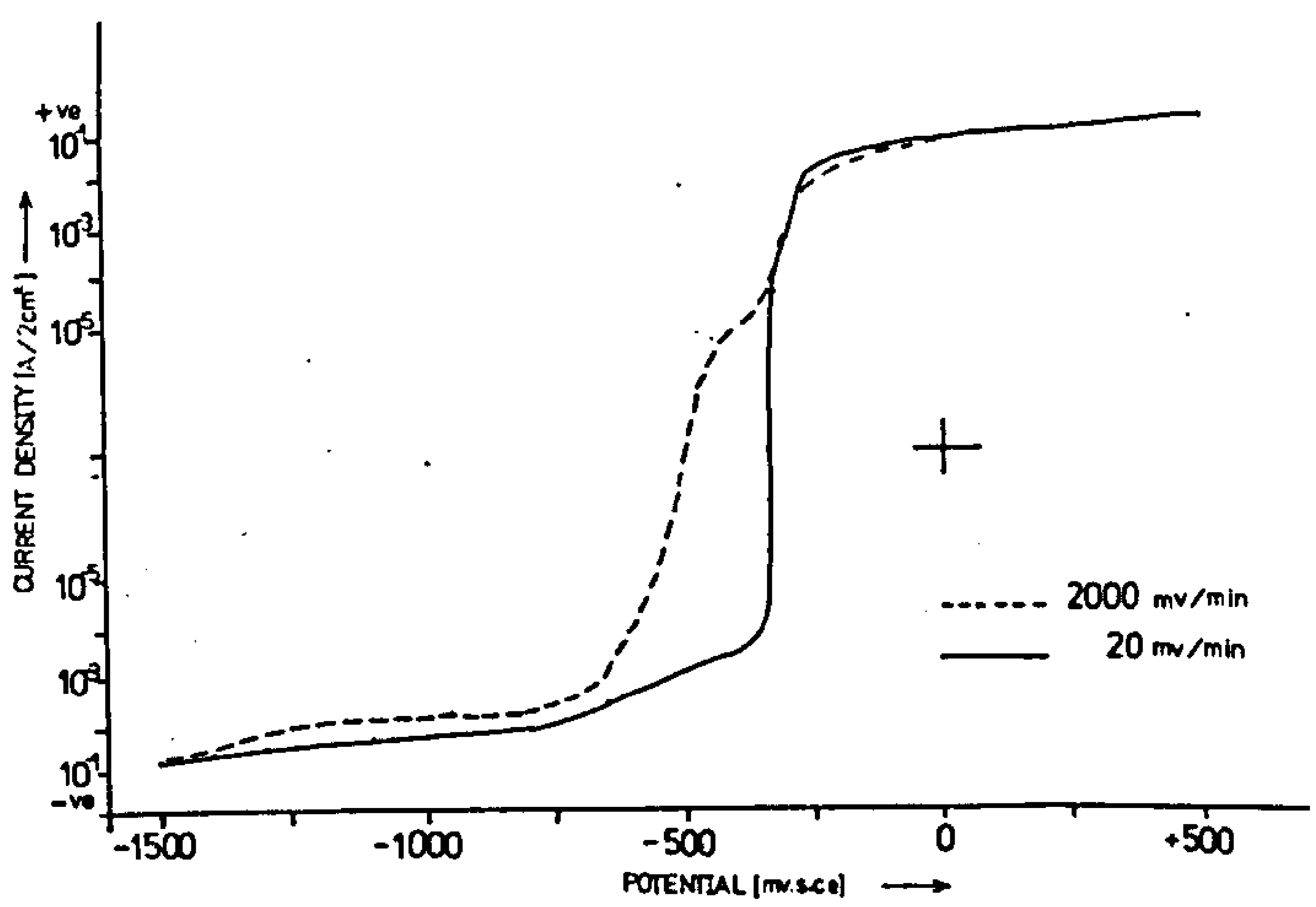

Fig. 3.8a

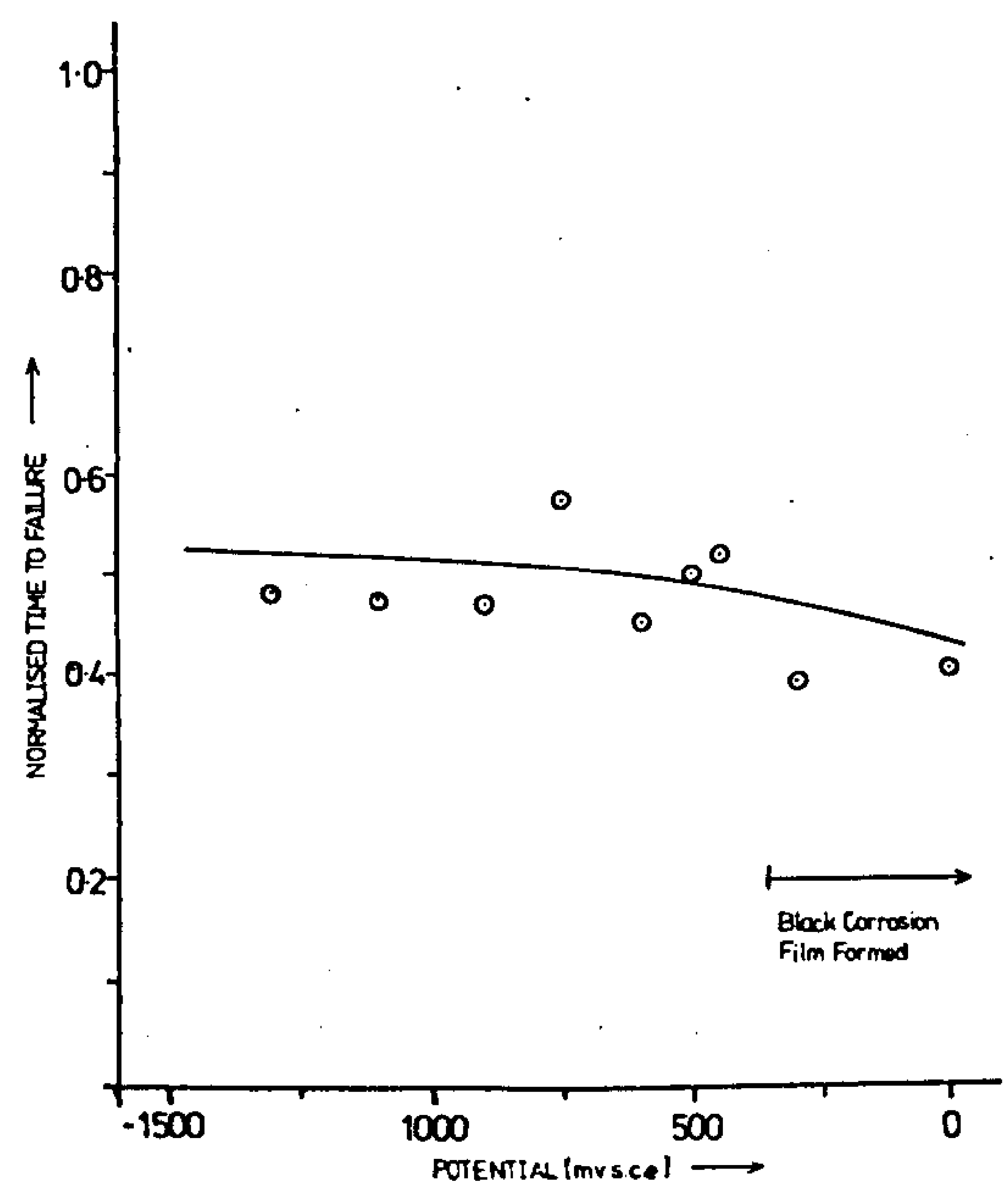

Fig. 3.8b

Fig. 3.9 The potentiodynamic fast and slow sweep rate polarisation curves, a) and the normalised time to failure versus applied potential relationship, b) for maraging steel specimens tested in 3.5 wt % NaCl solution of initial pH 6.0 (as madeup).

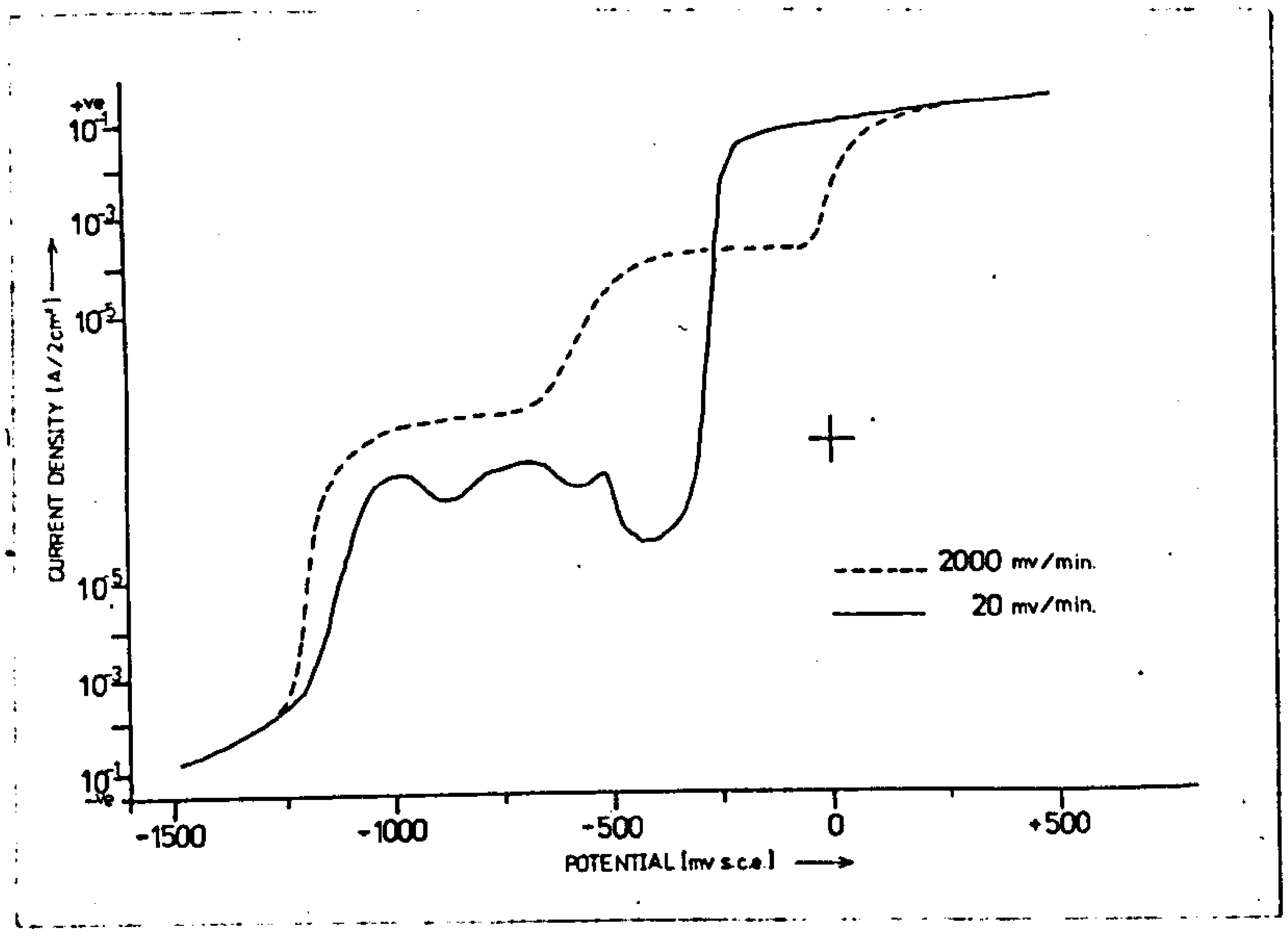

Fig. 3.9a

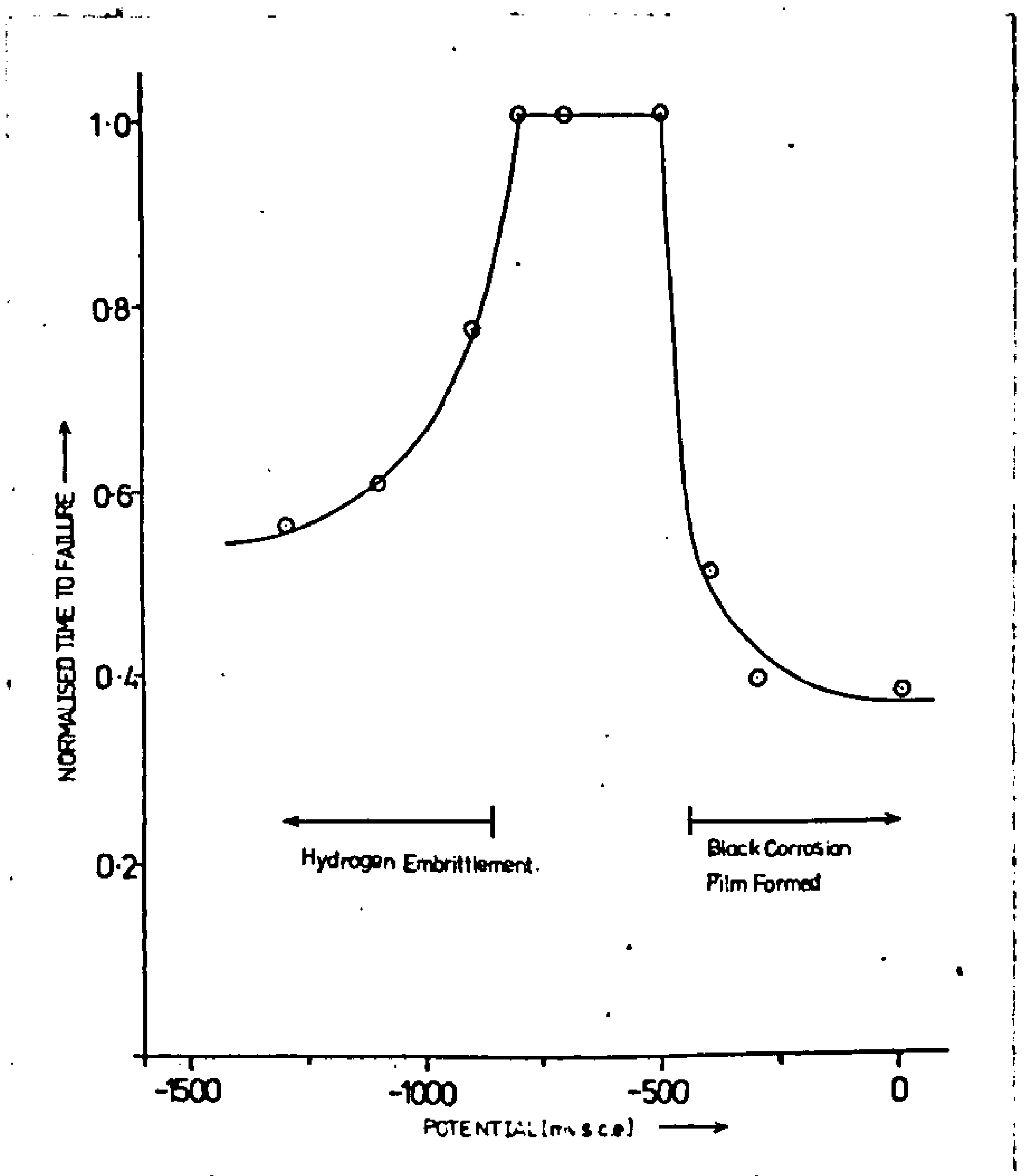

Fig. 3.9b

Fig. 3.10 The potentiodynamic fast and slow sweep rate polarisation curves, a) and the normalised time to failure versus applied potential relationship, b) for maraging steel specimens tested in 3.5 wt % NaCl solution of initial pH 11.0.

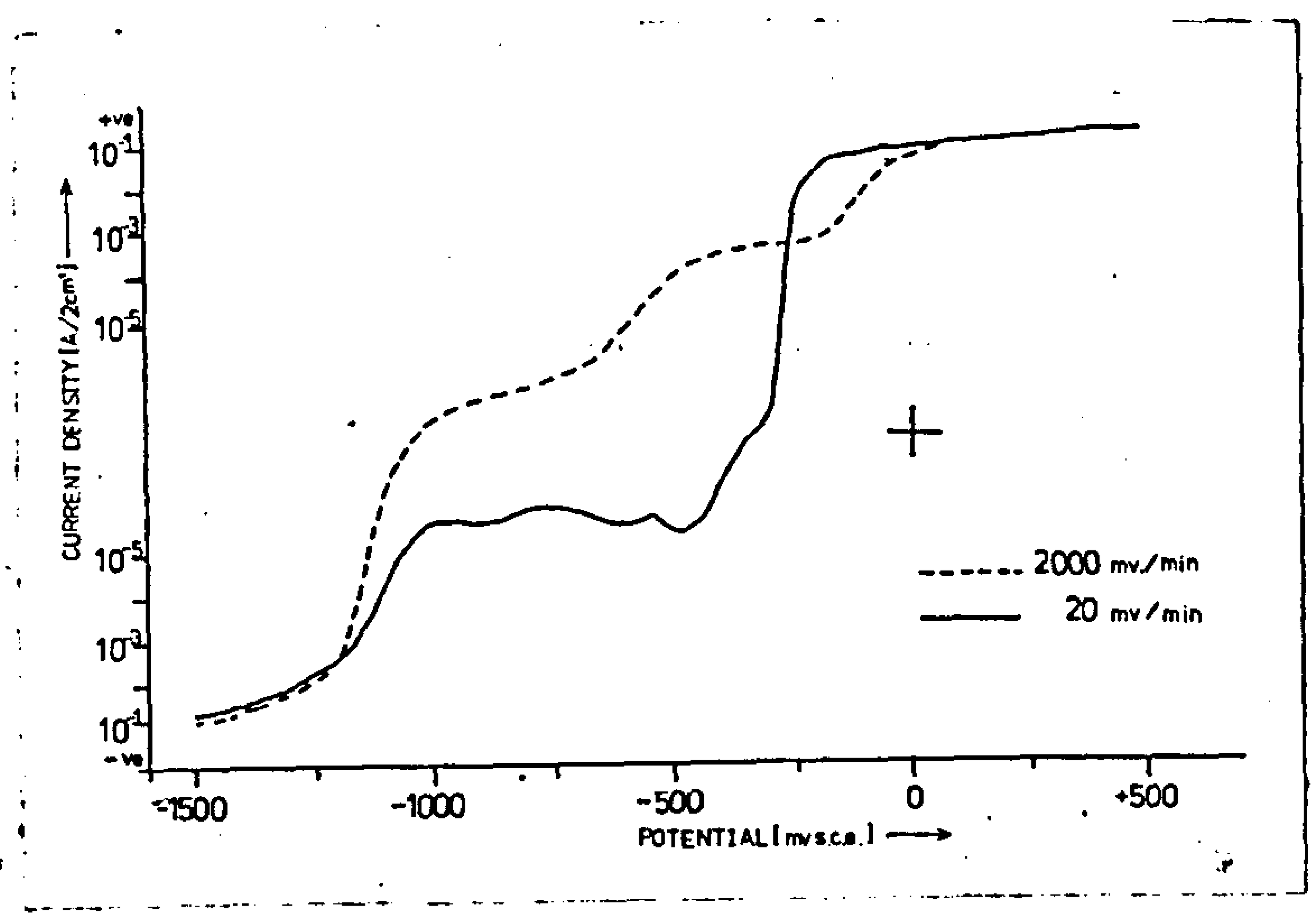

Fig. 3.10a

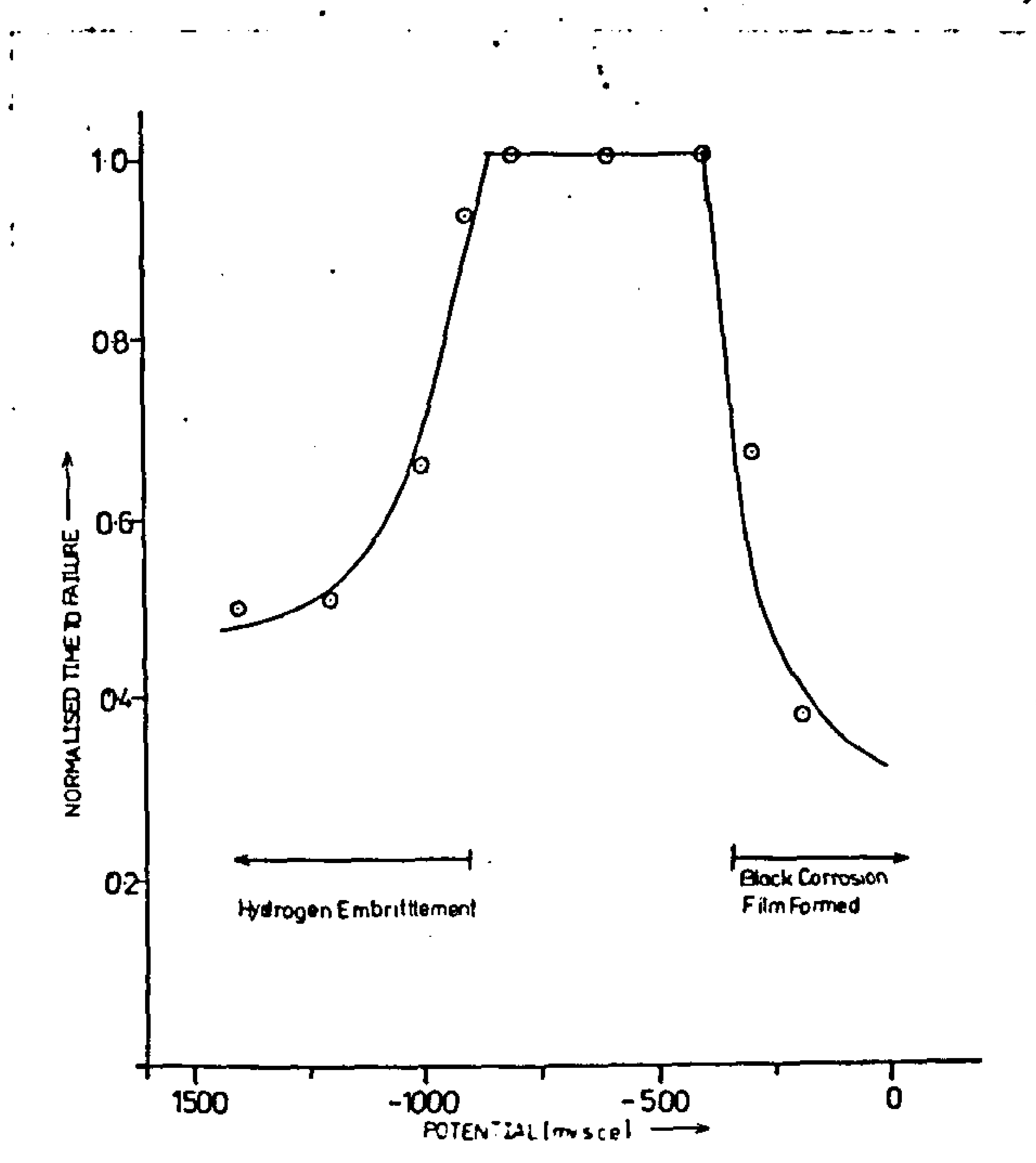

Fig. 3.10b

of hydrogen embrittlement.

The close relationship existing between the change in shape of the polarisation curves with applied potential and the corresponding change in cracking susceptibility with applied potential can be explained if we consider the nature of the anodic and cathodic reactions occurring on the metal surface.

Thus, at potentials noble to the free corrosion potential the predominating reaction occurring on the specimen surface is metal dissolution.

At potentials active to the free corrosion potential, however, dissolution is suppressed and it is necessary to look more closely at changes in the nature of the cathodic reaction brought about by changes in solution pH and/or potential in order to explain the observed dependence of cracking susceptibility on pH and applied potential.

The two competing cathodic reactions which are of interest in the present context are those of hydrogen evolution and oxygen reduction; the former being favoured by low pH and relatively active potentials and the latter by neutral or alkaline pH's, high O_2 content of the solution and relatively noble potentials.

In a solution of pH 2.0 at 25^{o}C, the thermodynamic equilibrium potential, E_H for the hydrogen evolution reaction is from $E_H = E_O - \cdot 059$ (pH) , -118mV N.H.E. i.e.-359 mV S.C.E.; so that hydrogen evolution becomes thermodynamically possible at potentials more active than the latter. It seems reasonable to assume therefore that, neglecting overpotential effects, the principle cathodic reaction occurring in a solution of pH 2.0 at potentials active to -360 mV S.C.E. will be that of hydrogen evolution and hence the observation of H.E. cracking at all potentials active to the f.c. potential (-340 mV according to the slow sweep rate curve) in pH 2.0 solutions (c.f. Fig. 3.8). The relatively high limiting cathodic current densities and the close similarity between the appearance of the fast and slow sweep rate curves in the corresponding polarisation curve (Fig. 3.8(a)) is indicative of the fact that the H.E.R. is not rate determined by bulk diffusion of reacting species (i.e. H^+ ions) to the metal surface as is the case, for example, in oxygen reduction.

As the pH of the solution is made more alkaline the equilibrium potential for the hydrogen evolution reaction, above which hydrogen evolution is no longer thermodynamically possible, is shifted in the active direction according to equation (1).

Thus, in as made up 3.5% NaCl solution of pH = 6.0, E_H = -600mV S.C.E; and for a solution adjusted to an initial pH of 11.0, E_H = -890 mV S.C.E. Consequently, neglecting effects of hydrogen over voltage, oxygen reduction becomes the predominant cathodic reaction in as made up and pH 11.0 solutions at potentials noble to -600 mV S.C.E. and -890 mV S.C.E. respectively. Therefore, specimens held at potentials between the free corrosion potential (as indicated by the slow sweep rate polarisation curve) and E_H should not experience stress corrosion cracking since neither metal dissolution nor cathodic evolution of hydrogen can take place, That this indeed is observed to be the case can be seen from Figs. 3.9 and 3.10. Cracking could not be induced at potentials between -450 mV and -850 mV SCE for solutions of pH = 6.0 or between -350 and -950 mV SCE for pH 11.0 solutions. Over these same potential ranges the polarisation curves show the following characteristics

a) very small limiting cathodic current densities on the slow sweep rate curves.

b) small anodic current densities on the fast sweep rate curves coupled with a displacement of the free corrosion potential in the active direction compared with that indicated by the slow sweep rate curves.

These differences between the fast and slow potential sweep rate curves may be rationalised as follows:-

Unlike the hydrogen evolution reaction, where the cathodic reactant species (H^+) is readily available from the dissociation of solvent water molecules; the solubility of O_2 in aqueous environments is rather low and consequently the rate of oxygen reduction can become controlled by the diffusion of oxygen to the metal surface. The rate of diffusion of oxygen molecules in water is several hundred times less than that of H^+ ions and so unless oxygen is equally available at all parts of a corroding metal surface an oxygen diffusion layer can soon build up resulting in an extremely small limting cathodic current density for the reaction according to the equation

$$i_L = \frac{zFDc_s}{\delta}$$ where D = diffusion coefficient of O_2, c_s = bulk concentration of O_2, δ = diffusion layer thickness

The relatively active free corrosion potentials exhibited by the fast potential sweep rate curves are a consequence of the times available for the diffusion of O_2 to the surface of the specimen being insufficient to maintain that level of O_2 concentration required to provide continued cathodic protection.

The discrepencies between the observed and calculated values ofthe equilibrium potential for hydrogen evolution can probably be explained by the effects of hydrogen overpotential.

Fig. 3.11 summarises the tensile testing

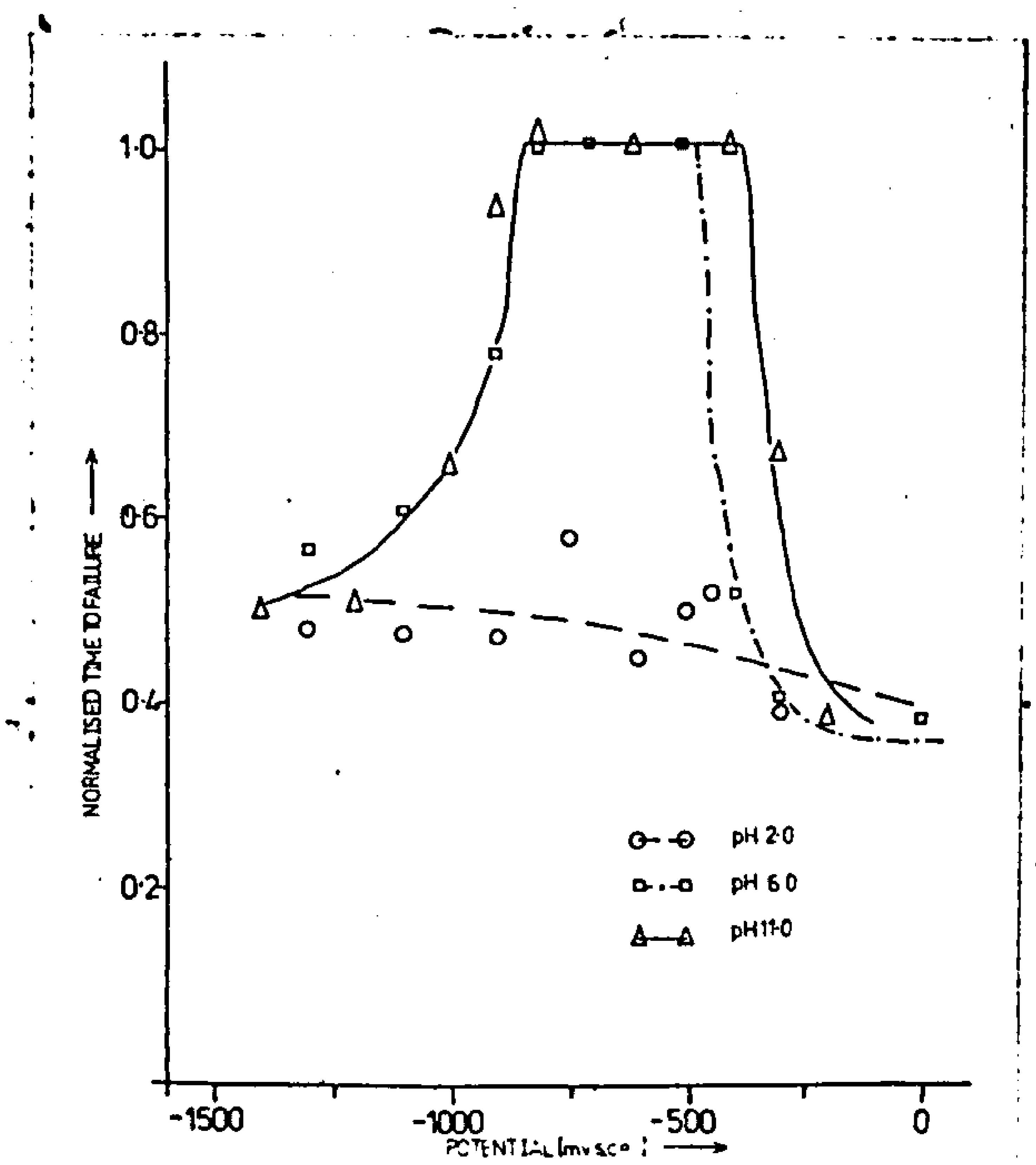

Fig. 3.11 Summary of the smooth tensile test results in 3.5 wt % NaCl solutions of various initial pH's.

results for all 3 solutions investigated and brings out a further point which was not immediately apparent from looking at Figs. 3.8-3.10 separately.

i.e. the upper limit of cathodic protection is displaced by approximately 100 mV in the noble direction as a result of increasing the initial pH from 6.0 to 11.0. In the next section it will be demonstrated that far greater increases in the upper limit of cathodic protection can be achieved by both reducing the Cl^- ion concentration and increasing the solution pH.

ii) <u>Fatigue Precracked Specimen Tests</u>

Although a full investigation of the influence of pH on the potential dependence of cracking of fatigue precracked specimens was not carried out; the influence of potential on the cracking susceptibility of fatigue precracked specimens in a solution of pH 11.0 was investigated primarily to observe the effect of potentials in that range previously observed to provide cathodic protection in smooth tensile tests.

Single-edge notch pin loaded tensile tests were performed at potentials of -250 mV, -500 mV, -700 mV and -1000 mV S.C.E. Specimens were loaded to an initial stress intensity of 15 KSI$\sqrt{IN}$ in all cases. In the absence of cracking over a period of 48hr the load was increased to provide a stress intensity approximately 5 KSI$\sqrt{IN}$ higher (i.e K_I = 20 KSI$\sqrt{IN}$) and this process was repeated every 24hr until cracking was initiated. This procedure enabled a $K_{I\ SCC}$ value for crack propagation to be determined for each potential investigated.

The results are tabulated in Table 3.4.

TABLE 3.4

The influence of applied potential upon the stress intensity required to initiate cracking and upon the average crack velocities in a 3.5 wt % NaCl solution adjusted to an initial pH of 11.0.

POTENTIAL (mV S.C.E.)	CRACK INITIATION	STRESS INTENSITY	AVERAGE CRACK VELOCITY	
	K.S.I.$\sqrt{IN}$	$MNm^{-3/2}$	INS^{-1}	ms^{-1}
-250	15	16.5	4.5×10^{-6}	1.14×10^{-7}
-500	20	22	4.5×10^{-6}	1.14×10^{7}
-700	30	33	5.0×10^{-6}	1.27×10^{-7}
-1000	15	16.5	2.0×10^{-5}	5.08×10^{-7}

It is apparent from these results that despite controlling the potential of fatigue precracked specimens within the range of potentials observed to provide cathodic protection in smooth tensile specimen tests crack propagation still occurred though a higher initial stress intensity was required to initiate cracking under these conditions. This suggests that potential and/or pH conditions can develop within the confines of the discontinuity associated with precracked specimens which are significantly removed from those conditions existing on the bulk surface of the specimen.

If, following Ateya and Pickering[108] it is assumed that the potential at the crack tip approaches the free corrosion potential, irrespective of the applied potential, then dissolution at the crack tip is possible and in the test on the precracked specimens at -500 mV SCE, for example, it was observed that a yellow brown precipitate, presumably of ferric hydroxide, formed along the sides of the precrack in support of this assumption.

It should not be overlooked, however, that Ateya and Pickering's work involved relatively high cathodic charging current densities and in this respect their arguments may not be strictly applicable in the present context. One possible alternative explanation may lie with the depletion of oxygen in the crack tip region which could conceivably promote a shift in the free corrosion potential to more active values with the consequence that dissolution becomes possible even though the crack tip potential remains the same as that on the bulk surface.

In either case it is tempting to suggest that, because cracking could not be initiated on smooth specimens at the free corrosion potential in either pH 6.0 or pH 11.0 solutions even though dissolution was observed to be taking place in these tests, the pH of the solution within the crack must also fall to a value where cracking can be initiated. However, this takes no account of the highly strained and yielding material at the crack tip which exists in precracked tests and which may facilitate the dissolution reaction so that even in the fairly unaggressive environments we are concerned with here, cracking may be initiated without recourse to arguments based upon lowering of the pH of the solution within the crack.

No evidence can be given which resolves the point unequivocally, however, it seems worthy to note that in a 3.5 wt % sodium chloride solution buffered to a pH of 9.0 with .01 mole/l of sodium borate, freely corroding precracked specimens of maraging steel were observed to

Fig. 3.12 The potentiodynamic fast and slow sweep rate polarisation curves a) and the normalised time to failure versus applied potential relationship, b) for maraging steel specimens tested in 3.5 wt % NaCl solution.

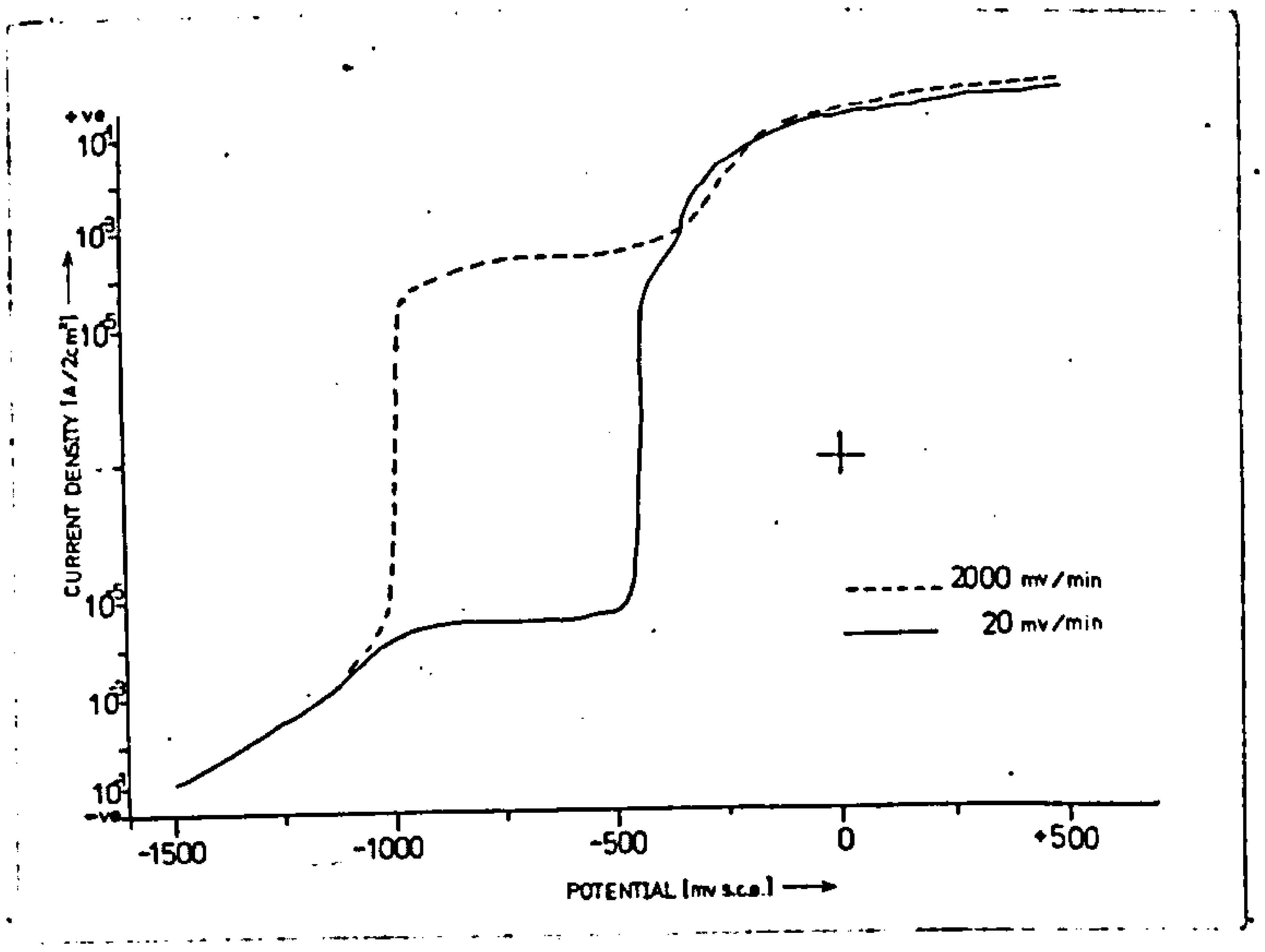

Fig. 3.12a

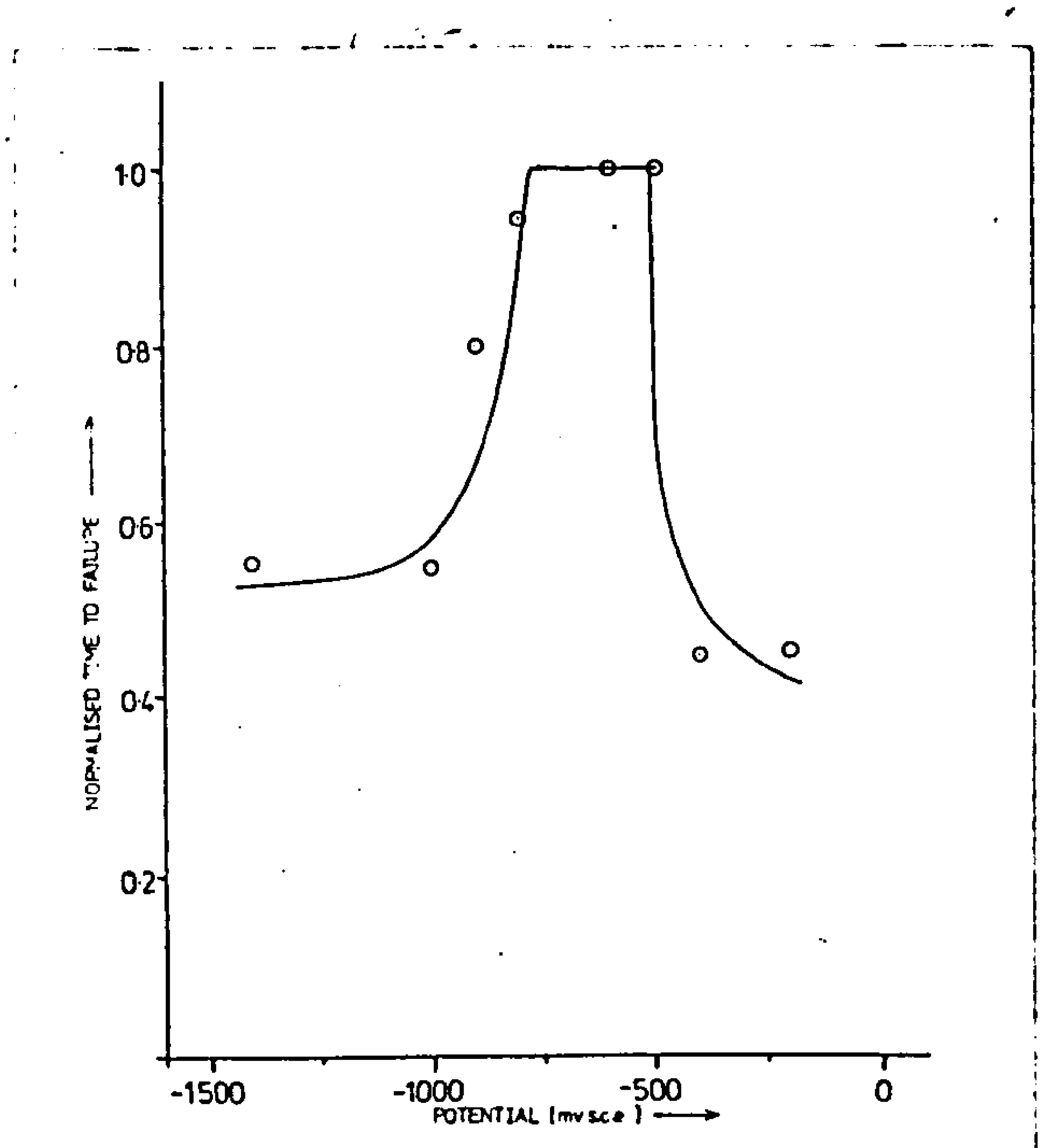

Fig. 3.12b

Fig. 3.13 The potentiodynamic fast and slow sweep rate polarisation curves, a) and the normalised time to failure versus applied potential relationship, b) for maraging steel specimens tested in .035 wt % NaCl solution.

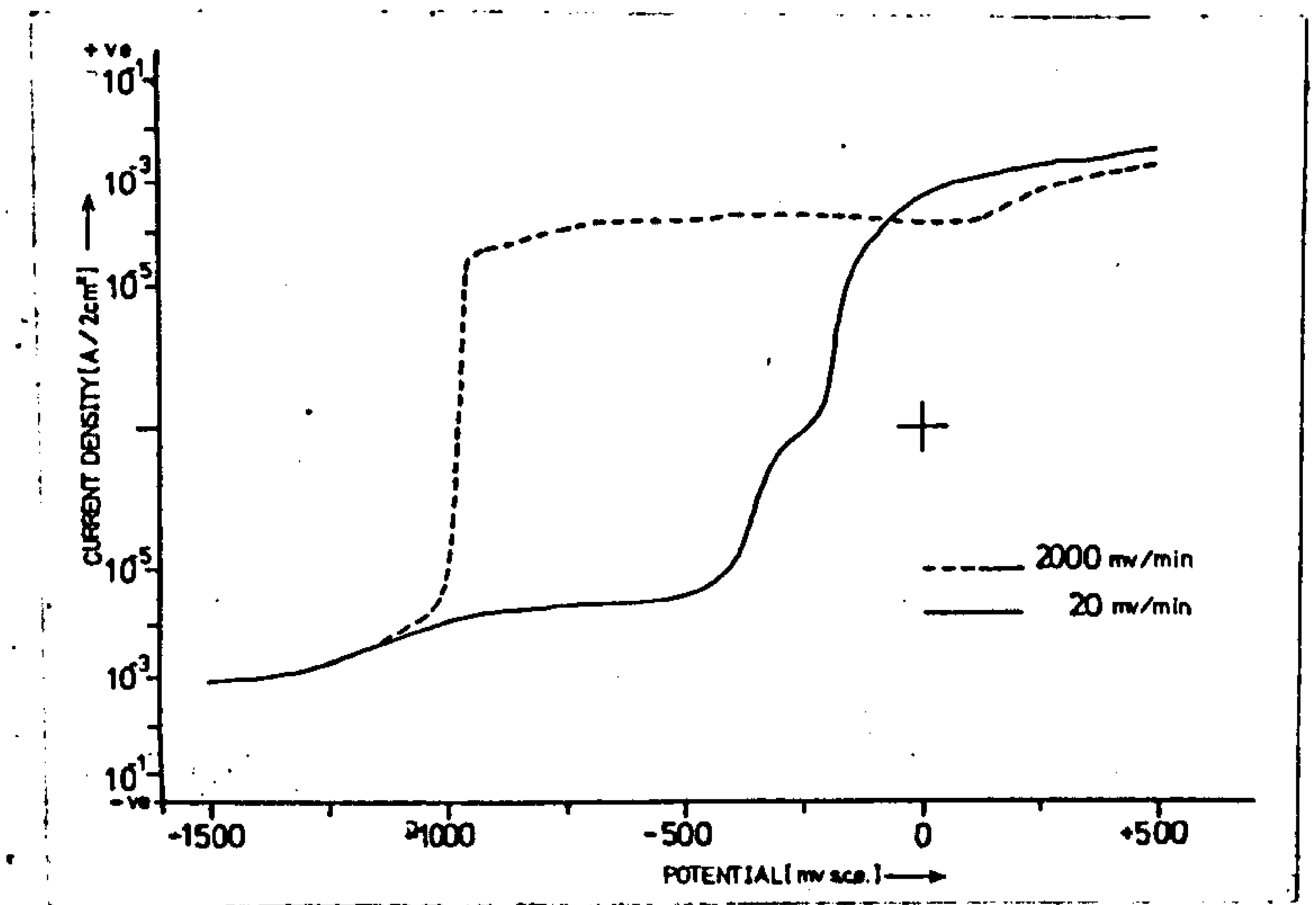

Fig. 3.13a

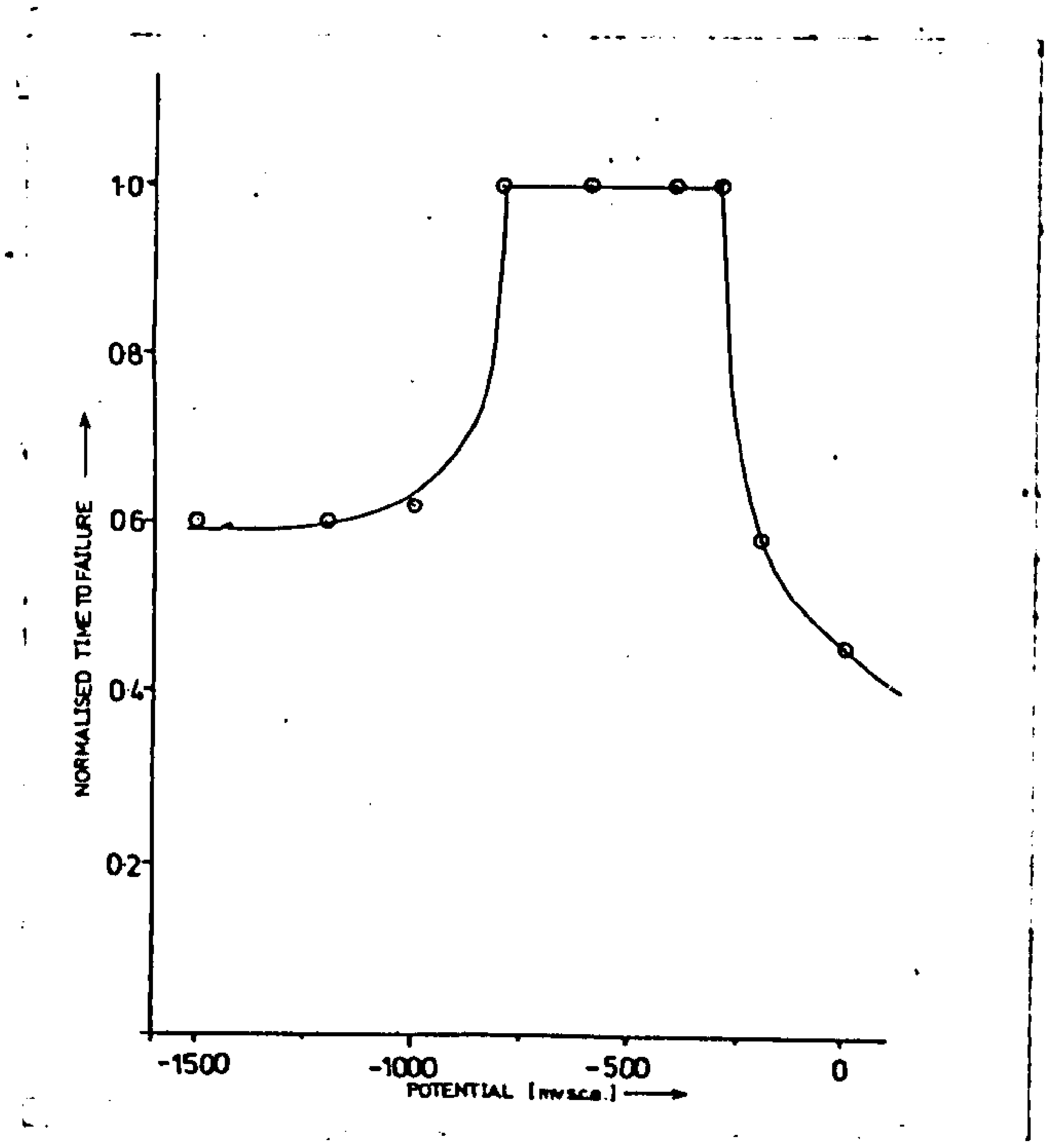

Fig. 3.13b

Fig. 3.14 The potentiodynamic fast and slow sweep rate polarisation curves, a) and the normalised time to failure versus applied potential relationship b) for maraging steel specimens tested in .0035 wt % NaCl solution.

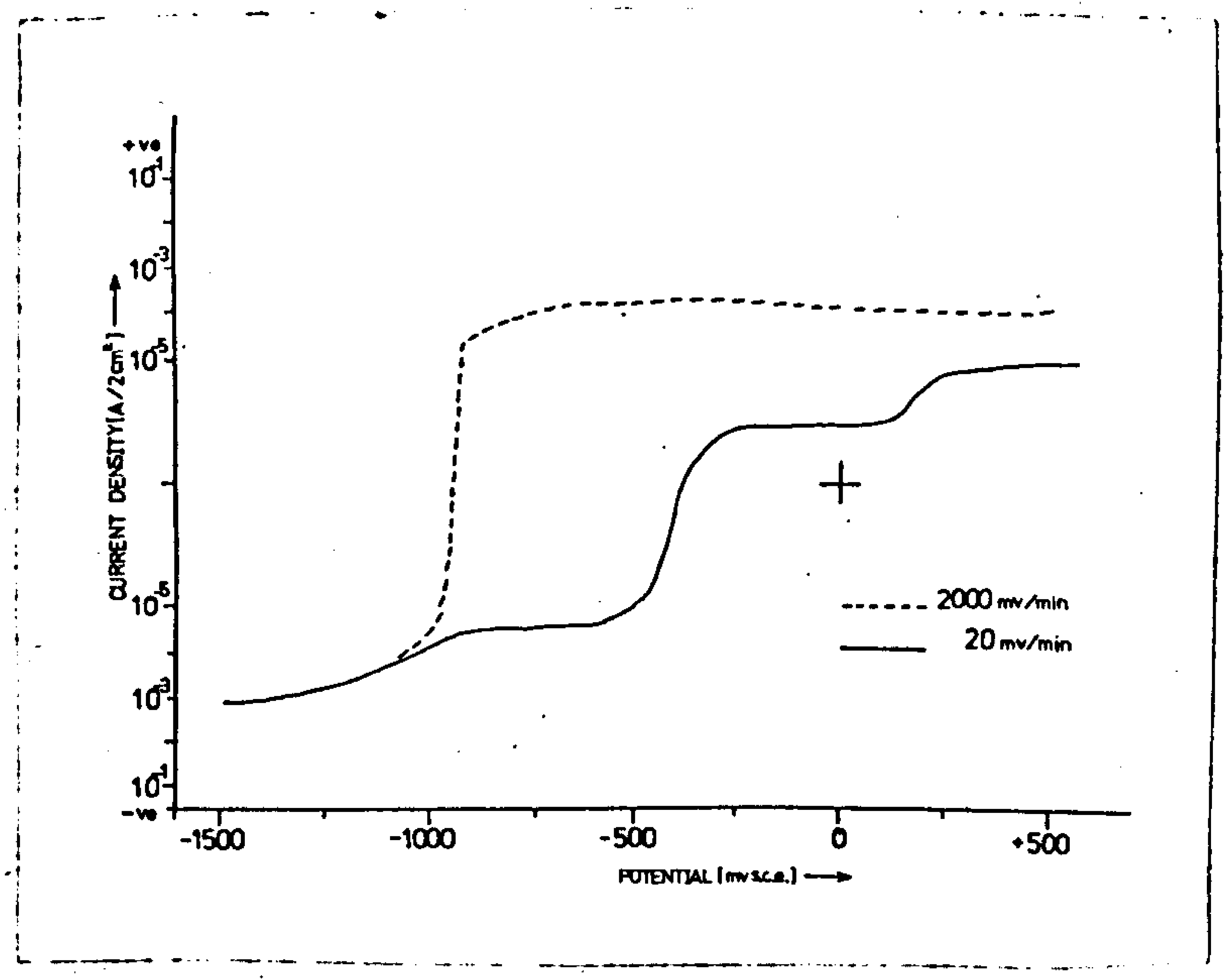

Fig. 3.14a

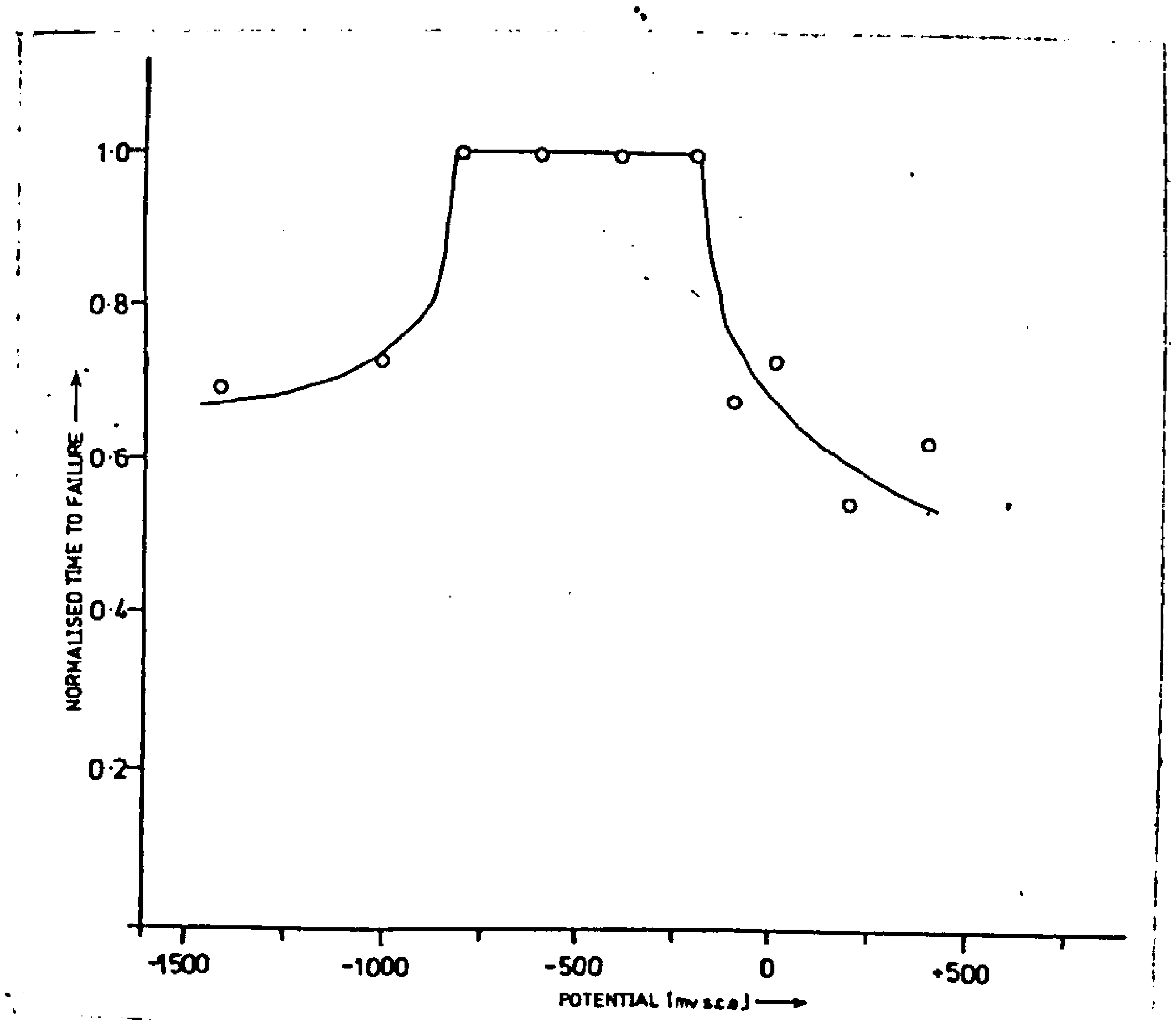

Fig. 3.14b

crack readily suggesting that a lowering of the pH of the solution within the confines of a discontinuity need not necessarily be a prerequisite to crack propagation in precracked specimens in the less aggresive environments.

3.2.2 The influence of chloride ion concentration on the potential dependence of SCC

In Figs. 3.12, 3.13, 3.14 are plotted potentiodynamic polarisation curves and the corresponding failure times as a function of applied potential for maraging steel specimens tested in solutions containing 35, .035 and .0035 wt % NaCl respectively. The reader is also referred back to section 3.2.1 (Fig. 3.9) to the results of tests performed in 3.5 wt % NaCl and which are of relevance in the present context.

In Fig. 3.15 the potentiostatic tensile test results have been replotted on common axes to enable the

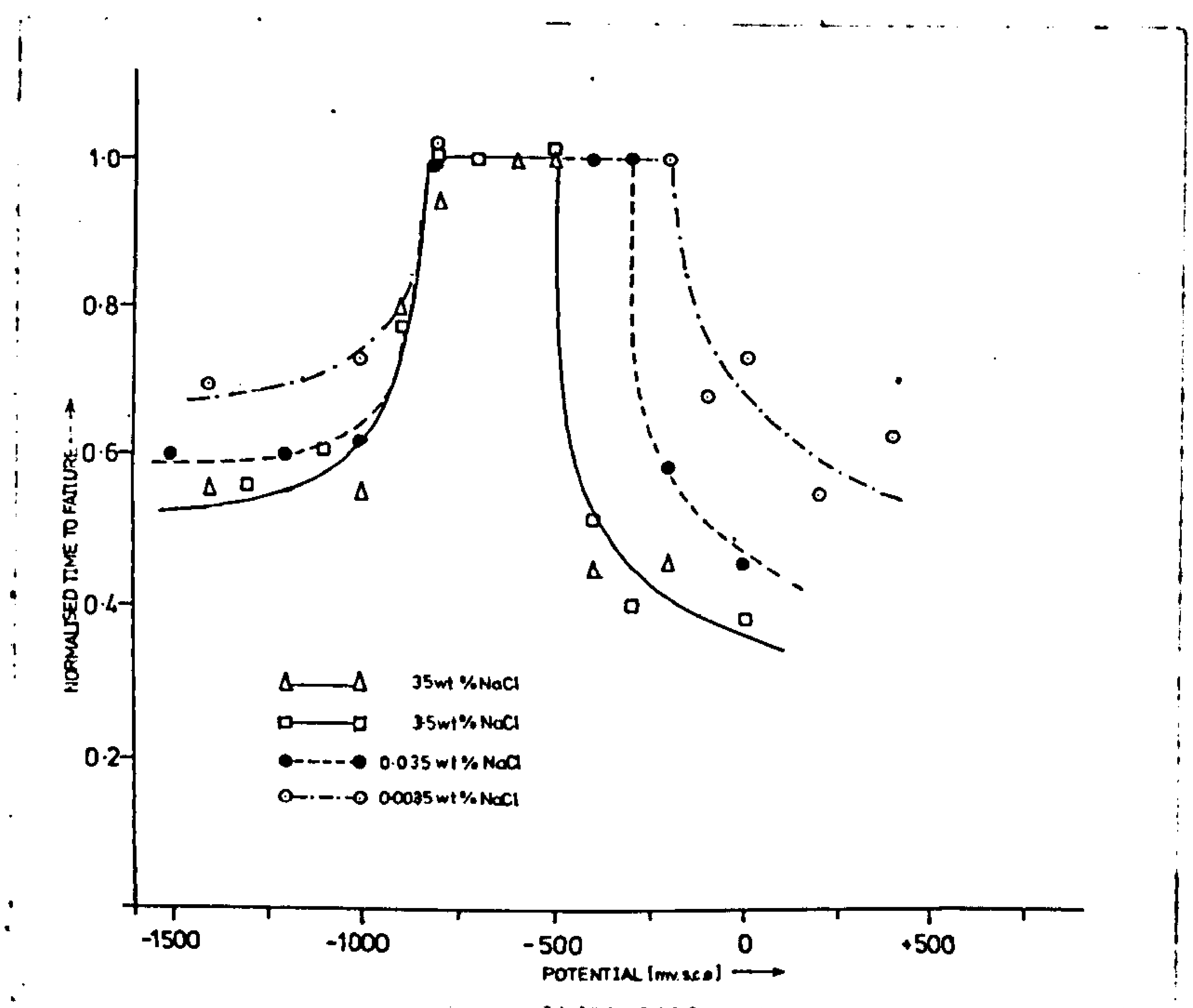

Fig. 3.15 Summary of the smooth tensile test results in sodium chloride solutions of various concentrations.

Fig. 3.16 The potentiodynamic fast and slow sweep rate polarisation curves, a) and the normalised time to failure versus applied potential relationship, b) for maraging steel specimens tested in .035 wt % NaCl solution adjusted to an initial pH of 11.0.

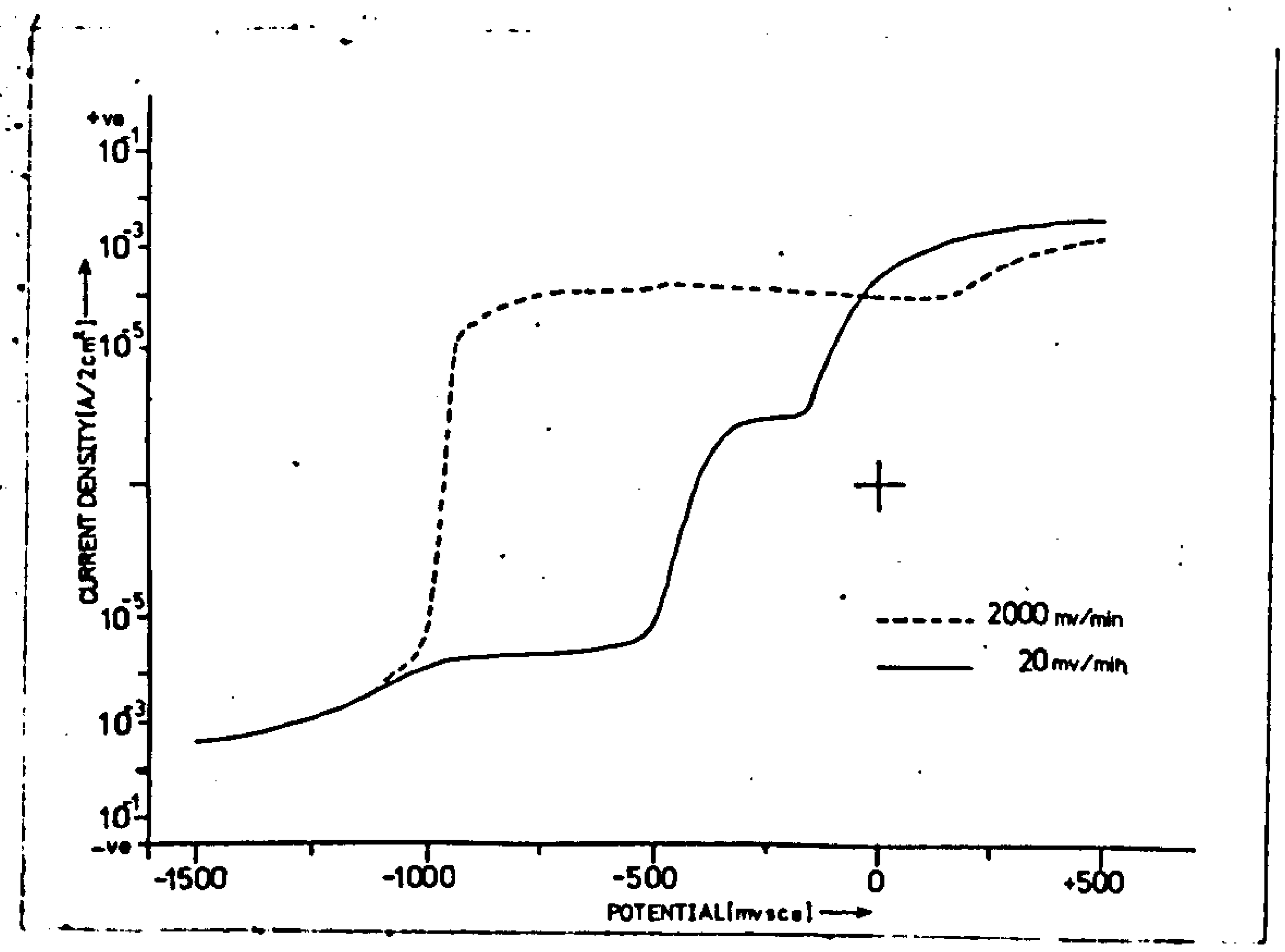

Fig. 3.16a

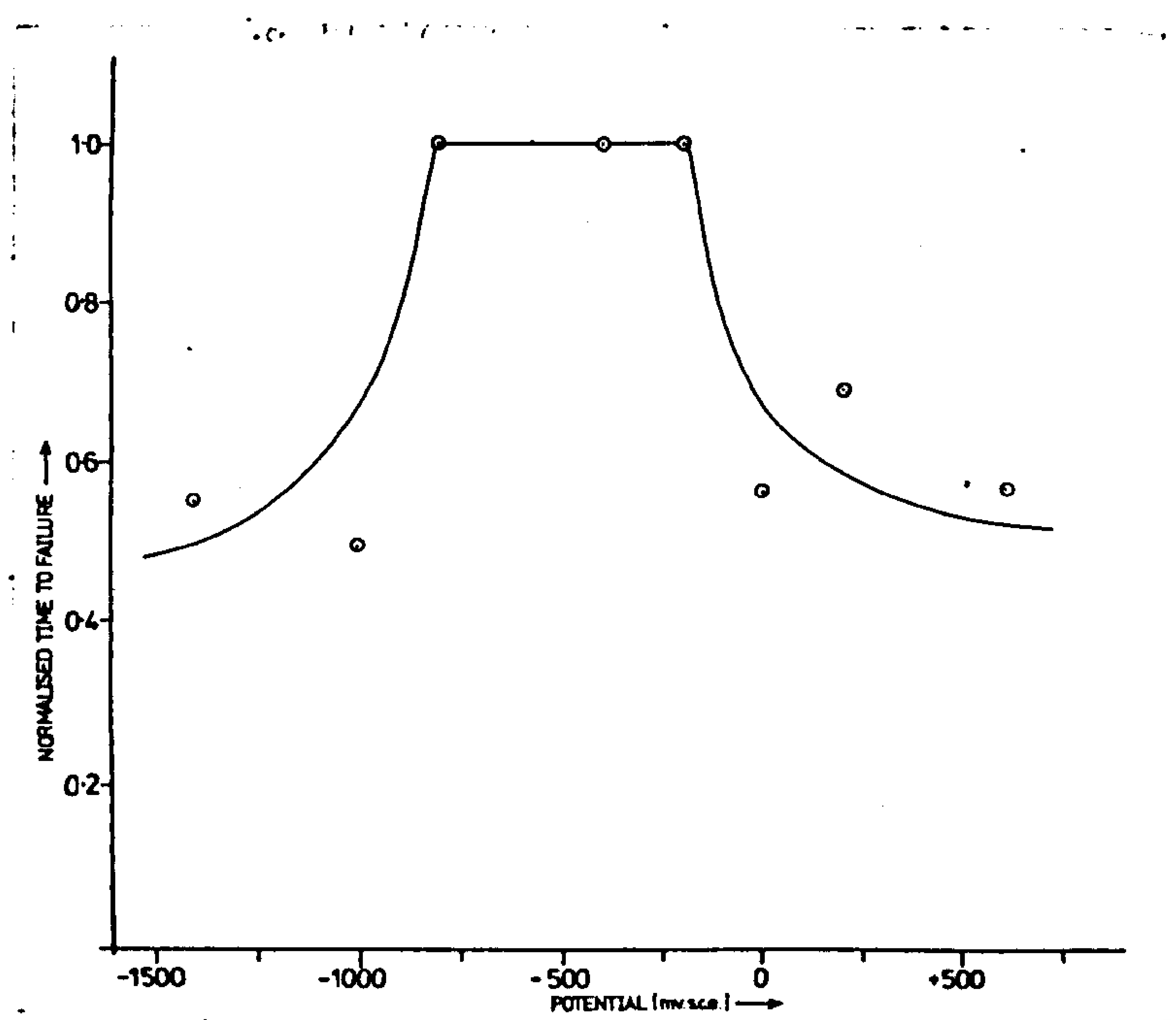

Fig. 3.16b

Fig. 3.17 The potentiodynamic fast and slow sweep rate polarisation curves, a) and the normalised time to failure versus applied potential relationship, b) for maraging steel specimens tested in .0035 wt % NaCl solution adjusted to an initial pH of 11.0.

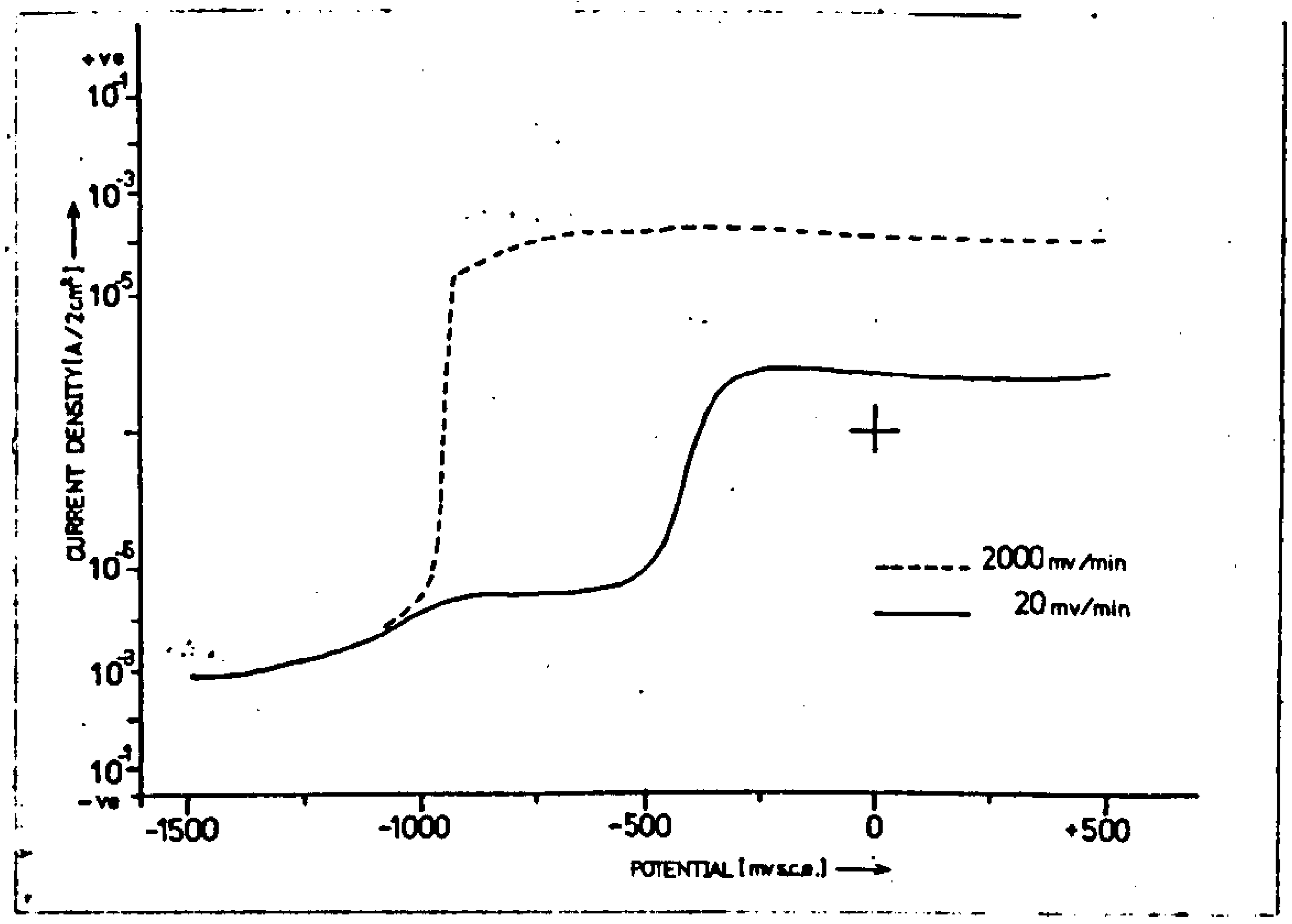

Fig. 3.17a

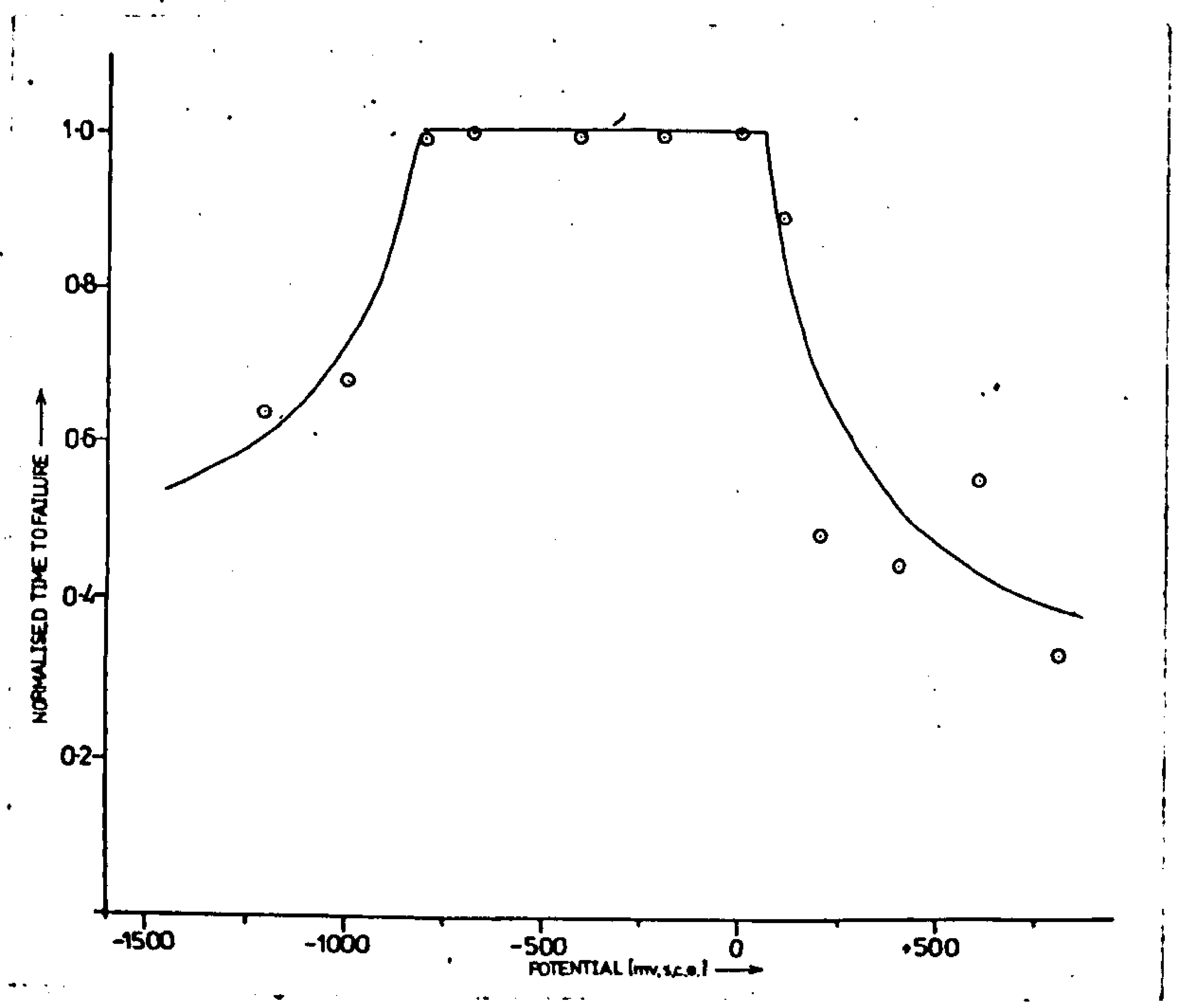

Fig. 3.17b

effect of Cl^- ion concentration on the susceptibility toward S.C.C. to be observed at a glance.

Figs. 3.16 and 3.17 show the polarisation curves and failure times as a function of applied potential of maraging steel specimens tested in solutions containing .035 and .0035 wt % NaCl respectively but adjusted to an initial pH of 11.0 with sodium hydroxide.

The results, described in section 3.2.1 (Fig. 3.10), of tests performed in 3.5 wt % NaCl adjusted to initial pH of 11.0 should also be referred back to here. Fig. 3.18 shows the tensile test results replotted on common axes for all 3 solutions adjusted to an initial pH of 11.0.

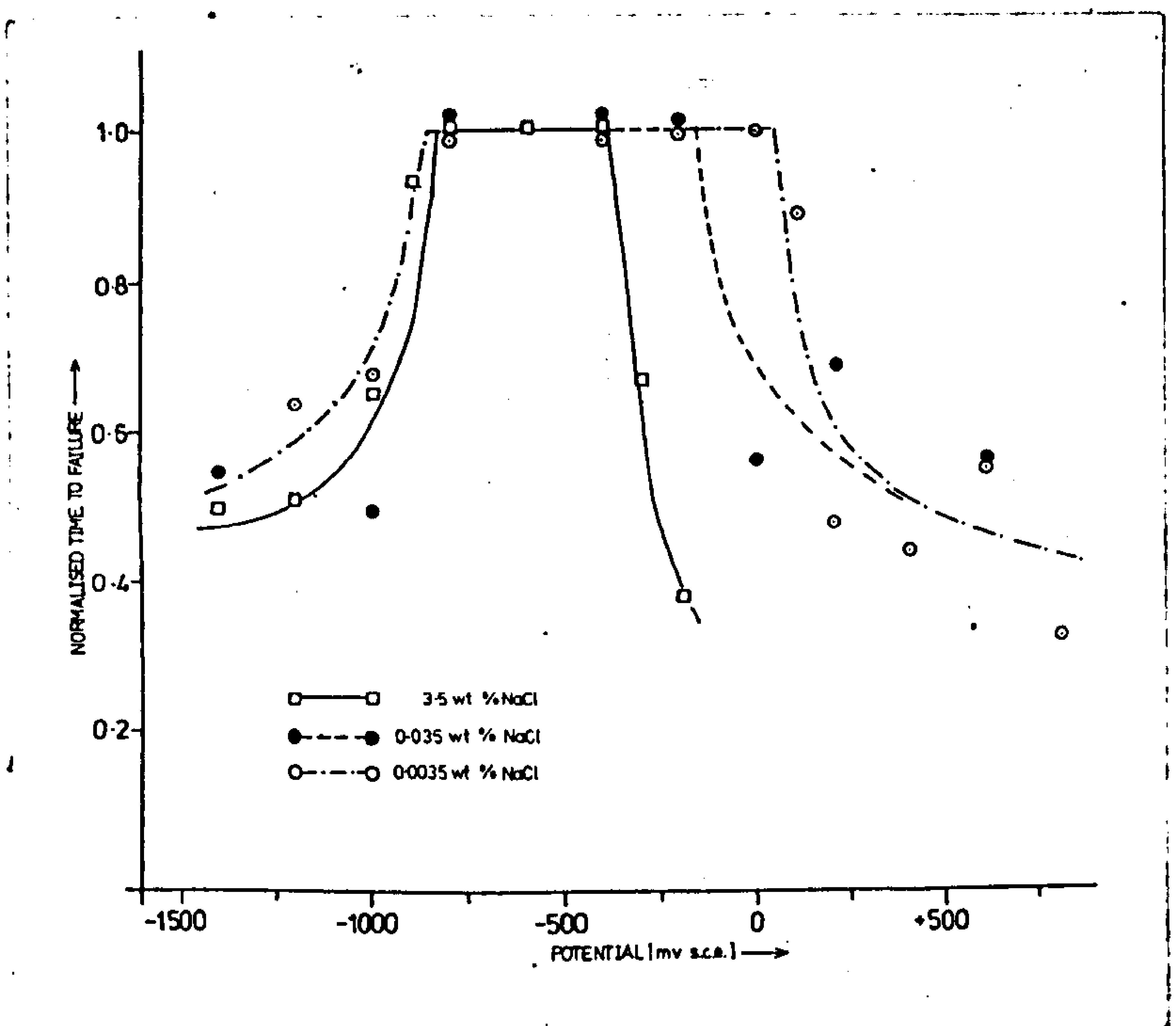

Fig. 3.18 Summary of the smooth tensile test results in sodium chloride solutions of various concentrations adjusted to an initial pH of 11.0.

It should be noted that the close relationship between the shape of the polarisation curves and the susceptibility towards stress corrosion cracking is again evident; at least in solutions containing $>$.0035 wt % NaCl. In the latter solution, however, the polarisation curves did not predict the upper limit of the range of cathodic protection for reasons which will be discussed later.

The following points emerge from these results.

i) Above a chloride ion concentration corresponding to 3.5 wt % NaCl (i.e. 0.6 M Cl^-); chloride ion concentration has a negligible effect on either the range of cathodic protection or the S.C.C. susceptibility.

ii) Chloride ion concentrations below this level, however, result in a noticeable increase in the range of cathodic protection and decrease in S.C.C. susceptibility.

iii) The upper limit of cathodic protection is extended to even more noble values (for a given Cl^- ion concentration) by an increase in initial pH of the solution.

The increase in the range of cathodic protection attendant on a decrease in Cl^- ion concentration is solely a consequence of a displacement of the upper potential limit of cathodic protection to more noble values. This displacement of the upper potential limit of cathodic protection was accompanied by a change in the nature of anodic attack from uniform surface dissolution and intergranular cracking to hemispherical pitting and intergranular cracking as the Cl^- ion concentration was reduced below the .035 wt % level. Even in the latter case some evidence of localised pitting attack was apparent.

Fig. 3.19 shows typical hemispherical pitting which resulted in intergranular cracking and failure in the tensile specimen tested in .0035 wt % NaCl of initial pH 11.0 at +200 mV S.C.E.

The above results are readily interpreted in terms of the effect of Cl^- concentration on the breakdown of the air or solution formed passive oxide film on the metal surface.

Anodic dissolution of the metal can begin at weak points in the air formed oxide film. Such weak points may include, for example, inclusions at the metal surface, which have oxidised less readily than the remainder of the surface; scratch lines; surface cavities or sheared edges etc.

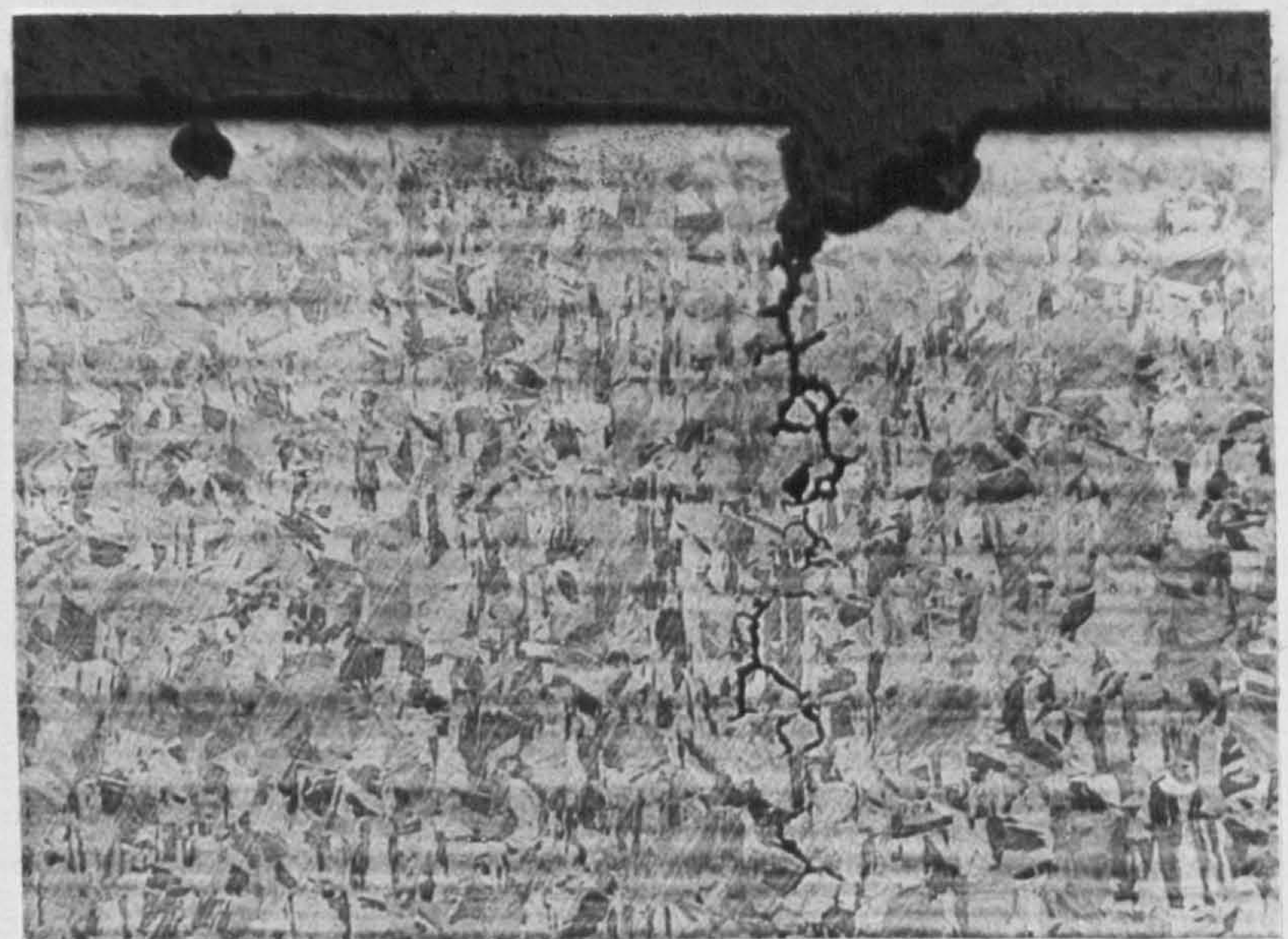

Fig. 3.19 Typical hemispherical pitting resulting in intergranular cracking in a tensile specimen tested in .0035 wt % NaCl of initial pH 11.0 at +200mV S.C.E. (x125).

In section 3.4 the influence of Ti(C,N) inclusions on crack initiation is discussed. Suffice it to say at this point Ti(C,N) inclusions are thought to be most significant in relation to their influence on crack initiation in smooth tensile specimens in the less aggressive environments.

If, as might be the case in dilute chloride solutions, the remainder of the surface remains relatively passive then corrosion proceeds confined to these weak points and pitting results. Intergranular SCC then occurs when the necessary conditions are established within the confines of the pit to initiate cracking i.e. lowering of the pH etc.

If, however, the solution is sufficiently aggressive, i.e. contains a high Cl^- ion concentration, then the passive film becomes contaminated with Cl^- ions and the lattice defects so produced enable cations to pass through the film more readily with the result that the remaining film is rapidly undermined and the metal is no longer protected i.e. general film breakdown.

Furthermore, as one might expect, the breakdown process is potential dependent and there exists a breakdown potential, E_b, above which appreciable corrosion can occur through the film. Only when the electric field within the film is sufficiently great will cations be pulled through the film. The breakdown potential depends upon the anion concentration and since the strength of the induced field will be greater at higher concentrations of Cl^- ion, a lower applied potential needs to be superimposed to breakdown the film.

The breakdown potentials are readily apparent on the slow sweep rate polarisation curves of the .035 wt % sodium chloride solutions and E_b is particularly evident in the solution of initial pH 11.0. The breakdown potentials correspond to those values at which the anodic dissolution currents 'break away' to comparatively high values (i.e. -200 mV SCE in a pH 6.0 solution and -100 mV SCE in the initial pH 11.0 solution Figs. 3.13, 3.16 respectively).

Breakdown potentials were not exhibited in the slow sweep rate polarisation curves determined in .0035 wt % NaCl solutions upto the maximum potential of +500 mV SCE investigated. Consequently it was expected that in these solutions pitting, intergranular cracking and failure would not occur in smooth tensile tests at potentials active to +500 mV SCE. That pitting, cracking and failure did occur at potentials as active as -100 mV SCE probably reflects the influence of tensile stress and/or strain in assisting breakdown of the otherwise protective film. In addition however it is conceivable that differences in surface contour between polarisation stub specimens and the exposed gauge length of tensile specimens (radius of curvature is greater in the former case) could result in greater tensile stresses being developed in the surface oxide films on tensile specimens compared with the oxide films formed on polarisation specimens. Furthermore since the breakdown of passive films is time dependent it may be dangerous to draw any conclusions about passive film breakdown from polarisation data in which the time taken, for example, to cover the final 400 mV (at a sweep rate of 20 mV/MIN) is only 20 MIN.

3.2.3 The influence of hydrogen peroxide additions on the stress corrosion cracking susceptibility in aqueous chloride environments

In the previous two sub-sections it was suggested that the oxygen reduction reaction was the principle cathodic reaction operating during the stress corrosion cracking of maraging steel in neutral or alkaline environments. Thus, the fact that smooth tensile specimens exposed to the latter environments under freely corroding conditions were observed to form shallow pits but that stress corrosion cracks did not subsequently propagate from the pits may be due, at least in part, to an insufficient rate of oxygen replenishment to the specimen surface to maintain the corrosion reactions required for crack propagation.

The oxygen reduction reaction is regarded as occurring in a number of successive steps one of which involves the formation of hydrogen peroxide, H_2O_2, as an intermediate reactant.

Thus:-

$$O_2\ (air) \rightarrow O_2\ (soln)$$
$$O_2\ (soln) \rightarrow O_2\ (ads)$$
$$O_2\ (ads) + H^+ + \varepsilon \rightarrow HO_2\ (ads)$$
$$HO_2\ (ads) + H^+ + \varepsilon \rightarrow H_2O_2$$
$$H_2O_2 + 2\varepsilon \rightarrow 2OH^-$$

the overall reaction being:-

$$O_2 + 2H_2O + 4\varepsilon \rightarrow 4OH^-$$

Therefore, if hydrogen peroxide is added to the corrosive environment of a metal environment system in which oxygen reduction is suspected as being the predominant cathodic reaction then it would be expected that the stress corrosion cracking propensity would be enhanced.

Fig. 3.20 shows the results of constant crosshead speed tensile tests performed on smooth tensile specimens exposed at the free corrosion potential to a 3.5 wt % sodium chloride solution containing an addition of 2% by volume of hydrogen peroxide and adjusted to an initial pH of 2.0 or 11.0 prior to testing with dilute HCl or NaOH respectively. The results of similar tests performed in solutions minus hydrogen peroxide are plotted on the same graphs for direct comparison.

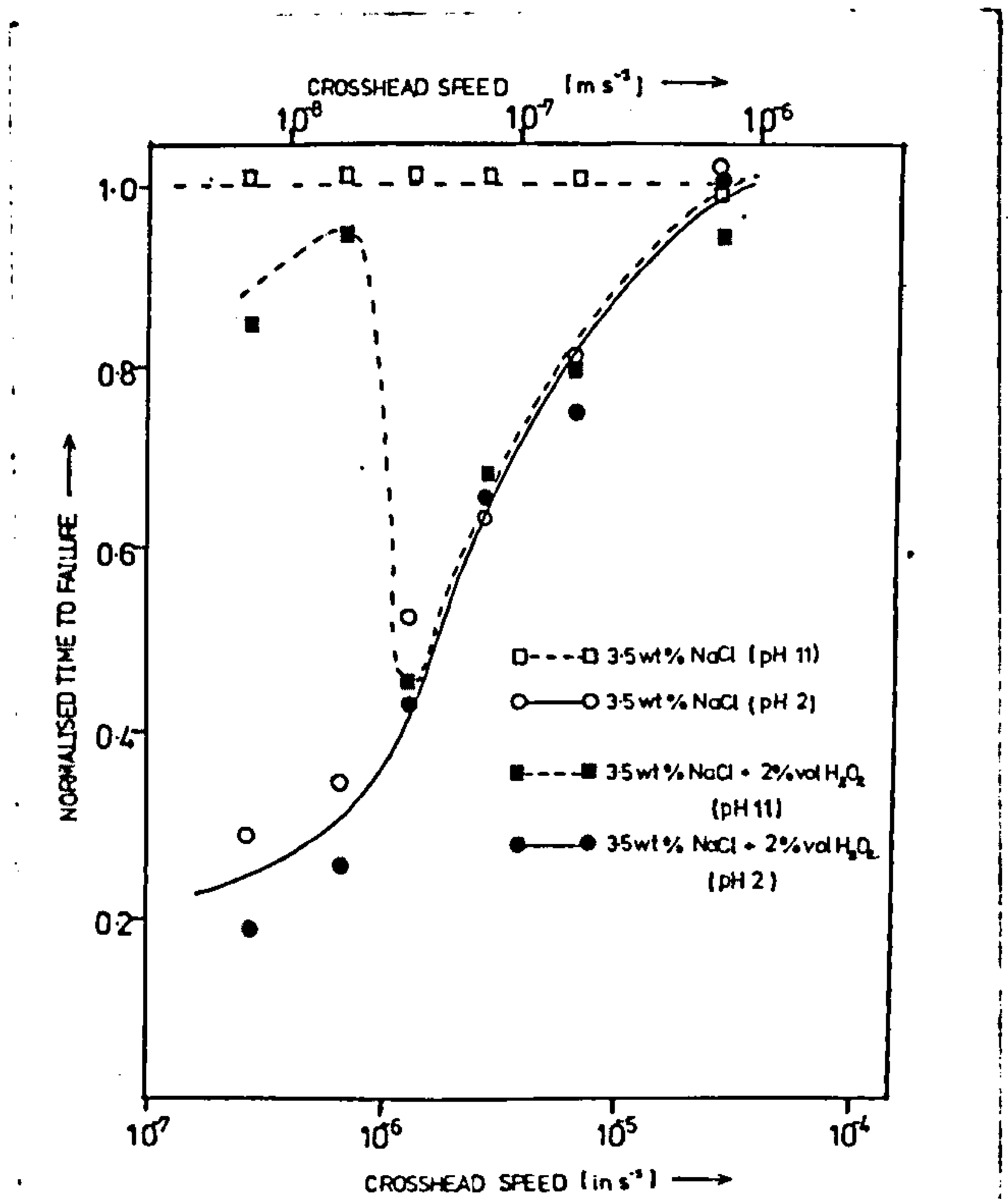

Fig. 3.20 Plot of the normalised failure times as a function of crosshead speed for a smooth maraging steel tensile specimens tested in a 3.5 wt % NaCl solution containing 2% by volume of H_2O_2 and adjusted to initial pH's of 2.0 and 11.0.

It is quite clear that the main effect of the hydrogen peroxide addition was to produce cracking in the solution made akaline to pH 11.0 the latter being a solution in which cracking could not be induced in its absence.

The above results appear to confirm that the oxygen reduction cathodic reaction may be the rate controlling factor in the stress corrosion cracking of maraging steel particularly in the less aggressive neutral or alkaline environments.

3.2.4 The influence of pH on the susceptibility towards SCC of freely corroding maraging steel in 3.5 wt % NaCl solution

In Fig. 3.21, the normalised failure times of smooth maraging steel specimens tested under freely corroding conditions in 3.5 wt % NaCl solutions adjusted to various initial pH's of between 1 and 12 with dilute solutions of hydrochloric acid (0.6N) or sodium hydroxide, and at a crosshead speed of 1.29×10^{-6} INS^{-1} are plotted as a function of initial pH.

It is evident that failures could only be produced in specimens tested in solutions of initial pH <3.0. Failure in these latter solutions was associated with the formation of a uniform black corrosion product on the exposed gauge lengths of the specimens. At pH's of between 3.0 and 11.0 dissolution was apparent as the formation of red rust spots along the exposed gauge lengths. In the test performed in a solution of initial pH = 12.0 the surface remained free of any visible signs of dissolution.

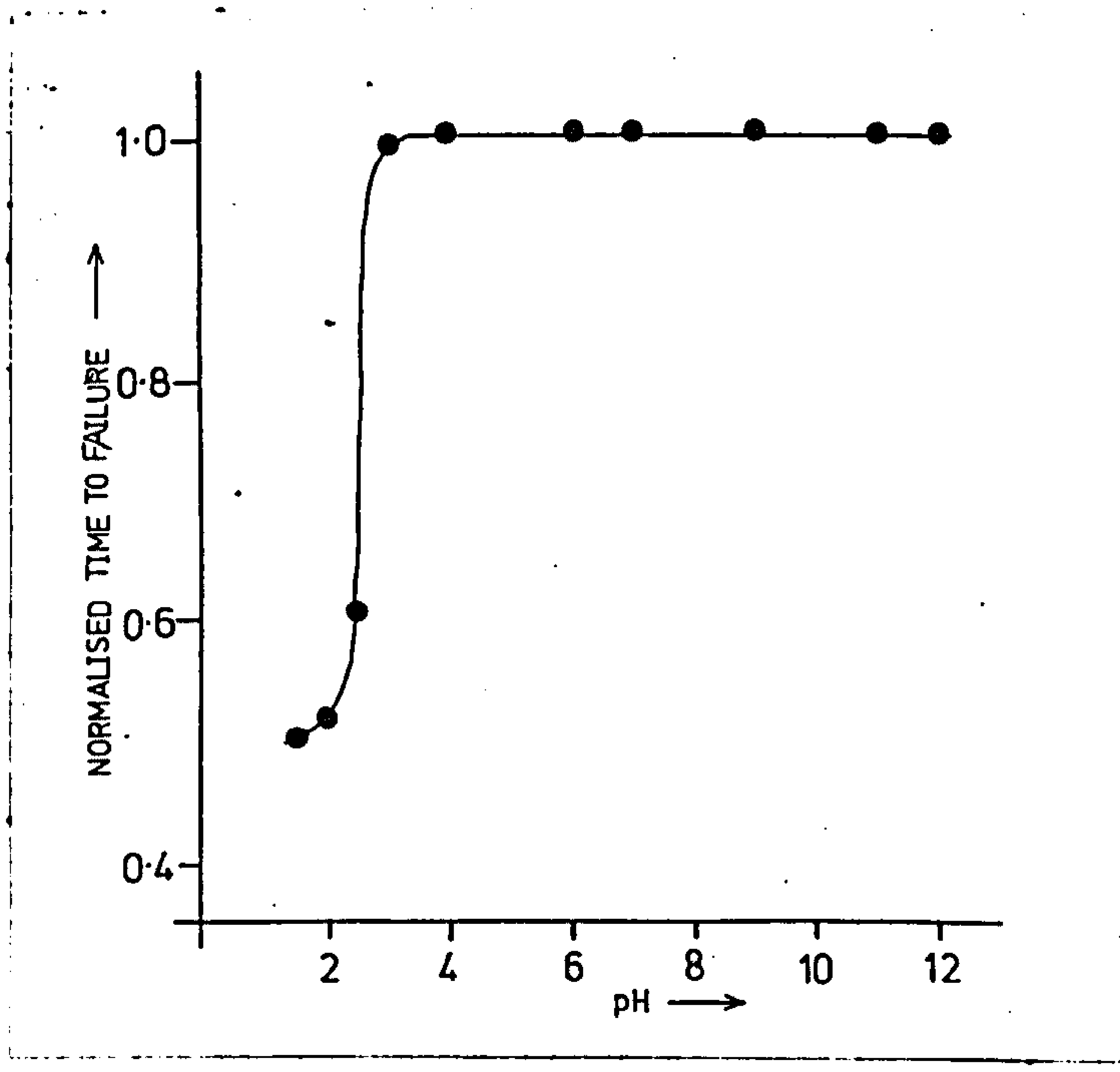

Fig. 3.21 Plot of the normalised failure times as a function of pH for smooth maraging steel tensile specimens tested at a crosshead speed of 1.29×10^{-6} INS^{-1} under freely corroding conditions in 3.5 wt % NaCl solutions adjusted to various initial pH's.

It could be argued that since the maximum exposure time in the above tests did not exceed 21hr (corresponding to the failure time on air of a specimen strained at a crosshead speed of 1.29×10^{-6} INS^{-1}), the failure of specimens to crack in the intermediate pH range, where dissolution was observed to be taking place at localised spots in the form of pitting, could be explained by insufficient time being available for the necessary cracking conditions to develop. It was decided, therefore, to carry out a series of tests in a solution of initial pH = 11.0 at various crosshead speeds in the range $2.5 \times 10^{-7} \rightarrow 2.5 \times 10^{-5}$ INS^{-1}, for which the maximum exposure time possible was 84 hr (at a crosshead speed of 2.5×10^{-7} INS^{-1}). Cracking could not be induced in these tests even in the specimen tested at the slowest crosshead speed. Indeed, as will be seen in section 3.4, cracking could only be induced in plain tensile specimens exposed to neutral and alkaline solutions of 3.5 wt % NaCl when tested in the constant total strain loading mode and only then when loaded to initial stresses exceeding the yield strength of the material.

The results described above are at variance with the observations of Green and Haney[48] and Leckie[59].

It may be recalled; (cf. Literature review) that Green and Haney using thin foil (.002" thick) tensile specimens of an 18Ni maraging steel observed pronounced minima at pH values of 2.0 and 11.0, when failure times were plotted as a function of initial pH. Leckie observed similar minima in the failure times of fatigue precracked specimens of a 12Ni-5Cr-3Mo maraging steel, at pH's of 2.0 and 12.0.

The discrepancy between the results of the present investigation and those of Green and Haney and Leckie may be explained as follows:-

i) Green and Haney used foil specimens in their investigations. Accordingly what their results probably reflect is not the influence of pH on the resistance to stress corrosion crack initiation and propagation but the influence of pH on the resistance to pitting.

Furthermore, since pitting attack is initiated at weak sites such as inclusions, scratch lines etc in the otherwise protective air formed oxide film; then the failure times of thin foil specimens would depend upon the number and distribution of such sites on the metal surface. Consequently, a considerable amount of scatter in the experimental failure times could be expected in such tests It is conceivable therefore that the minimum in failure time observed by Green and Haney at pH 11.0 could simply reflect experimental scatter in their tests as a consequence of pitting.

ii) Leckie's results, on the other hand, while undoubtedly reflecting the true resistance to stress corrosion cracking do not distinguish between the initiation and propagation stages of crack growth; it being assumed that the use of fatigue precracked specimens circumvents the initiation stage in crack propagation. However, though it may be true to say that precracking may shorten or modify the crack initiation period, it does not circumvent it altogether. In the present work, for example, it was rarely observed that fatigue precracked specimens began to crack immediately upon the application of the desired electrochemical conditions. Indeed, often several hours elapsed before cracking was initiated. Consequently, the minimum in failure times observed by Leckie at a pH of 12 could simply be indicative of a comparatively shorter crack initiation period in the specimen tested at the latter pH compared with those initiation periods in solutions of pH 6, 8 and 10 for example.

The absence of cracking in plain tensile specimen tests of pH's in excess of 3.0 prompted the execution of similar tests on fatigue precracked specimens, principally to determine whether or not the presence of precracks are a necessary precursor to crack propagation in plain specimens exposed to the less aggressive environments.

Table 3.5 lists the initial pH's, initial stress intensities and average crack velocities of tests performed on pin loaded single edge notch tensile specimens freely corroded in 3.5 wt % NaCl solution adjusted to the initial pH indicated with dil HCL solution or NaOH solution.

TABLE 3.5

Results of S.E.N. tensile specimens tested in 3.5 wt % NaCl of various initial pH's under freely corroding conditions.

Ksi $\sqrt{in}$

Initiation Time (HR)	pH	Initial Stress Intensity KSI $\sqrt{IN}$	Initial Stress Intensity $MNm^{-3/2}$	Crack Velocity ins^{-1}	Crack Velocity ms^{-1}
10	2.0	22.4	24.61	$1x10^{-6}$	$2.54x10^{-8}$
11.5	6.0	22.0	24.17	$6x10^{-6}$	$1.52x10^{-7}$
25	6.6	24.9	27.36	$5.2x10^{-6}$	$1.32x10^{-7}$
12	8.5	22.0	24.17	$5.5x10^{-6}$	$1.4x10^{-7}$
12	11.0	21.3	23.4	$1.8x10^{-6}$	$4.57x10^{-8}$
-	12.0	No cracking in 30hr.			

Crack velocities were determined on the basis of the time for which crack propagation was seen to be taking place (as indicated by the D.C. resistance technique for crack growth monitoring) and not on the basis of the time from addition of the test solution. Therefore, unlike Leckie's results the above results are characteristic only of actual crack propagation; the influence of varying initiation times having been effectively eliminated as explained above.

Macroscopic crack branching was observed in the specimens tested in solutions of pH 5.5, 6.6 and 8.5 at stress intensities of 27, 31.75 and 30.6 KSI $\sqrt{IN}$ respectively. The average crack velocities quoted in Table 3.5 were calculated from the maximum crack growth in the plane of the precrack.

The most significant feature of these results is the fact that cracking took place at all under conditions which, as we have seen, were not amenable to the initiation of cracking in plain tensile specimens. The importance of sharp discontinuities in promoting the stress corrosion cracking of maraging steel in the less aggressive environments has been adequately demonstrated therefore.

3.2.5 The influence of applied current on the failure times of smooth tensile specimens of maraging steel

As has been seen (cf. section 1.4 Literature review) the application of anodic and cathodic currents to specimens subjected to stress corrosion conditions has been used in deciding whether failure of freely corroding stressed specimens in a given corrosive environment is due to hydrogen embrittlement or stress corrosion cracking.

Fig. 3.22 shows that for maraging steel exposed to 3.5 wt % NaCl solution acidified to an initial pH of 2.0 anodic currents reduced the cracking time while

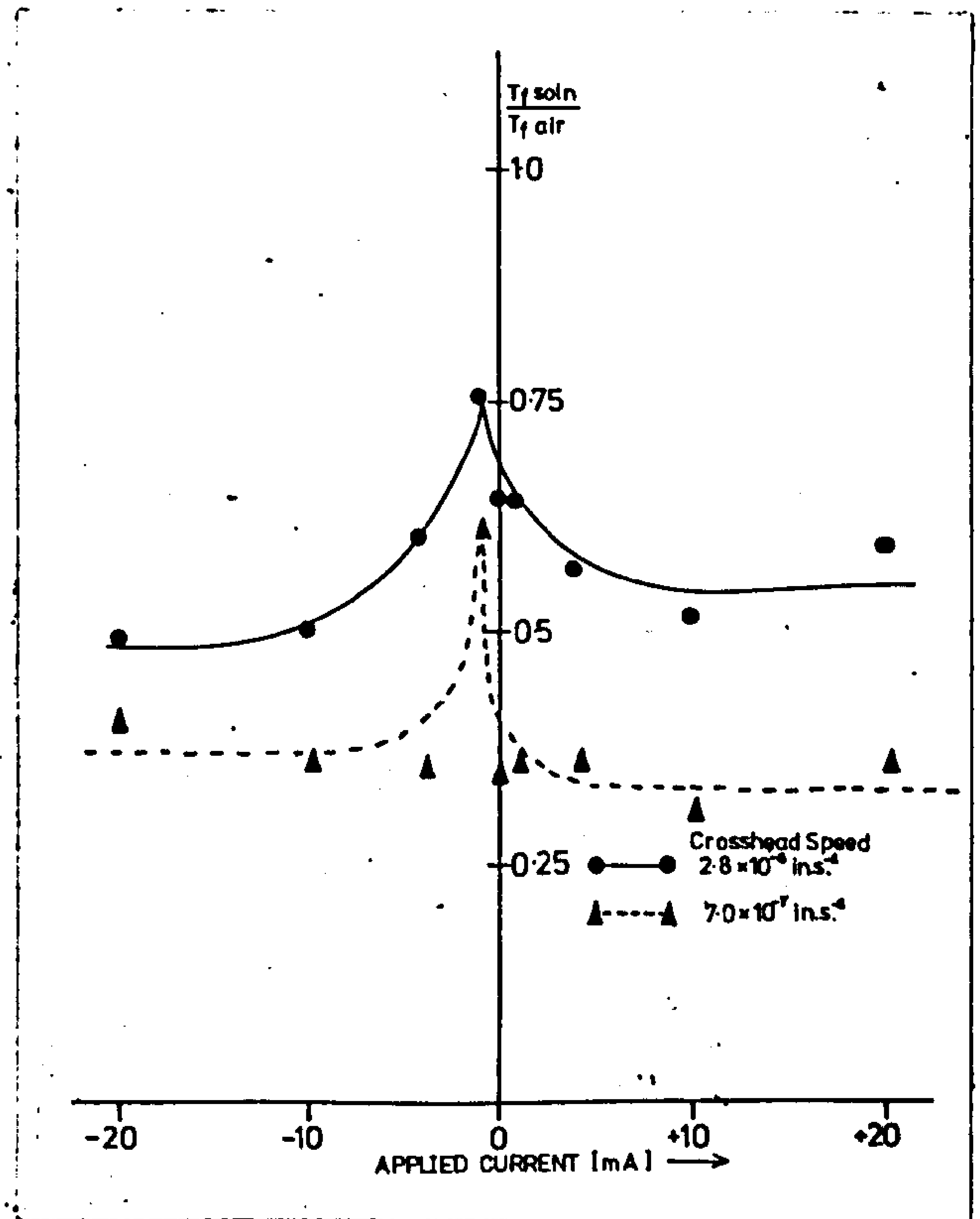

Fig. 3.22 The influence of applied current density on the stress corrosion cracking susceptibility of smooth maraging steel specimens strained at the crosshead speeds indicated in a 3.5 wt % NaCl solution of initial pH 2.0.

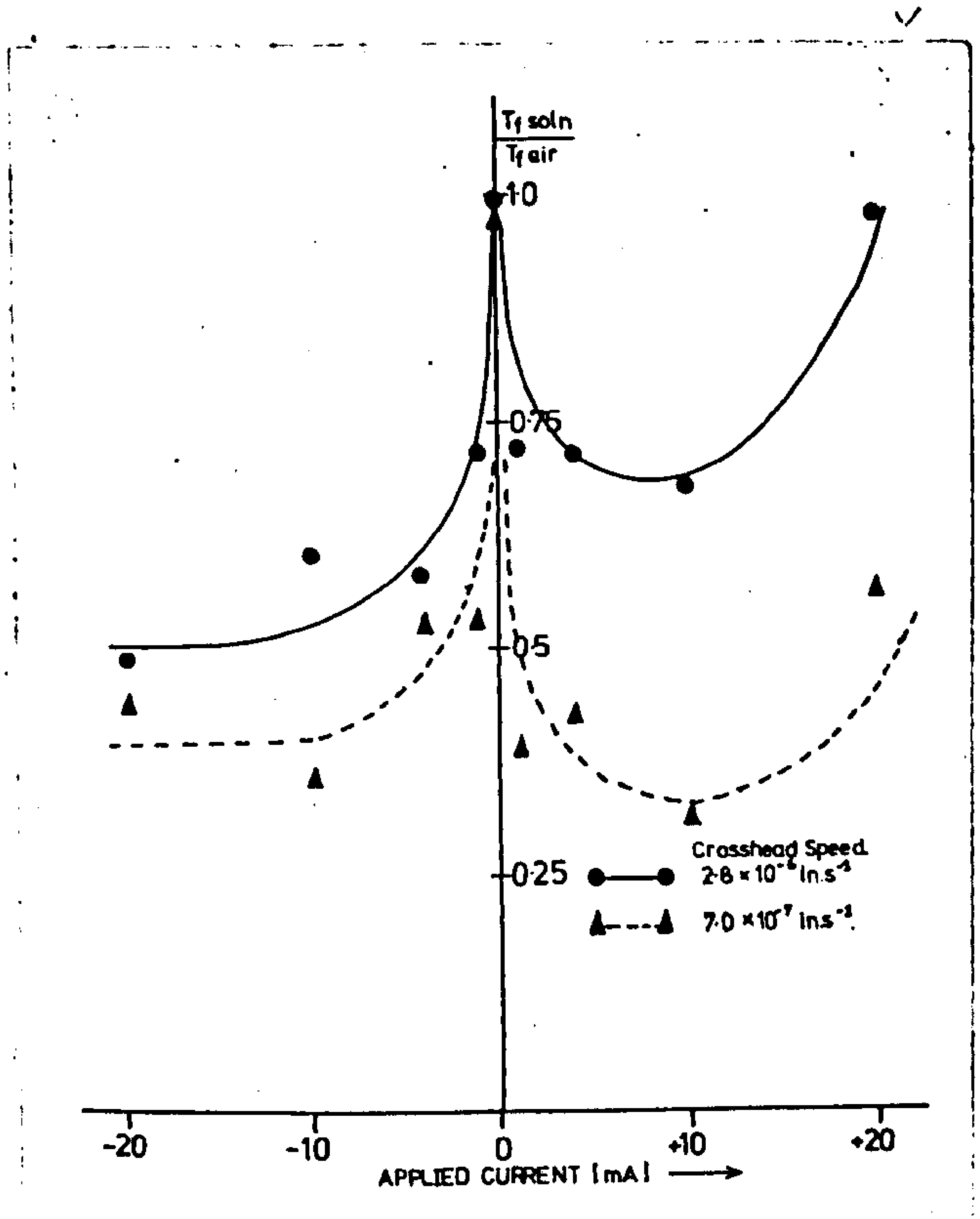

Fig. 3.23 The influence of applied current density on the stress corrosion cracking susceptibility of smooth maraging steel specimens strained at the crosshead speeds indicated in a 3.5 wt % NaCl solution of initial pH 11.0.

small cathodic currents significantly prolonged the cracking time; behaviour that is characteristic of a classical stress corrosion system. Relatively high cathodic currents reduced the time to failure and indicate that the system is one in which hydrogen embrittlement can be induced but that under freely corroding conditions failure is by stress corrosion cracking as a result of anodic dissolution.

Fig. 3.23 shows the effect of applied current on the times to failure of maraging steel specimens exposed to a 3.5 wt % NaCl solution adjusted to an initial pH of 11.0. In this environment failure of smooth tensile specimens could not be induced at the free corrosion potential. Anodic and cathodic currents both reduced the time to failure; however, very high anodic current densities produced general dissolution followed by necking and ductile failure. The latter probably reflects the polarising influence of the heavy ferrous/ferric hydroxide precipitate which was observed to form readily in this alkaline solution. Thus, the hydroxide precipitate was evidently stifling the anodic dissolution process at the grain boundaries and even the highest strain rates employed were insufficient to depolarise the reaction - particularly at the high current densities employed. Consequently localised grain boundary dissolution was replaced by general dissolution and specimen thinning.

3.2.6 The influence of various additions made to the basic test solution

In an extensive programme initiated to try to determine the cracking mechanism(s) operating during the S.C.C. of maraging steel in aqueous saline environments, the effects of various ingredients added to the basic 3.5 wt % NaCl test solution on

a) the failure times of smooth constant crosshead speed tensile specimens

b) crack velocities of fatigue precracked cantilever loaded beam specimens

and c) hydrogen permeation characteristics through thin membranes were investigated as a function of applied polarisation.

The various additives chosen were as follows:-

1) Chloroplatine acid solution 5% w/v (25 cc/l of basic test solution).

2) Sodium arsenate (hydrated). $Na_2A_sO_47H_2O$ (5 gm of hydrated salt/l of test solution).

3) Thiourea (5 gm/l of test solution).

These additives were selected because of their known catalysing or poisoning influences on the hydrogen evolution reaction (HER).

$$2H^+ + 2\varepsilon \rightarrow H_2 \text{ gas}$$

via $H^+ + 1\varepsilon \rightarrow H_{ads}$; $H_{ads} + H_{ads} \rightarrow H_2$ or $H_{ads} + H^+ + \varepsilon \rightarrow H_2$

a) Additions of chloroplatnic acid, cause cathodically polarised sites to be decorated with platinum black. The latter exhibits a high exchange current density and low overpotential for the hydrogen evolution reaction and consequently any hydrogen ions reduced at these sites will be more readily evolved as molecular hydrogen than absorbed into the metal lattice to produce hydrogen embrittlement. Consequently, if cracking is a result of hydrogen embrittlement, the susceptibility towards cracking should be decreased by chloroplatinic acid additions made to the test solution.

b) Group V metals or metalloids including P, As or Sb are well known to act as poisons of the hydrogen evolution reaction when added in compound form to corrosive environments. As such these additions have been employed to prevent corrosion in acidified corrosive environments where hydrogen reduction is considered to be the principle cathodic reaction taking place.

It is thought that while the proton reduction step $H^+ + 1\varepsilon \rightarrow H_{ads}$ is allowed to go on unhindered the subsequent combination of these adsorbed hydrogen atoms to form diatomic hydrogen molecules is largely prevented. The precise mechanism of the inhibition of the recombination reaction is uncertain but it has been suggested[121] that, for example, the arsenious ion A_sO^+ is sufficiently surface active to adsorb at those sites at which hydrogen atoms may recombine (e.g. at growth edges). The arsenious ion may then be cathodically reduced by reactions such as

$$AsO^+ + 2H_{ads} + \varepsilon \rightarrow As + H_2O$$

or

$$As_2O_3 + 6H_{(ads)} \rightarrow 2As + 3H_2O$$

It can be seen therefore that the introduction of arsenical compounds into mildy acidic environments can result in a high population of uncombined hydrogen atoms on the metal surface thereby encouraging the absorption of hydrogen into the metal lattice which can result in hydrogen embrittlement cracking. If, therefore, cracking is attributed to hydrogen embrittlement then the addition of sodium arsenate to the corrosive environment ought to increase the S.C.C. susceptibility.

c) Thiourea is an adsorption inhibitor often used in acid pickling to restrain active dissolution of the substrate metal whilst permitting mill scale removal to continue unhindered. Unfortunately, whilst inhibiting metal dissolution; the use of thioureas in acid pickling is also know to increase hydrogen uptake and can therefore result in hydrogen embrittlement.

Thioureas bond strongly to the metal surface by sharing electrons with surface metal atoms (σ bonding) and do so indiscriminantly over the entire surface. Therefore they tend to be very effective corrosion inhibitors interfering with both the anodic and cathodic reactions. The interference is thought to be a simple steric effect such that solvating water molecules are prevented from uniting to form hydrogen molecules. It is because of this latter affect that the presence of thiourea in solution can lead to hydrogen embrittlement of steels and particularly of the high strength steels which are particularly susceptible to hydrogen embrittlement cracking.

Therefore, the effects of thiourea additions on the cracking susceptibility of maraging steel might be expected to be similar to those produced by sodium arsenate additions if cracking is a consequence of hydrogen embrittlement.

a) <u>The influence of solution additions on the susceptibility to SCC of smooth tensile specimens tested at constant crosshead speeds</u>

Constant crosshead speed tensile tests

were performed on maraging steel specimens, austenitised for 1hr at 950°C and aged for 3hr at 530°C, in 3.5 wt % NaCl solutions containing the above ingredients and acidified in all cases to an initial pH of 2.0. Tests were performed under freely corroding conditions and also with anodic or cathodic polarisation applied to the specimen gauge length using the simple galvanostatic circuit described in section 2.4.1.

In order to avoid carrying out repetitive confirmatory tests in a given testing situation, an extensive testing programme was carried out in which

i) Two different crosshead speeds were chosen. Failure times at these crosshead speeds were then determined as a function of applied current.

ii) Failure times were determined as a function of crosshead speed for specimens tested under freely corroding conditions and with 10 mA anodic or cathodic current applied to the specimen gauge length.

Failure times in solution were in all cases normalised on the corresponding failure times in air.

Figs. 3.24, 3.25 show the normalised failure times plotted as a function of applied current for tests performed at crosshead speeds of 2.8×10^{-6} and 7.0×10^{-7} INS^{-1} respectively.

In Figs. 3.26, 27, 28 normalised failure times are plotted as a function of crosshead speed for tests performed with cathodic polarisation at the free corrosion potential, and with anodic polarisation respectively.

Fig. 3.24 The influence of additions of a) 5gm/l of sodium arsenate ($Na_2AsO_4\ 7H_2O$), b) 5gm/l of thiourea and c) 25cc/l of chloroplatinic acid solution (5% w/v) to the corrosive environment (3.5 wt % NaCl, initial pH 2.0) on the cracking susceptibility of smooth maraging steel tensile specimens tested at a cross-head speed of 2.8×10^{-6} INS^{-1}.

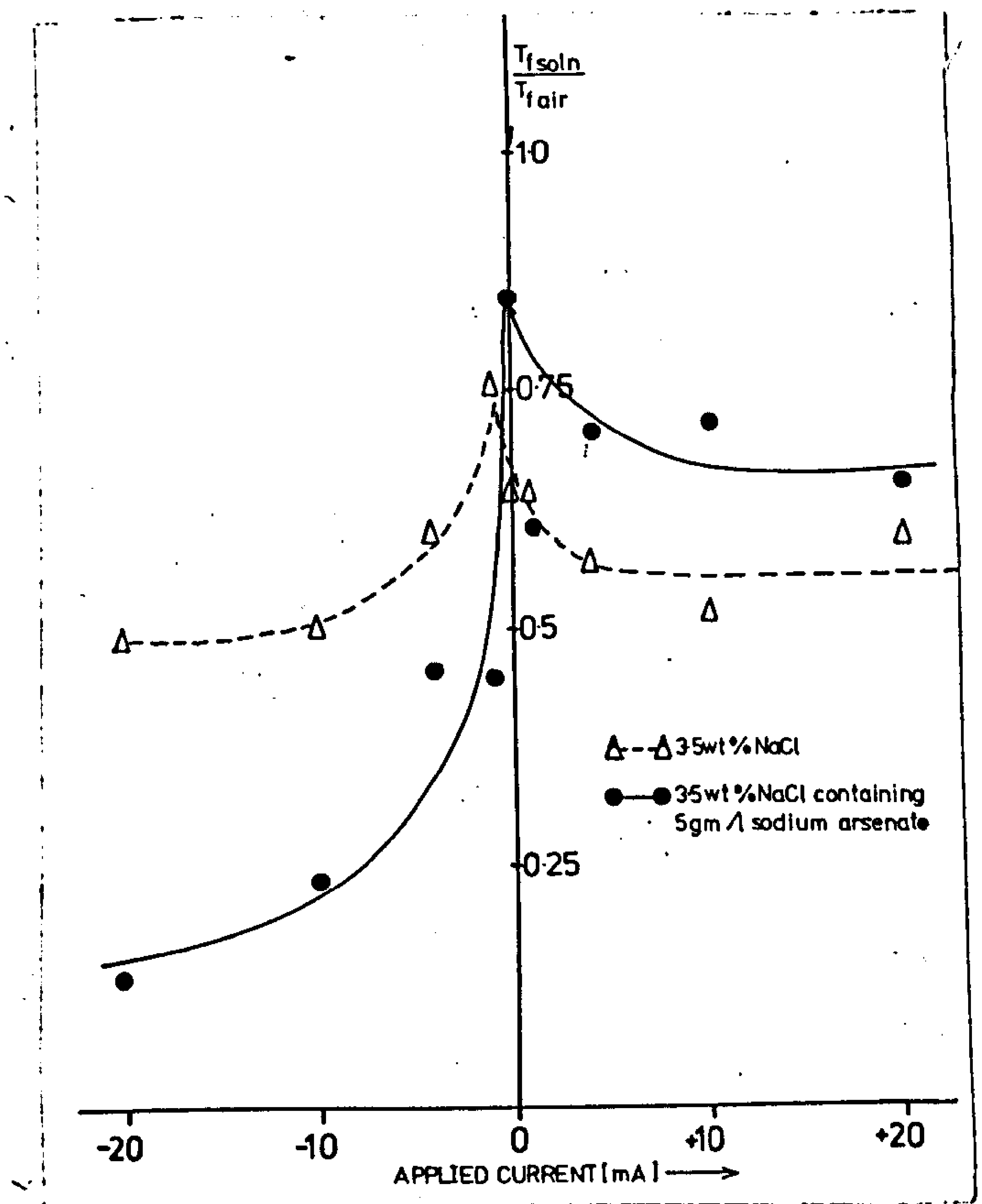

Fig. 3.24a

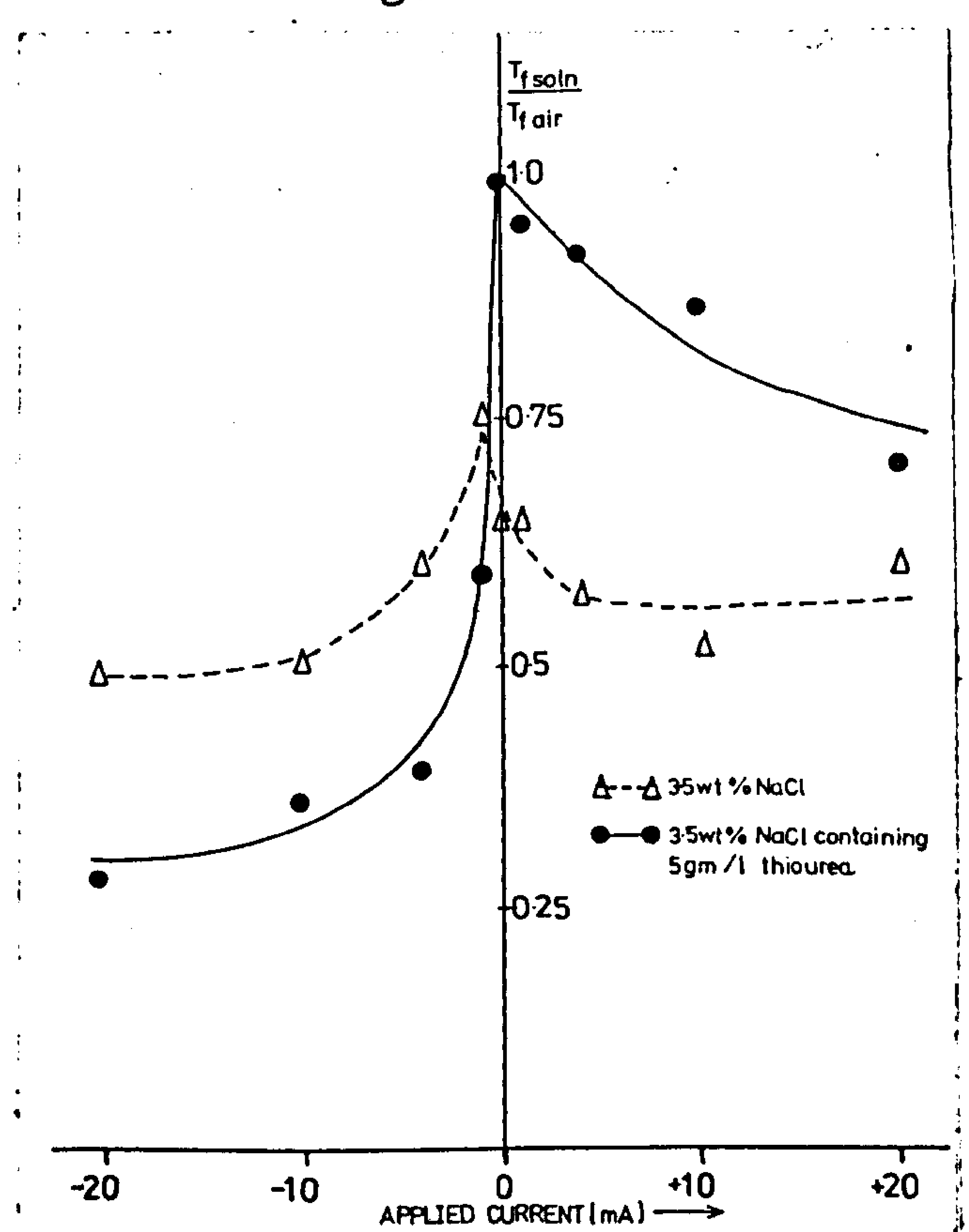

Fig. 3.24b

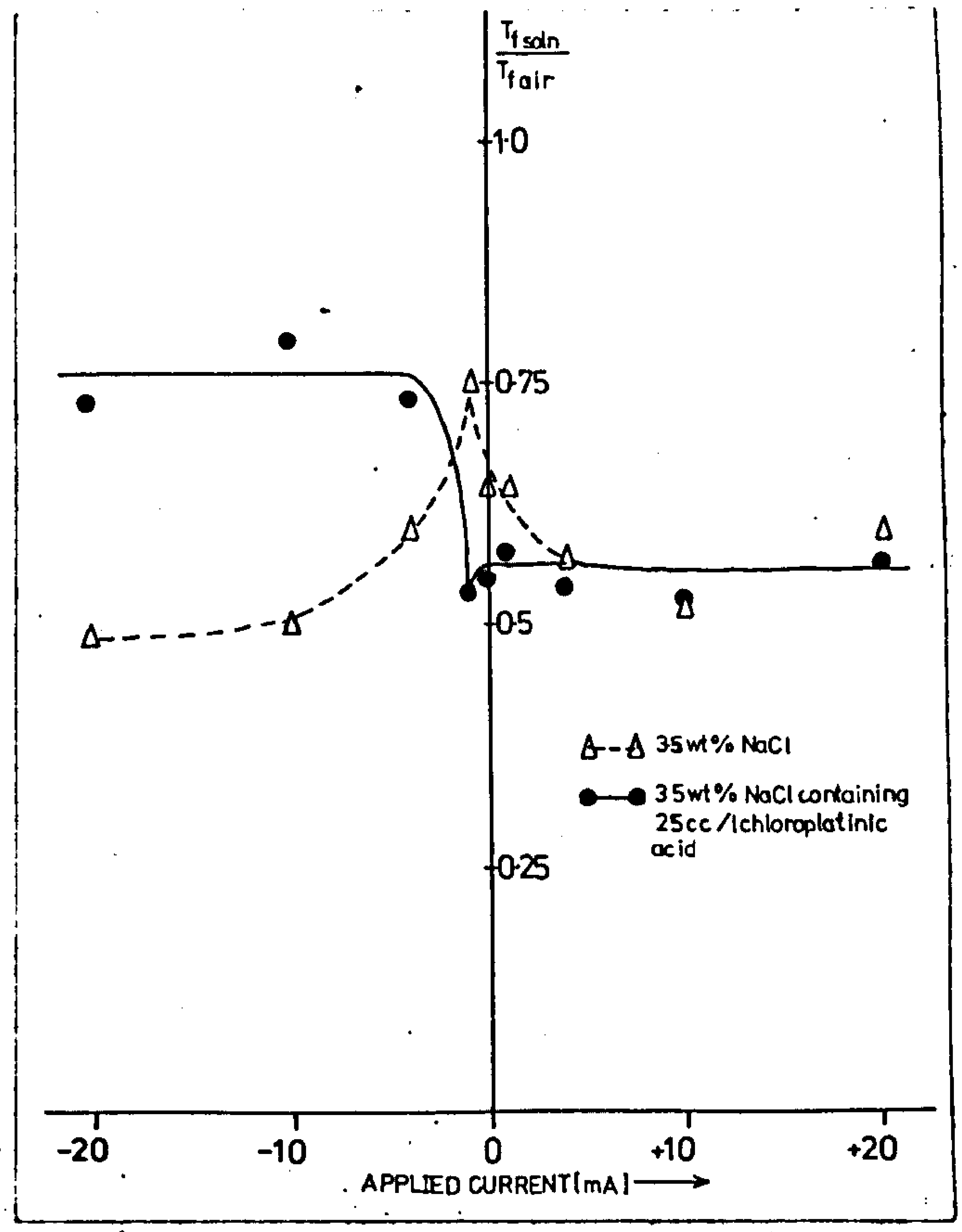

Fig. 3.24c

Results of tests performed in solutions containing no added ingredients are plotted on the same graphs for comparison.

The different additives can be seen to have had different effects on the cracking susceptibilities depending upon the nature and extent of polarisation applied to the specimen.

The results of tests performed on highly cathodically polarised specimens (i.e. more negative than 1 mA) illustrate the catalysing effect of chloroplatinic acid and the poisoning effect of thiourea and sodium arsenate on the recombination step in the hydrogen evolution reaction in accordance with the arguments outlined above.

Fig. 3.25 The influence of additions of a) 5gm/l of sodium arsenate (Na_2AsO_4 $7H_2O$) b) 5gm/l of thiourea and c) 25cc/l of chloroplatinic acid solution (5% w/v) to the corrosive environment (3.5 wt % NaCl, initial pH 2.0) on the cracking susceptibility of smooth maraging steel tensile specimens tested at at crosshead speed of 7.0×10^{-7} INS^{-1}.

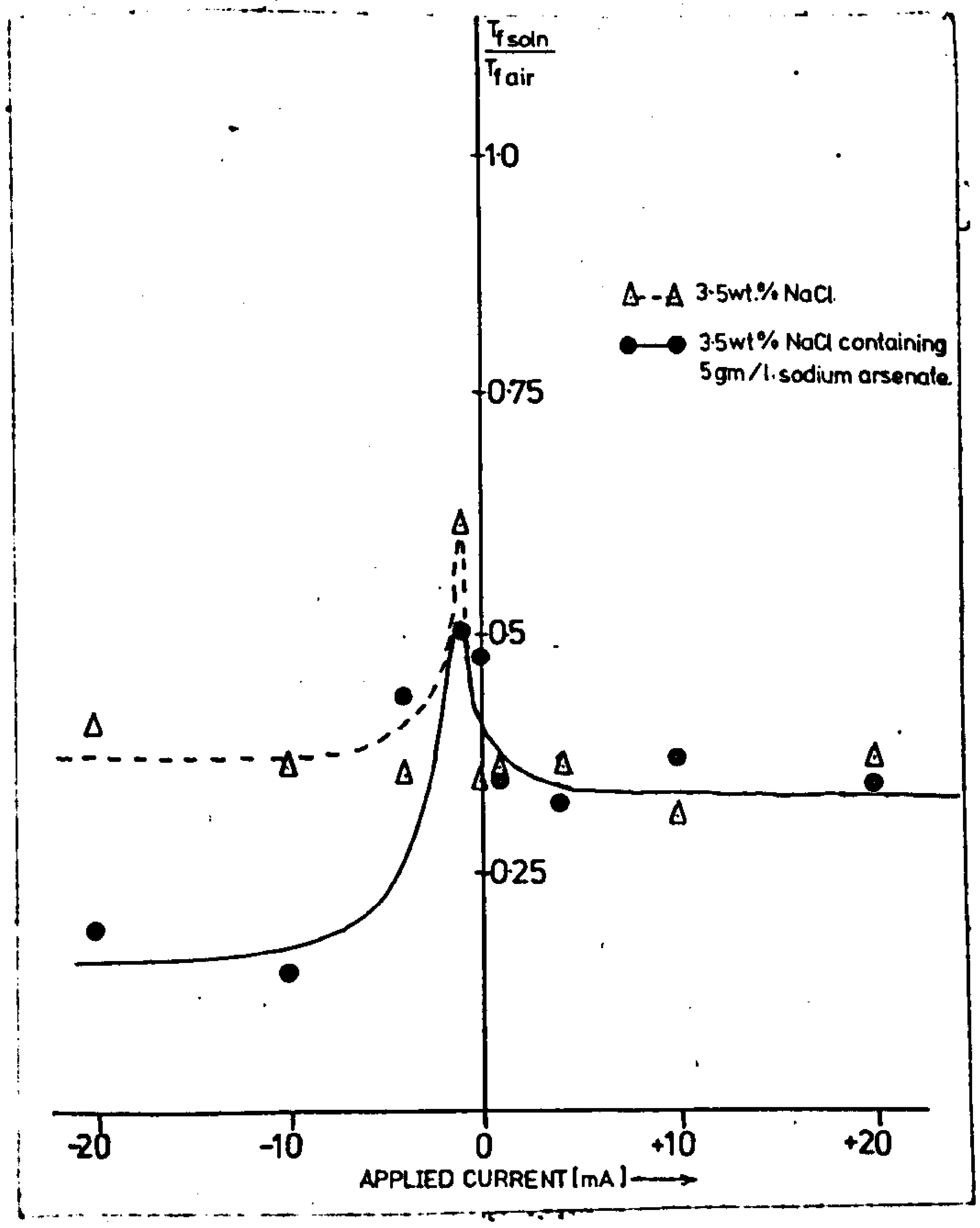

Fig. 3.25a

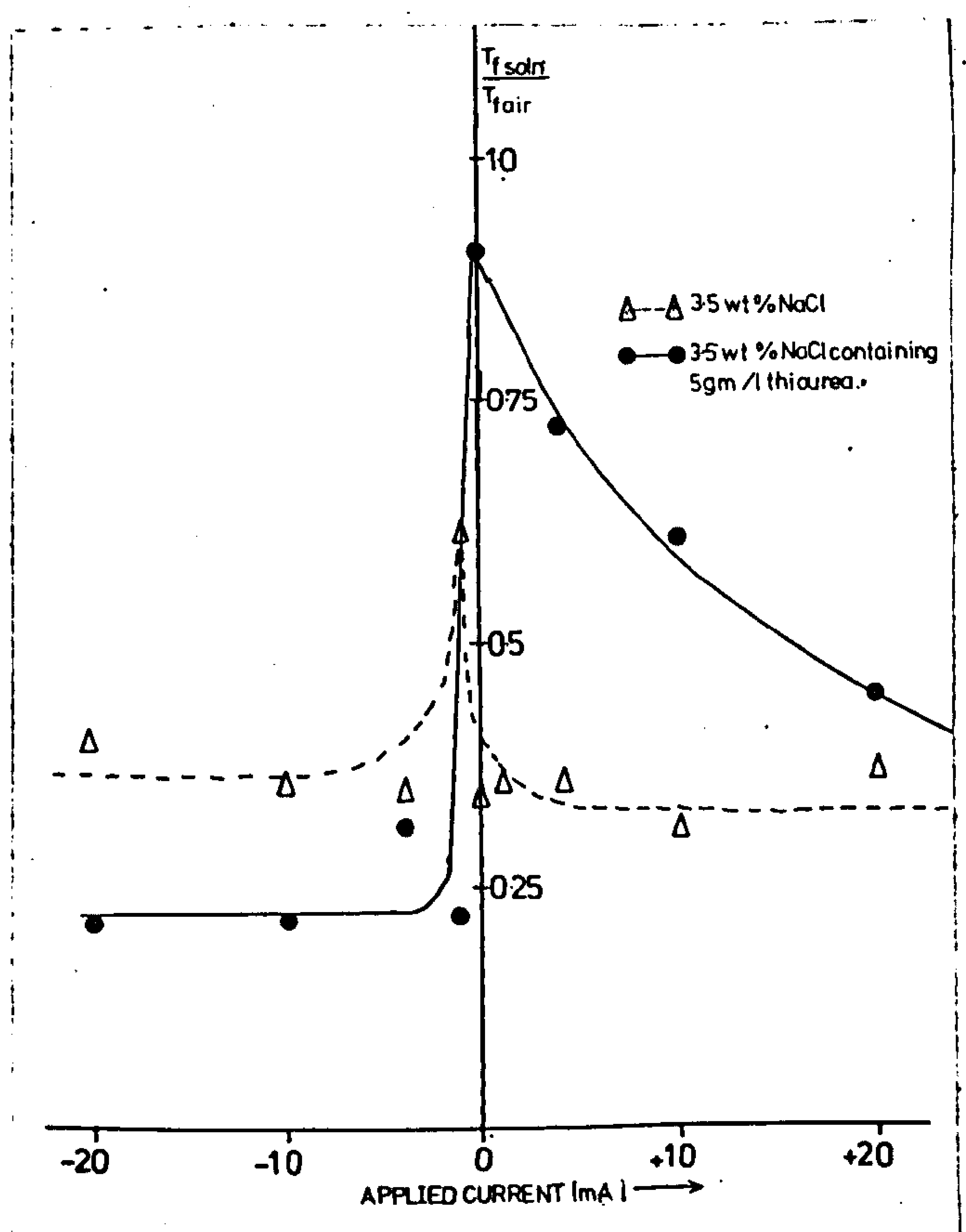

Fig. 3.25b

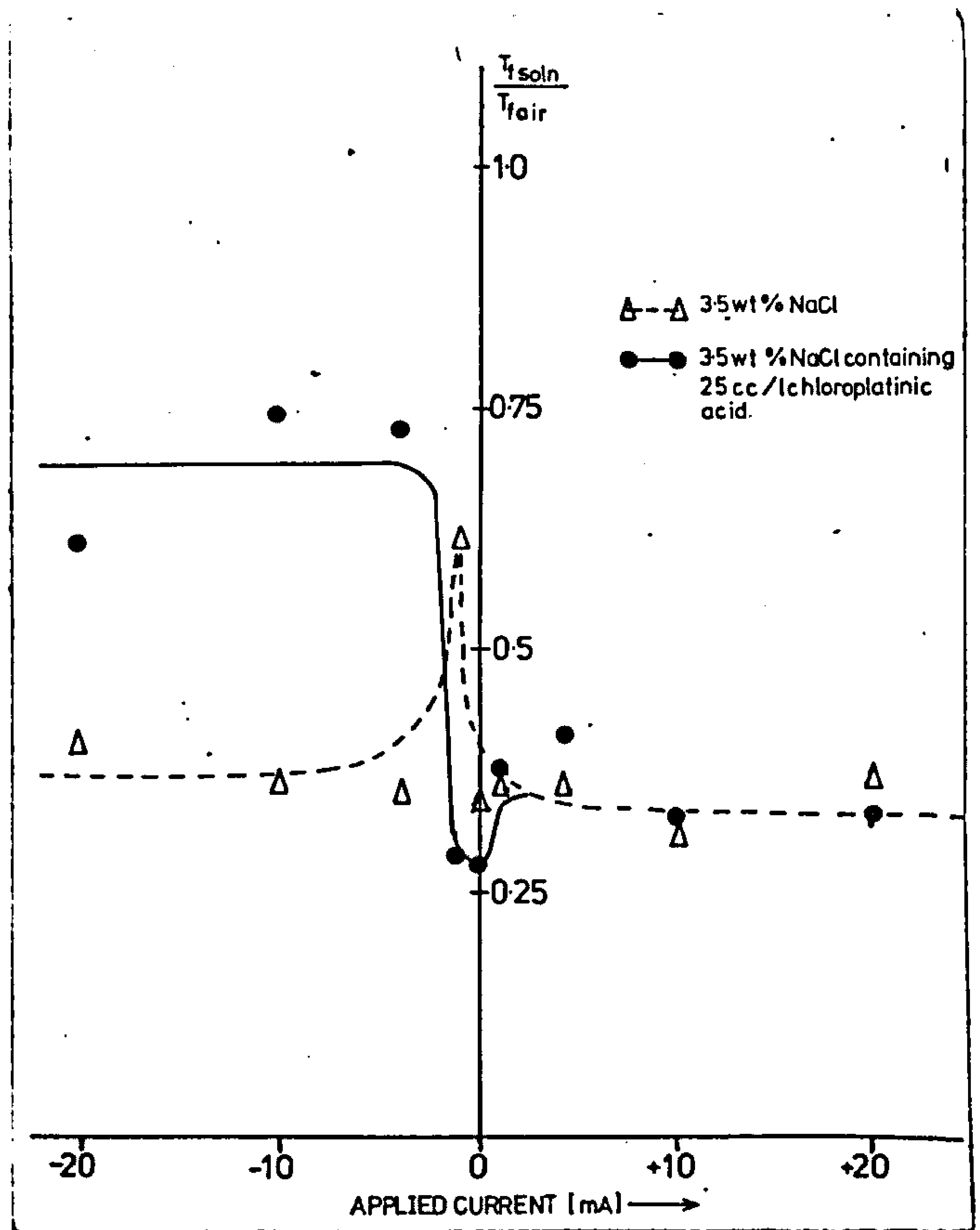

Fig. 3.25c

The influence of the solution additions on the stress corrosion cracking susceptibility at or close to the free corrosion potential are of particular interest.

Chloroplatinic acid additions significantly reduced the failure times of specimens tested with small cathodic polarisation (-1 mA). The latter value, it should be noted is coincident with that current density at which the maximum resistance to stress corrosion cracking was exhibited in uncontaminated test solutions. At the free corrosion potential, chloroplatinic acid additions were again effective in reducing failure times compared with the uncontaminated solution.

If we accept that the cracking mechanism

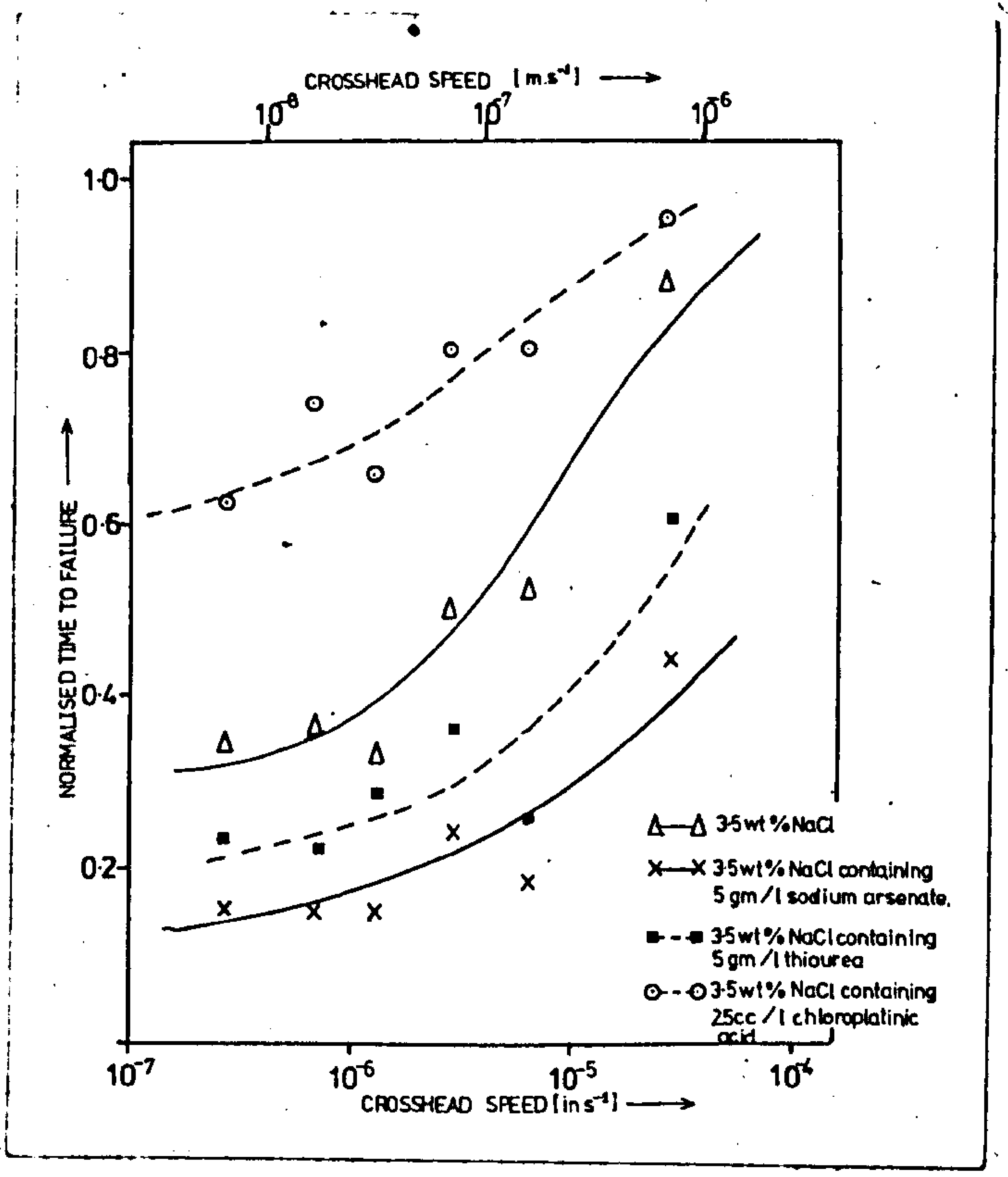

Fig. 3.26 The influence of various additions made to the corrosive environment (3.5 wt % NaCl initial pH 2.0) on the cracking susceptibility of smooth maraging steel tensile specimens subjected to cathodic polarisation.(3.65 mA cm^{-2}).

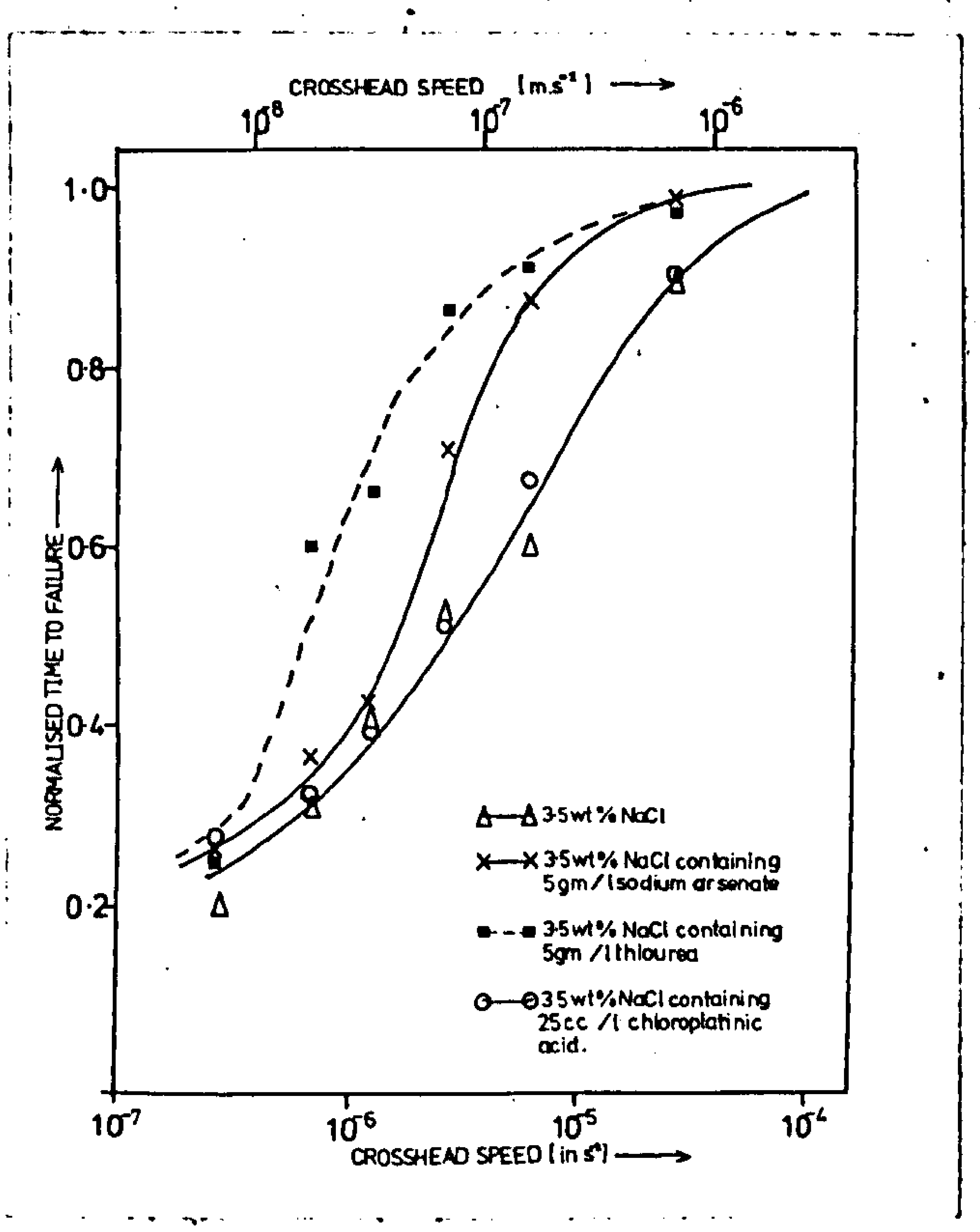

Fig. 3.27 The influence of various additions made to the corrosive environment (3.5 wt % NaCl initial pH 2.0) on the cracking susceptibility of freely corroding smooth maraging steel tensile specimens.

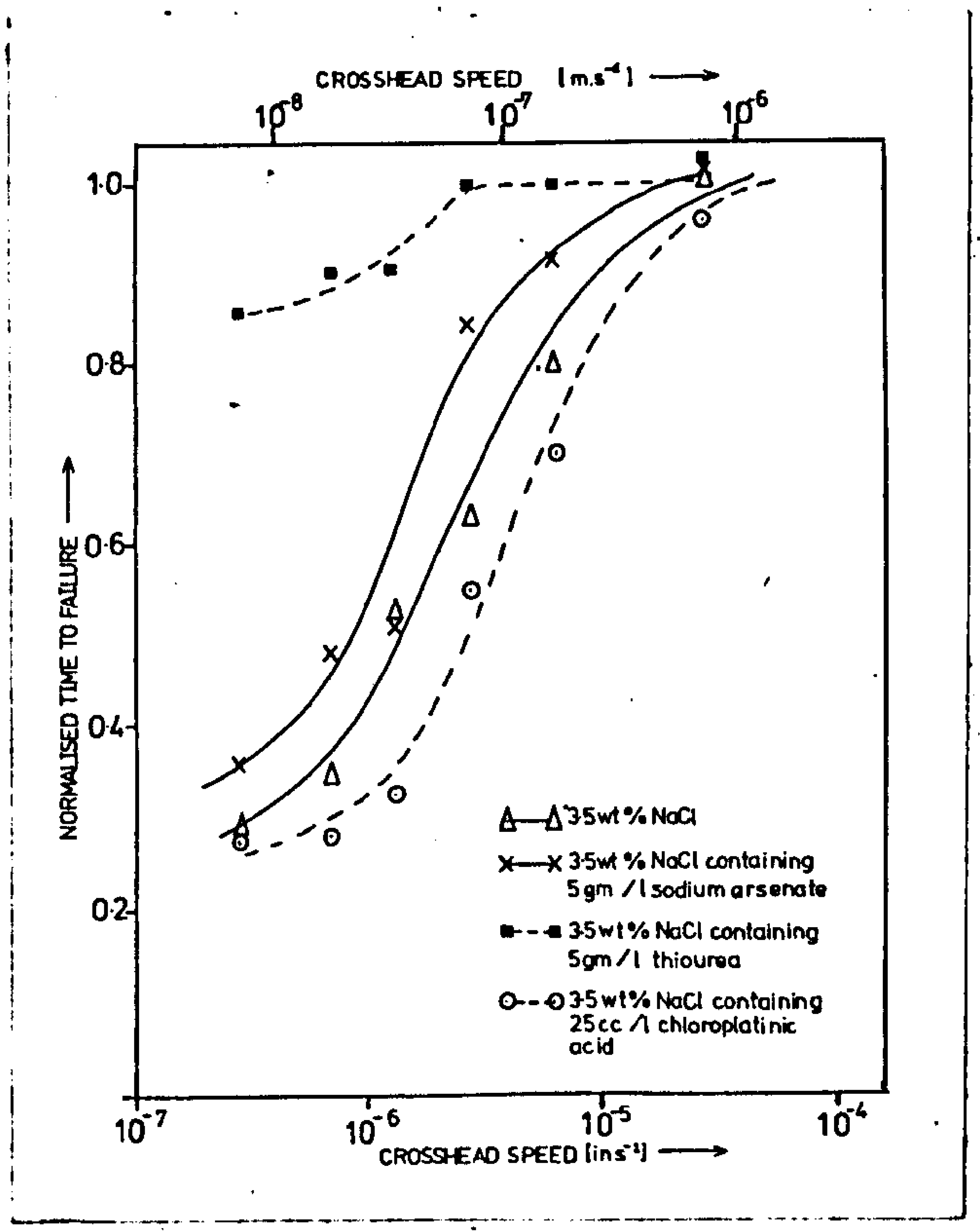

Fig. 3.28 The influence of various additions made to the corrosive environment (3.5 wt % NaCl initial pH 2.0) on the cracking susceptibility of smooth maraging steel tensile specimens subjected to anodic polarisation (3.65 mA/cm^2).

changes from one of predominantly hydrogen embrittlement cracking to predominantly active path corrosion at a current density corresponding to approximately 1 mA cathodic applied to the gauge length of the specimen (as the results of tests performed in uncontaminated solutions would imply according to arguments set out in section 1.4) then the influence of chloroplatinic acid additions on the failure times with slight cathodic polarisation and at the free corrosion potential can be explained by an increase in the corrosion current brought about by the reduced overpotential for the hydrogen evolution reaction at the deposited platinum cathodes.

Thus referring to Fig. 3.29 the corrosion current on the steel is increased from $I_{CORR\ Fe}$ to $I_{CORR\ Pt}$ by the deposition of platinum on cathodic sites.

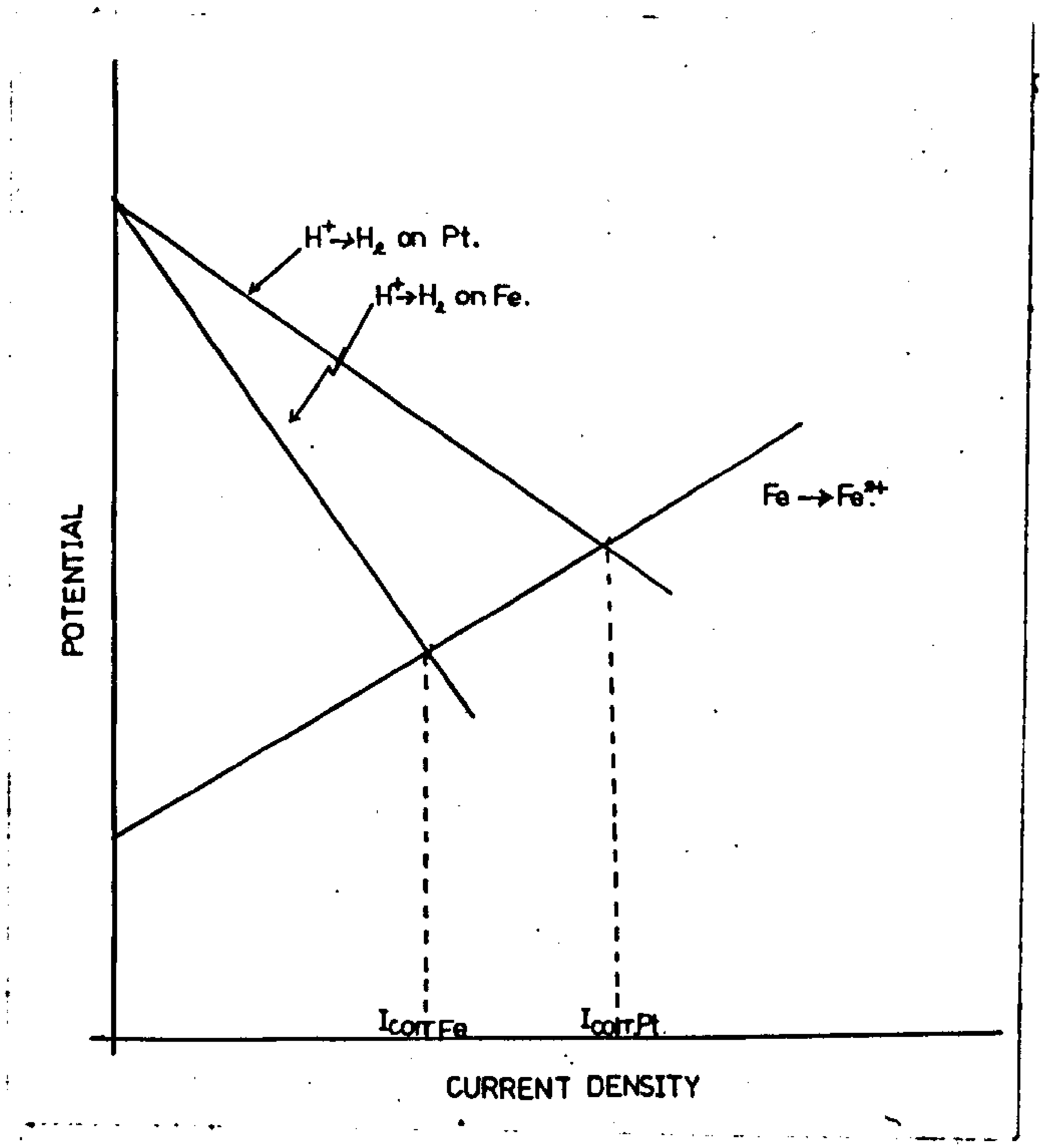

Fig. 3.29 The effect of the addition of a platinum salt on the corrosion of iron in acidic solutions. Schematic only.

Sodium arsenate additions slightly increased and thiourea additions significantly increased failure times of specimens tested under freely corroding conditions. These observations can also be interpreted on the basis of an active path dissolution model. Thus the dissolution reaction in the former case may be inhibited either as a consequence of poisoning of the hydrogen recombination step in the hydrogen evolution reaction or more likely as a consequence of the deposition of metallic arsenic which has been observed to occur from arsenate solutions at potentials more noble than approximately -400 mV (NHE). With reference to the influence of arsenate additions on stress corrosion cracking susceptibilities at or close to the free corrosion potential, Smialowski[122] reports that hydrogen uptake in arsenic containing solutions is only possible at potentials less noble than -0.4V (NHE) i.e. -650 mV SCE corresponding to a potential range over which AsH_3 can be formed at low partial pressures. Consequently, sodium arsenate probably does not have a poisoning effect on the hydrogen evolution reaction at the surface of freely corroding maraging steel exposed to this acidic chloride environment since the corrosion potential of maraging steel in this environment is approximately -400 mV SCE (i.e. -160 mV NHE). Furthermore the arsenite ion, AsO_2 is reduced at a potential of +.2475V NHE according to the reaction:-

$$2HAsO_4 + 6H^+ \rightarrow 2As + 4H_2O + 6\varepsilon$$

and it is probable, therefore, that the surface of the steel will be covered with a layer of As which tends to protect the metal from further corrosion and inhibits hydrogenation. In the latter case the dissolution reaction is inhibited directly by the adsorption of thiourea molecules at active anodic sites.

Under conditions of anodic polarisation the influence of chloroplatinic acid additions was negligible. Sodium arsenate additions proved to be slightly beneficial but only at crosshead speeds in excess of

10^{-6} INS^{-1} whilst thiourea additions proved to be decidedly beneficial at all crosshead speeds and current densities investigated.

In all 3 test solutions under conditions of cathodic polarisation cracking was intergranular along the prior austenite grain boundaries.

At the free corrosion potential; cracking in sodium arsenate and chloroplatinic acid containing solutions was also intergranular along prior austenite grain boundaries . In thiourea containing solutions where premature failure had occurred (i.e. crosshead speeds $< 10^{-6}$ INS^{-1}) some evidence of superficial intergranular cracking was observed on the fracture surfaces of broken specimens.

Anodically polarised specimens tested in arsenate and chloroplatinic acid containing solutions exhibited intergranular cracking. Anodically polarised specimens tested in solutions containing thiourea, however, were characterised, almost without exception by narrow transgranular fissures that had propagated in a direction perpendicular to the tensile axis. (Fig. 3.30). The single exception was in the test performed at the slowest crosshead speed. In the latter, intergranular cracking was observed, which appeared to have initiated from the base of the initially formed transgranular fissures.

In table 3.6 the measured mean fissure depths and mean fissure penetration rates (calculated from measured fissure depth divided by failure times) are tabulated as a function of crosshead speed for tests

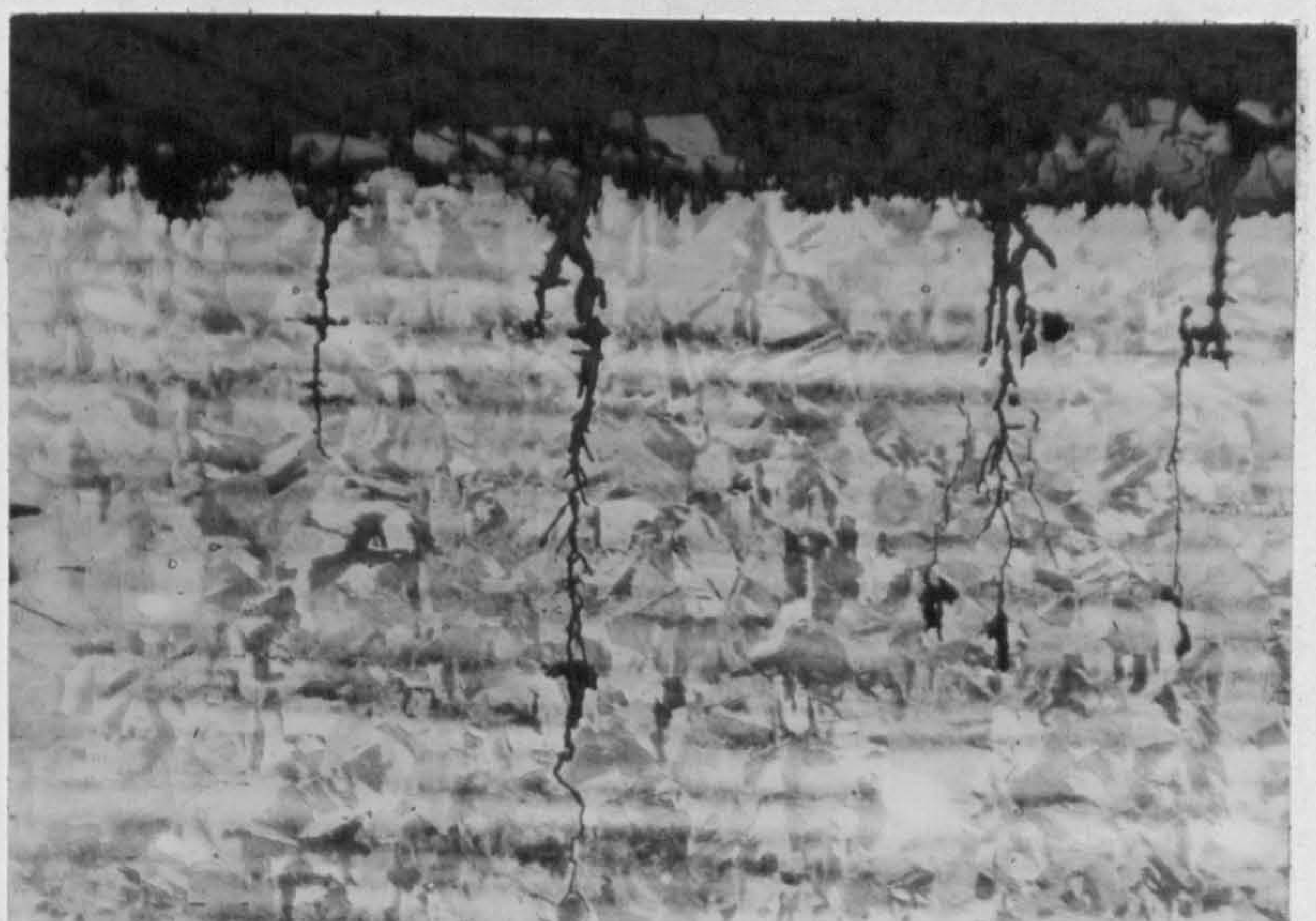

Fig. 3.30 Transgranular fissuring observed in an anodically polarised maraging steel tensile specimen strained to failure at a crosshead speed of 7×10^{-7} INS^{-1} in 3.5 wt % NaCl solution containing 5gm/l of thiourea and adjusted to an initial pH of 2.0 (x125).

TABLE 3.6

Mean fissure depths and penetration rates as a function of crosshead speed for tests on smooth tensile specimens performed with anodic polarisation (3.65 mA/cm^2) in a 3.5 wt % NaCl solution containing 5gm/l thiourea and acidified to an initial pH of 2.0.

CROSSHEAD SPEED		FISSURE DEPTH		FAILURE TIME	MEAN FISSURE PENETRATION RATE	
INS^{-1}	MS^{-1}	IN	M	MIN	INS^{-1}	MS^{-1}
2.5×10^{-5}	6.35×10^{-7}	3.03×10^{-3}	7.7×10^{-5}	46.5	1.08×10^{-6}	2.74×10^{-8}
6.4×10^{-6}	1.63×10^{-7}	9.92×10^{-3}	2.52×10^{-4}	185	8.9×10^{-7}	2.26×10^{-8}
2.8×10^{-6}	7.11×10^{-8}	1.37×10^{-2}	3.48×10^{-4}	395	5.79×10^{-7}	1.47×10^{-8}
1.29×10^{-6}	3.28×10^{-8}	2.05×10^{-2}	5.21×10^{-4}	830	4.11×10^{-7}	1.04×10^{-8}
7.0×10^{-7}	1.78×10^{-8}	2.95×10^{-2}	7.5×10^{-4}	1240	3.97×10^{-7}	1.01×10^{-8}

performed with 10 mA anodic polarisation in a 3.5 wt % NaCl solution containing 5gm/l thiourea and acidified to an initial pH of 2.0.

These penetration rates are consistent with anodic dissolution at the tip of the crack or fissure-based upon dissolution of iron as Fe^{2+} - of between 25 and 75 mA/cm^2. These values are obtained despite the presence of an anodic adsorption inhibitor. It seems reasonable to assume therefore, that in the absence of the said inhibitor the current densities that can be maintained particularly at active sites in the neighbourhood of grain boundaries will be significantly higher than these values i.e. approaching the limiting current densities observed in polarisation curves (i.e. $\sim$ 100 mA/cm^2 cf. section 3.2.1).

The change of crack path concomitant on the addition of thiourea to the test solution of anodically polarised specimens can be explained as follows. Thiourea molecules are preferentially adsorbed at those sites which in their absence would suffer intense anodic dissolution e.g. grain boundaries.

Eventually however, when all such sites are occupied the remainder of the surface will be covered with an adsorbed monolayer. In the absence of an applied stress the net effect of adsorption is that of uniform dissolution occurring at a reduced rate through the adsorbed surface layer. The application of stress to such a system has the effect of breaking down the protective monolayer at localised sites resulting in intense anodic activity at these localities until such time as further adsorption can stifle further attack. The process is then repeated again and again resulting eventually in intense fissuring. The situation may be loosely regarded as analogous to the transgranular stress corrosion cracking of, for example, 18-8 stainless steel in chloride environments where it has been suggested that a balance between passivation kinetics and strain rate provide conditions amenable to stress corrosion cracking.

In conclusion, therefore, the effects of various additions made to the basic test solution on the susceptibility towards cracking of smooth tensile specimens of maraging steel are not inconsistent with a mechanism of cracking at the free corrosion potential and with anodic polarisation, based upon a pre-existing (or strain generated) active path dissolution model.

b) <u>The influence of additions made to the corrosive environment on crack velocities determined on fatigue specimens loaded in cantilever bending</u>

Brown type cantilever beam tests were performed on 0.3" thick fatigue precracked maraging steel specimens inthe same solutions investigated above and the results compared with similar tests performed in non-contaminated 3.5 wt % NaCl solution acidified to an initial pH of 2.0.

Tests were carried out at the free corrosion potential and with galvanostatic anodic and cathodic polarisation (approximately +2mA cm^{-2} and $-2mA/cm^2$

respectively) in all test solutions.

Crack growth was monitored continuously throughout the test using the D.C electrical resistance technique. This permitted graphs of crack length as a function of time to be plotted, from which crack velocities and stress intensity factors (calculated using equation 2.1) at any instant could be derived. Results were thereby plotted in terms of instantaneous crack velocity versus instantaneous stress intensity.

Fig. 3.31 shows the results of tests at the free corrosion potential and with anodic and cathodic polarisation in a solution containing 25cc/l of chloroplatinic acid. For comparison the results of testsperformed in the uncontaminated solution are plotted on the same graph.

The results of tests performed in solutions containing 5gm/l of sodium arsenate and thiourea were plotted in a similar fashion (Fig. 3.32 and Fig. 3.33 respectively).

The following points are clear from these results:-

i) In each case crack velocity was virtually independent of stress intensity over the range of stress intensities investigated (20-35 KSI$\sqrt{\text{IN}}$). This behaviour is typical of the plateau crack velocity regime designated Region II by Carter, Brown and others.

ii) A comparison of Figs. 3.31, 3.32 and 3.33 shows that chloroplatinic acid, sodium arsenate and thiourea additions had a negligible effect on the

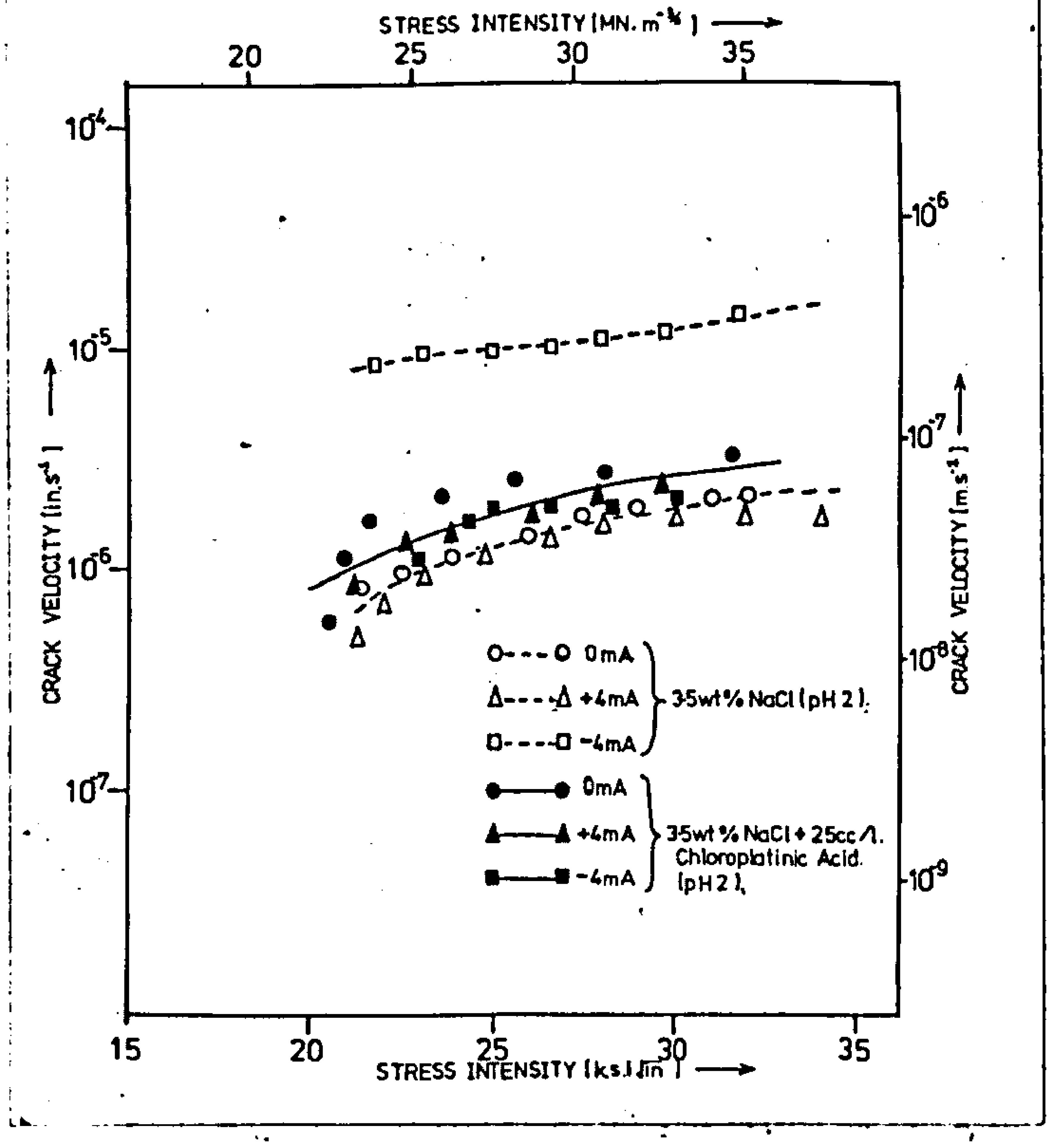

Fig. 3.31 Crack velocity vs stress intensity data determined on fatigue precracked cantilever bend specimens loaded in 3.5 wt % NaCl solution containing 25cc/l of chloroplatinic acid. Solution (5% w/v) and acidified to an initial pH of 2.0.

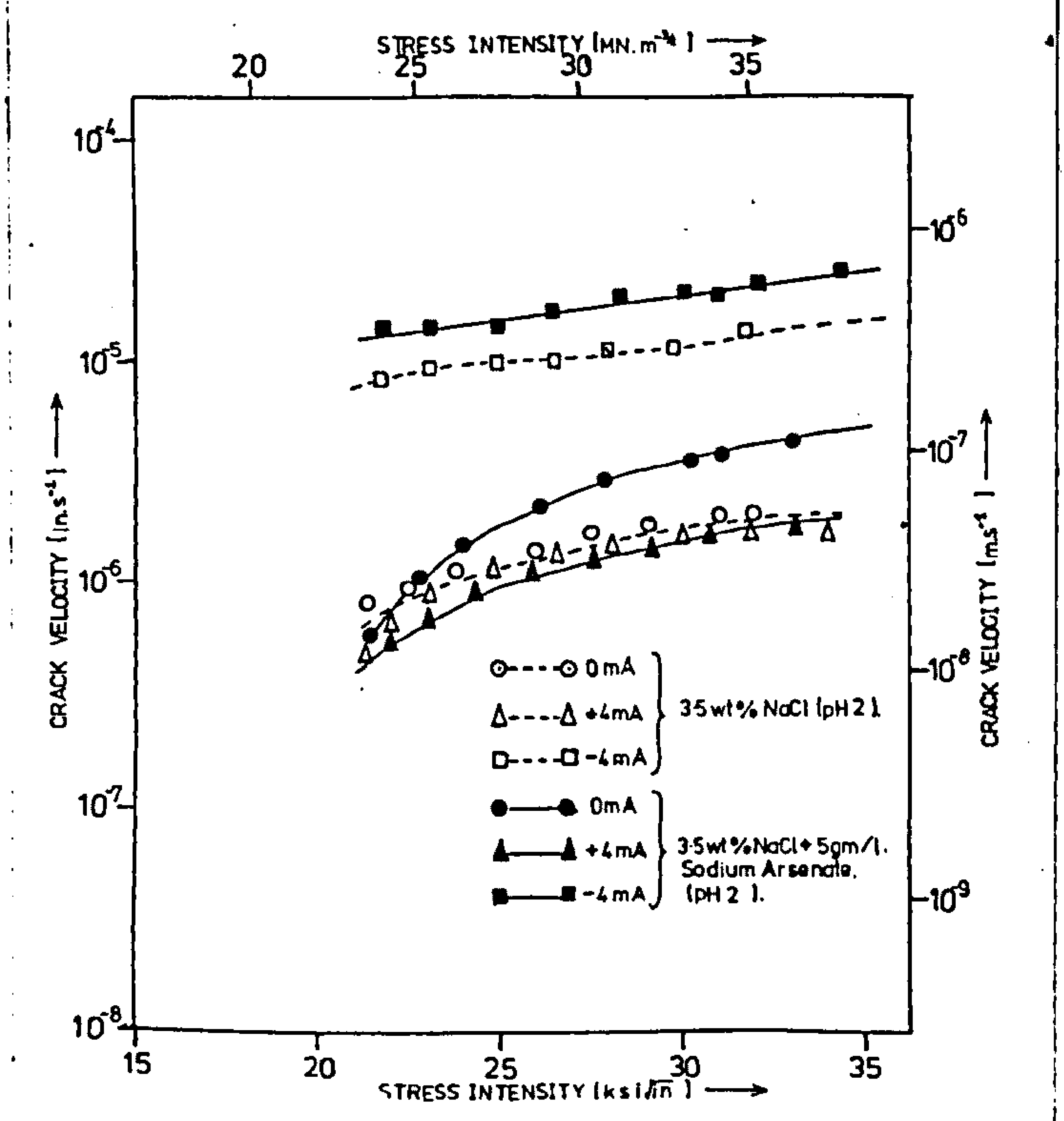

Fig. 3.32 Crack velocity vs stress intensity data determined on fatigue precracked cantilever bend specimens loaded in 3.5 wt % NaCl solution containing 5gm/l of sodium arsenate and acidified to an initial pH of 2.0.

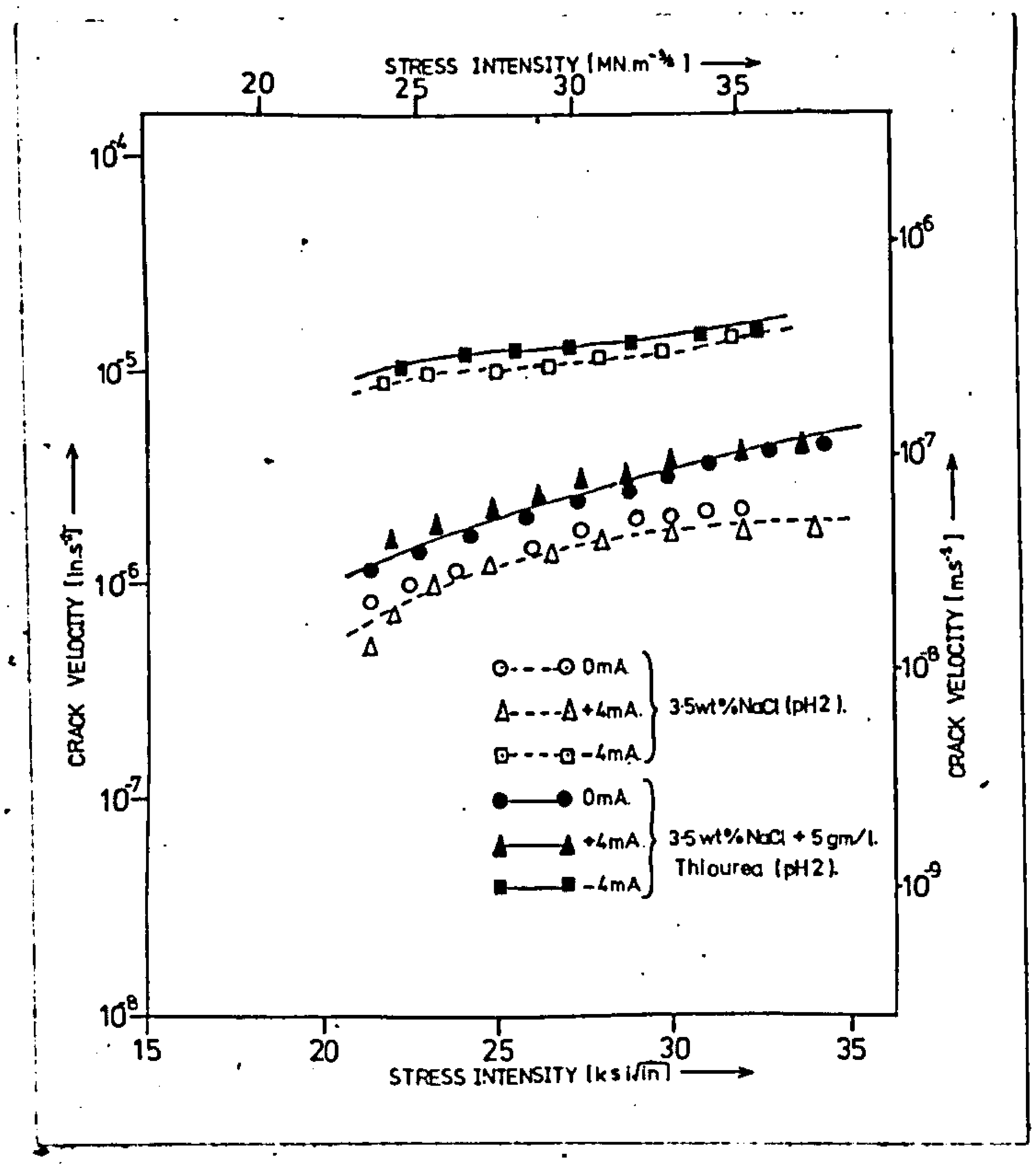

Fig. 3.33 Crack velocity vs stress intensity data determined on fatigue precracked cantilever bend specimens loaded in 3.5 wt % NaCl solution containing 5gm/l thiourea and acidified to an initial pH of 2.0.

plateau crack velocity as determined under freely corroding conditions in non contaminated 3.5 wt % NaCl test solution. The same is true of tests performed with anodic polarisation.

iii) Under conditions of cathodic polarisation, however, chloroplatinic acid additions were observed to lower the plateau crack velocity by approximately an order of magnitude. Thiourea and sodium arsenate additions, on the other hand, produced only a slight increase in the plateau crack velocity.

The former result suggests that chloroplatinic acid additions can be effective not only in increasing crack initiation times of smooth specimens subjected to cathodic polarisation but also in reducing absolute crack propagation rates. The influence of thiourea and sodium arsenate additions on the plateau crack velocities suggests on that other hand, that these additions are effective primarily in reducing initiation times presumably by increasing the rate of hydrogen absorption and thereby reducing the time required to attain the minimum concentration of lattice dissolved hydrogen, c_o, necessary for crack initiation. Once, c_o for crack propagation from a smooth surface is exceeded crack propagation can commence. Thereafter crack propagation can be maintained by a much reduced adsorbed surface hydrogen concentration (i.e. typical of that existing in non contaminated solutions), possibly because the concentration of hydrogen required to maintain crack propagation at the tip of a sharp stress concentrator (microcrack) is very much less than that required to initiate cracking from a smooth defect free surface.

Examination of fracture surfaces on the scanning electron microscope revealed cracking to be intergranular in all cases irrespective of solution composition or polarising conditions. In view of the nature of cracking observed in anodically polarised tensile specimens tested in solutions containing thiourea; this was a somewhat surprising observation. It will be recalled that in these tests failure was invariably preceded by the propagation of transgranular fissures and it seemed reasonable to expect that some fissuring would be observed in the corresponding fatigue precracked tests. In fact cracking was predominantly intergranular with no evidence of propagating fissures as such. However, a peculiar feature of the fatigue precracked specimen was the intense general dissolution that had taken place on the sides and prenotch zones close to the fatigue precrack. This pronounced form of general dissolution was not observed on the other anodically polarised fatigue precracked specimens.

These observations may in some way be related to the observation of intergranular cracking initiated from narrow fissures in the test performed with anodic polarisation and at the slowest crosshead speed in smooth tensile tests; the implication being that the presence of crevices, notches or fissures are a pre-requisite for intergranular cracking in this environment. The effect may be simply mechanical in origin, possibly related to the stress concentrating influence of crevices, notches or fissures which are of course absent on initially smooth tensile specimens. Alternatively, the effect may be related to the development of different electrochemical conditions within the confines of the crevice, notch or fissure such that, for example hydrogen discharge becomes possible; the embrittling tendency being enhanced by the presence of thiourea in such circumstances. If the latter hypothesis was correct however, a correspondingly higher crack velocity would have been expected and since this was not observed to be the case then the only other explanation is that the concentration of inhibiting species within the cracks were eventually depleted by initial adsorption at active sites and thereafter could not be replenished because of the barrier to ingress of thiourea molecules by the build up of corrosion product on the crack sides.

3.2.7 The influence of various additions made to the corrosive environment on the galvanostatic polarisation curves

In section 3.2.6 the effect that various ingredients added to the test solution had on the failure times of smooth constant crosshead speed tensile specimens and on the crack velocities of fatigue precracked cantilever bend specimens were reported.

In this section galvanostatic polarisation curves determined in the same environments will be described and used to explain the aforementioned results. The polarisation curves were determined in the following manner. Commencing at the free corrosion potential the specimen was polarised anodically or cathodically to a given current density using the simple galvanostatic circuit described previously. The current density was increased in stepwise fashion every five minutes and the potential of the specimen was recorded along with the corresponding current density immediately prior to a further increase in the latter.

Fig. 3.34a shows the anodic and cathodic polarisation curves so determined in the solution containing 25cc/l of chloroplatinic acid. Plotted on the same graph for comparison are the anodic and cathodic curves determined in the uncontaminated environment. Figs. 3.34b and c show similar cuves for solutions containing 5gm/l each of sodium arsenate and thiourea respectively. In all cases the anodic curves are represented by lines passing through triangles and the cathodic curves by lines passing through circles.

Fig. 3.34 Galvanostatic anodic and cathodic polarisation curves for maraging steel in a 3.5 wt % NaCl solution containing a) 25cc/l of chloroplatinic acid solution (5% w/v), b) 5gm/l of sodium arsenate and c) 5gm/l thiourea. Solutions acidified to an initial pH of 2.0 in all cases.

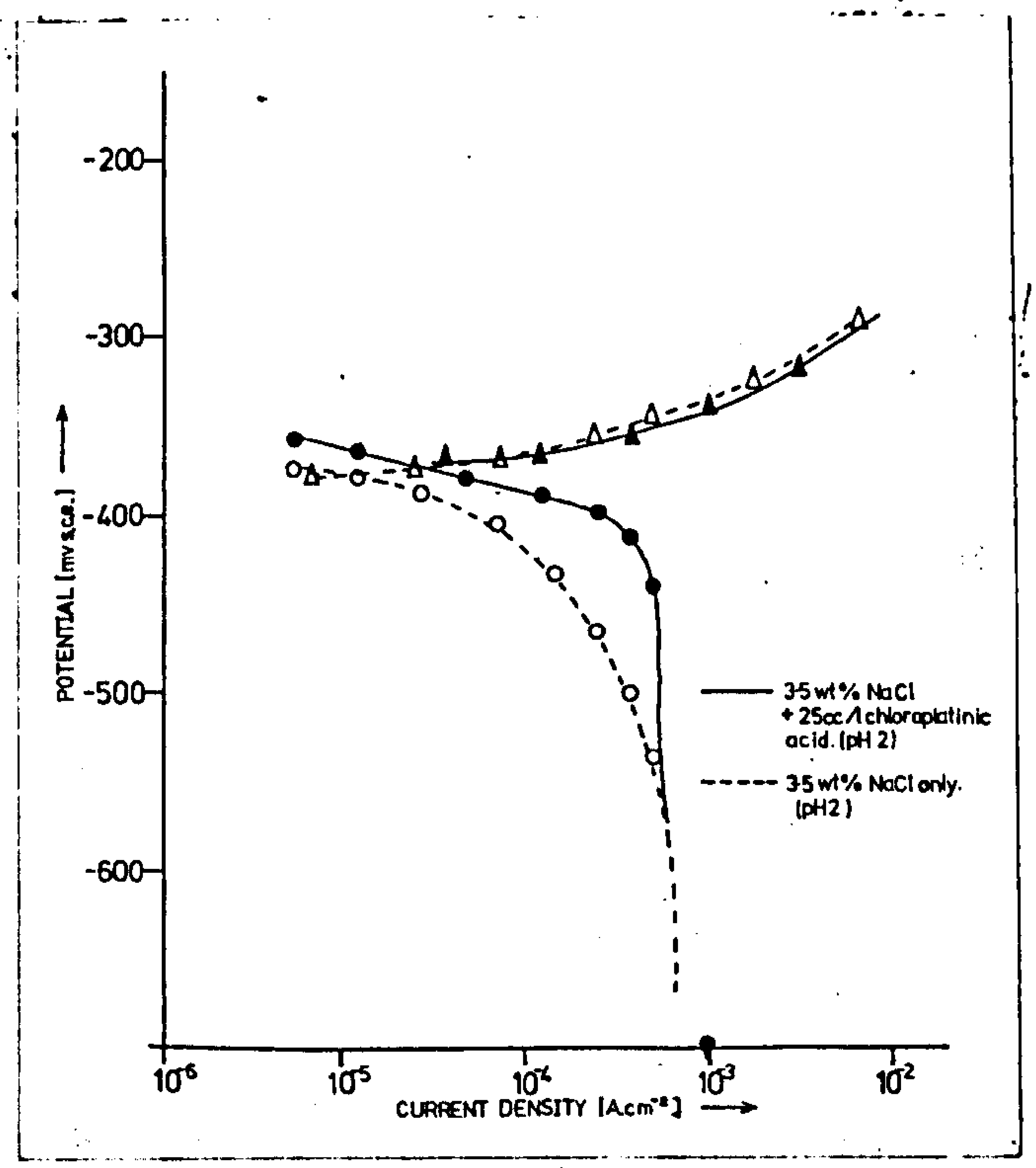

Fig. 3.34a

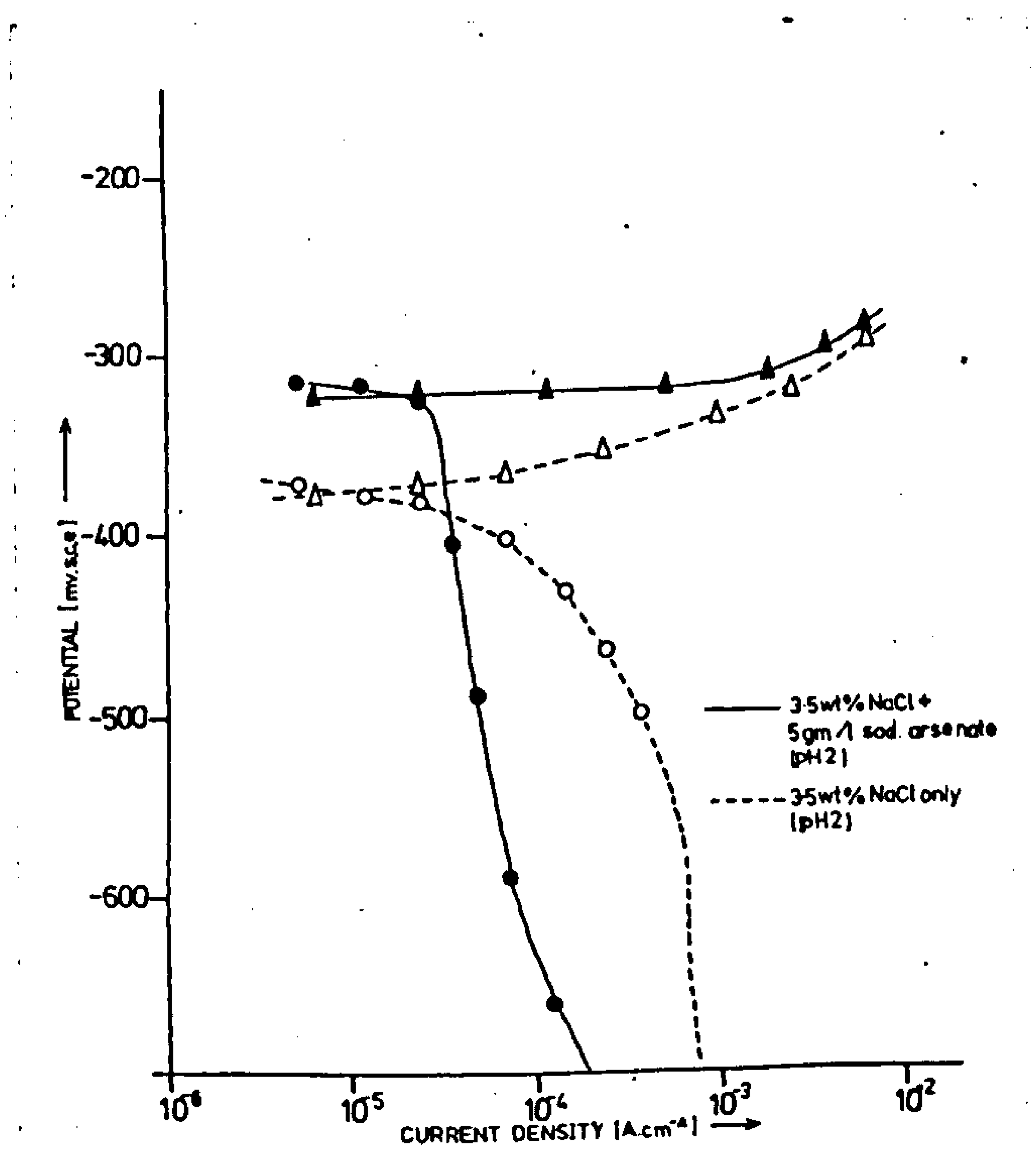

Fig. 3.34b

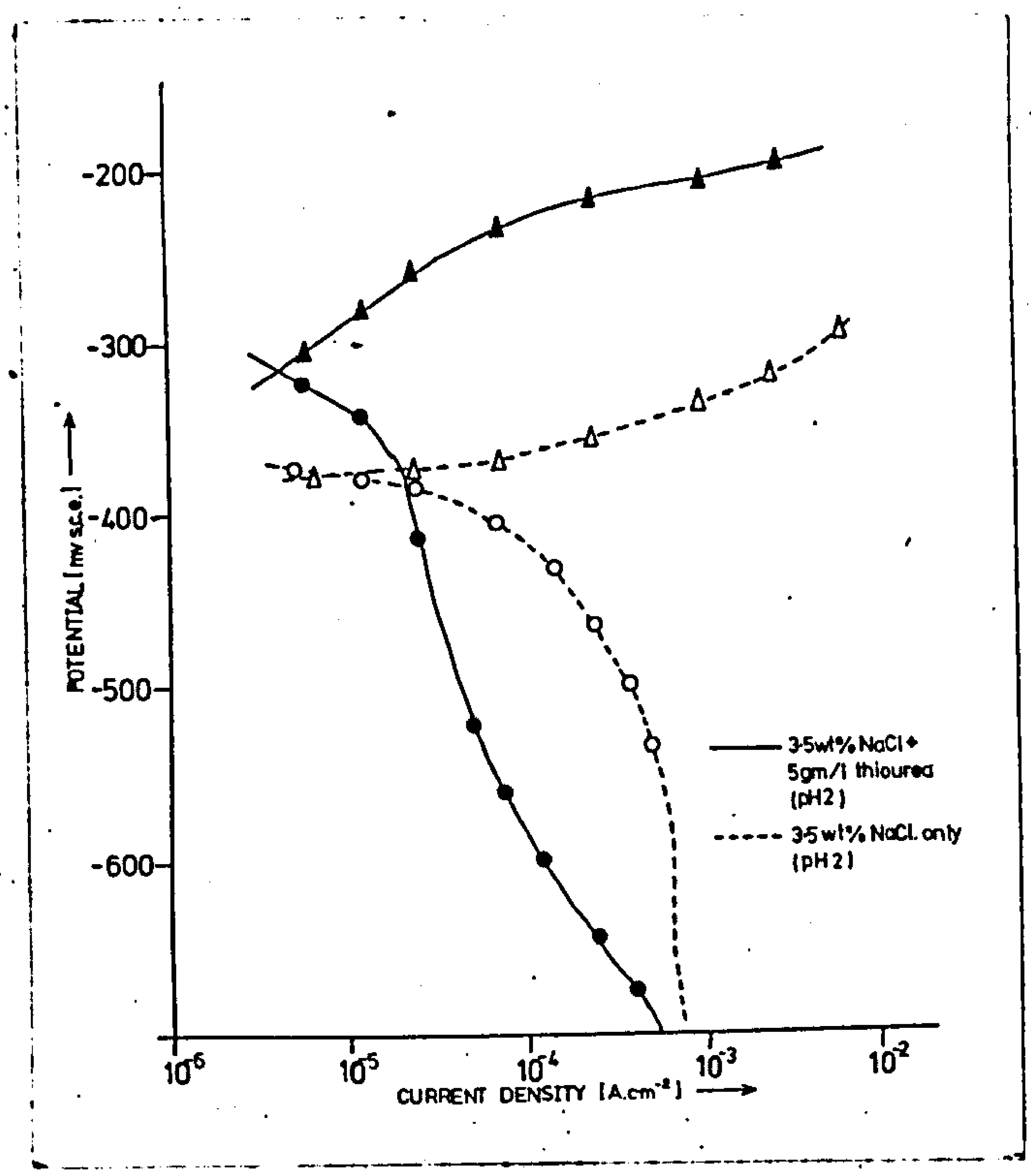

Fig. 3.34c

It is apparent that the different contaminants interfere with the anodic and cathodic reactions to different extents. Thus:-

i) Thiourea has significantly increased the overpotentials for both the anodic (dissolution) and cathodic (hydrogen evolution) reactions at the metal surface.

ii) Sodium arsenate has increased, slightly, the overpotential for the anodic reaction but significantly increased that for the cathodic reaction.

iii) Chloroplatinic acid on the other hand, has not influenced the dissolution reaction but has reduced the overpotential for the hydrogen evolution reaction.

These observations reflect the effect these additions were expected to have on the reactions occurring on the surface of maraging steel specimens subjected to anodic and cathodic polarisation and consequently they concur with the constant crosshead speed tensile results carried out in these environments and described previously (see sections 3.2.6).

3.3 Hydrogen Permeation Experiments

Introduction

The electrochemical hydrogen permeation technique has been widely used for the determination of the diffusivities and solubilities of electrolytic hydrogen in a variety of metals and alloys ranging from palladium in one of the earliest investigations[120] to armco iron,[123,124] Fe-Ni alloys[125] and high strength steels[126] in more recent studies. Furthermore, the technique has provided useful information concerning the effect of cathodic poisons[127] e.g. As, Se, Te, S and electroplating solutions[128] on the adsorption and absorption of atomic hydrogen into the lattice of iron and steels during cathodic charging and/or electroplating.

In all of the examples quoted above a hydrogen concentration profile was maintained within the metallic membrane by cathodically polarising one side of the membrane in the solution under investigation. However, the demonstration of acidification (and therefore conditions thermodynamically favourable for hydrogen discharge) that can occur in areas of localised geometry such as precracks pits or fissures even under conditions of bulk anodic polarisation of the specimen surface, indicates that hydrogen may permeate through metallic membranes under these conditions.

Consequently, the electrochemical permeation technique, in addition to providing information about the diffusivity of hydrogen in the metal or alloy under investigation, could shed some light on the SCC mechanism of the same alloy at the free corrosion potential and under anodically polarising conditions in a given environment. Wilde[110] appreciated that the permeation technique could provide useful information in this respect, and he used the technique to demonstrate that hydrogen absorption occurred in a 12% Cr martensitic stainless steel under conditions of exposure previously thought to preclude this possibility. This lead him to the conclusion that 'environmentally induced cracking of high strength martensitic stainless steels occurs by a hydrogen embrittlement process <u>at all potentials</u>'.

In the present investigations, the permeation technique was used both quantitatively, to provide values of the diffusivity coefficient of hydrogen in maraging steel, and qualitatively to compare the permeation of hydrogen through maraging steel under freely corroding conditions and with anodic or cathodic polarisation in acidified 3.5 wt % NaCl solutions with and without additions made to catalyse or inhibit absorption of hydrogen into the metal lattice (cf. section 3.2.6.).

Theoretical Basis of the Technique

In the electrochemical hydrogen permeation technique a thin metallic membrane is cathodically charged with hydrogen on one side while the other side is maintained at a constant potential sufficiently anodic to oxidise hydrogen atoms passing through. The current in the anodic potentiostatic circuit which maintains a zero coverage of hydrogen on this side of the membrane is, by Faraday's Law, a direct measure of the instantaneous rate of permeation of hydrogen. It is possible to obtain a continuous record of the hydrogen permeation rate with the sensitivity associated with current measurement. Thus with a current recorder in the anodic circuit of sensitivity of the the order of 1 μA f.s.d and a membrane of area 1 cm^2, fluxes of hydrogen of the order of 10^{-11} moles of H/sec can be detected.

Now, from Fick's first law of diffusion, the flux of hydrogen at the anodic side of the membrane is given by

$$\text{Flux} = - D \left(\frac{\partial c}{\partial x}\right)_{x=L} \qquad (1)$$

whence the permeation current density J is given by:-

$$J = -nFD \left(\frac{\partial c}{\partial x}\right)_{x=L} \qquad (2)$$

where c = concentration, $mol cm^{-3}$

n = no. of electrons involved in the oxidation of hydrogen

F = Faraday Constant (96,500 coulombs)

D = Diffusion coefficient, $cm^2 s^1$

McBreen et al[129] solved the diffusion equation (see eqn. 3 below for the concentration gradient as a function of time (Ficks second Law) in order to evaluate the concentration gradient at x=L in equations (1) and (2) and thereby develop a mathematical basis for the permeation technique

$$D \frac{\partial^2 c}{\partial x^2} = \frac{\partial c}{\partial t} \quad \text{for } 0 < x < 1 \qquad (3)$$

The initial and boundary conditions applying to the permeation technique are

$$c = Co; \; x = 0; \; t = 0 \qquad (4)$$

$$c = 0; \; x = L; \; t > 0 \qquad (5)$$

$$c = 0; \; 0 < x < L; \; t < 0 \qquad (6)$$

By applying Laplace Transforms to eqn. (3) and to the boundary conditions (4) and (5) gives

$$\frac{\partial^2 \bar{c}}{\partial x^2} - \frac{p}{D} \bar{c} = 0 \qquad (7)$$

$$\bar{c} = \frac{Co}{p} ; \quad x = 0 \qquad (8)$$

$$\bar{c} = 0, \; x = L \qquad (9)$$

where $\bar{c} = L\left[c(x,t)\right]$ is the Laplace Transform operator and p is the Laplace Transform parameter. A homogeneous solution for equation (7) is

$$\bar{c} - ae^{-qx} = be^{+qx} \qquad (10)$$

where a, b are unknown coefficients and $q = (\frac{p}{D})^{\frac{1}{2}}$.

Using eqns. (8) and (9) to solve for a and b and applying inverse transformation gives

$$\frac{C(x,t)}{co} = \sum_{n=0}^{\infty} (-1)^n \operatorname{erfc} \frac{x+2nL}{2\sqrt{Dt}}$$

$$- \sum_{n=0}^{\infty} (-1)^n \operatorname{erfc} \frac{2L(n+1)-x}{2\sqrt{Dt}} \qquad (11)$$

where c(x,t) is the concn of hydrogen at x at any time t.

From (2) the steady state permeation current density is given by

$$J = \frac{DzF}{L} (co - C_L) \qquad (12)$$

and $c_L = 0$

Combining equations (2), (11) and (12) gives

$$\frac{J_\tau}{J_\infty} = \frac{2}{\pi^{\frac{1}{2}}} \frac{1}{\tau^{\frac{1}{2}}} \sum_{n=0}^{\infty} (-1)^n e^{-\frac{(2n+1)^2}{4\tau}} \qquad (13)$$

where τ is a dimensionless parameter

given by $\tau = \frac{Dt}{L^2}$ (13a)

Using the first term approximation (n=0) of equation (13) gives

$$\frac{J_\tau}{J_\infty} = \frac{2}{(\pi\tau)^{\frac{1}{2}}} e^{-\frac{1}{4\tau}} \qquad (14)$$

which is valid up to $J_\tau = 0.965\ J_\infty$ and is particularly applicable to short times including the so called 'breakthrough time'.

An equivalent solution of equation (3) may be obtained by using the Fourier method. The corresponding first term approximation is

$$\frac{J_\tau}{J_\infty} = 1 - 2e^{-\pi^2\tau} \qquad (15)$$

This solution is particularly applicable to long times ($\tau > 0.2$).

Table 3.7 lists values of J_τ / J_∞ as a function of τ calculated from equations (14) and (15)

Diffusion coefficents for hydrogen in the metal or alloy can be calculated by finding the time to attain any fraction of the steady state permeation rate and then applying equation (13a) with a knowledge of τ, t and L to calculate D e.g. from Table 3.7 it can be seen

TABLE 3.7

Normalised permeation currents, as calculated from the first term Fourier and Laplace Transform solutions of equation (3)

τ	$\frac{2}{(\pi\tau)^{\frac{1}{2}}} e^{\frac{1}{4\tau}}$	$1-2e^{-\pi^2\tau}$
0.00	0.0000	-10
0.01	0.0000	-0.8122
0.02	0.0000	-0.6481
0.05	0.0339	-0.2210
0.1	0.2924	+0.2546
0.15	0.5500	+0.545
0.20	0.7227	0.7222
0.25	0.8303	0.8304
0.30	0.8955	0.8966
0.4	0.9470	0.9614
0.5	0.9677	0.9856
0.6	0.9596	0.9946
0.7	0.9435	0.9980
0.8	0.9178	0.9992
0.9	0.8962	0.9997
1.0	0.8788	0.9998

that if $\tau = 0.15$, $J_\tau / J_\infty = 0.55$. Thus if the permeation current reaches 55% of J_∞ in a time, t then

$$D = 0.15 \frac{L^2}{t}$$

It should be noted here that the above mathematical analysis is based on the assumption of a constant value of diffusivity coefficient. Consequently if the initial and boundary conditions were correctly chosen, a plot of $\frac{J_\tau}{J_\infty}$ vs. log time and $\frac{2}{(\pi\tau)^{\frac{1}{2}}} e^{-\frac{1}{4\tau}}$ for $\tau < 0.3$ and $1-2e^{-\pi^2\tau}$ for $\tau > 0.3$ against log τ. should have identical shapes. Any dissimilarity between the experimental and theoretical build up curves is therefore indicative of anomalous permeation behaviour such as for example concentration dependence of hydrogen diffusivity.

3.3.1 The influence of applied polarisation on the absorption and permeation of hydrogen through 18 Ni maraging steel membranes exposed to 3.5 wt % NaCl

For these investigations .008" (.020 cm) thick membranes, prepared by cutting discs from the 1" diameter bar stock and grinding to the desired thickness, were employed.

Hydrogen permeation experiments were conducted on these membranes under the following conditions of applied polarisation, in a 3.5 wt % NaCl solution, acidified to an initial pH of 2.0 with 0.6NHCl solution.

i) At a cathodic current density of $4mAcm^{-2}$

ii) At the free corrosion potential

iii) At an anodic current density of $4mAcm^{-2}$

The permeation transients are shown in Fig. 3.35 from which it would appear that hydrogen is absorbed into the steel no matter what polarisation is applied to the charging side of the membrane.

The cathodically polarised specimen exhibited a steady state permeation current density, J_{∞} of 2.75 $\mu A/cm^2$ which was attained after approximately 800 minutes. The anodically polarised specimen, however, showed no sign of attaining a steady state value - the permeation current density rising steadily to about 8$\mu A/cm^2$ after a total of

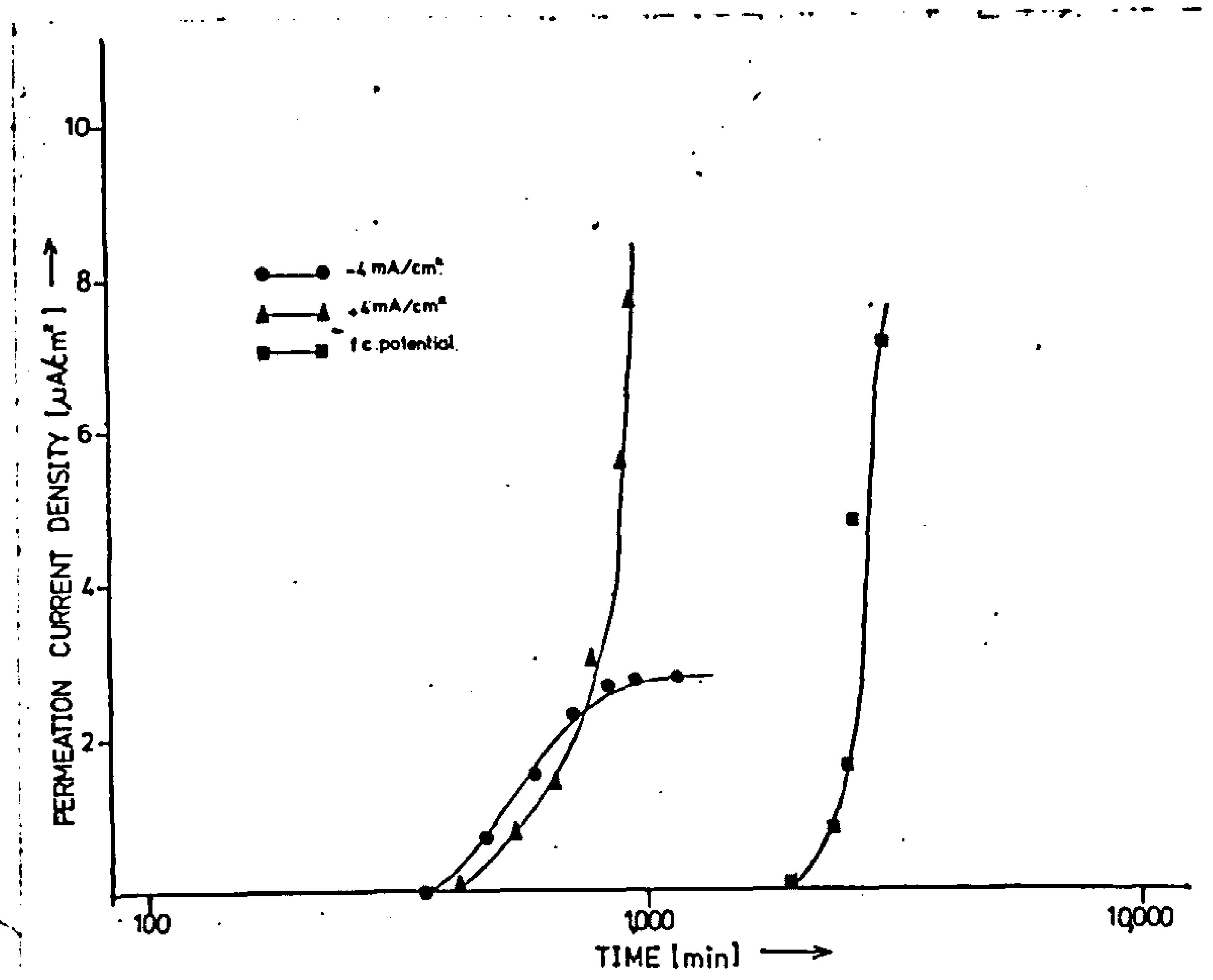

Fig. 3.35 Hydrogen permeation transients determined on maraging steel membranes subjected to various conditions of applied polarisation in a 3.5 wt % NaCl solution of initial pH 2.0.

17 hours on test. Assuming the rising permeation transient was indeed due to hydrogen permeating through the material in advance of the anodically dissolving interface, this behaviour can be readily explained when it is remembered that the specimen was being continually thinned down by the anodic current density so that a gradual increase in permeation current could be anticipated in accordance with equation (12).

Visual examination of anodically polarised membranes after testing revealed the presence of 'blisters' on the anodic side of the membrane (i.e. that side held potentiostatically at +100 mV SCE in NNaOH solution). Such blisters were not apparent on cathodically polarised specimens. Detailed examination of the blisters on the scanning electron microscope revealed the presence of cracks in the domes of the blisters. By adhering the surface of the blistered side of the membrane to a glass slide with araldite and separating the slide from the membrane after curing, the blister domes could be easily removed to permit examination of the interior sufaces of the blisters. Fig. 3.36a shows the interior surface of a blister after removal of the blister dome whilst Fig. 3.36b shows the interior surface of a removed blister dome.

Tests at the free corrosion potential showed permeation current rises only after a period of 30-40 hours and examination of the anodic side of the membrane after completion of the tests revealed 'blistering' similar to that observed on anodically polarised membranes.

The observation that permeation current rises in freely corroded and anodically polarised specimens appeared to be closely linked with the development of blistering and that the blisters were inevitably cracked or perforated prompted the question 'Is the permeation current increase observed in freely corroded and anodically polarised specimens due to true hydrogen permeation or to the microscopic perforation of the membrane with its consequent solution contact effects?' The fact that a permeation current was detected under freely corroding conditions is a clear indication that if the permeation current transients observed during anodic polarisation of the membranes were not as a result of diffusing hydrogen then they must have been a consequence of solution contact (and reaction) between the solutions on either side of the membrane and not as a consequence of some

Fig. 3.36 Appearance of the interior surfaces of blisters produced on maraging steel membranes during anodic polarisation in a 3.5 wt % NaCl solution of initial pH 2.0 after removal of the blister domes.

a) blister pits

b) blister domes

Fig. 3.36a

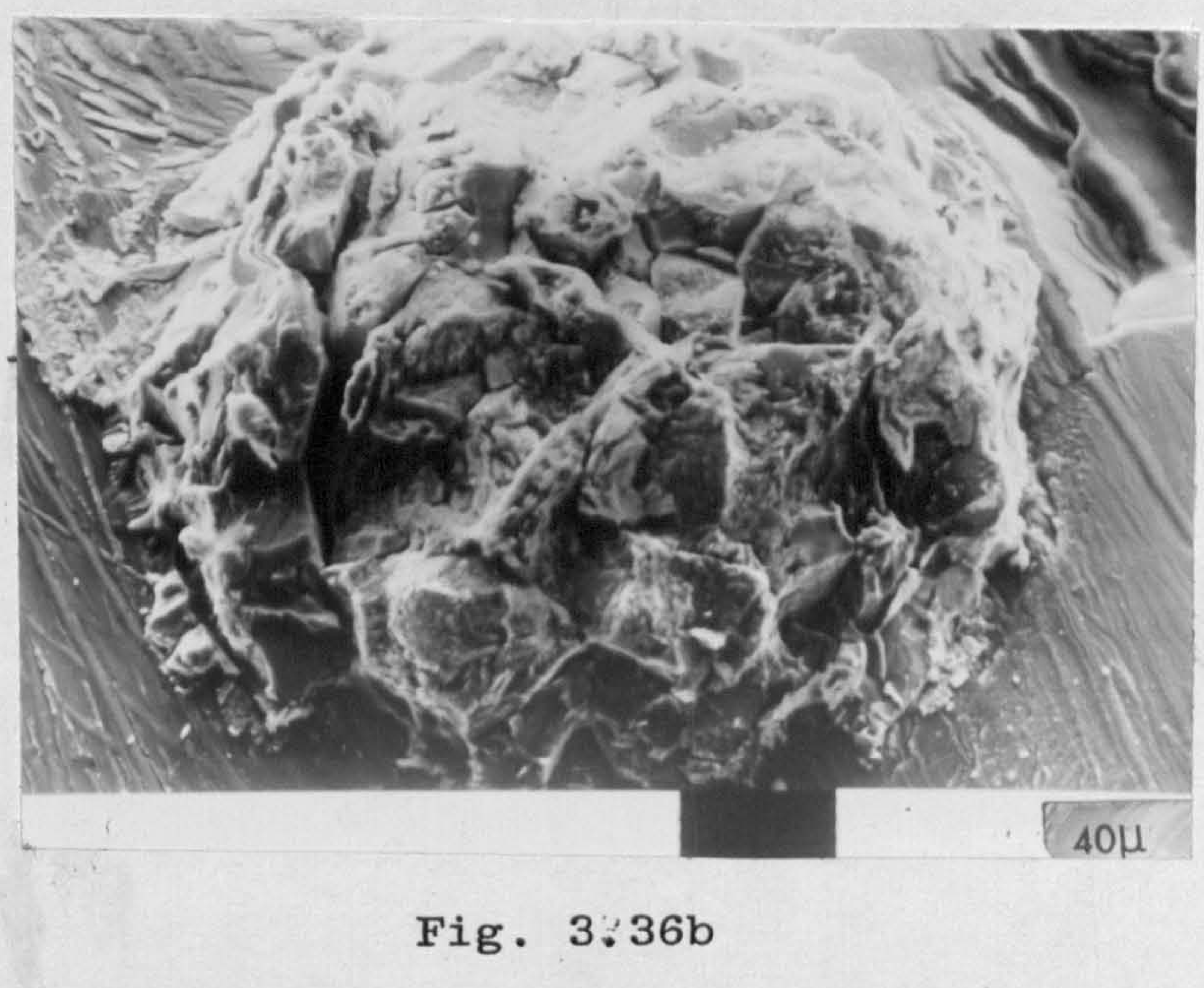

Fig. 3.36b

interaction between the two electrical circuits on either side of the membrane.

It is suggested that permeation current transients observed in freely corroded and anodically polarised specimens may be explained not by the oxidation reaction $H \rightarrow H^+ + \varepsilon$ but by the alternative reaction $Fe \rightarrow Fe^{2+} + 2\varepsilon$ which would be detected in the auxiliary potentiostatic circuit upon perforation of the membrane.

To test this hypothesis permeation transients were obtained for anodically polarised specimens polarised to identical current densities, but of different thicknesses. The permeation transients are shown in Fig. 3.37a and the corresponding specimen thicknesses plotted as a function of breakthrough time are shown in Fig. 3.37b. In each case 'blisters' were observed on the membranes after testing. The linear relationship between specimen thickness and breakthrough time can be explained in terms of Faradays laws assuming that the current density at certain localised sites (corresponding to the blisters on the reverse side of the membrane) was somewhat greater than the uniformly applied current density of 4mA cm^{-2}. That this assumption is justified can be seen from Fig. 3.38 which shows the intense localised fissuring that has occurred.on the surface of a specimen anodically polarised at a uniform current density corresponding to 4 $mAcm^{-2}$. The relationship between specimen thickness and breakthrough time exhibited in Fig. 3.37b could not, however, be explained by a hydrogen diffusion model since according to equation (13a) the breakthrough time ought to be proportional to the square of the specimen thickness.

Fig. 3.37 Permeation transients, a) and the corresponding specimen thickness - breakthrough time relationship, b) for maraging steel membranes of various initial thicknesses anodically polarised (4mA cm^{-2}) in a 3.5 wt % NaCl solution of initial pH 2.0.

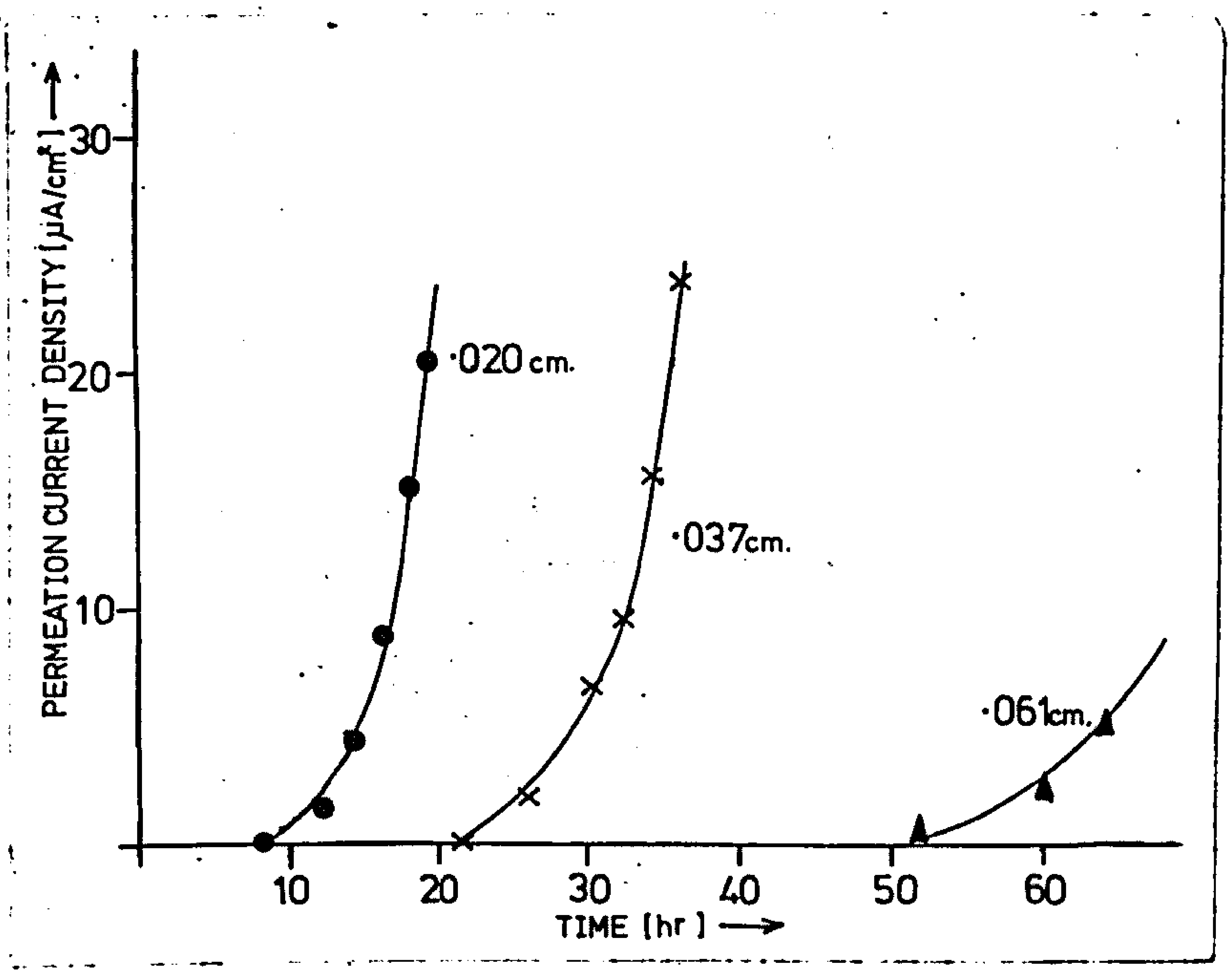

Fig. 3.37a

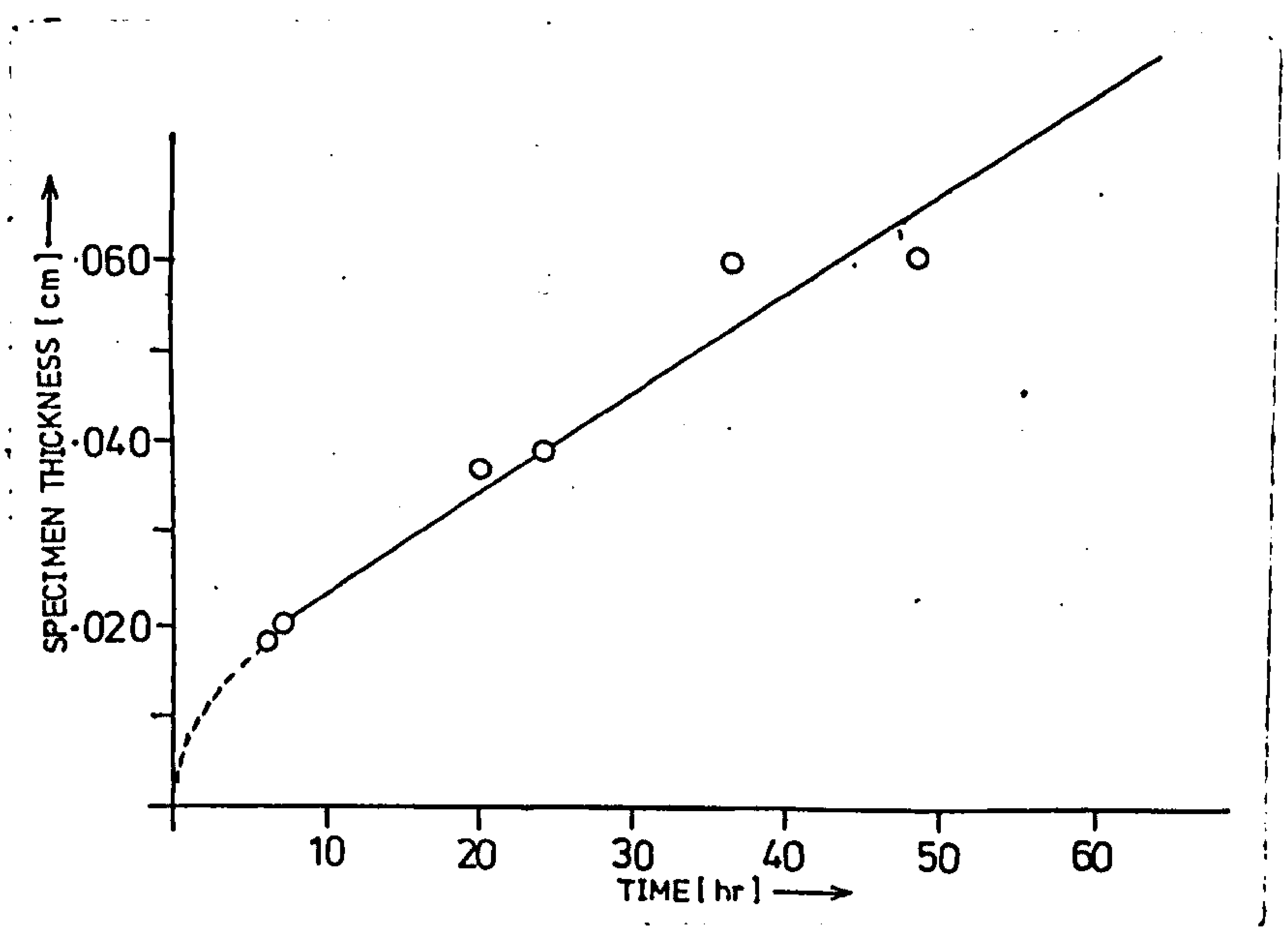

Fig. 3.37b

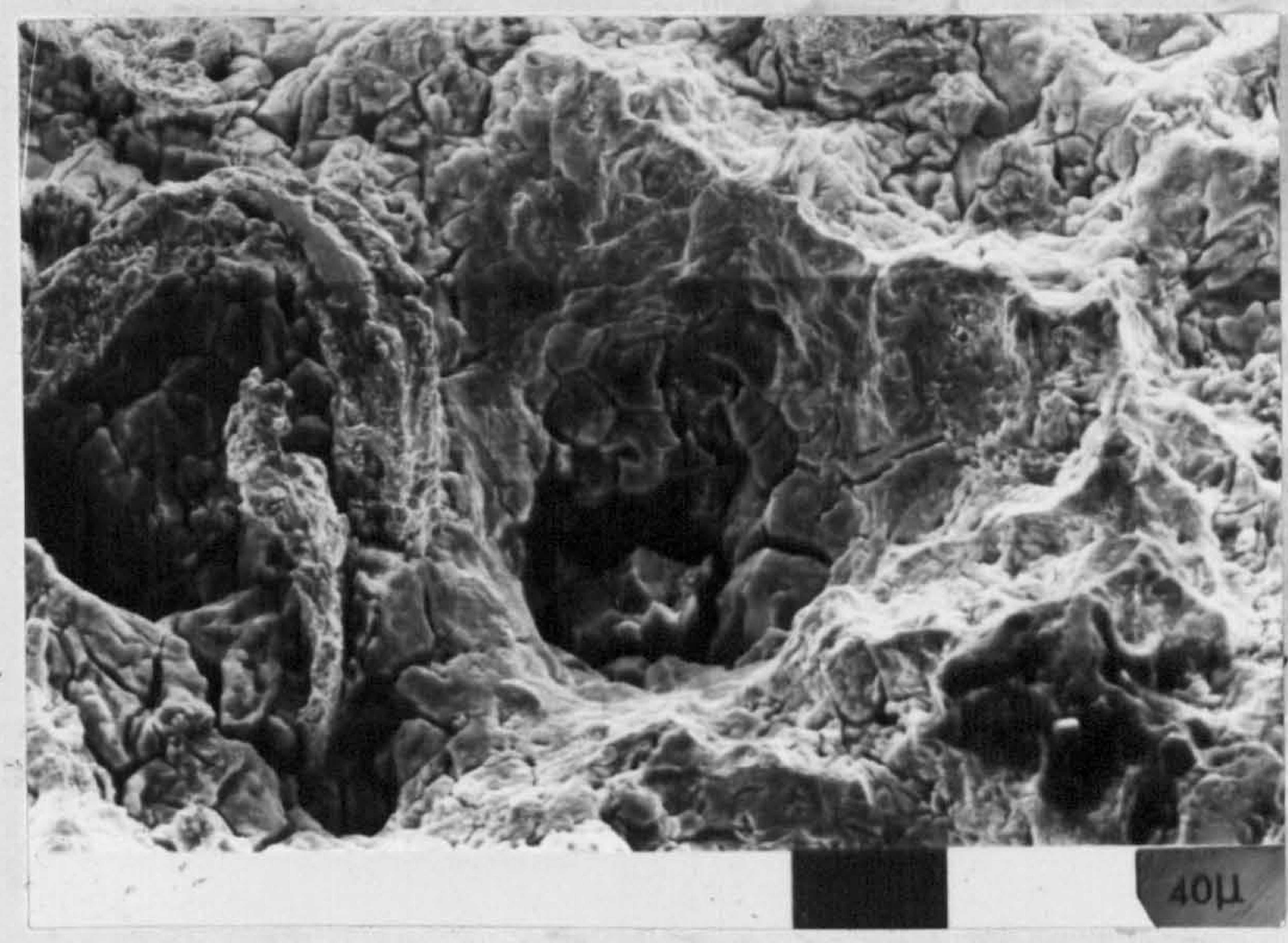

Fig. 3.38 Intense localised fissuring observed on the 'charging' side of a maraging steel membrane anodically polarised (4mA cm^{-2}) in a 3.5 wt % NaCl solution of initial pH 2.0. Transversely prepared specimen.

In conclusion, therefore, it would appear that whilst the results of permeation experiments carried out with applied anodic polarisation would appear, at first sight to imply that hydrogen is absorbed into the steel under these conditions; a more detailed examination of the circumstances associated with the permeation transients under these conditions indicates that the transient may equally be explained by perforation of the specimen membranes resulting in a rise in the current in the potentiostatic circuit as a consequence of the dissolution reaction

$$Fe \rightarrow Fe^{2+} + 2e$$

If the latter is correct then the observations of Barth (et al)[109], Shively (et al)[130] and Wilde,[110] who employed permeation techniques to demonstrate that absorption of hydrogen into high strength and austenitic stainless steels occurs during anodic polarisation, could be explained on the same grounds.

3.3.2 The influence of specimen orientation on the absorption and permeation of hydrogen through maraging steel

In the preceding section the results were described of hydrogen permeation experiments performed on maraging steel membranes, prepared in such a way that the through thickness diffusion of hydrogen corresponded to diffusion of hydrogen in a direction parallel to the longitudinal axis of the 1" diameter bar stock (hereafter referred to as transverse section specimens).

In this section, results will be described of permeation experiments carried out on membranes prepared in such a way that the through thickness diffusion of hydrogen in the membrane corresponded to diffusion of hydrogen in a direction perpendicular to the longitudinal axis of the 1" diameter bar stock (hereafter referred to as longitudinally prepared specimens).

The latter specimens were prepared in one of two ways and for the reasons given below:

a) Approximately .05" (0.127cm) thick plate was hot rolled from the 1" diameter bar stock in a direction parallel to the longitudinal axis of the bar. After annealing for 1hr at 950°C, .008" (.020cm) thick strips were machine ground from the hot rolled plate and 1" diameter discs stamped from the strip. The latter were then aged for 3hr at 530°C under vacuum.

b) In order to check whether or not the heavy deformation introduced by the hot rolling procedure described in (a) was having any influence on permeation behaviour as a consequence of for example the introduction of preferred orientation, a few specimens were prepared by grinding .008" (.020cm) thick longitudinal strip directly from the annealed bar stock. One inch diameter membranes were stamped from the strip which were then aged for 3hr at 530°C under vacuum.

Hydrogen permeation experiments were carried out on the resulting specimens, under identical conditions to those used previously i.e. $4mAcm^{-2}$ anodic, freely corroding and $4mA\ cm^{-2}$ cathodic polarisation in acidified 3.5 % NaCl solution.

Cathodic polarisation produced identical permeation transients to those described in the preceding section. However, the freely corroded and anodically polarised specimens, produced markedly different results.

A typical permeation transient for an anodically polarised longitudinally prepared specimen is shown in Fig. 3.39 along with that for a transverse section specimen. It is noticeable that the breakthrough time for the longitudinally prepared specimen is approximately 3 times longer than that for the specimen prepared by transverse sectioning. The freely corroded specimens showed no permeation current rise even after 72 hour on test.

The permeation curves obtained for specimens prepared as in (a) and (b) were indistinguishable so that

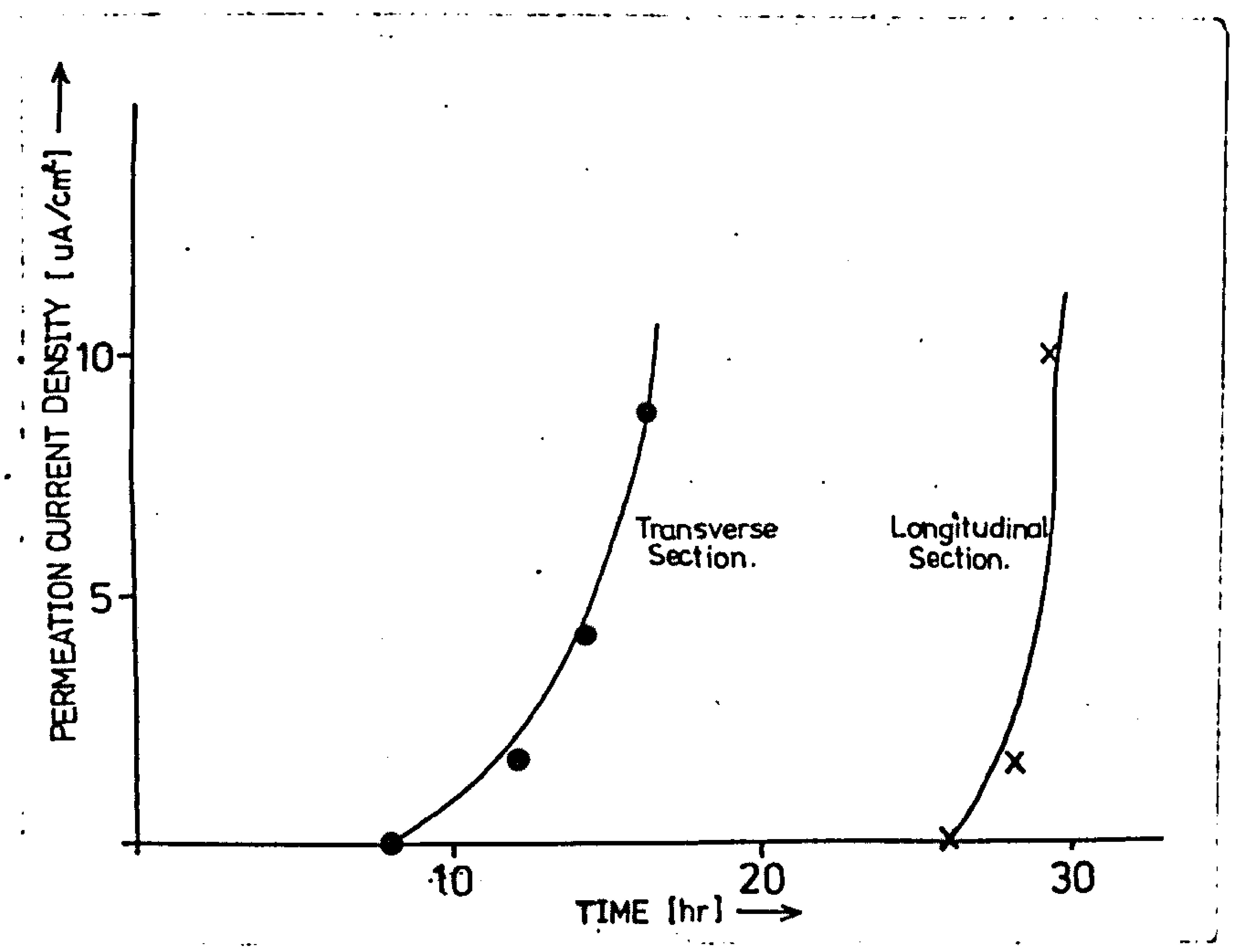

Fig. 3.39 A comparison of the permeation transients of longitudinally and transversely prepared (see text) maraging steel membranes anodically polarised ($4mA/cm^2$) in a 3.5 wt % NaCl solution of initial pH 2.0.

the markedly different permeation behaviour described can in no way be attributed to preferred orientation effects introduced by the heavy hot rolling schedule employed in preparation (a).

Fig. 3.40 shows scanning electron microscope phototgraphs of the anodically polarised face of a specimen prepared as in (a). It would appear that unlike specimens prepared by transverse sectioning, in which localised fissures were observed, dissolution has taken place uniformly over the entire exposed surface area of the membranes. Bearing in mind the markedly different nature of attack produced by the different specimen preparations; it is interesting to compare 'perforation' rates of longitudinally and transversely prepared permeation specimens with calculated values based on (a) an applied

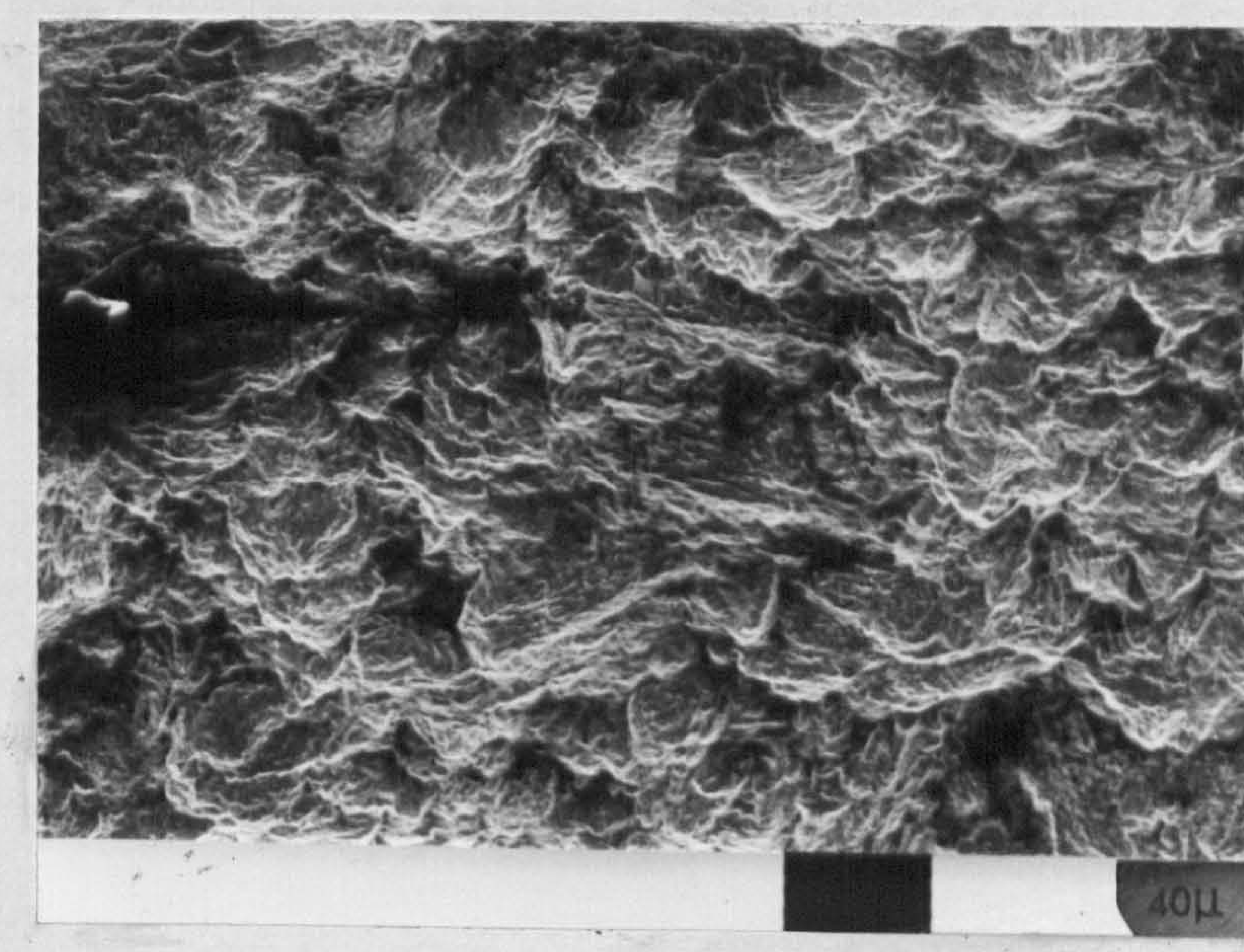

Fig. 3.40 Scanning electron micrograph of the anodically polarised face of a longitudinally prepared maraging steel hydrogen permeation membrane.

anodic current density of 4mA cm^{-2} (as employed in the permeation experiments) and (b) an applied anodic current density of 100mAcm^{-2} (the maximum value observed in polarisation curves cf. Fig. 3.8(a))

i) Transverse section specimen preparation.

Break through time 7hr; thickness .008".

Actual 'perforation' rate 3.18×10^{-7} INS^{-1}
(8.1×10^{-9} ms^{-1})

ii) Longitudinal section specimen preparation.

Break through time 28.5hr, thickness .008".

Actual 'perforation' rate 7.8×10^{-8} INS^{-1}
(1.98×10^{-9} ms^{-1})

iii) Perforation rate based on applied current density of 4mA cm^{-2}.

$$r_{+4} = \frac{.004 \times 56}{2 \times 96{,}500 \times 7.85 \times 2.54} = 5.8 \times 10^{-8}\ INS^{-1}$$
$$(1.47 \times 10^{-9}\ ms^{-1})$$

iv) Perforation rate based on applied current density of 100mA cm^{-2}

$$r_{+100} = \frac{.1 \times 56}{2 \times 96{,}500 \times 7.85 \times 2.54} = 1.45 \times 10^{-6}\ INS^{-1}$$
$$(3.68 \times 10^{-8}\ ms^{-1})$$

The close similarity between the perforation rate observed for the longitudinally prepared specimen and that calculated on the basis of an applied current density of 4mA cm^{-2} implies that the permeation transients observed for the longitudinally prepared specimens were a consequence of membrane perforation and not, as the results may initially suggest true hydrogen permeation.

A comparison of the perforation rate of the transversely prepared specimen with the calculated values

iii) and iv) indicates that the permeation transients observed for this specimen preparation could also be attributed to perforation rather than true hydrogen permeation, if it is assumed that dissolution occurs at localised sites (corresponding to the observed fissures) at current densities of between 4 and 100mA cm^{-2}.

3.3.3 <u>The influence of additions made to the charging solution on the hydrogen permeation characteristic.</u>

Specimens for these investigations were prepared by transverse sectioning of the as received bar stock. Permeation transients were obtained for each charging solution the charging side of the membrane being exposed at the free corrosion potential and to cathodic and anodic polarisation at current densities of 4mA cm^{-2} chosen to be typical of those employed in the constant crosshead speed tensile tests described in section 3.2.6.

Fig. 3.41 shows a plot of the permeation current density as a function of $\log_{10}$ (time) for tests carried out in a charging solution of 3.5 wt % NaCl containing 5gm/l of solution of sodium arsenate and acidified to an intial pH of 2.0. Figs. 3.42 and 3.43 show similar plots for charging solutions containing 5gm/l of thiourea and 25cc/l chloroplatinic acid respectively (in each case acidified to an initial pH of 2.0). The results of similar tests in a solution containing no added ingredients are reproduced on each graph for comparison.

The results can be most conveniently described according to the nature of the polarising

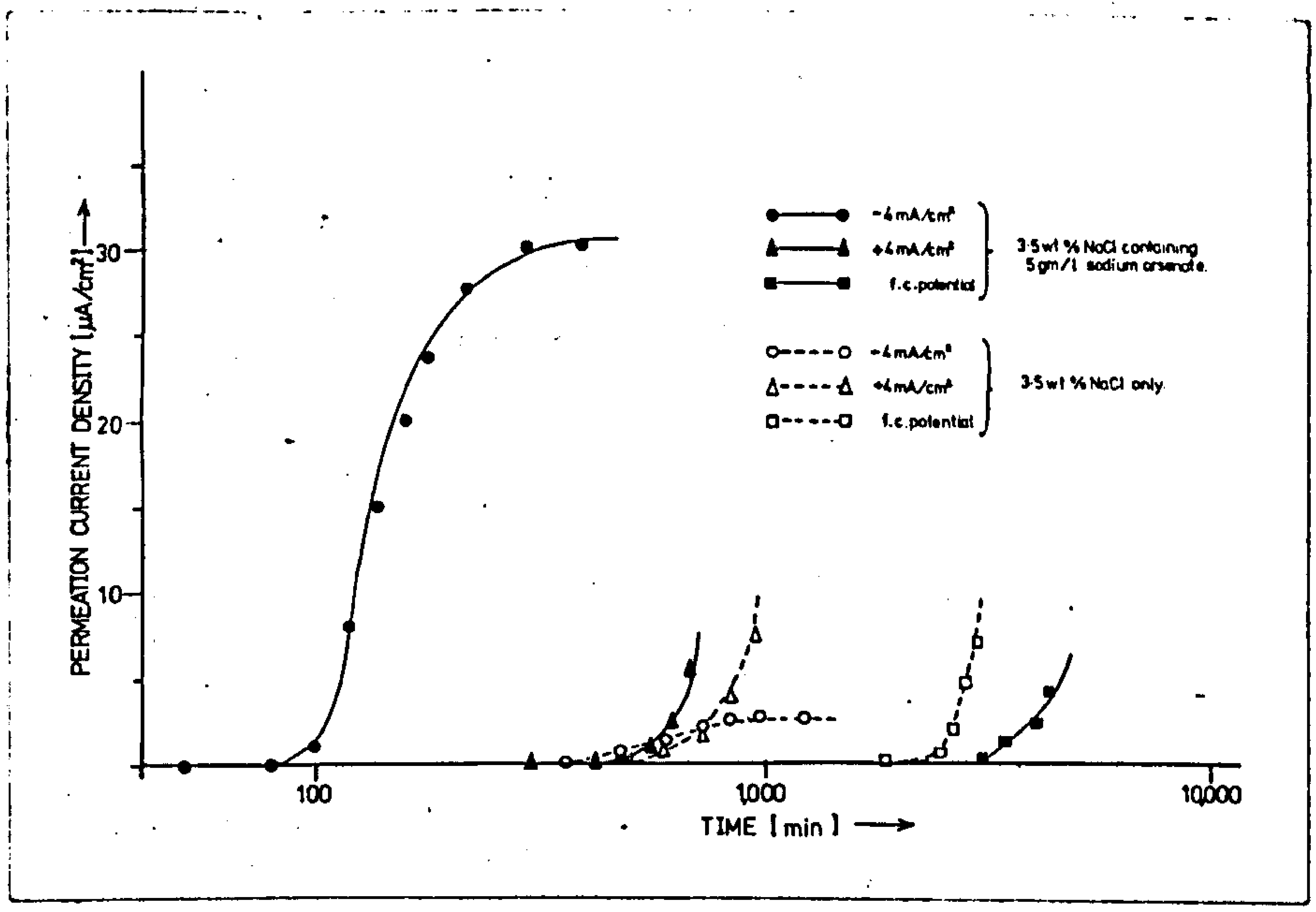

Fig. 3.41 Hydrogen permeation transients determined on maraging steel membranes subjected to various conditions of applied polarisation in a 3.5 wt % NaCl solution containing 5gm/l of sodium arsenate acidified to an initial pH of 2.0.

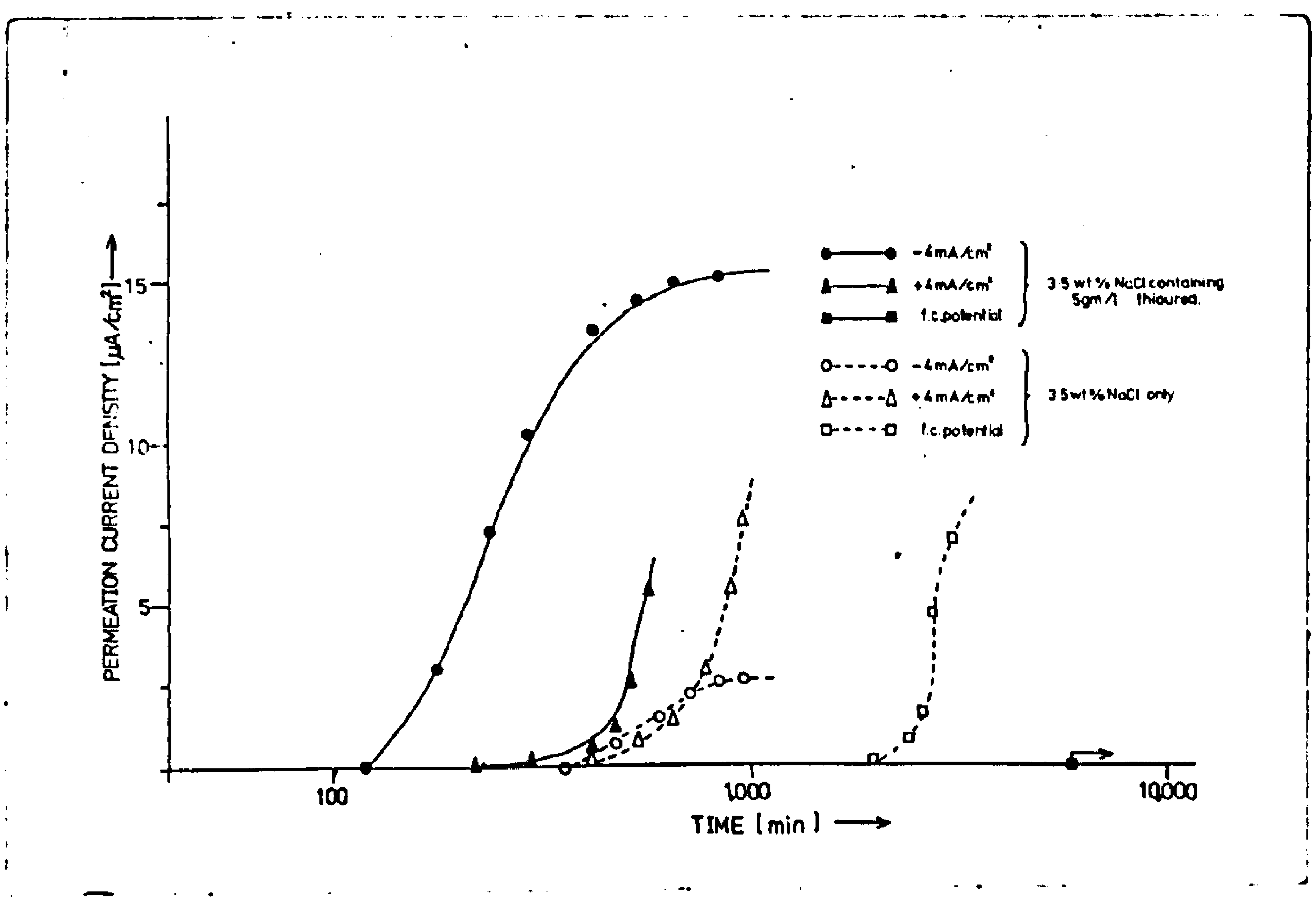

Fig. 3.42 Hydrogen permeation transients determined on maraging steel membranes subjected to various conditions of applied polarisation in a 3.5 wt % NaCl solution containing 5gm/l of thiourea acidified to an intial pH of 2.0.

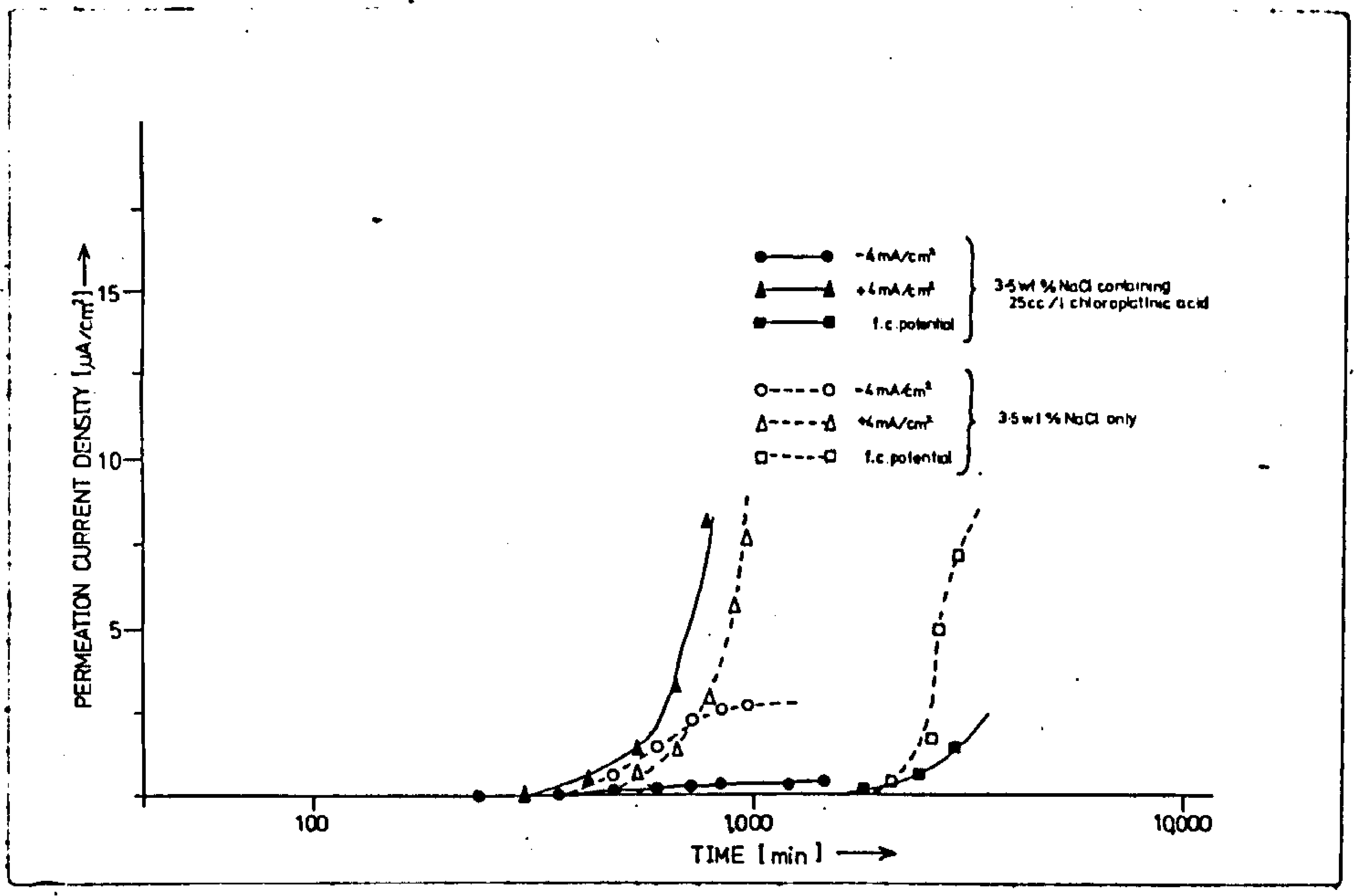

Fig. 3.43 Hydrogen permeation transients determined on maraging steel membranes subjected to various conditions of applied polarisation in a 3.5 wt % NaCl solution containing 25cc/l of chloroplatinic acid solution (5% w/v) acidified to an initial pH of 2.0.

conditions to which the charging side of the membranes were subjected:-

i) Cathodic polarisation

The results clearly demonstrate that sodium arsenate and thiourea additions are effective in increasing both the rate and amount of hydrogen adsorbed and absorbed into the metal. Furthermore, it is apparent that sodium arsenate is much more effective than thiourea in this latter respect; since the steady state permeation current density is higher and the rate of attainment of steady state more rapid in the case of the sodium arsenate addition. Chloroplatinic acid additions, however, can be seen to significantly reduce hydrogen uptake into the metal.

(witness the extremely low permeation current density of $0.25\ \mu A\ cm^{-2}$ in the case of the chloroplatinic acid addition Fig. 3.43).

The above observations are in agreement with the effect the additions were observed to have on the failure times of smooth tensile specimens tested at constant crosshead speed (cf. section 3.2.6).

ii) Anodic polarisation

The permeation transients obtained for specimens exposed to contaminated NaCl solutions were similar in all respects to one another and to the transients obtained for specimens exposed to non-contaminated solution. In all cases, the rising permeation transients appeared to be associated with perforation - by dissolution - of the specimen membranes as described in the previous sub-section.

No significance is attached to the fact that the time scales are slightly different for each solution since, for the purposes of clarity, only the transients for one run were plotted from a batch of 3 similar runs and some variation in time scale can be expected from run to run under otherwise identical test conditions. This is a consequence of the density and morphology of TiC(N) inclusions varying from specimen to specimen as explained more fully in section 3.4.

iii) Freely corroding

The effect of the addition of thiourea to the charging solution was to prevent a rise in permeation transient even after the maximum time permitted for a run (100 hr). In solutions contaminated with sodium arsenate and chloroplatinic acid permeation transients were recorded although the breakthrough time in the former case was almost doubled. The doubling of the breakthrough time in the case of the sodium arsenate contaminated solution may also be explained by the density and morphology of intermetallic (TiCN) inclusions varying from specimen to specimen as was thought to be the case in anodically polarised specimens. However, this certainly could not be the explanation in the case of the thiourea contaminated solution, since examination of that side of the membrane exposed to the charging solution at the end of the run revealed that very little dissolution had occurred.

These observations are in agreement with the results of constant crosshead speed tensile tests in which it was observed that thiourea additions were effective, particularly at the free corrosion potential, in preventing SCC presumably because of the inhibiting influence of thiourea on the dissolution reaction.

3.3.4 Quantitative aspects of the permeation technique - the determination of hydrogen diffusivities

For this aspect of the permeation work it was decided that a promoter should be added to the charging electrolyte in order to ensure consistent results. This is advisable since even traces of, for example, sulphur and phosphorous can have a strong promoting effect on hydrogen absorption. An intentional and strictly controlled addition of a promoter swamps any influence such contaminant may have on the adsorption reaction, thereby enabling hydrogen penetration rates to be measured more precisely than would be possible using so called pure electrolytes. Consequently, an addition of 5gm/l of sodium arsenate was made to the charging electrolyte (3.5 wt % NaCI) the pH of the latter then being adjusted to an initial pH of 2.0 with dilute hydrochloric acid solution (0.6N).

i) The influence of specimen thickness at constant charging current density.

Permeation curves were determined on specimens of various thicknesses in the range .008" - .032" (.025 - .08cm) and at a constant cathodic charging current density of 4 mAcm^{-2}.

Under steady state conditions, and assuming Fick's first law of diffusion is obeyed, then a plot of the reciprocal of the specimen thickness should be linear and of slope $F_D C_O$ (c.f. eqn.12).

Fig. 3.44a shows the peak permeation currents plotted as a function of the reciprocal of the specimen thickness. It can be seen that although a best straight line could be fitted to the points (dashed) this line would not then pass through the origin. Consequently, the relationship is considered to be as shown by the solid curve i.e. non linear.

A further test of the applicability of Fick's first law of diffusion to describe the diffusion of hydrogen through maraging steel is apparent from eqn. (13a) Thus, for any characteristic value of τ, equation (13a) indicates that the corresponding time interval, t should be proportional to the square of the specimen thickness. Two such time intervals are the so called breakthrough time, t_b, for which τ = .0653[120] and the so called time lag, t_L for which τ = .166.[120]

Fig. 3.44b shows the breakthrough times and time lags for specimens of various thicknesses (corresponding to the results of Fig. 3.44a) plotted as a function of the square of the specimen thickness. It is apparent that the points curve upwards as the thickness is increased.

The diffusion coefficients calculated from the above results using equation (13a) are tabulated below from which it is apparent that the diffusion coefficient apparently decreases with increasing specimen thickness above a thickness of .020" (.052cm).

TABLE 3.8

Diffusion coefficients for maraging steel calculated from the breakthrough and time lag times.

THICKNESS (cm)	$L^2 (cm^2)$	$D_{tb} (cm^2\ s^{-1})$	$D_{Tl} (cm^2\ s^{-1})$
2.2×10^{-2}	4.84×10^{-4}	5.98×10^{-9}	8.67×10^{-9}
2.5×10^{-2}	6.25×10^{-4}	6.81×10^{-9}	1.02×10^{-8}
2.92×10^{-2}	8.53×10^{-4}	6.3×10^{-9}	1.08×10^{-8}
5.2×10^{-2}	2.7×10^{-3}	6.7×10^{-9}	1.08×10^{-8}
7.88×10^{-2}	6.21×10^{-3}	3.9×10^{-9}	5.9×10^{-9}

Furthermore, the diffusivity coefficients calculated from 'time lag' times are almost twice those calculated from the 'breakthrough times', indicating that the diffusion coefficient apparently increases with time.

Fig. 3.44 A plot of (a) the peak permeation current densities as a function of $^1/$spec thickness and (b) the breakthrough and time lag times as a function of (spec thickness)^2 for maraging steel membranes cathodically charged at a current density of 4mA cm^{-2} in a 3.5 wt % NaCl solution containing 5gm/l of sodium arsenate acidified to an initial pH of 2.0.

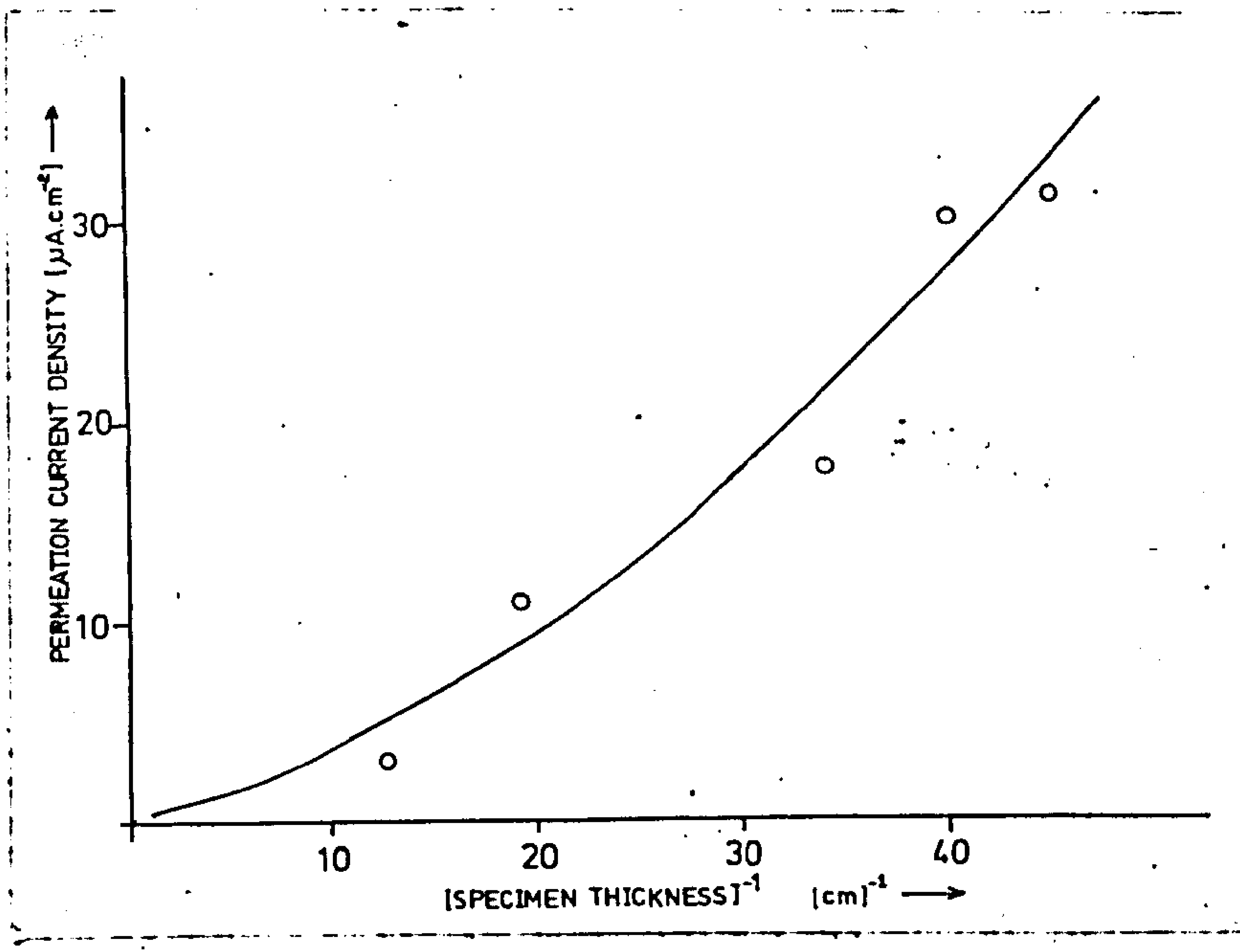

Fig. 3.44a

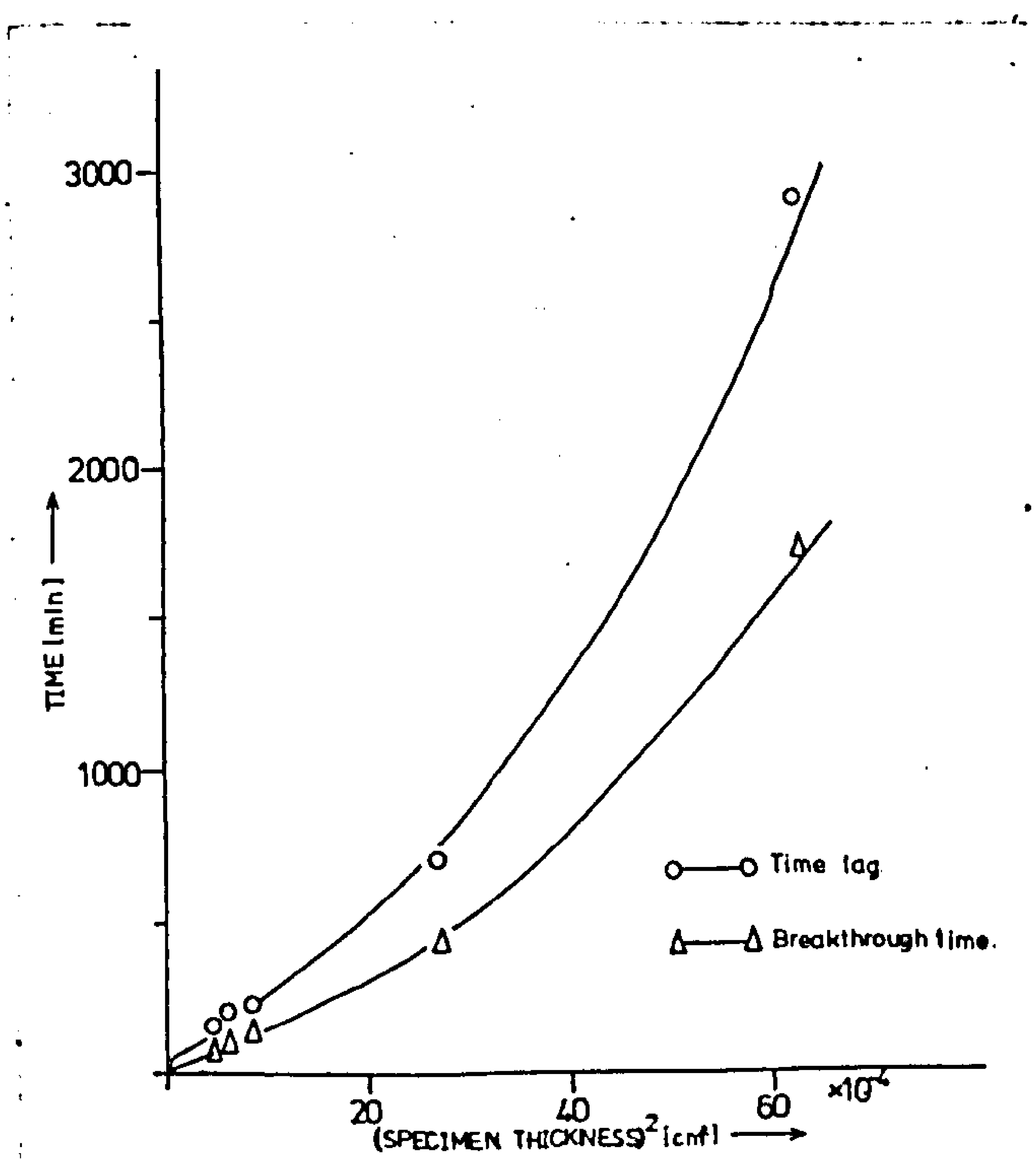

Fig. 3.44b

This apparently anomalous behaviour will be considered in greater detail in the following sub-section.

ii) The influence of charging current density at constant specimen thickness.

Fig. 3.45 shows the hydrogen permeation transients for .0115" (.0292cm) thick maraging steel coupons charged at cathodic current densities of between 0.25mA cm^{-2} and 8mA cm^{-2}.

The curves determined with charging current densities of 0.25 and 1mA cm^{-2} show normal permeation transients in that they do not exhibit peak permeation currents followed by a gradual decline. The latter behaviour in permeation curves has been observed in other metal-environment systems e.g. armco iron polarised cathodically in 0.1NH_2SO_4[124] and has been explained as being either a consequence of irreversible processes occurring within the membranes such as the formation of microcracks or blisters which act as traps for the absorbed hydrogen above a certain critical hydrogen concentration, (Bockris); or as a result of changes in surface phenomena at the cathodic side of the membrane or a combination of the two. Arguments concerning the validity of either theory will not be entered into at this point; suffice it to say that both theories appear to be equally plausible to account for the anomalies in the permation behaviour. It may be of interest to note, however, that specimens pre-charged at a current density of 8mA cm^{-2} in the same charging electrolyte and subsequently annealed under vacuum at 200°C for 16hr to remove the absorbed hydrogen and then pulled to failure in air; showed no obvious evidence of microcrack formation on the fracture surface. Specimens similarly precharged and tested in air immediately after charging failed in a brittle fashion the fracture surface showing an annulus of intergranular crack propagation surrounding the central 'dimpled' region characteristic of ductile overload (see also section 3.7).

More importantly, perhaps, is the fact that the permeation transients were shifted to shorter times as the charging current density was increased. This implies that the permeation transients cannot be described by the theoretical equations derived on the assumption of concentration independant diffusivity (equations (14), (15)). Nevertheless; by selective fitting of the experimental data in each of the short, intermediate and long, time regions of the theoretical 'build up' curve (at values of J_{τ}/J_{∞} = 0.175, 0.496, 0.895) values of diffusion coefficient were calculated for each of the curves. The latter results are plotted graphically in Fig. 3.46 which shows the variation of diffusion coefficient - so calculated - with charging current density and time. In general, it can be seen that there is a consistent increase in diffusivity with time as the transient progresses at any particular charging current density and also with charging current density (up to 4mA cm^{-2}) at any particular time thus reflecting a trend towards concentration dependent diffusivity.

The above 'apparent' diffusion coefficients for hydrogen in maraging steel should be compared with the quoted values of the diffusion coefficient of hydrogen

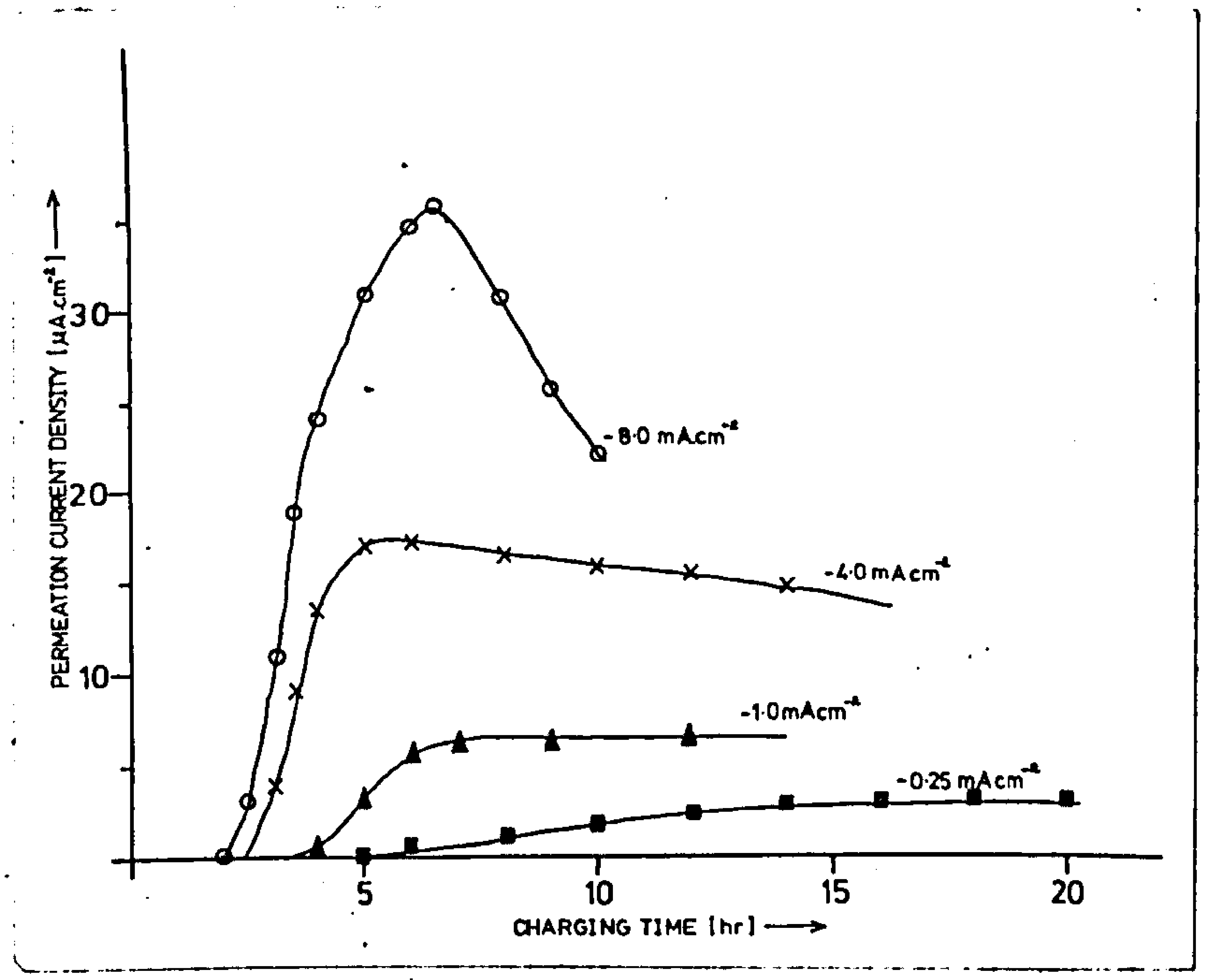

Fig. 3.45 The influence of cathodic charging current density on the hydrogen permeation transients observed on maraging steel membranes hydrogen charged in a 3.5 wt % NaCl solution containing 5gm/l of sodium arsenate acidified to an initial pH of 2.0.

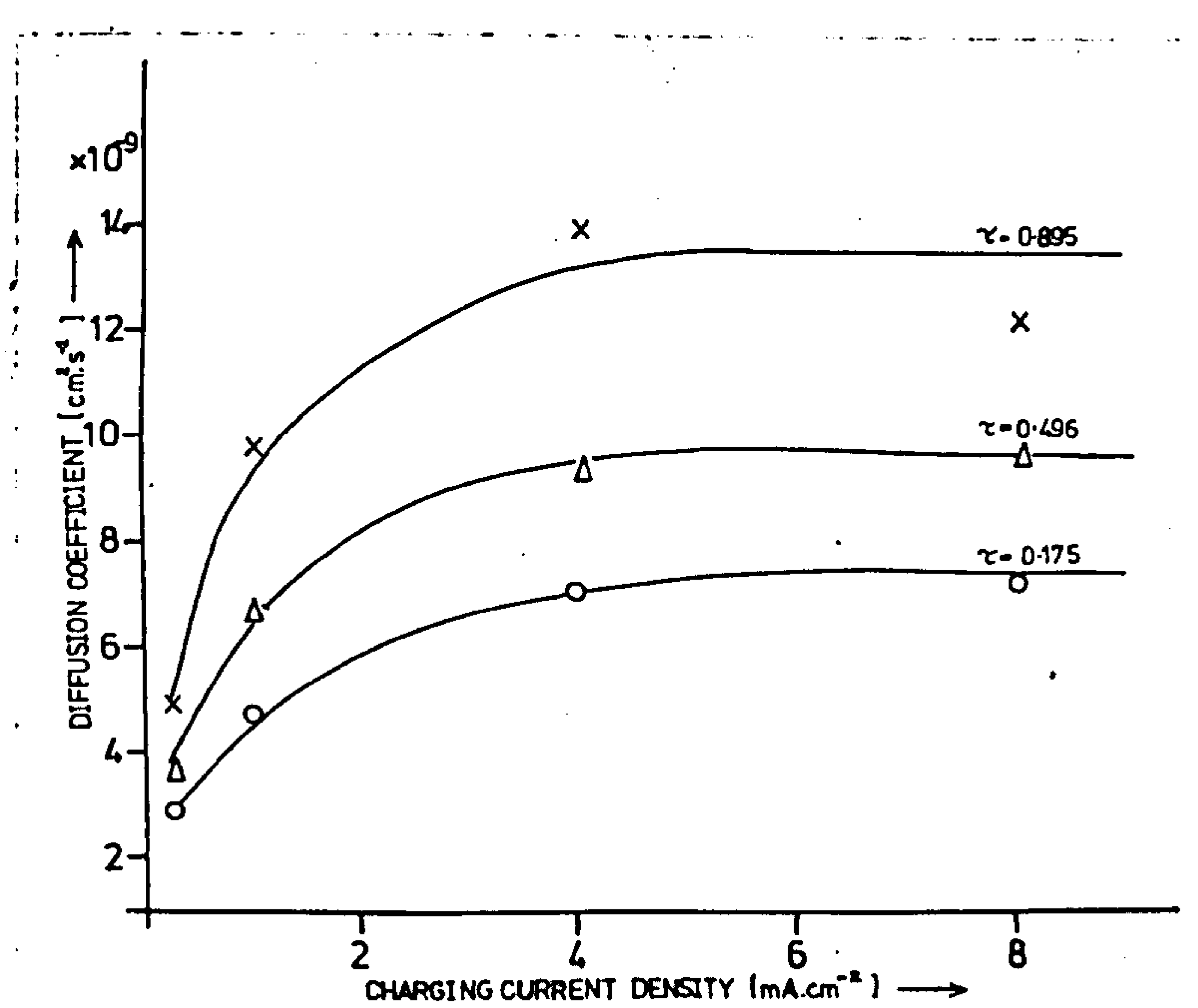

Fig. 3.46 The variation of diffusion coefficient with charging current density and times, calculated from the curves shown in Fig. 3.45.

in iron at 22°C e.g. 3.06×10^{-5} cm^2s^{-1}.[131] Such anomalous diffusion behaviour is almost certainly explained by the theory of hydrogen trapping first suggested by Darken and Smith[132] to explain anomolous diffusion coefficients in a cold worked steel and subsequently developed on a mathematical basis by McNabb and Forster[133] and more recently extended by Oriani.[131] According to the trapping theory, hydrogen moving through the metal matrix is assumed (and, indeed, has been shown to be) trapped at a variety of positions within the metal or alloy. Hydrogen atoms trapped in this way will not be as mobile as hydrogen atoms occupying normal lattice sites with the consequence that diffusivities determined on bulk specimens will be lower than the true lattice diffusivities. The nature and density of trapping sites is a function of the composition and the physical state of the metal or alloy and in particular, the amount of prior cold work to which the material has been subjected. Thus, in an annealed pure metal apart from grain boundaries, solid-solid interfaces are absent the only other likely trapping sites being dislocations or chemical impurities. In a precipitation age-hardening alloy such as maraging steel, solid-solid interfaces between matrix and precipitate particles are abundant thereby providing many more trapping sites for absorbed hydrogen.

3.4 The Influence of Specimen Orientation on the Stress Corrosion Cracking Susceptibility

It will be recalled that in 'hydrogen permeation' tests performed with anodic polarisation on the charging side of the membranes, it was observed that the rate of perforation of the specimens was strongly dependent upon the orientation of the specimen with respect to the original rolling direction.

The implication of the above results is that because of for example, segregation of alloying elements into stringers or the elongation of inclusions in directions parallel to the original rolling direction, particularly susceptible paths for dissolution are provided. Consequently, the effect of specimen orientation on the stress corrosion cracking susceptibility of both smooth tensile specimens and fatigue precracked single-edge notch tensile specimens was investigated.

Because the maximum cross sectional area of bar stock available to provide specimens with the original rolling direction perpendicular to the tensile axis, was only $\pi/4$ IN^2; smooth tensile and single edge notch fatigue precrack specimens of the reduced dimensions shown in Figs. 2.1b and 2.4 respectively were employed in these investigations.

The influence of specimen orientation with respect to the original rolling direction on the cracking susceptibility of smooth tensile specimens of 18Ni maraging steel exposed to acidified 3.5 wt % NaCl solution (initial pH = 2.0) at the free corrosion potential and with galvanostatic anodic and cathodic polarisation is shown in Tables 3.9 and 3.10. The results in Table 3.9 are for dynamically strained specimens tested at a constant crosshead speed of 1.29×10^{-6} INS^{-1} and those in Table 3.10 for specimens loaded to an initial stress of 150,000 p.s.i and held at a constant strain throughout the duration of the test.

TABLE 3.9

The influence of specimen orientation on the failure times of smooth tensile specimens dynamically strained at 1.29×10^{-6} INS^{-1} under various conditions of applied polarisation in 3.5 wt % NaCl (initial pH 2.0).

APPLIED CURRENT (mA)	TIME TO FAILURE (MIN)	
	Rolling direction ⊥ to tensile axis	Rolling direction // to tensile axis
-2.5	395	500
-0.63	505	590
0	375	390
+0.63	310	335
+2.5	325	350

TABLE 3.10

The influence of specimen orientation on the failure times of smooth tensile specimens loaded to an intial stress of 150,000 p.s.i.and held at constant strain throughout the tests.

APPLIED CURRENT (mA)	TIME TO FAILURE (MIN)	
	Rolling direction ⊥ to tensile axis	Rolling direction // to tensile axis
0	230	290
+0.63	140	192
+2.5	112	144

The above results, and particularly the latter, demonstrate quite clearly that specimen orientation with respect to the original rolling direction can significantly influence the susceptibility towards stress corrosion cracking. The fact that as much as 90% of the total failure times in smooth tensile tests can be associated with crack initiation, implies that the main influence of specimen orientation is on the crack initiation step. To check the validity of the latter; single edge notch fatigue precracked tensile tests were carried out, in the same environment, on specimens prepared in such a way that the original rolling direction was parallel to the cracking plane. The crack velocities so determined are set out in Table 3.11 along with crack velocities determined previously on specimens prepared such that the original rolling direction was perpendicular to the cracking plane and parallel to the tensile axis.

TABLE 3.11

The influence of specimen orientation on the average crack velocities determined on S.E.N tensile specimens.

APPLIED CURRENT DENSITY (mA/cm^2)	AVERAGE CRACK VELOCITIES			
	Rolling direction // to cracking plane		Rolling direction ⊥ to cracking plane	
	ins^{-1}	ms^{-1}	ins^{-1}	ms^{-1}
+2.6	$5x10^{-6}$	$1.27x10^{-7}$	$5.4x10^{-6}$	$1.37x10^{-7}$
0	$3x10^{-6}$	$7.62x10^{-8}$	$2.0x10^{-6}$	$5.08x10^{-8}$
-2.6	$2.1x10^{-5}$	$5.34x10^{-7}$	$1.8x10^{-5}$	$4.57x10^{-7}$

The close similarities between the two sets of crack velocity data indicates that the above deduction, i.e. that the principle influence of specimen orientation in smooth tensile tests is on the crack initiation step, was indeed correct.

The above results prompted the execution of tests under freely corroding conditions in as made up 3.5 wt % NaCl solution; conditions under which, it may be recalled, stress corrosion cracking could not be induced in dynamically strained tensile specimens (cf. section 3.2.4).

For these investigations the constant strain static tensile loading mode was employed in which the smooth tensile specimens were loaded to various initial stress levels on a hardbeam tensometer, the crosshead was then locked in position and the load allowed to relax as crack propagation proceeded to failure.

The results which are shown in Fig. 3.47 were plotted in terms of initial stress versus time to failure.

Specimens prepared such that the tensile axis was at 90° to the original rolling direction were evidently much more susceptible to crack initiation than those specimens prepared in such a way that the tensile axis was parallel to the original rolling direction.

Cracking, when it occurred was intergranular and appeared to have initiated from the base of pits which had

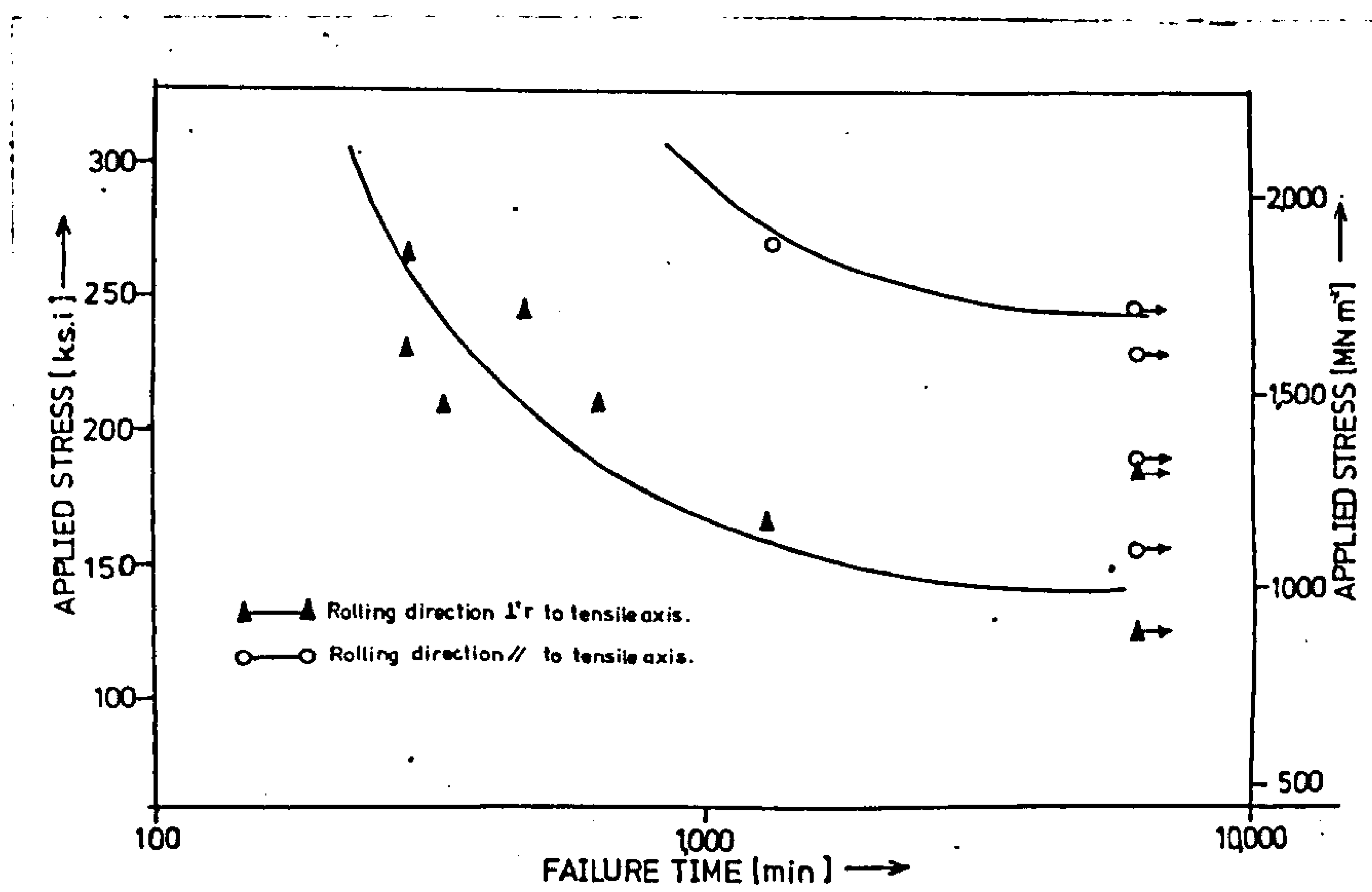

Fig. 3.47 The influence of specimen orientation with respect to the original rolling direction on the SCC susceptibility of smooth maraging steel tensile specimens tested under conditions of constant strain in a 3.5 wt % NaCl solution of initial pH 6.0.

formed on the surface as a result of intense localised dissolution. Although dissolution at localised sites was observed on the surface of specimens whose tensile axis was parallel to the original rolling direction, cracking was not initiated from the base of the pits so formed, presumably because pitting was only occuring to a shallow depth - this depth being insufficient to permit either extensive plastic deformation at the base of the pits or to allow electrochemical changes to take place within the pits whereby the necessary cracking conditions could be developed.

The significance of the specimen orientation with respect to the original rolling direction in this context may be related to differences in the morphology of TiC(N) inclusions produced by the different specimen preparations. Thus in the case of specimens prepared such that the original rolling direction was perpendicular to the tensile axis the inclusions are present as stringers orientated at 90^{o} to the tensile axis whereas in the case of specimens prepared such that the original rolling direction was parallel to the tensile axis the inclusions are present as stringers lying parallel to the tensile axes. Consequently, if pitting is initiated in the immediate vicinity of TiC(N) inclusions as a result of marked differences between the electrochemical characteristics of TiC(N) and the matrix material, then much deeper fissures (or pits) would be produced in the former case than in the latter case.

TiC(N) inclusions appear as distinctive pink, angular particles under the optical microscope and they are fairly easily identified within the lighter background of the matrix material on polished but unetched surfaces. Such inclusions were quite abundant in the maraging steel used in these investigations where they were often observed to be present in the form of intermittent stringers of fragmented particles orientated parallel to the original rolling direction.

To demonstrate that pitting was often associated with these inclusions the following procedure was adopted. A freshly polished section of maraging steel was exposed to as made up 3.5 wt % NaCl solution for approximately 30 seconds, rinsed in deionised water and methanol, and dried under a hot air blower. Examination of the polished and corroded surface on the optical mirco-scope revealed the presence of numerous sites of anodic attack; each site being associated with an angular inclusion at its centre (Fig. 3.48). Because of the discolouration

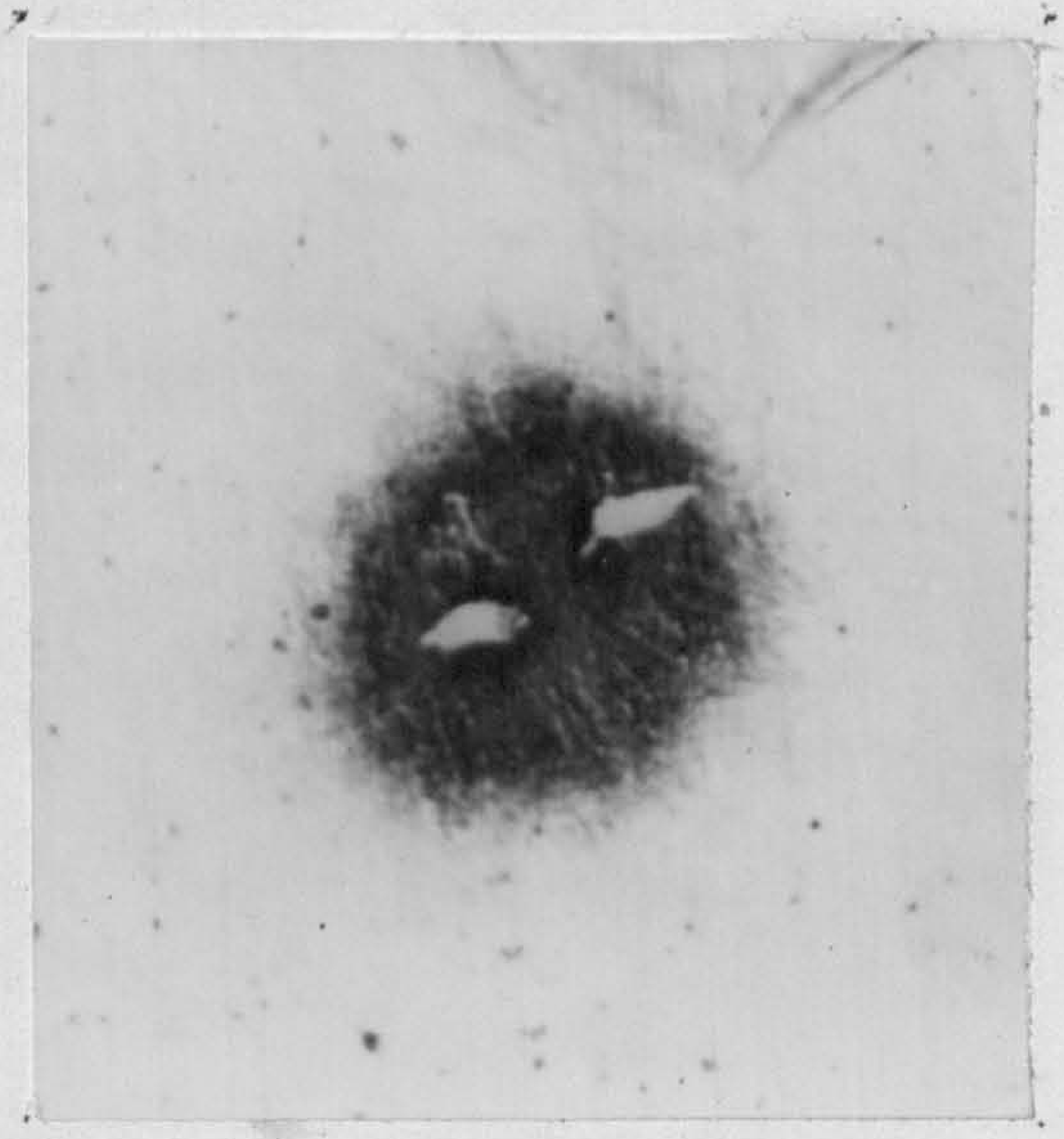

Fig. 3.48 Optical micrograph of the freshly polished surface of a maraging steel specimen exposed to 3.5 wt % NaCl solution of initial pH 6.0 for 30 seconds showing dissolution of the matrix material immediately adjacent to angular inclusions in the steel (x125).

of the inclusion and the surrounding matrix material by the black corrosion products formed; the true colour of the inclusions could not be identified; however, from the shape and general size of the inclusions it seemed fairly certain that they were in fact TiC(N) particles.

By way of confirmation, a number of the inclusions associated with anodic dissolution were labelled with a Vickers hardness indentor (load 1kg) and the metallographic section mounted on a stub and the inclusions examined on a scanning electron microscope fitted with EDAX facilities.

A typical inclusion is shown in Fig. 3.49a. Figs. 3.49b, c and d show the corresponding element distributions of Fe, Ni and Ti respectively as represented by their characteristic x-rays generated by the electron beam. Fig. 3.50 shows the full x-ray spectrum from the area shown in Fig. 3.49a.

These results confirm that the inclusions associated with the pitting localities are of a Titanium bearing compound - probably TiC(N) derived from the melting procedure where Ti is added to scavenge elemental carbon from the melt.

The corrosion potentials, determined on sintered discs of TiC, in 3.5 wt % NaCl solutions adjusted to various initial pH's are listed in Table 3.12.

<u>TABLE 3.12</u>

The corrosion potentials of TiC in 3.5 wt % NaCl of various initial pH's.

pH	Corrosion Potential (mV vs SCE)
2.0	+250
as made up (6.0)	+40
11.0	0

Fig. 3.49 Scanning electron micrograph (a) of an inclusion associated with anodic dissolution and the corresponding elemental distributions (b), (c) and (d) of Fe, Ni and Ti respectively as revealed by the characteristic x-rays generated by the electron beam.

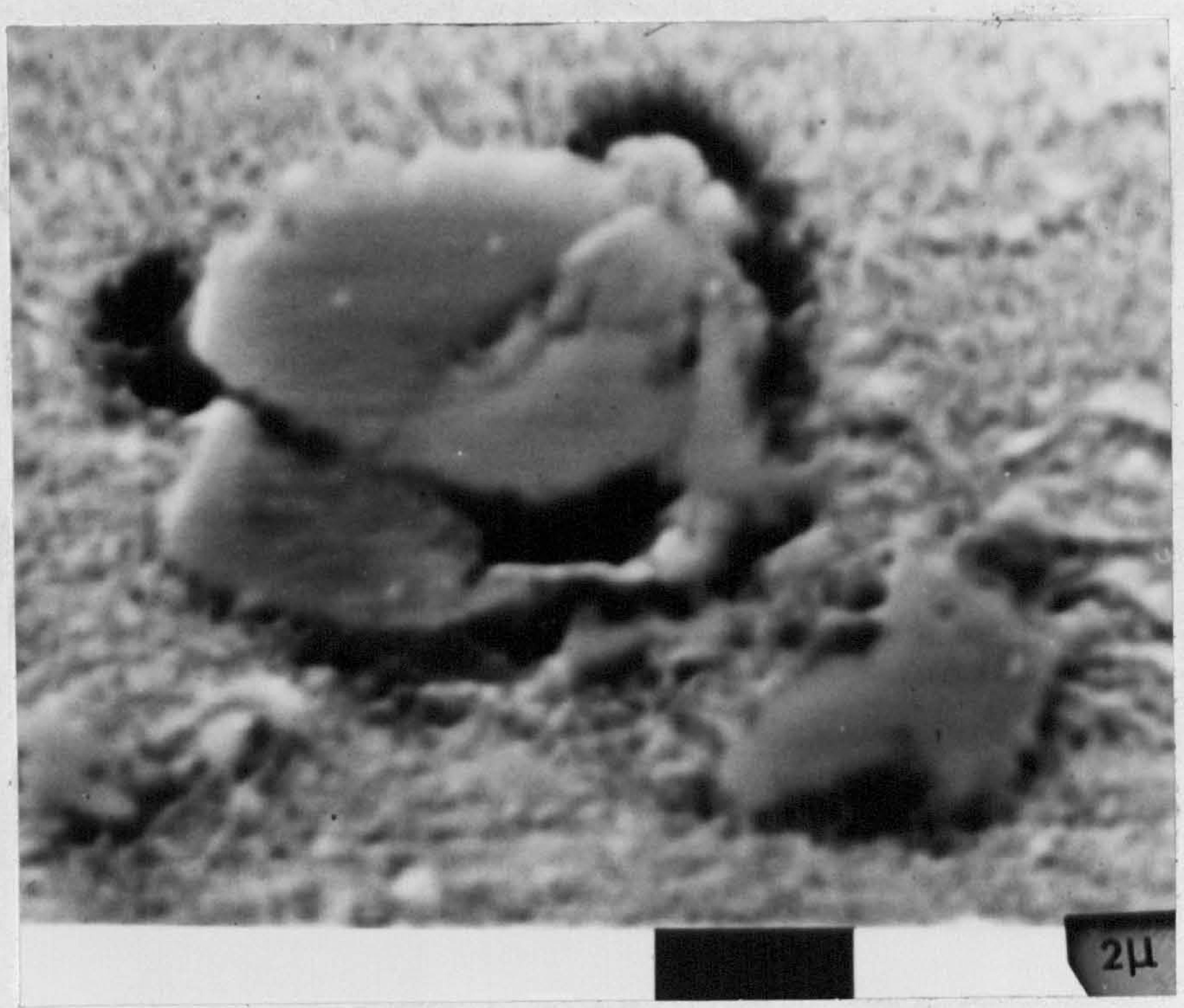

Fig. 3.49a

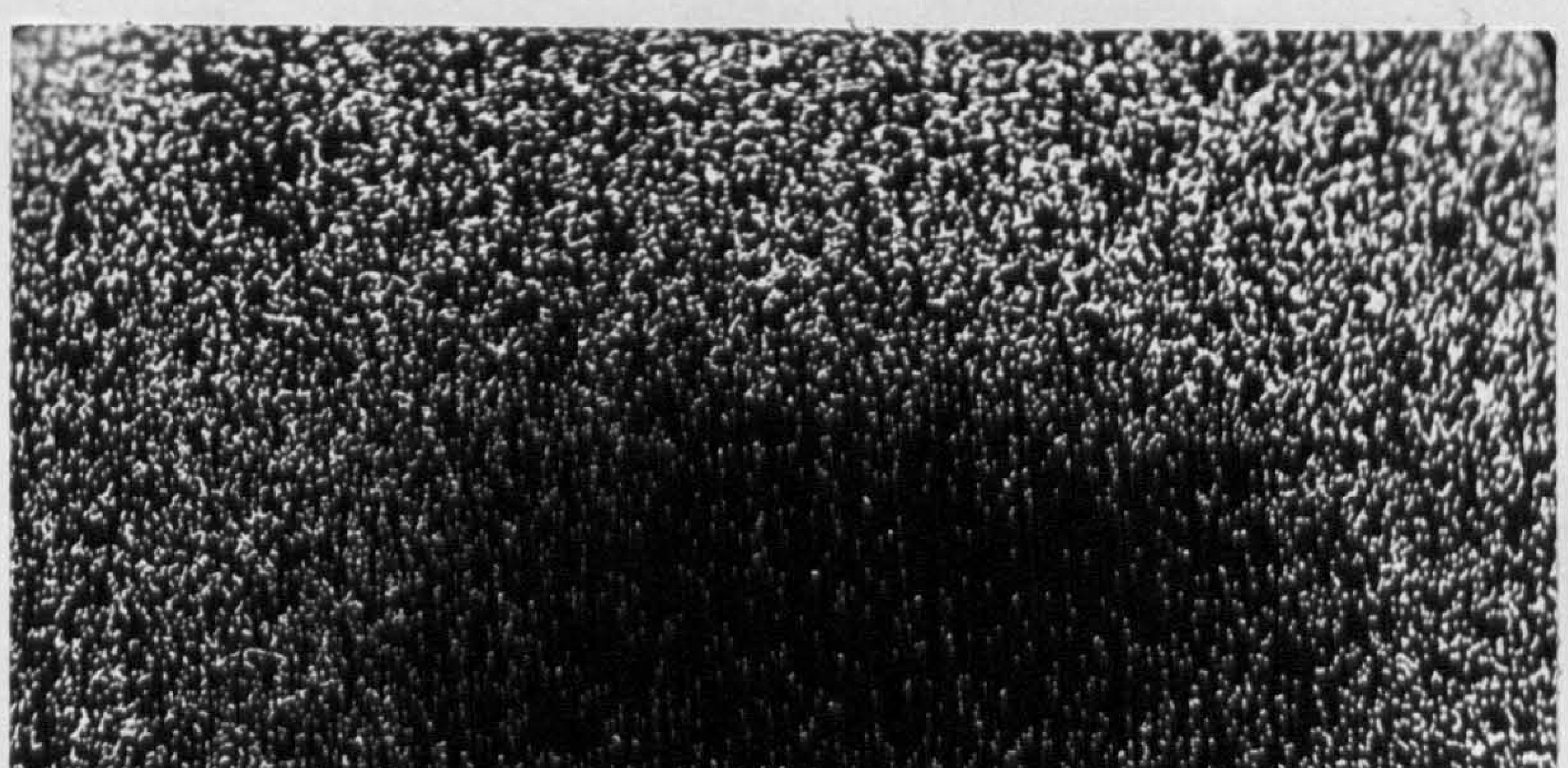

Fig. 3.49b

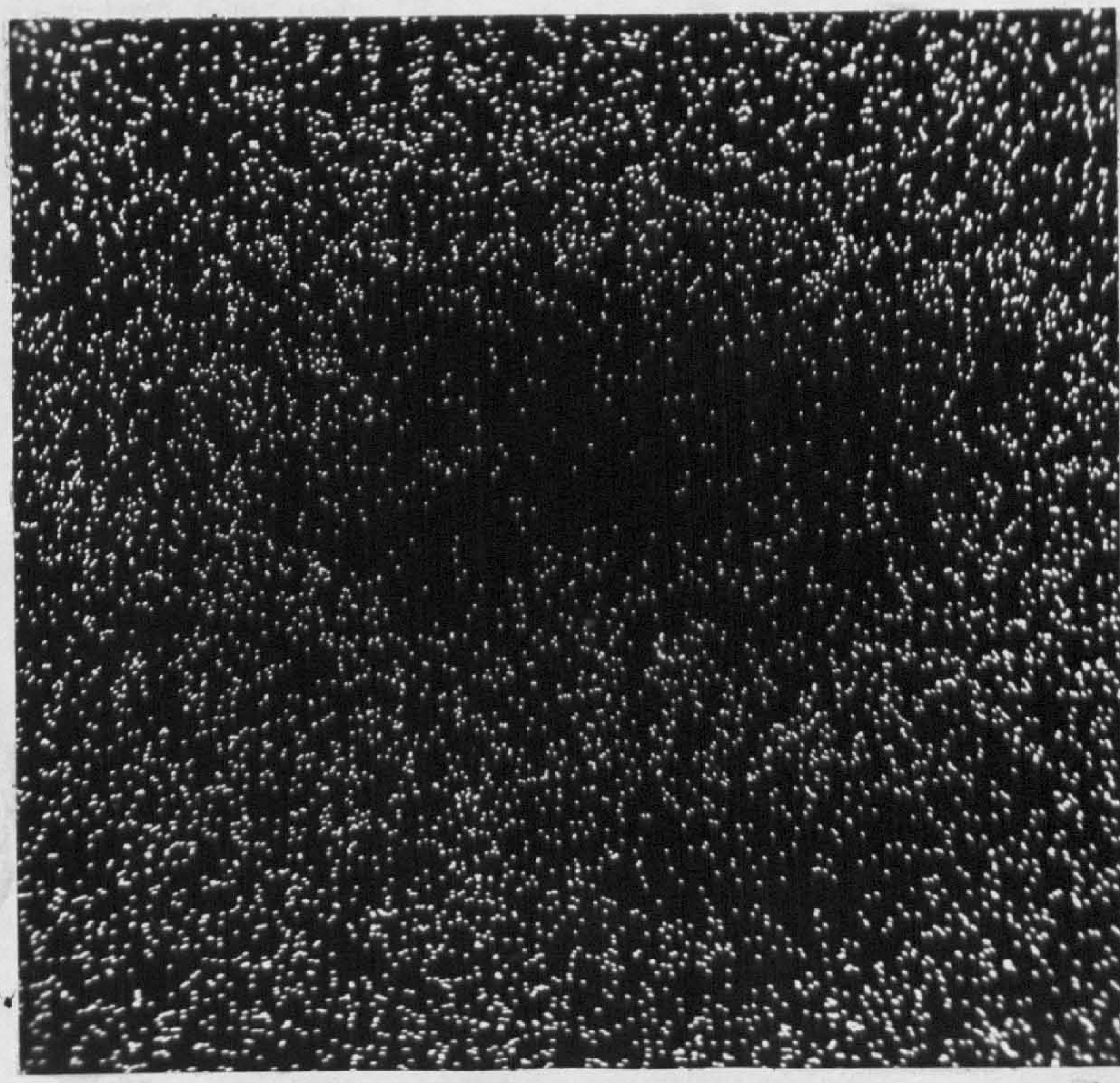

Fig. 3.49c

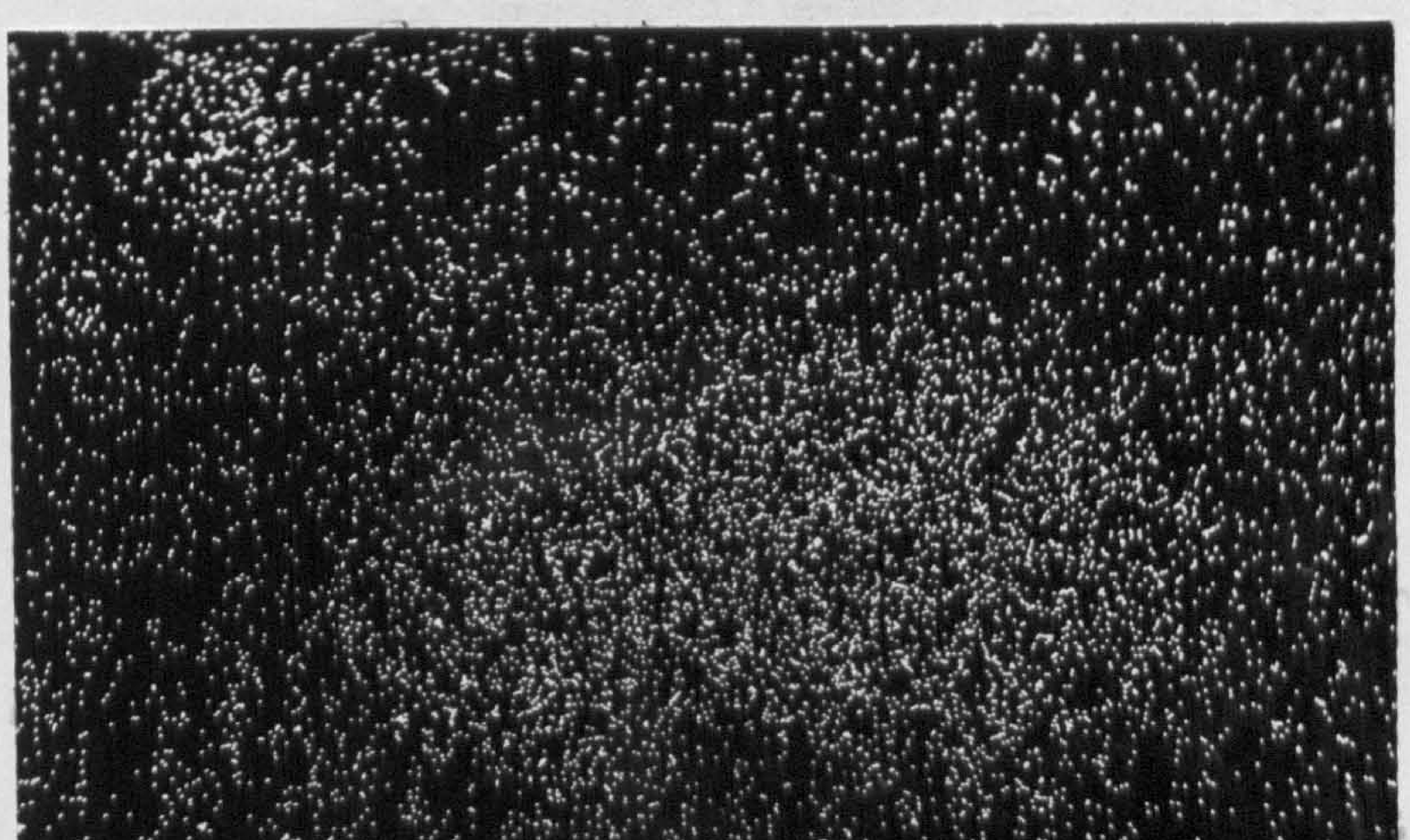

Fig. 3.49d

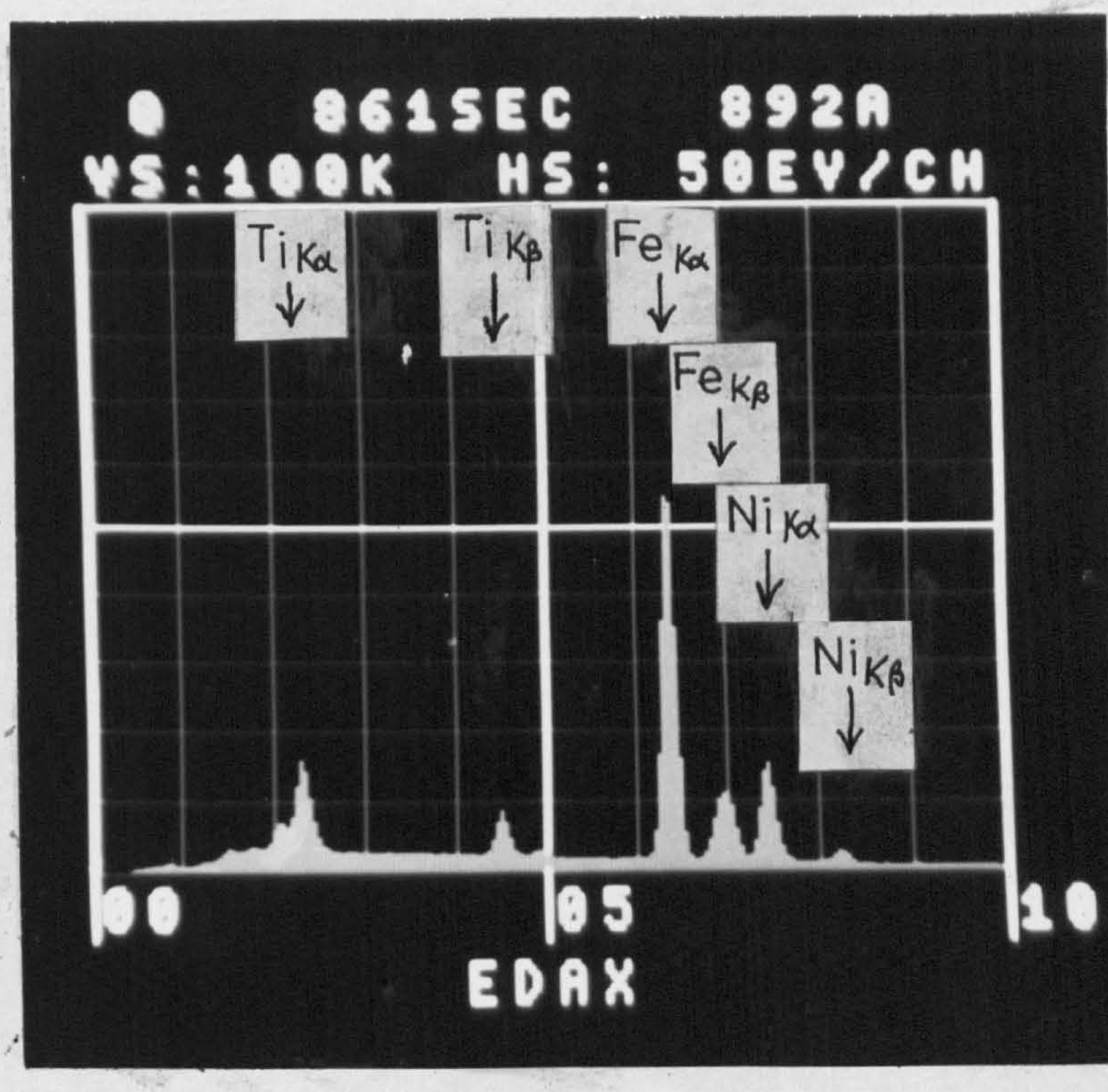

Fig. 3.50 The full x-ray spectrum generated by the electron beam scanned across the area shown in Fig. 3.49. Sampling time as shown.

These potentials being some 400-600 mV noble to the corrosion potential of iron in the same environments indicate that TiC(N) inclusions in maraging steel probably act as particularly efficient cathodes in a local galvanic cell produced between the TiC(N) inclusions and the immediately adjacent matrix material. It is not surprising therefore that marked dissolution was observed to take place in the vicinity of such inclusions.

3.5 The Determination of Threshold Stress Intensity Values for Stress Corrosion Cracking and the Effect of Creep Relaxation on the Threshold Stress Intensity

It has been suggested[134] that the threshold stress intensity value in a given metal-environment system corresponds 'to the initiation by a process of slip deformation, of resolvable stretch zone formation at the crack tip' and that the atomically clean metal so formed acts as suitable sites for either the cathodic reduction of hydrogen or the anodic dissolution of the metal. The implication is that the stretch zone formation results in plastic deformation in the metal at the crack tip so that the otherwise protective air formed oxide film is intersected and the necessary corrosion reactions can take place on the clean metal so produced. As McIntyre[135] points out an exception to this rule will be under conditions where reductive dissolution of the oxide film can expose fresh metal and thereby by-pass the initiation processes giving rise to reduced apparent threshold stress intensities.

On the basis of this theory information concerning the protective (or otherwise) nature of the air formed oxide films may be gleaned since, assuming the oxide film to be protective, then one might expect $K_{I\ SCC}$ to be improved if the oxide film is allowed to reform at the crack tip after loading and before exposure to the cracking conditions. Another factor, associated with plastic deformation produced at the crack tip, and which may influence the ease of crack initiation and propagation, is the rapidly yielding material produced at the crack tip. This may be important even in the absence of protective films formed on the metal surface. Thus, Hoar and his co-workers[136,137,138] have clearly demonstrated that yielding assists the anodic dissolution process and reduces activation overpotential to negligible proportions in 18Cr- 8Ni stainless steels and some Fe-Ni alloys in 42 wt % $MgCl_2$. The explanation of the rapid attack under yielding conditions is thought to be connected with certain microstructural features in the face centred cubic lattice in these alloys. These alloys (like the maraging steels) have very low stacking fault energies and very high dislocation densities on slip planes. Electron microscopic studies have shown[139] that these features are almost exclusively attacked and this might explain the connection between strain rate and dissolution rate in some stress corroison systems.

The purpose of the work described in this section was to determine fundamental $K_{I\ SCC}$ data whilst at the same time obtaining information about the protective (or otherwise) nature of the air formed oxide film and about the influence of the strain rate at the crack tip on $K_{I\ SCC}$ data which might help to elucidate the mechanisms of crack initiation and propagation in maraging steel exposed to aqueous environments.

Threshold stress intensities were determined by the technique of 'bracketing'. Specimens were loaded to various chosen initial stress intensity levels either directly in contact with the corrosive environment or initially in air. In the latter case the corrosive environment and the polarising conditions were applied to the specimen after 72 hr on load during which time creep processes were assumed to have gone to completion and the air formed oxide film - initially disrupted by deformation at the crack tip - to have reformed. Crack growths were monitored using the D.C. electrical resistance technique so that crack initiation could be readily detected thereby permitting crack growth rates to be more accurately determined. Tests were terminated which showed no evidence of crack propagation within 50hr of exposure. Specimens were broken open after testing and any crack growth measured on the travelling microscope.

Threshold stress intensities were determined under freely corroding conditions in as made up (pH 6.0) 3.5 wt % NaCl and in 3.5 wt % NaCl solution acidified to an intial pH of 2.0 with dilute hydrochloric acid. In addition threshold stress intensities were determined for the latter environment under conditions of anodic and cathodic polarisation.

The influence of strain rate on crack initiation and propagation was investigated under freely corroding conditions in 3.5 wt % NaCl acidified to an initial pH of 2.0. The procedure adopted was as follows:- Specimens were loaded to an initial stress intensity of 10 KSI$\sqrt{\text{IN}}$ (to ensure complete separation of fatigue precrack faces and thereby ensuring no ambiguity as to crack initiation as indicated by the D.C electrical resistance crack growth monitor) the solution added and the specimen strained at the desired crosshead speed until substantial crack growth had occurred. At the end of the run, the specimen was unloaded, broken open and crack growth measured as described above.

Fig. 3.51 shows the effect of pre-loading to exhaust creep processes on the $K_{I\ SCC}$ data obtained on freely corroding S.E.N. maraging steel tensile specimens in a 3.5 wt % NaCl solution of initial pH 6.0. It is evident that pre-loading has not influenced the threshold stress intensity the latter having a value of between 25 and 30 KSI$\sqrt{\text{IN}}$. The implication of these results is that the air formed oxide film on maraging steel is not sufficiently stable to prevent stress corrosion cracking under the above

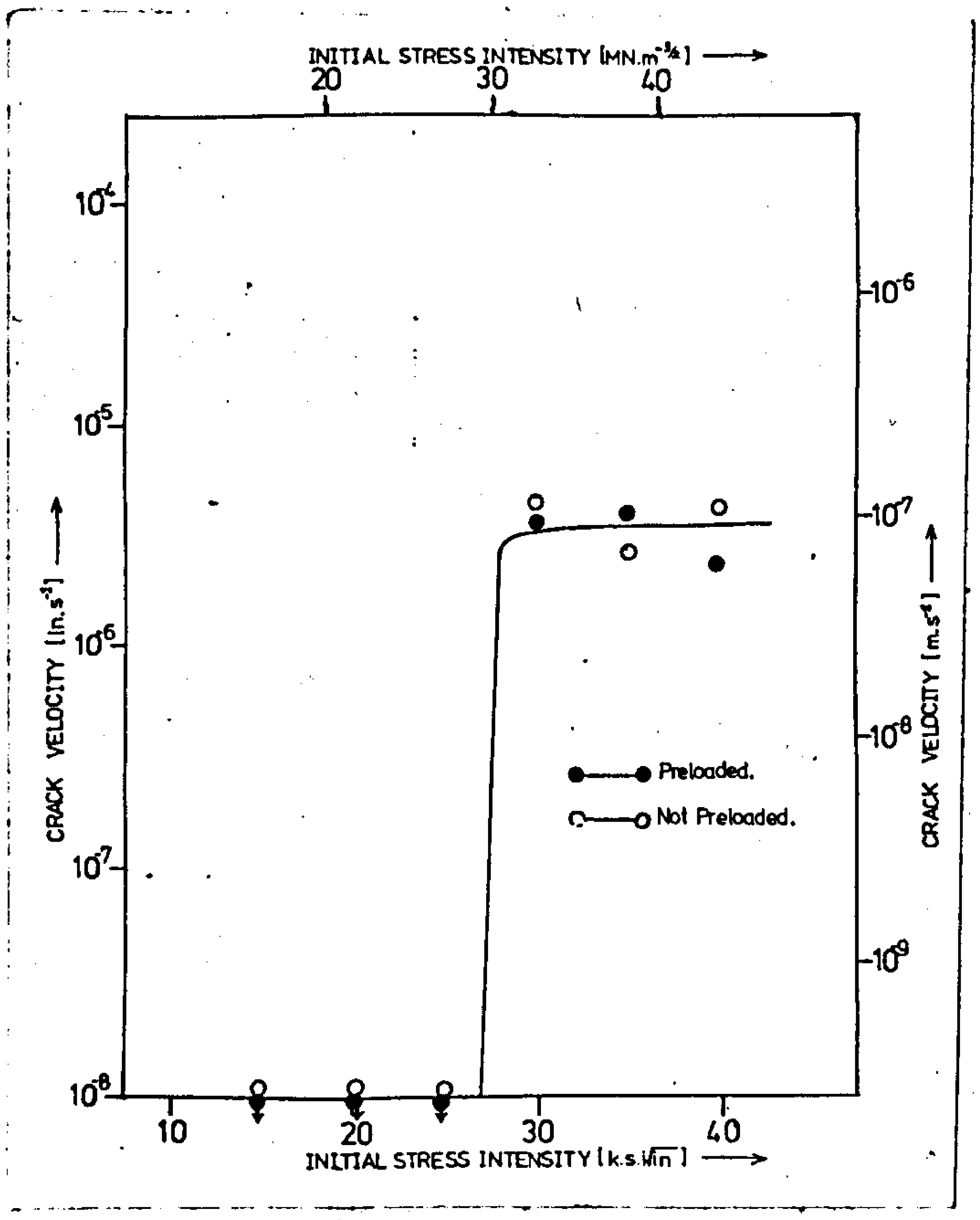

Fig. 3.51 The influence of preloading for 72hr in the absence of the corrosive environment on the threshold stress intensity for cracking of maraging steel precracked SEN tension specimens exposed under freely corroding conditions to a 3.5 wt % NaCl solution of initial pH 6

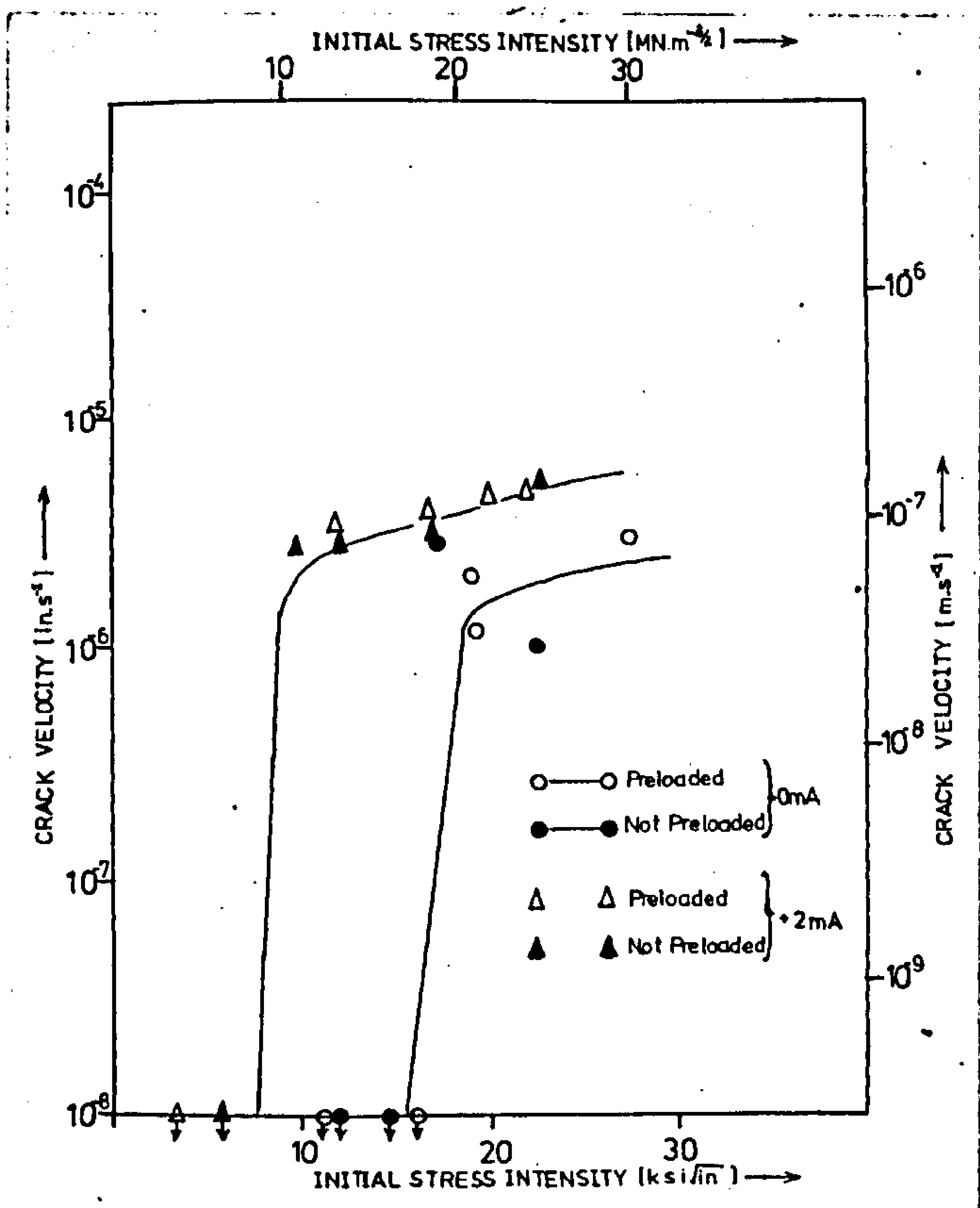

Fig. 3.52 The influence of preloading for 72hr in the absence of the corrosive environment on the threshold stress intensities for cracking of maraging steel under freely corroding conditions and with applied anodic and cathodic polarisation in a 3.5 wt % NaCl solution of initial pH 2.0.

TABLE 3.13

The influence of crosshead speed in the average crack velocity of S.E.N tensile specimens tested under freely corroding conditions in 3.5 wt % NaCl of initial pH 2.0.

CROSSHEAD SPEED		CRACK INITIATION STRESS INTENSITY		INITIATION TIME	AVERAGE CRACK VELOCITY	
INS^{-1}	MS^{-1}	KSI $\sqrt{IN}$	$MNm^{-3/2}$	HR	INS^{-1}	MS^{-1}
2.5×10^{-7}	6.35×10^{-9}	23.6	25.93	38	1.8×10^{-6}	4.57×10^{-8}
7.0×10^{-7}	1.78×10^{-8}	20	21.97	15	2.55×10^{-6}	6.47×10^{-8}
1.29×10^{-6}	3.28×10^{-8}	32.7	35.93	15	2.4×10^{-6}	6.1×10^{-8}

conditions. In this respect it is probable that metallurgical features within the metal matrix, which oxidise less readily, act as weak sites at which dissolution can be initiated e.g. inclusions (see section 3.2.2).

The results of tests performed in the acidified solution at the free corrosion potential and with applied anodic and cathodic polarisation are shown in Fig. 3.52.

Again, pre-loading has had a negligible effect on $K_{I\ SCC}$ data. The latter results are entirely as one might expect, since the conditions prevailing in the latter tests were conducive to easy reduction of the air formed oxide film.

Table 3.13 summarises the results of the constant crosshead speed tensile tests.

If it is assumed that the strain rate at the crack tip increases proportionally with crosshead speed then the fact that the average crack velocity remains independent of strain rate - despite an order of magnitude increase on the latter - indicates that, (over the effective range of strain rates investigated) the strain rate at the crack tip is of secondary importance in determining the kinetics of cracking of maraging steel in this environment.

3.6 The Use of the Acoustic Emission Technique to Study the Stress Corrosion Cracking Mechanism

The detection of stress waves emitted from growing stress corrosion cracks may provide further insight into the mechanisms operating during the stress corrosion cracking of different materials in different environments. In a recent paper,[113] the acoustic emission technique was used in association with the D.C. electrical resistance technique for crack growth monitoring to distinguish hydrogen embrittlement from active path corrosion as the cracking mechanism operative in the stress corrosion cracking of high strength and stainless steels in aqueous saline environments. The underlying assumption that must be made in using the acoustic emission technique as a mechnistic tool is that in active path corrosion, where cracks are assumed to propagate by anodic dissolution along preferential active paths, significant acoustic emission can not be expected to occur in contrast to hydrogen induced cracking where high amplitude acoustic signals have been detected accompanying crack propagation.

In view of the apparent success of the above workers in being able to distinguish between the two possible mechanisms operating in the stress corrosion cracking of high strength steels it was decided to carry out tests of a similar nature on maraging steel specimens in 3.5 wt % NaCl in order to complement the other results of the current work aimed at determining the cracking mechanism(s) operating in the SCC of maraging steel in aqueous environments.

Single edge notch fatigue precracked tensile specimens were tested in as made up 3.5 wt % sodium chloride solutions under the following conditions of applied polarisation:-

i) $2 mAcm^{-2}$ cathodic polarisation. Initial stress intensity 20 KSI $\sqrt{IN}$.

ii) Freely corroding. Initial stress intensity 25 KSI $\sqrt{IN}$

and iii) $2mAcm^{-2}$ anodic polarisation.
Initial stress intensity 20 KSI$\sqrt{IN}$.

The results were plotted in terms of cumulative acoustic emission counts and potential drop across the growing crack as a function of time (see Figs. 3.53 → 3.57).

It was apparent from the outset that significant background noise would be generated as a consequence of hydrogen bubble collapse at the specimen surface, (in the case of the cathodically polarised specimens), or on the platinum counter electrode (in the case of the anodically polarised specimens).

At the time, this background noise was unavoidable and it was decided to continue the investigations in the belief that any hydrogen embrittlement cracking that might occur would be readily detectable as an increase in the cumulative count rate above that due to hydrogen bubble collapse.

As can be seen from Fig. 3.53 there appears to be some correlation between the onset of cracking and an increase in the acoustic emission count rate for the cathodically polarised ($2mAcm^{-2}$) specimen. However, a small but noticeable time lag was observed between initiation of cracking - as indicated by an increase in p.d. across the crack - and the acoustic emission count rate increase. Fig. 3.54 shows the results of a similar test with applied cathodic polarisation but at reduced applied current density of $1\ mAcm^{-2}$ and again a time lag was apparent.

Turning now to the freely corroded specimen (Fig. 3.55) it is apparent that the acoustic emission

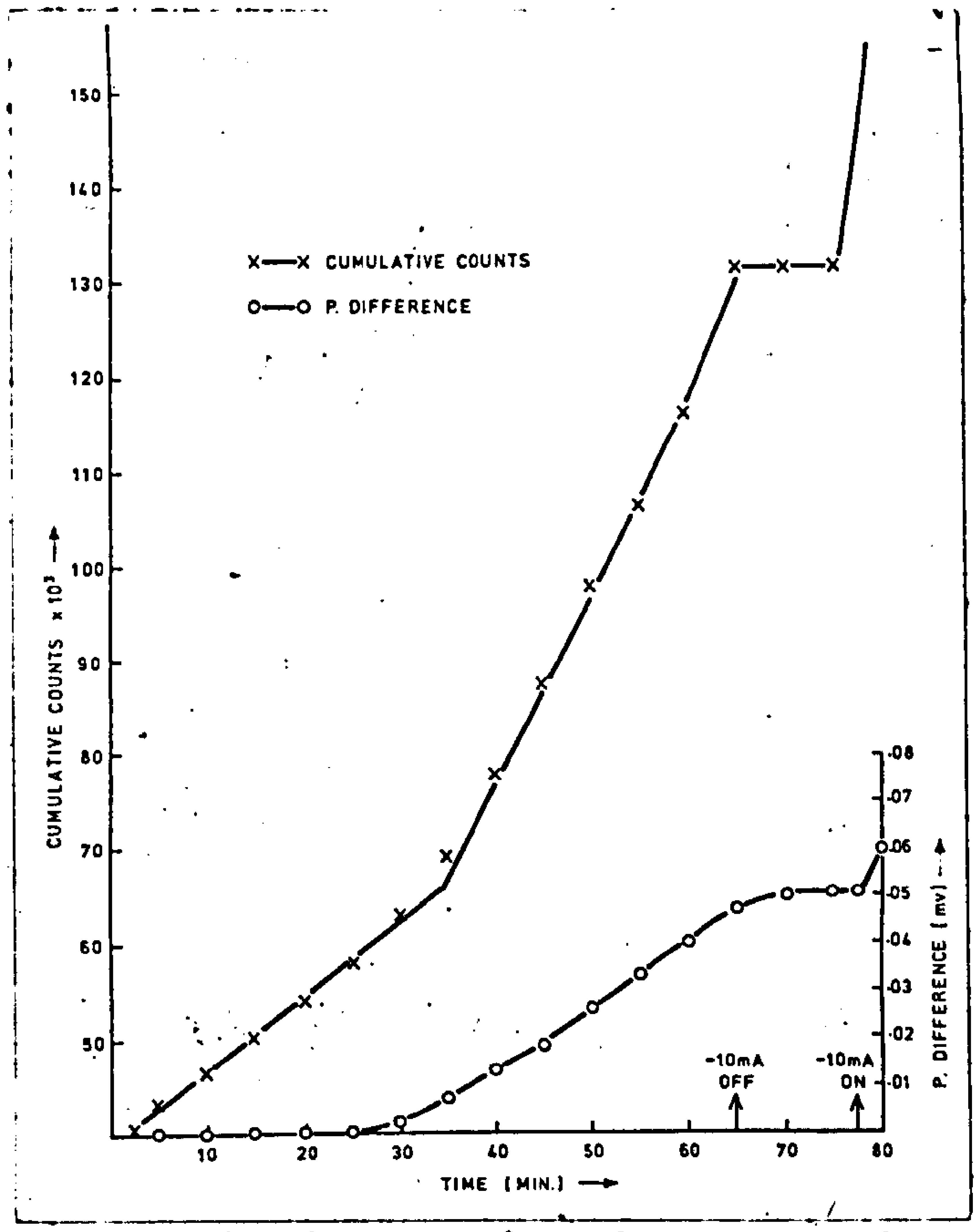

Fig. 3.53 Acoustic emissions and p.d across the crack as a function of time for SEN fatigue precracked tensile specimens of maraging steel exposed to a 3.5 wt % NaCl solution (initial pH 6.0) with an applied cathodic current density of 2mA cm^{-2}.

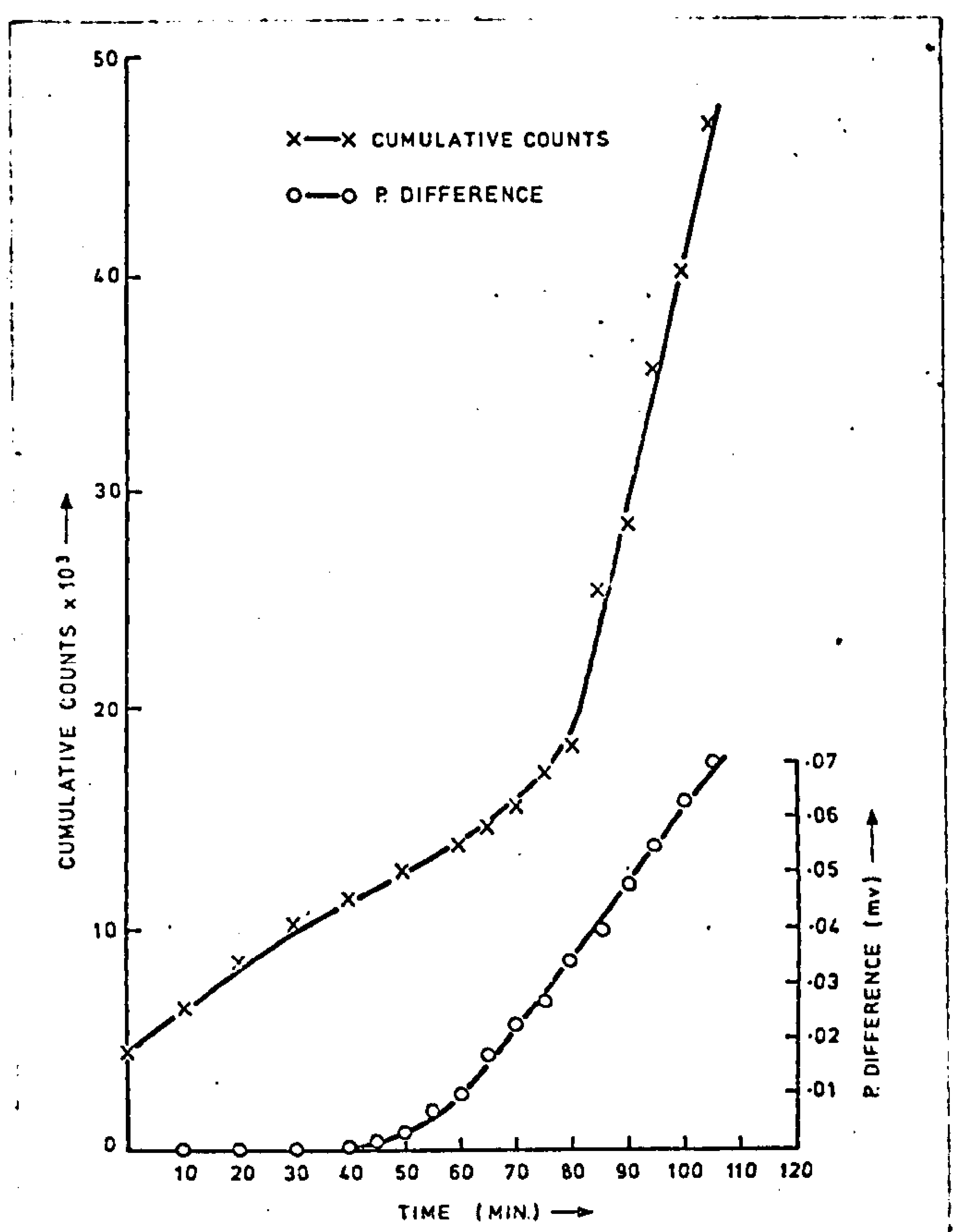

Fig. 3.54 Acoustic emissions and p.d across the crack as a function of time for SEN fatigue precracked tensile specimens of maraging steel exposed to a 3.5 wt % NaCl solution (initial pH 6.0) with an applied cathodic current density of 1mA cm^{-2}.

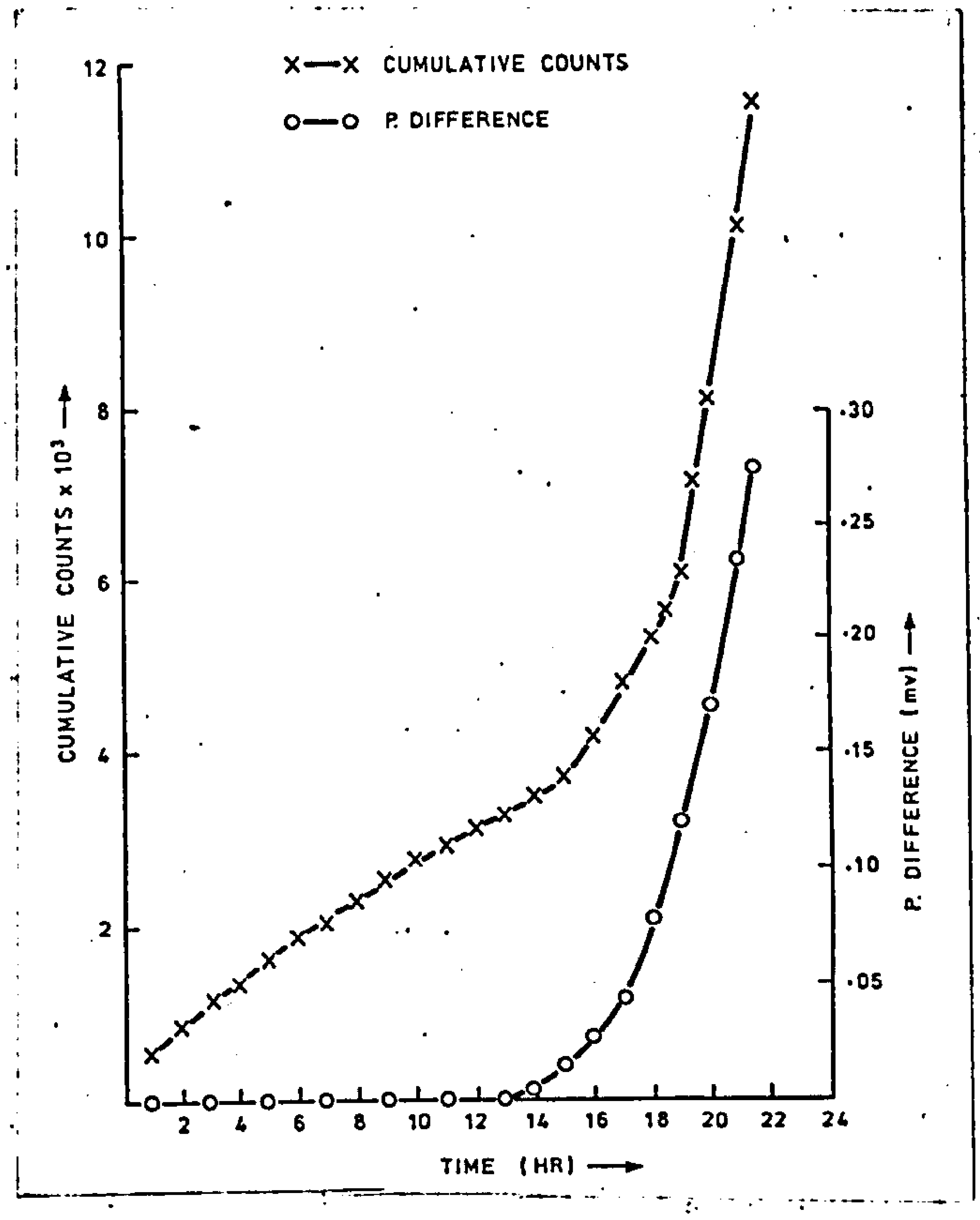

Fig. 3.55 Acoustic emissions and p.d across the crack as a function of time for SEN fatigue precracked tensile specimens exposed to a 3.5 wt % NaCl solution (initial pH 6.0) under freely corroding conditions.

count rate remained virtually constant at the background count rate to between the 15th and 16th hour on test after which a two fold increase in the count rate was observed continuing at a steady rate for the next 3-4 hours. A further increase in the count rate was then observed which remained fairly constant until the specimen was unloaded after a total of 21.5 hours on test. The crack growth monitor indicated detectable crack growth after 14 hours on test so that once again a time lag was observed between an increase in the acoustic emission count rate and crack initiation.

The reasons for the time lag behaviour are purely conjectural, at the present time, especially when the relatively high background count rate due to hydrogen bubble collapse and its tendency to vary with time greatly confuses matters. However, it is conceivable that hydrogen embrittlement cracking may occur, at least in the initial stages of crack growth, in a continuous fashion which does not necessarily entail intermittent release of short bursts of energy due to a quasi-cleavage fracture mode. The above is confirmed, to some extent, by the observation that fractographs of broken hydrogen embrittlement specimens show smooth intergranular facets looking remarkably similar to those observed on specimens subjected to anodic polarisation the latter showing no evidence of cleavage type fracture having occurred in the earlier stages of crack propagation.

Fig. 3.56 shows the results for the anodically polarised specimen and it is apparent that the acoustic emission count rate decreased with time despite the fact that the crack monitoring technique indicated continuous crack growth from an early stage. The diminution in the acoustic emission count rate can be attributed to the decreasing efficiency for the hydrogen evolution reaction as the solution within the cell became increasingly alkaline.

In an attempt to produce a constant background count rate due to hydrogen evolving at the platinum in the latter case it was decided to replenish the solution within the corrosion cell continuously by running fresh solution through the cell under gravity from an external reservoir (flow rate approximately 500cc/hr). The results of this test are shown in Fig. 3.57 and it is evident that replenishment of test solution did even out the background count rate quite considerably. None

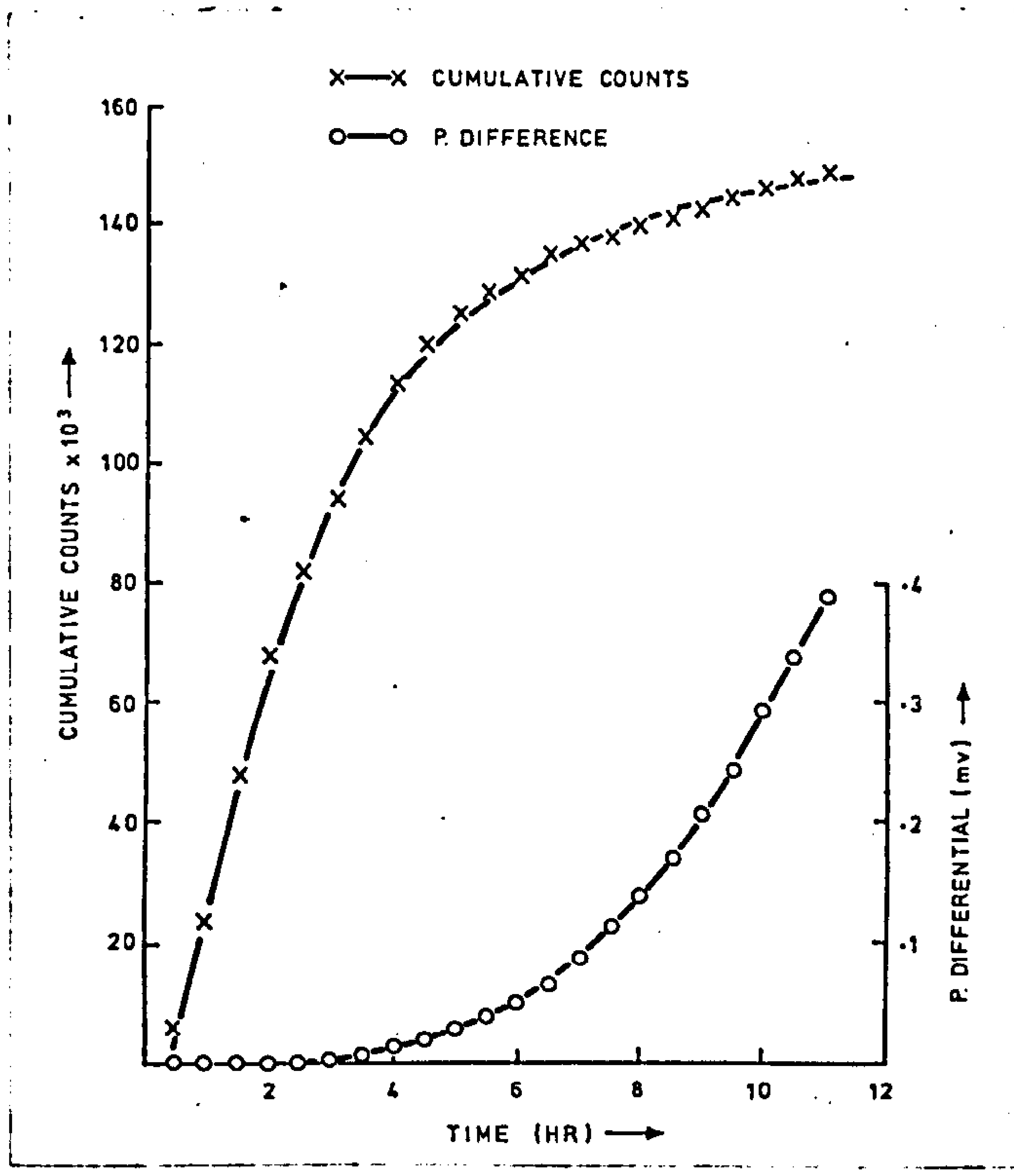

Fig. 3.56 Acoustic emissions and p.d across the crack as a function of time for SEN fatigue precracked tensile specimens exposed to a 3.5 wt % NaCl solution (initial pH 6.0) with an applied anodic current density of 2mA cm^{-2}.

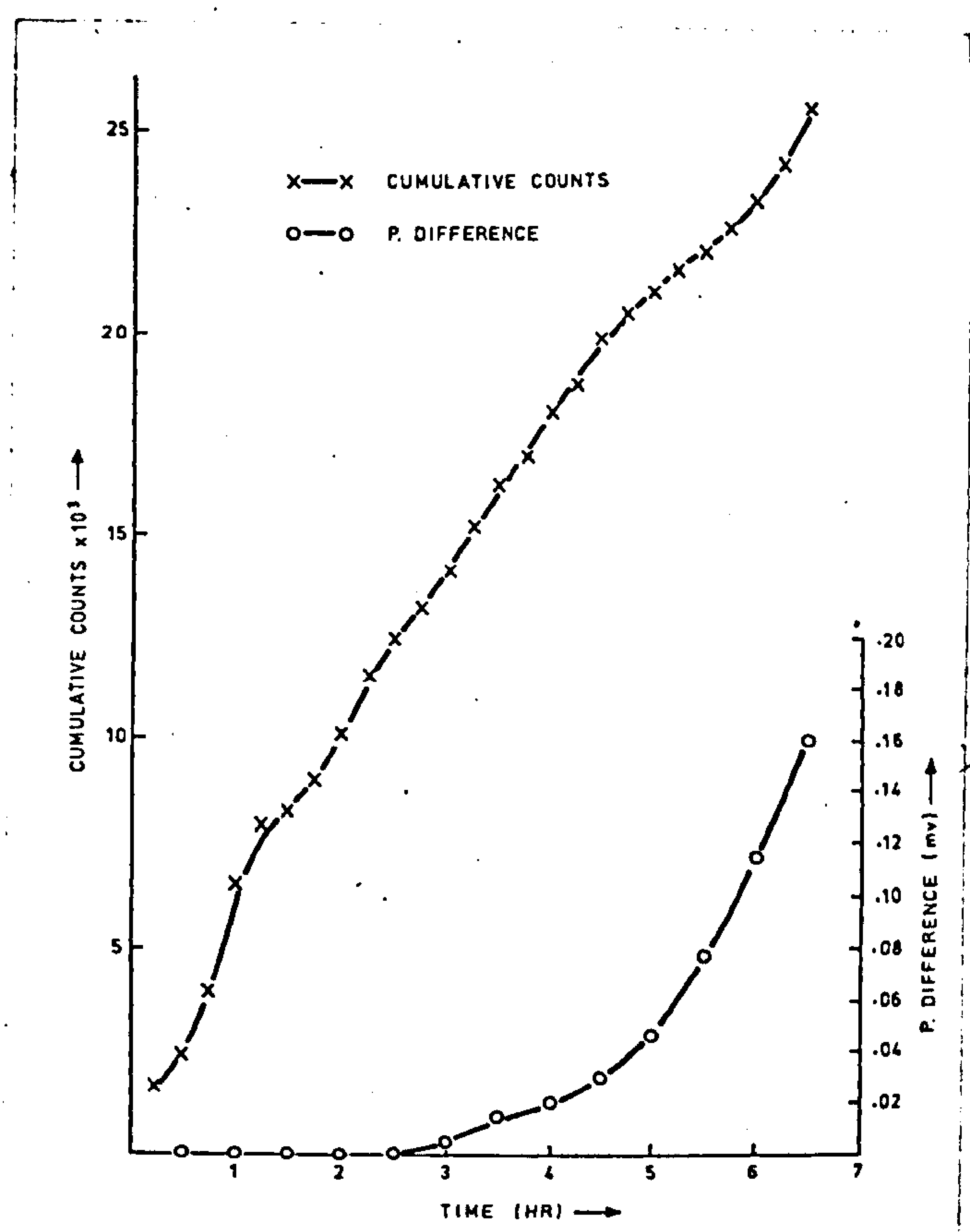

Fig. 3.57 Acoustic emissions and p.d across the crack as a function of time for SEN fatigue precracked tensile specimens exposed to a 3.5 wt . NaCl solution (initial pH 6.0) with an applied anodic current density of 2mA cm^{-2}. Solution continuously replenished.

the less, there is room for further improvement in this direction.

If we consider the background count rate due to hydrogen bubble collapse at the platinum as being represented by the first 2hr of test where no crack growth was detected, we can see that, apart from a short interval towards the end of the run when a barely noticeable increase in count rate was detected, at no time during the test did the count rate exceed the background value despite evidence of crack growth indicated by the increasing potential drop across the crack. These observations would appear to provide evidence of a confirmatory nature indicating that crack growth is due to an active path dissolution mechanism when 18Ni (300) grade maraging steel is anodically polarised with respect to its free corrosion potential.

The main conclusions from this work are as follows:

1) Acoustic emissions were detected which appeared to correlate with crack propagation both at the free corrosion potential and under cathodic polarisation conditions. Based on the assumptions outlined above these results could be taken to be evidence that maraging steels crack by a hydrogen embrittlement mechanism at the free corrosion potential in artificial sea water.

2) Acoustic emissions, over and above those due to background noise, could not be detected for anodically polarised specimens. This implies that the mechanism of cracking at potentials noble to the free corrosion potential is one of active path dissolution.

3) Time lags were observed between the onset of cracking and detectable increases in the emission rate suggesting that in the intial stages of hydrogen embrittlement cracking, crack growth may occur in a continuous and comparatively quiet manner.

4) Background noise due to hydrogen bubble collapse tended to confuse the interpretation of the results.

Although it appears to be impossible to eliminate this background noise completely in the case of cathodically polarised specimens, the following refinements to the technique may provide for either a total elimination of background noise due to hydrogen evolution at the platinum counter electrode, or at the very least for the attainment of a more uniform rate of hydrogen evolution during anodic polarisation of the specimens.

a) Deposition of a Pt black layer onto the surface of the platinum counter electrode. The microscopically rough surface so produced would provide more numerous sites for hydrogen bubble nucleation and so produce uniformity in bubble size with a consequent smoothing of the hydrogen evolution reaction.

The above refinement must be used in association with continuous replenishment of the solution, <u>at a slow rate</u>, within the corrosion cell since, as we have seen, uniformity of solution pH is another pre-requisite for a uniform rate of hydrogen evolution.

In addition to improvement a); by isolating the platinum counter electrode from the corrosion cell it maybe possible to eliminate the background noise altogether. Thus, if a second cell is constructed to contain the platinum electrode and is connected via a sintered glass disc to the corrosion cell; the sintered glass disc whilst providing ionic contact between the solution in the two compartments could also provide some barrier to the passage of stress waves through the solution from the platinium counter electrode to the specimen surface.

3.7 The Influence of Gaseous and Electrochemical Hydrogen Precharging on the Cracking Susceptibility of Maraging Steel

Constant crosshead speed tensile tests were performed on Hounsfield No.11 tensile specimens (Fig. 2.2) charged with hydrogen

i) from the gaseous phase and tested in situ

and ii) electrochemically pre-charged from a poisoned and acidified chloride solution and subsequently pulled to failure in air.

The main aim of these experiments was to see if there was any significant difference in the cracking modes of specimens subjected to normal stress corrosion cracking conditions and specimens charged with hydrogen either from the gaseous phase or electrolytically; since it has been reported[28] that hydrogen embrittlement failures in maraging steel showed a mixed mode of cracking but with transgranular cracks predominanting, whereas stress corrosion failures were predominantly intergranular in nature.

Fig. 3.58 shows a plot of specimen

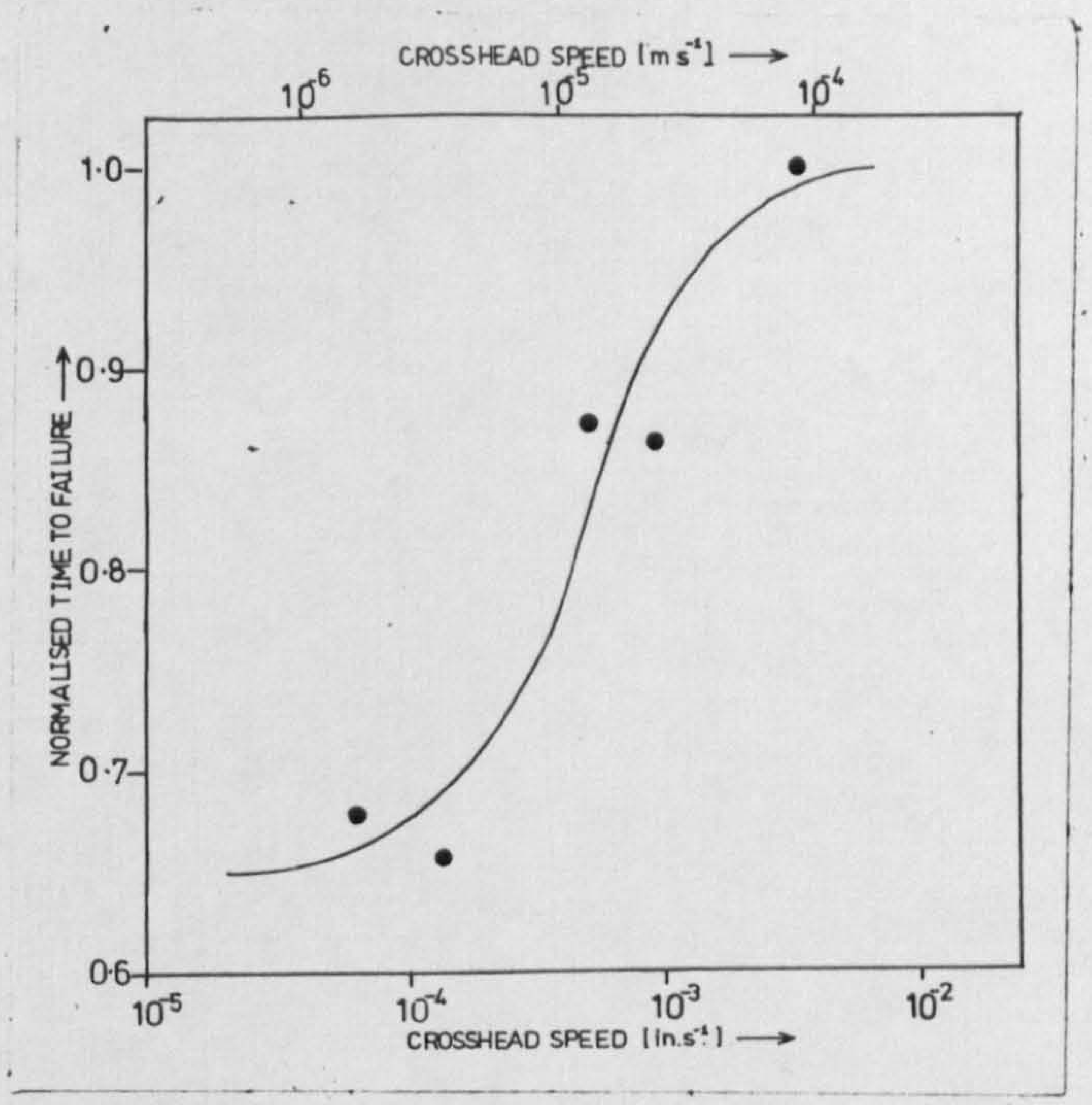

Fig. 3.58 The influence of crosshead speed on the failure times of smooth tensile specimens of maraging steel (Aust. 1hr 950°C; Aged 3hr 530°C) tested in a 760 TORR purified gaseous hydrogen atmosphere. Failure times in gaseous hydrogen were normalised on the corresponding failure times in air.

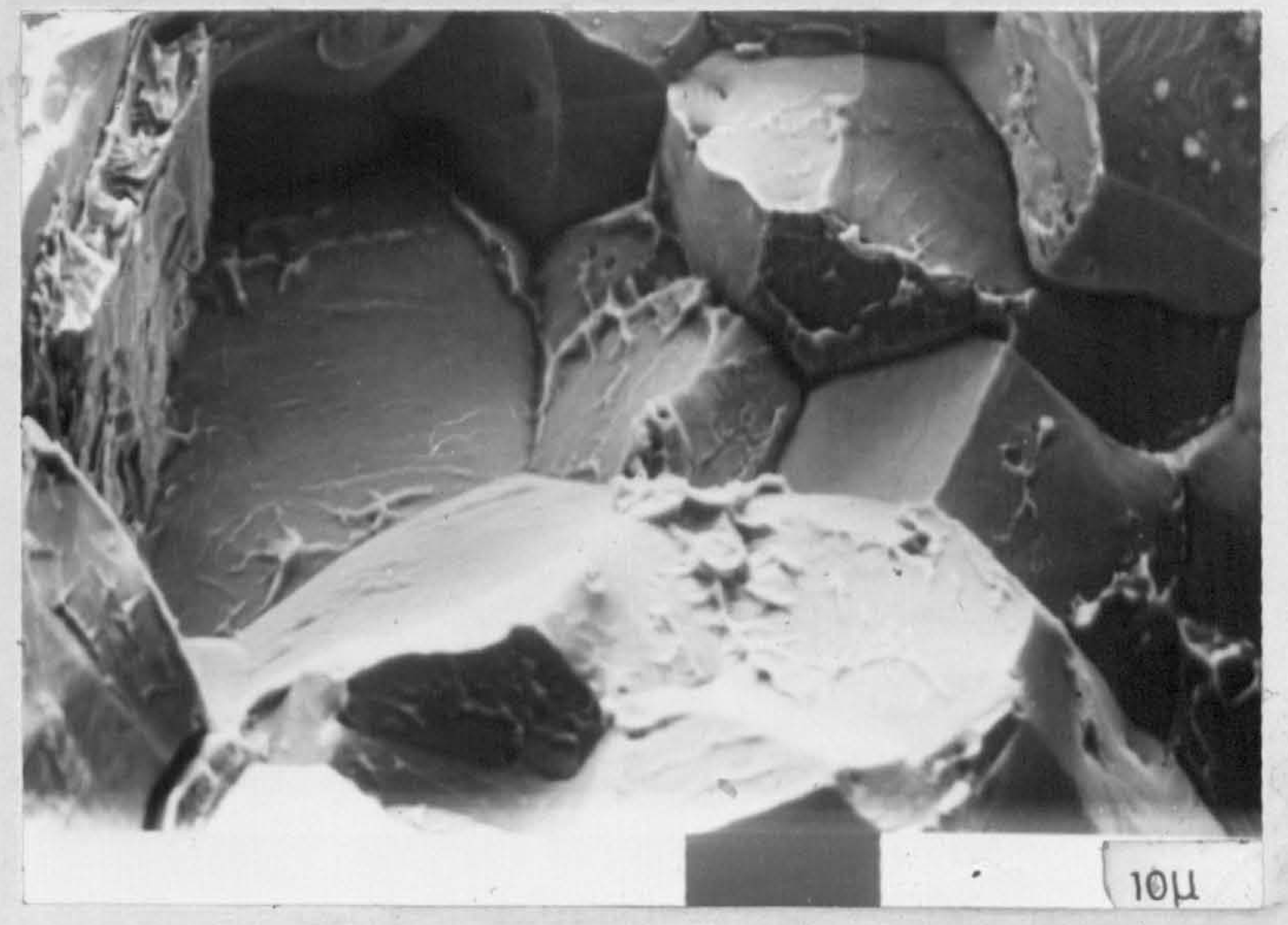

Fig. 3.59 Scanning electron micrograph of the fracture surface of a maraging steel tensile specimen strained to failure in 760 TORR gaseous hydrogen showing typical intergranular facets.

failure times (normalised on air failure times) as a function of crosshead speed for specimens strained in 760 TORR of purified gaseous hydrogen. It is clear that the material is embrittled by gaseous hydrogen at crosshead speeds of $< 10^{-3}$ INS^{-1}. Examination of fracture surfaces revealed small thumbnail areas of predominantly intergranular cracking of which Fig. 3.59 is typical. Evidence of ductile tearing on the intergranular facets is presumably a consequence of cracking initiating at loads close to those representative of the ultimate tensile strength of the material.

Specimens electrolytically charged for various times in the poisoned acidified chloride solution (3.5 wt % NaCI containing 5 gm/l of sodium arsenate acidified to pH 2.0) and pulled to failure in air all exhibited an annulus of material that had separated in an intergranular fashion along the prior austenite grain boundaries. Table 3.14 lists results of the latter experiments. The figures in the final column are values of diffusivity calculated on the assumption that at the interface between the intergranularly cracked material and the central ductile zone the hydrogen concentration had fallen to essentially zero and therefore for non steady state diffusion in a semi-infinite medium

$$\frac{x}{\sqrt{Dt}} = 6.0 \quad 140$$

where x = maximum diffusional distance i.e. the depth of t he intergranular annulus.

D = diffusion coefficient

t = time

TABLE 3.14

The results of constant crosshead speed tensile tests performed on specimens electrolytically charged with hydrogen at a cathodic current density of $10mA/cm^2$ in 3.5 wt % NaCl containing 5gm/l sodium arsenate adjusted to intial pH 2.0.

Prepolarising Time (secs)	Crosshead Speed INS^{-1}	MS^{-1}	Depth of Annulus (Cm)	$D(Cm^2s^{-1})$
300	$2.7x10^{-5}$	$6.86x10^{-7}$	negligible	-
900	$2.7x10^{-5}$	$6.86x10^{-7}$	$1.336x10^{-2}$	$5.44x10^{-9}$
1800	$2.7x10^{-5}$	$6.86x10^{-7}$	$1.455x10^{-2}$	$3.22x10^{-9}$
5400	$2.7x10^{-5}$	$6.86x10^{-7}$	$2.79x10^{-2}$	$4.0x10^{-9}$
5400	$1.3x10^{-4}$	$3.3x10^{-6}$	$2.22x10^{-2}$	$2.52x10^{-9}$
5400	$1.3x10^{-3}$	$3.3x10^{-5}$	$2.62x10^{-2}$	$3.52x10^{-9}$

The above diffusivities, calculated on the basis of concentration independent diffusivity are in fair agreement with those diffusivites calculated from hydrogen permeation data despite the fact that the latter work suggested the possibility of a concentration dependence of diffusivity.

The observation of a strain rate dependency of hydrogen embrittlement cracking in gaseous hydrogen gives some indication that hydrogen induced cracking in maraging steel is dependent upon the rate of bulk (or surface) diffusion of hydrogen to the material in the vicinity of the crack tip and that it is not simply due to direct adsorption of hydrogen at the crack tip surface. The results of a single precracked specimen test electrolytically charged with hydrogen from a 3.5 wt % NaCl solution are of interest in this context.

In this test crack growth was monitored with time by using the D.C. electrical resistance technique. The current density was controlled and varied galvanostatically. Fig. 3.60 shows part of the effective crack growth versus time curve for this test. It is evident that a change in the charging current from 5mA to freely corroding conditions caused a diminution of crack velocity to essentially zero within 60 seconds. Now the change in the mean crack velocity is limited only by the kinetics of hydrogen transport within the material at the crack tip. This is important as to the question of how far into the steel the hydrogen can be reasonably expected to penetrate in order to effect cracking. If, as is suggested by some workers, the hydrogen must diffuse to the region of maximum triaxiality ahead of

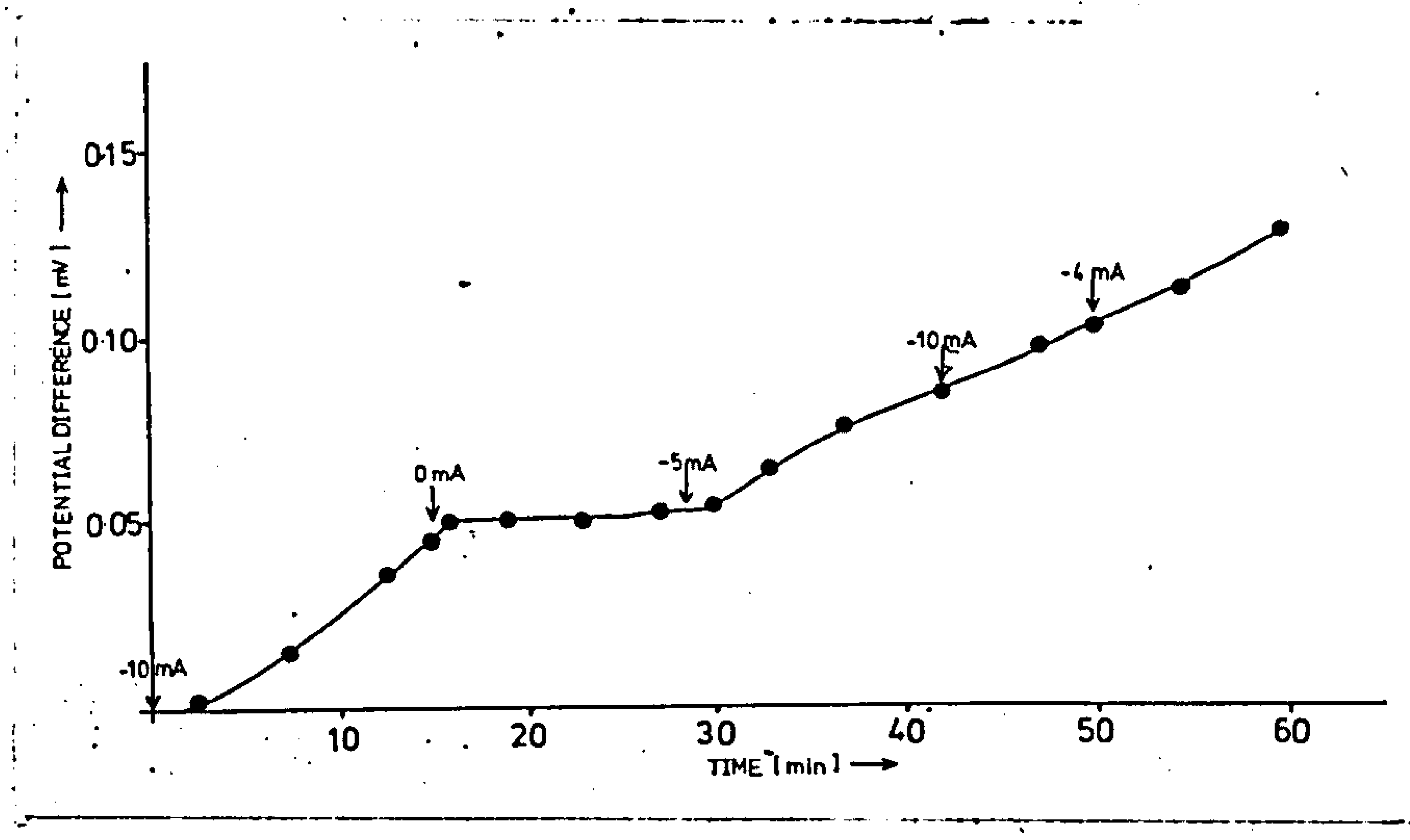

Fig. 3.60 P.d across the crack as a function of time for a SEN fatigue precracked tensile specimen of maraging steel subjected to alternate periods of cathodic polarisation and free corrosion in a 3.5 wt % NaCl solution of initial pH 2.0.

the growing crack then the response time of a moving crack to a sudden change in hydrogen concentration must be at least as long as the time required to diffuse through the plastic zone formed at the crack tip.

The plastic zone size is given by continuum mechanics as[141]

$$r_y = \frac{K^2}{\pi \sigma_y^2}$$

where K = stress intensity

σy = yield stress of the material.

For maraging steel in the heat treated condition employed here, σy = 280 KSI and at the stress intensity employed in these tests of 20 KSI $\sqrt{\text{IN}}$ the latter equation gives a value of 4.1×10^{-3} cm for the length of the plastic zone. For an effective diffusivity of hydrogen in maraging steel of between 10^{-9} and 10^{-8} cm^2 s^{-1}, the minimum response time of the crack to a sudden change of hydrogen concentration lies between 47 and 470 secs. This compares with the observed response time of less than 60 secs and implies that the depth to which hydrogen must diffuse in order to effect cracking can be anything from a maximum distance corresponding to the length of the plastic zone to a minimum distance of about an order of magnitude less than the radius of the plastic zone. This result whilst not being inconsistent with the decohesion theory of hydrogen embrittlement of Oriani equally does not unequivocally negate the possibility of hydrogen diffusion to the region of maximum triaxiality at the crack tip.

3.8 Brief Summary

1) Increasing austenitising temperatures above 760°C have been shown to be increasingly detrimental to the resistance to environmental cracking of smooth maraging steel specimens. However, crack propagation rates appear to be less influenced by austenitising temperature than do crack initiation periods.

The susceptibility to cracking of maraging steel has been shown to be a maximum at ageing temperatures of 480-530°C. The latter heat treatments were associated with an intergranular cracking mode. Less susceptible heat treatments were associated with an increasing tendency towards transgranular fracture. Maximum susceptibility to cracking was observed to correspond almost exactly with maximum strength associated with the ageing heat treatments.

2) In neutral and alkaline solutions of NaCl a range of potentials was observed over which

cathodic protection could be afforded to smooth tensile specimens of maraging steel. In acid environments however, cathodic protection could not be afforded to maraging steel. Increasing pH and decreasing chloride ion concentrations were observed to extend the range of potentials over which cathodic protection was observed.

Precracked specimens were observed to crack even over the range of potentials observed to provide cathodic protection of smooth tensile specimens.

3) Freely corroding smooth tensile specimens of maraging steel tested at constant crosshead speed were observed to crack only in solutions of pH < 3.5. Fatigue precracked specimens, however, were observed to crack readily in solutions of all pH's < 12.0.

Cracking could be induced in freely corroding smooth tensile specimens of maraging steel when tested in the constant strain mode at stresses above the yield stress or at lower stresses if the orientation of the specimen with respect to the original rolling direction was changed. In this respect maximum susceptibility to cracking was observed when the original rolling direction was perpendicular to the tensile axis. These effects are probably related to the morphology of titanium rich inclusions (probably TiC(N)) in the steel. It was demonstrated that sites for the initiation of corrosive attack were associated with such inclusions.

The importance of the oxygen reduction reaction in the stress corrosion cracking of freely corroded maraging steel specimens in neutral and alkaline environments has been demonstrated by tests in solutions containing H_2O_2

in which cracking could be induced even in solutions of initial pH 11.0.

4) The relationship between the failure times of smooth tensile specimens and the galvanostatically applied current density in a 3.5 wt % NaCl solution adjusted to an initial pH of 2.0 was observed to pass through a maximum at small cathodic current densities implying that under freely corroding conditions in this solution crack propagation is dissolution controlled.

5) The results of experiments carried out on smooth tensile specimens subjected to galvanostatic anodic and cathodic polarisation in solutions containing compounds which were added to influence the hydrogen evolution reaction and/or the dissolution reaction suggest that environmental cracking of the maraging steels occurs by two different mechanisms (HEC and APC or strain generated dissolution) according as to whether cathodic or anodic polarisation is applied to the steel.

6) Hydrogen permeation experiments on maraging steel membranes cathodically polarised in 3.5 wt % NaCl solutions permitted values of hydrogen diffusivities in the steel to be calculated. Some evidence for concentration dependent diffusivity was noted. Typical diffusivities were calculated to be between 10^{-9} to 10^{-8} $cm^2\ s^{-1}$ which are some four orders of magnitude greater than the diffusivity of hydrogen in pure iron. These large differences were related to the large number of trapping sites for dissolved hydrogen that exist in maraging steels.

Permeation transients were also observed for membranes anodically polarised on the charging side which would appear to indicate that hydrogen can diffuse into the steel ahead of the dissolving metal solution interface thereby implying that hydrogen could be the cause of cracking of specimens subjected to anodic polarisation.

However, the bulk of the evidence presented in this work points to the fact that these so called, permeation transients were almost certainly not due to hydrogen diffusing through the steel but were due to perforation of the membranes and rises in the current in the potentiostatic circuit due to the dissolution reaction, $Fe \rightarrow Fe^{2+} + 2\varepsilon$, occurring at the perforations.

7) Increases in acoustic emission count rate were observed for cathodically polarised and freely corroding precracked specimens of maraging steel stressed in a 3.5 wt % NaCl solution of initial pH 6.0 which may indicate that 18Ni maraging steels crack by a hydrogen embrittlement mechanism when tested at its free corrosion potential in artificial sea water.

Acoustic emission count rate increases were not observed, however, for anodically polarised specimens. This may be indicative of an active path or strain generated active path dissolution mechanism operating at potentials noble the free corrosion potential. Further work is needed, however, to clarify the situation by tests with improved experimental techniques to eliminate or reduce background counts due to hydrogen bubble collapse.

8) Hydrogen embrittlement cracking of the maraging steel investigated in the current work was readily induced by exposure to 760mm of purified hydrogen

gas or by electrochemical precharging. In the particular heat treatment employed (AUST 1hr 950°C; AGED 3hr 530°C) cracking was along the prior austenite grain boundaries. Fully ductile mechanical properties could be restored by removal of the absorbed hydrogen in vacuo at 150°C for several hours.

Experiments on fatigue precracked specimens subjected to intermittent cathodic polarisation in 3.5 wt % NaCl solutions indicate that the maximum possible distance over which hydrogen can diffuse in order to influence crack growth kinetics of non-precharged material is of the order of 10^{-2} to 10^{-3} cm.

4 Discussion

Most of the results have already been discussed in detail under the appropriate sub-headings in the Results section. Consequently it is proposed, here, only to bring together the main points that have emerged from this work and attempt to explain the general sequence of events by which initially smooth maraging steel members fail by stress corrosion cracking - paying particular attention to the mechanism(s) of crack propagation under various conditions of applied potential.

In general, the sequence of events which leads to the failure of a high strength steel component by stress corrosion cracking in a moderately aggressive environment is as follows:-

i) Initiation or incubation

The protective oxide film (if any) breaks down locally and corrosion pits or fissures are formed.

ii) Propagation

A stress corrosion crack grows from the pit or fissure and

iii) Fast fracture

When the crack has grown sufficiently long and if the stress has not been able to relax, the unbroken ligament separates by fast fracture. In the maraging steels the final fast fracture appears to be characteristic of simple overload ductile failure (i.e. dimpling) and will not be discussed further.

4.1 Crack Initiation in Maraging Steels

The ease with which the protective air formed oxide film on maraging steels is broken down has been shown to be principally dependent upon environmental factors and upon the degree and nature of polarisation applied to the specimen surface. In general, high concentrations of chloride ion (cf. section 3.2.2.), acidic environments (cf. sections 3.2.1, 3.2.3) and a shift in the potential of the specimen in the noble direction (cf. section 3.2.1, 3.2.2) assist in the removal of the air formed oxide film.

Under freely corroding conditions in the less aggressive environments (i.e. neutral or alkaline low chloride aqueous solutions) the orientation and electrochemical characteristics of certain metallurgical features intersecting the specimen surface appear to be of some importance in undermining the air formed oxide film. For example, TiC(N) inclusions exposed at the surface appear to provide weak sites in the oxide film at which corrosion pits are formed (cf. section 3.4). However, corrosion pits of the necessary shape and/or depth to initiate crack propagation are only produced when these inclusions are suitably orientated with respect to the tensile axis (see 'Crack propagation in maraging steels' - below).

4.2 Crack Propagation in Maraging Steels (APC v HEM)

At potentials more active than about -400 mV SCE in acid environments (pH 2.0) or -800 mV SCE in alkaline environments (pH 11.0) there seems to be little doubt that at least in the initial stages of cracking initiated from a smooth surface hydrogen embrittlement is the cause of cracking in the maraging steels. At more noble potentials, however, the cracking mechanism is not so clearly defined.

At the free corrosion potential in neutral or alkaline environments the formation of corrosion pits or fissures appears to be necessary though not sufficient condition for crack propagation. Once such corrosion pits have developed whether or not stress corrosion cracking is subsequently observed appears to depend upon pit (or fissure) depth and/or acuity. For example, the shallow pits and fissures formed at the sites of TiC(N) inclusions when the latter were orientated parallel to the tensile axis and the round bottom pits formed by polarising at potentials noble to the free corrosion potential in dilute aqueous chloride solutions appeared to be of insufficient depth or sharpness to initiate cracking when these specimens were subsequently exposed to neutral or alkaline 3.5 wt % NaCl at the free corrosion potential. However, cracking was observed in tests on fatigue precracked specimens under identical test conditions. What, then, is the significance of pit or fissure profiles on the propensity to stress corrosion cracking?

There would appear to be two ways in which discontinuities can influence the cracking propensity. The first is associated with the zone of plastically deformed material producedat the tip of the discontinuity by an applied stress, which facilitates the dissolution reaction at that location.[136] A high anodic current density is sustained at the crack tip by the relatively large cathodic area over the remainder of the specimen surfaces and crack sides and by removal of the corrosion products tending to stifle the reactions at the crack tip by the ingress of fresh electrolyte as a consequence of yawning. The constant total strain tests on smooth tensile specimens described in section 3.4 may be of some significance in this respect. It may be recalled that specimens prepared in the conventional manner (i.e. such that the original rolling direction was parallel to the tensile axis of the specimens) were observed to fail only when loaded to stresses in excess of the yield stress (see fig. 3.47). This maybe indicative of the fact that in circumstances where crack initiation and propagation is difficult the plastically deformed material produced by yielding can facilitate dissolution and thereby assist in the formation and propagation of stress corrosion cracks.

The second is associated with the fact that the discontinuity provides the necessary confined space within which, because of oxygen starvation and hydrolysis of ferrous ion and the restricted access of bulk solution to the tip of the crack because of the build up of corrosion product along the sides and mouth of the crack, low pH's and/or shifts of potential in the active direction can occur such that hydrogen discharge becomes thermodynamically feasible and cracking can be attributed to hydrogen embrittlement. Much of the work in support of the latter theory has involved either the demonstration that the pH and potential at the tip of a growing stress corrosion crack is conducive to the discharge of hydrogen or that under freely corroding conditions and even at potentials noble to the latter hydrogen can permeate through thin membranes of the steel.

There have been several reported successful measurements of the pH and potential existing in the solution at the tips of discontinuities however, the validity of such measurements must in many cases be questioned since apart from technical difficulties associated with the use of micro-electrodes for accurate pH and potential measurements and which in many cases appear to have been overlooked (e.g. contamination of electrode surfaces by adsorbed corrosion products and dehydration of the pH sensitive membrane - where glass electrodes are used - producing asymmetry potentials), it seems unlikely that such measurements, made as they are, on the outer surfaces of growing cracks can be truely representative of those conditions actually existing within the cracks. Notwithstanding these reservations it can not be disputed that electrochemical changes within pits, crevices and cracks are possible as a consequence of, for example, hydrolysis of ferrous or ferric ions or oxygen depletion in the solution confined within the discontinuity and indeed it is difficult to explain the observed differences in cracking behaviour of smooth and precracked specimens in many instances unless such electrochemical changes are deemed to have taken place. However, even if we accept what little evidence there is available on the conditions existing close to the tips of growing cracks it can not be stated that crack propagation is unequivocally a consequence of hydrogen embrittlement since whilst the pH close to the crack tip has been shown to be acidic and the potential amenable to hydrogen discharge the latter has not been shown to be sufficiently active to preclude dissolution of the metal. Consequently, enhanced dissolution of the metal in the vicinity of the crack tip will occur and it may then be argued that cracking is just as likely to be a consequence of enhanced dissolution as of hydrogen embrittlement.

The hydrogen permeation technique to distinguish between active path corrosion and hydrogen embrittlement mechanisms of cracking also appears to have its limitations, as has been demonstrated in the present work. It seems highly probable that the many reports of the observation of hydrogen permeating through thin membranes of high strength steels when subjected to anodic polarisation may simply be a consequence of perforation of the membranes as explained in section 3.3.

Having rejected the apparently more direct and hitherto widely accepted methods used to determine the cracking mechanisms in the high strength steels we are left only with indirect methods of tackling the problem. For example, we know that if cracking is a consequence of hydrogen embrittlement then the introduction of a species into the environment which facilitates the ingress of hydrogen into the metal will be expected to enhance cracking whilst species that facilitate the discharge of hydrogen in the molecular form will retard cracking. The results reported in section 3.2.6, on the influence of sodium arsenate, thiourea and chloroplatinic acid additions on the failure times in smooth tensile tests seems to point to the fact that stress corrosion by anodic dissolution and hydrogen embrittlement in the maraging class of high strength steels can be characterised as two distinctive mechanisms of failure depending upon the sign of the current density applied to the material. The results of a preliminary study on the effect of applied current density on the acoustic stress waves emitted from growing cracks in maraging steel specimens (cf. section 3.6) tends to confirm this observation if the basic assumption is correct that cracking as a consequence of dissolution processes is 'quiet' whereas hydrogen embrittlement cracking is noisy. Stress wave emissions were also detected when the material was caused to crack under freely corroding conditions which is indicative of a hydrogen embrittlement cracking mode, but the fact that noticeable time lags were observed between the onset of cracking and detectable increases in the acoustic emission count rate implies that, under freely corroding conditions at least some part of the crack propagation process may be attributed to metal dissolution.

In conclusion , therefore it is proposed that the 18% Ni maraging steels suffer stress corrosion cracking by dissolution along pre-existing active paths at potentials noble to the free corrosion potential (-350mV S.C.E.) and hydrogen embrittlement cracking at potentials more active than about -400mV S.C.E. to -800mV S.C.E. depending upon the pH of the environment. In the intervening potential range including the free corrosion potential, where cracking only occurs in the presence of a discontinuity it is suggested that both dissolution and hydrogen embrittlement may contribute towards crack propagation.

5 Conclusions

For the system studied in the current work, a high strength 18Ni maraging steel in aqueous chloride environments it would appear that sufficiently active potentials promote hydrogen induced cracking whereas sufficiently noble potentials promote cracking by a dissolution controlled mechanism. The crack growth kinetics and the influence of various chemical and electrochemical parameters on crack growth processes are consistent with such a conclusion.

Over the intermediate range of potentials, however, there is some uncertainty as to which mechanism of crack growth is operative and in these circumstances it seems not unreasonable to suggest that both hydrogen induced and dissolution controlled cracking can occur in these circumstances. The kinetic requirements of a model involving such a mixed mode of cracking are that the crack growth rates by the individual processes should be of the same order in the appropriate potential range and the results presented herein appear to satisfy this requirement.

Whilst for certain metal-environment systems it may be demonstrated that a particular crack growth mechanism is operative there are other systems in which the significance of a particular cracking mechanism is not immediately obvious and there appears to be no reason why a multiple mechanism of crack growth should not then be considered. This may be the case in some of those systems (e.g. those including aluminium and titanium alloys) in which the cracking mechanism continues to be disputed. However, for a process so complex as stress corrosion cracking it is very important to consider all of the evidence at hand,

and particularly in relation to so called 'definitive experiments', before conclusions are reached concerning the mechanism of cracking operative under given conditions.

REFERENCES

1 Haynes, A.G., Fielding, J., 'Machinability' Spec. Rpt. No.94, I.S.I. London 1967, p. 103.

2 Floreen, S., Met. Rev. 13, 115, 1968.

3 International Nickel Co., 'Summary data for 18Ni maraging steels', 1965.

4 Perkas, M.D., 'Structure and Properties of High Strength Maraging Steels', Met. Sci. Heat Treatment, p.558, 1970.

5 Legendre, P., Castagne, J.L. Met. Constr. Mec. 100, 105, 1968.

6 Cheng, I., Thomas, G., Trans. A.S.M. 61, 14, 1968.

7 Reisdorf, B.G., Baker, A.J., 'The Kinetics and Mechanisms of Strengthening of Maraging Steels', A.F.M.L. Tech. Rpt. 64-390, 1965.

8 Floreen, S. and Speich, G.R., Trans. A.S.M. 57, 714, 1964.

9 Banerjee, B.R., Hauser, J.J. and Caperes, J.M., Metal Sci. Journal 2, 76, 1968.

10 Parkins, R.N., 'Stress Corrosion Spectrum', Br. Corr. Journal, Vol. 7, Jan 1972.

11 Despic, Raicheff, R.C., Bockris, J.O.M., Journal Chem. Phys. 48, 1968.

12 Sandoz, G., 'High Strength Steels - S.C.C. in high strength steels and in Ti and Al alloys'. Naval Res. Lab, Washington D.C. 1972, p.79.

13 Benjamin, W.D., Steigerwald, E.A., 'Environmentally induced delayed failures in martensitic high strength steels'. Tech. Rpt. AFML-TR-68-80, Wright Patterson Air Force Base, 1968.

14 Carter, C.S., Corrosion, 25, 423, 1969.

15 Procter, R.P.M. and Paxton, H.W., Corr. Sci. 11, 723, 1971.

16 Dautovitch, D.P., Floreen, S., 'The Stress Corrosion and Hydrogen Embrittlement Behaviour of Maraging Steels', Conference Proceedings on the S.C.C. and H.E. of iron base alloys, Firminy 1973, NACE, to be published.

17 Phelps, E.H. and Loginow., Corrosion, 16, p. 325-335, 1960.

18 Davis, R.A., Dreyer, G.A. and Gallaugher, W.C., Corrosion, 20, p. 93-103, 1964.

19 Brown, B.F., 'S.C.C. of high strength steels' from Theory of S.C.C. in alloys. NATO Scientific Committee Research Evaluation Conference, 1971.

20 Phelps, E.H., Proc. Conf. on the Fundamental Aspects of S.C.C., Houston, 1969 NACE.

21 Procter, R.P.M. and Paxton, H.W., Trans. A.S.M., 62, 989, 1969.

22 Webster, D., 'The Improvement of Mechanical Properties of AFC.77 by Austinite Grain Refinement'. Trans, A.S.M. 62, 759, 1969.

23 Parkins, R.N. and Haney, E.G., Trans. Met. Soc. of AIME, 242, 1943, 1968.

24 Castagne, Corr Trait, Prot. Fin. 18, 218, 1970.

25 Carter, C.S., Met. Trans. 1, 1551, 1970.

26 Carter, C.S., Met. Trans. 2, 1621, 1971.

27 Stavros, A.J. and Paxton, H.W., Met. Trans. 1, 3049, 1970.

28 Haigh, P.M., Ph.D Thesis, University of Newcastle upon Tyne, 1970.

29 Copen, H.R. and Van Rooyen, D., unpublished work from ref. 16.

30 Setturlund, R.B., Mat. Prot. 4, (12), 27, 1965.

31 Novak, S.R., U.S. Steel Project No. 39-018-007(20), 1968.

32 Carter, C.S., Met. Trans., 3, 548, 1972.

33 Carter, C.S., Boeing Document, D6-25275, 1970.

34 Dautovitch, D.P., unpublished work reported in ref. 16.

35 Burdekin, F.M., Stone, D.E.W., J. Stress Analysis 1, 145, 1966.

36 Dean, S.W., Copson, H.R., Corrosion, 21, 95, 1965.

37 Phelps, E.H., 'Stress corrosion behaviour of high yield strength steels', Problems, prevention and theories of corrosion. Panel Discussion No.27, 7th World Congress. Procs, Elsevier Pub. Co.

38 Phelps, E.H., Meers, R.B., Proc. 1st International Cong. Metallic Corrosion, p.319, Butterworths, 1961.

39 Bloom, F.F., Corrosion, 11, p.325-335, 1960.

40 NACE Committee T-1B Report, Matls Protection, 3, 89-96, 1963.

41 Hudgins, C.M., McGlasson, R.L., Mehdizadeh, P., Rosborough, W.M., Corrosion, 22, p. 238-251, 1966.

42 Rpt. of Tech. Practices Committee I.G. 'Field experience with the cracking of high strength steels in sour gas and oil wells', Corrosion, 8, pp 351-354, 1952

43 Schultz, A.E., and Robertson, W.D., Corrosion, 13, p. 437t-458t, 1957.

44 Smialowski, M., 'Hydrogen in steels', Pergammon, 1962.

45 Newman, J.F. and Shrier, L.L., Corr. Science 9, p. 631, 1969.

46 Fresder, J.P. and Fresder, R.S., Corrosion, 8, 342, 1958.

47 Bhatt, H.J., Phelps, E.H., Corrosion, 17, 430t, 1961.

48 Green, J.A.S. and Haney, E.G., 'A Stress Corrosion Test for Foil and Strip', presented at A.S.T.M. Conf., Atlantic City, N.J. 1966.

49 Steigerwald, E.A., Proc. ASTM, 60, 750, 1960.

50 Parkins, R.N., private communication.

51 Hanna, G.L., Troiano, A.R. and Steigerwald, E.A., Trans. A.S.M., 57, 658, 1964.

52 Johnson, H,H.J. and Willner, A.M., Applied Matls Research, 4, p. 34-40, 1965.

53 Kenyon, N., Kirk, W.W. and Van Rooyen,D., Corrosion, 27, 390, 1971.

54 Leckie, H.P. and Loginow, A.W., Corrosion, 24, 291, 1968.

55 Green, J.A.S. and Haney, E.G., Corrosion, 23, 5, 1967.

56 Freedman, A.H., J. Materials Sci., 5(12), 431, 1970.

57 Mostovy, S., Smith, H.R., Lingwall, R.G., and Ripling, E.J., Eng. Fract. Mechanics 3, 291, 1971.

58 Carter, C.S., Corrosion, 27, 471, 1971.

59 Leckie, H.P., Proc. Conf. on Fund. Aspects of S.C.C., NACE, p.411, 1967.

60 Sonnins, C.B., Gulbransen, L.B., Hasan, S.Z., Coffey, F.Z. and Skelton, M.W., 'Investigations of the S.C.C. behaviour of maraging steels in various environments'. Rev. Met., 66, 741, 1969.

61 Hancock, G.G. and Johnson, H.H., 'H_2, O_2 and subcritical crack growth in high strength steels', Trans. Met. Soc. AIME, 236, p. 513-516, 1966.

62 Sawicki, V.R., Ph.D. Diss, Cornell University, N.Y., 1971.

63 McIntyre, P. and Priest, A.H., 'Accelerated Test Technique for Determination of $K_{I\ SCC}$ in Steels'. British Steel Corpn. Corporate Labs Report MG/31/72, 1972.

64 Kern, G.E., Ph.D Thesis, Ohio State University, Columbus, Ohio, 1973.

65 Walter, R.J., Jewett, R.P. and Chandler, W.T., Metal Science and Eng., 5, 99, 1970.

66 Hudak, S.J., and Wei, R.P., unpublished work reported in ref. (16).

67 Williams, D.P. and Nelson, H.G., Met. Trans, 1, 63, 1976.

68 Oriani, R.A. and Josephic, P.H., Scripta Met., 6, 681, 1972.

69 Haynes, A.G., Metallurgical Developments in High Alloy Steels Spec. Rpt. No.86, I.S.I. London, p.125, 1964.

70 Gray, H.R. and Troiano, A.P., Metal Progress, p.75, April 1964.

71 Bonizewski, T., Brit. Weld Journal 12, 557, 1965.

72 Dautovitch, D.P. and Floreen, S., Met. Trans., 74, 2627, 1973.

73 Haynes, A.G., Rev. de Met. 63, 555, 1966.

74 Wang, M.T., Tech. Rpt. AFML. -72-102 Part 1, 1972.

75 Jones, P.M.S., Gibson, R. and Evans, J.A., UKAEA Rpt. O-19/66, 1966.

76 Oriani, R.A., Fundametal aspects of stress corrosion testing, NACE Houston, p.32, 1969.

77 Baldy, M.F. and Bowden, R.C., Corrosion, 11, 417t, 1955.

78 Prange, F.A., Corrosion, 8, p.355, 1952.

79 Davies, R.A., Corrosion, Vol. 19, p.45t, 1963.

80 Lillys, P. and Nehrenberg, A.E., Trans. A.S.M., 48, p. 327-355, 1956.

81 Trozzo, P.S. and McCartney, R.F., Corrosion, 16, 26, 1960.

82 Oriani, R.A., 'A decohesion theory for hydrogen induced crack propagation.' S.C.C. and HE of iron base alloys, NACE conference, Firminy, 1973, to be published.

83 Carter, C.S., Boeing Co. Rpt. D6-19770, 1967.

84 Beachem, C.D., Met. Trans., 3, p.347, 1972.

85 Wang, M.T. and Staehle, R.W., H_2 in metals, International Conf. Paris, p.342, May-June 1972.

86 Speidel, M.O., H_2 in metals, International Conf. Paris, p.3, May-June 1972.

87 Carter, C.S., Eng. Fracture Mech, Vol. 3, p.1, 1971.

88 Jeanfils, C., Pampillo, C.A., Rosenberg, J. and Paxton, H.W., Carnegie Mellon Tech. Rpt. 1, 1971 US Naval Research Contract N 00014-67-A-0314-0004.

89 Bobshtein, C.Z., Ginzberg, S.S. Kishkin, S.T. and Moroz, L.M., Metal Science and Heat Treatment 56, 396, 1969.

90 Laurent, J.P., Lapasset, G., Aucouturier, M. and Lacombe, P., Corros. Trait. Prot. Finition, 20, No.2, 113, 1972

91 Lapasset, G., Laurent, J.P., Aucouturier, M. and Lacombe, P., L'hydrogène dan les Metaux, Editions Science et Industrie, Paris, p. 108, 1972.

92 Toy, S.M. and Phillips, A., Corrosion, 26, 200, 1970.

93 Clark, A.B.J. and Irwin, G.R., Exp. Mech,, 23, 321, 1966.

94 Syrett, B.C. and Trudeau, L.P., Corrosion, 27, 216, 1971.

95 Haydon, H.W. and Floreen, S., Corrosion, 27, 429, 1971.

96 Parkins, R.N., Mazza, F., Royeula, J.J. and Scully, J.C., 'Stress corrosion test methods', BR. Corr. Journal 7, 154, 1972

97 Uhlig, H.H., Metal Progress, 57, p. 486-487, 1950.

98 Bhatt, H.J. and Phelps, E.H., Proc. 3rd International Congress on Metallic Corrosion Moscow, USSR, May 16-26, 1966.

99 Brown, B.F., 'Cracking of martensitic 410 stainless steel in corrosive environments', Rpt. NRL Progress p.40, May 1958.

100 Brown, B.F., 'S.C.C. and related phenomena in high strength steels', NRL Rpt. 6041, Nov. 1963.

101 Brown, B.F., 'S.C.C. and corrosion fatigue of high strength steels'. Defense Metals Info. Centre, Battelle Mem.

Institute, Columbus, Ohio, DMIC Rpt. 210, p.91, Oct, 1974.

102 Truman, J.E., Perry, R. and Chapman, G.N., J.I.S.I., p.745-756, 1964.

103 Hughes, P.C., Lamborn, I.R. and Leibert, B.B., 'Delayed fracture of a low alloy high strength steel at controlled corrosion rates', J.I.S.I. p. 728-731, (1965).

104 Baylis, J.R., Met. Chem. Eng. 32, 874, 1925.

105 Hoar, T.P., Trans. Faraday Soc. 33, 1152, 1937.

106 Edeleanu, C. and Evans, U.R., Trans. Faraday Soc., 47, 1121, (1951).

107 Brown, B.F., Fujii, C.J. and Dahlberg, E.P., J. Electrochem. Society, 116, 218, 1969.

108 Ateya, B.G. and Pickering, H.W., J. Electrochem. Soc. p. 1018-1026, 1975.

109 Barth, C.F., Steigerwald, E.A. and Troiano, A.R., Corrosion, 25, No.9, p. 353-358, 1969.

110 Wilde, B.E., Corrosion, 27, p. 326-333, 1971.

111 Swann, P.R. and Embury, J.D., 'Microstructural aspects of stress corrosion failure'. High Strength Materials, ed. V.F. Zackay, Wiley & Son N.Y., p.351, 1965.

112 Elsea, A.R. and Fletcher, E., 'H_2 induced delayed brittle failures of high strength steels'. D.M.I.C Rpt. 196, January, 1964.

113 Okada, H. Ken-Ichi Yikawa, Tamura, H., Corrosion, 30, No.7, p. 253, 1974.

114 Parkins, R.N., N.A.T.O. A.S.I., 1975 to be published 1976.

115 Beachem, C.D. and Brown, B.F., 'A Comparison of 3 precracked specimens for evaluating the Stress Corrosion

Susceptibility of 3 high strength steels', Stress Corrosion Testing, ASTM STP425 Philadelphia, Pa 1967.

116 Brown, W.F. and Srawley, J.E., 'Plane Strain Crack Toughness Testing of High Strength Metallic Materials'. ASTM STP 410 Philadelphia, Pa, 1966.

117 Procter, R.P.M. and Paxton, H.W., Trans. ASM 62, 989-999, 1969.

118 Barnett, W.J. and Troiano, A.R., Trans. AIME, 209, 486-494, 1957.

119 McIntyre, P. and Priest, A.H., B.I.S.R.A. Open Report MG/54/71.

120 Devanathan, M.A.V. and Stachurski, Z.O.J., Proc. Royal Society, A.270, 90, 1962

121 West, J.M., 'Electrodeposition and Corrosion Processes'. Van Nostrand Reinhold. 1971

122 Smialowski, M., 'Hydrogen in Metals', p. 368-369, Pergammon Press, 1962.

123 Govindan Namboodhiri, T.K. and Nanis, L., Acta. Met. 21, 663, 1973.

124 Beck, W., Bockris, J.O.M., McBreen, J. and Nanis, L. Proc. Royal Soc. A290, 220, 1965.

125 Beck, W., Bockris, J.O.M. Genshaw, M.A. and Subramanyan, P.K., Met. Trans., 2, 883, 1971.

126 Kim, C.D. and Loginow, A.W., Corrosion, 24, p. 313, 1968.

127 Radhakrishnan, T.P. and Shreir, L.L., Electrochemica ACTA, 11, p.1007-1021, 1966.

128 Devanathan, M.A.V., Stachurski, Z. and Beck W., J. Electrochem Soc, 110, No. 8, 886, 1963.

129 McBreen, J. Nanis, L. and Beck, W., J. Electrochem Soc., 113, 1218, 1966.

130 Shively, J., Corrosion, 23, 215, 1967.

131 Oriani, R.A., Acta Met. 18, 147, 1970.

132 Darken, L.S. and Smith R.P., Corrosion, 5, 1, 1949.

133 McNabb, A., Foster, P.K., Trans. A.I.M.E., 227, 618, 1963.

134 McIntyre, P., Priest, A.H., Paper 13. Agard Conf. 98 Specialists meeting on stress corrosion test methods.

135 McIntyre, P., Proceedings of a Conference on 'Mechanics and Mechanisms of Crack Growth', organised by the Physical Metallurgy Centre of the B.S.C., Cambridge, 1973.

136 Hoar, T.P. and West, J.M., Proc. Royal Soc., A268, 304, 1962.

137 Hoar, T.P. and Scully, J.C., J. Electrochem. Soc., 111, 348, 1964.

138 Hoar, T.P. and Scully, J.C., Proceedings of 2nd International Congress on Metallic Corrosion, New York, 1966.

139 Tromans, D. and Nutting, J., Fracture of Solids, p.637, Interscience, New York 1963.

140 Darken, L.S. and Gurry, R.W., Physical Chemistry of Metals, p.444, McGraw-Hill.

141 Knott, J.F., Mater. Sci. Eng. 7, 1, 1971.

ACKNOWLEDGMENTS

The author would like to thank Professor R N Parkins for his encouragement and useful discussions relating to this work. The author is also indebted to Professor Parkins for permission to use the facilities of the Metallurgy Department and to the Science Research Council for financial support. The author is grateful to Mr D Birchon of the Admiralty Materials Laboratory, Poole, Dorset for permission to use the acoustic emission facilities of that laboratory.

Finally, the author would like to express his gratitude to the technical staff of the Metallurgy Department without whose able assistance and co-operation this work would not have been possible.